PB81-156960

Near-Wall Similarity in a Pressure-Driven Three-Dimensional Turbulent Boundary Layer

Virginia Polytechnic Inst. and State Univ.
Blacksburg

Prepared for

National Aeronautics and Space Administration
Moffett Field, CA

Sep 80

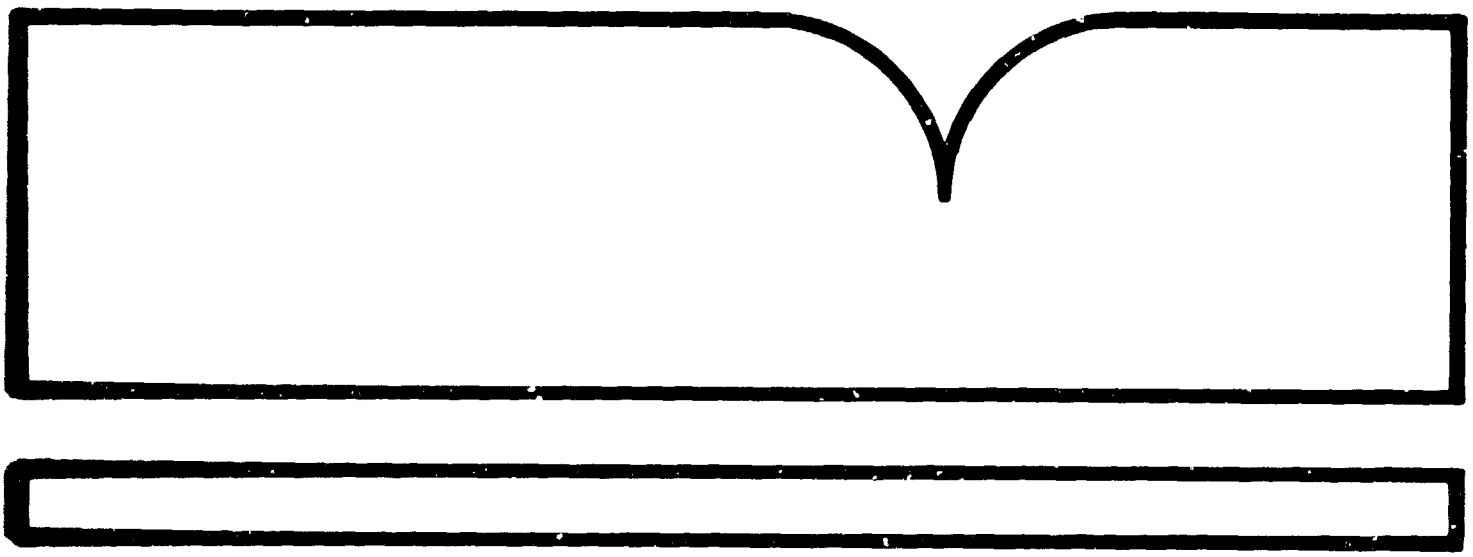

Near-Wall Similarity in a Pressure-Driven Three-Dimensional Turbulent Boundary Layer

F. J. Pierce
J. E. McAllister

Mechanical Engineering
Virginia Polytechnic Institute & State University
Blacksburg, Virginia 24061

Report VPI-E-80.32 September 1980

Prepared for the
National Aeronautics and Space Administration
NASA Grant NSG 2301

Grant Monitor
Joseph Marvin
NASA-Ames Research Center

BIBLIOGRAPHIC DATA SHEET	1. Report No. VPI-E-80.32	2.	3. Recipient's Accession No. PB81 156960
4. Title and Subtitle Near-Wall Similarity in a Pressure-Driven Three-Dimensional Turbulent Boundary Layer			5. Report Date September 1980 6.
7. Author(s) F. J. Pierce J. E. McAllister			8. Performing Organization Rept. No.
9. Performing Organization Name and Address Mechanical Engineering Department Virginia Polytechnic Institute and State University Blacksburg, Virginia 24061			10. Project/Task/Work Unit No. 11. Contract/Grant No. NASA NSG 2301
12. Sponsoring Organization Name and Address NASA-Ames Research Center University Affairs Office, 241-25 Moffett Field, California 94035			13. Type of Report & Period Covered Interim 14.

15. Supplementary Notes

16. Abstracts

Extensive measurements of the mean velocity, wall pressure and wall shear stress fields were made in a three-dimensional pressure-driven turbulent boundary layer created by a cylinder with trailing edge placed normal to a flat plate floor.

The direct force wall shear stress measurements were made with a unique, floating element direct force sensing shear meter that responded to both the magnitude and direction of the local wall shear stress.

These data were used to test the ability of ten near-wall similarity models proposed in the literature to describe the near-wall velocity field for the measured flow under a wide range of skewing conditions and a variety of pressure gradient and wall shear vector orientations.

17. Key Words and Document Analysis. 17a. Descriptors

three-dimensional flow
boundary layer
turbulent
wall shear meter
wall shear stress
near-wall similarity
pressure-driven
law of the wall

17b. Identifiers/Open-Ended Terms

17c. COSATI Field/Group

18. Availability Statement	19. Security Class (This Report)	21. No. of Pages
Release Unlimited	UNCLASSIFIED	242
	20. Security Class (This Page) UNCLASSIFIED	22. Price

INSTRUCTIONS FOR COMPLETING FORM NTIS-35 (Bibliographic Data Sheet based on COSATI Guidelines to Format Standards for Scientific and Technical Reports Prepared by or for the Federal Government, PB-180 600).

1. **Report Number.** Each individually bound report shall carry a unique alphanumeric designation selected by the performing organization or provided by the sponsoring organization. Use uppercase letters and Arabic numerals only. Examples: FASEB-NS-73-87 and FAA-RD-73-09.

2. Leave blank.

3. **Recipient's Accession Number.** Reserved for use by each report recipient.

4. **Title and Subtitle.** Title should indicate clearly and briefly the subject coverage of the report, subordinate subtitle to the main title. When a report is prepared in more than one volume, repeat the primary title, add volume number and include subtitle for the specific volume.

5. **Report Date.** Each report shall carry a date indicating at least month and year. Indicate the basis on which it was selected (e.g., date of issue, date of approval, date of preparation, date published).

6. **Performing Organization Code.** Leave blank.

7. **Author(s).** Give name(s) in conventional order (e.g., John R. Doe, or J.Robert Doe). List author's affiliation if it differs from the performing organization.

8. **Performing Organization Report Number.** Insert if performing organization wishes to assign this number.

9. **Performing Organization Name and Mailing Address.** Give name, street, city, state, and zip code. List no more than two levels of an organizational hierarchy. Display the name of the organization exactly as it should appear in Government indexes such as Government Reports Index (GRI).

10. **Project/Task/Work Unit Number.** Use the project, task and work unit numbers under which the report was prepared.

11. **Contract/Grant Number.** Insert contract or grant number under which report was prepared.

12. **Sponsoring Agency Name and Mailing Address.** Include zip code. Cite main sponsors.

13. **Type of Report and Period Covered.** State interim, final, etc., and, if applicable, inclusive dates.

14. **Sponsoring Agency Code.** Leave blank.

15. **Supplementary Notes.** Enter information not included elsewhere but useful, such as: Prepared in cooperation with . . . Translation of . . . Presented at conference of . . . To be published in . . . Supersedes . . . Supplements . . . Cite availability of related parts, volumes, phases, etc. with report number.

16. **Abstract.** Include a brief (200 words or less) factual summary of the most significant information contained in the report. If the report contains a significant bibliography or literature survey, mention it here.

17. **Key Words and Document Analysis. (a). Descriptors.** Select from the Thesaurus of Engineering and Scientific Terms the proper authorized terms that identify the major concept of the research and are sufficiently specific and precise to be used as index entries for cataloging.
(b). Identifiers and Open-Ended Terms. Use identifiers for project names, code names, equipment designators, etc. Use open-ended terms written in descriptor form for those subjects for which no descriptor exists.
(c). COSATI Field/Group. Field and Group assignments are to be taken from the 1964 COSATI Subject Category List. Since the majority of documents are multidisciplinary in nature, the primary Field/Group assignment(s) will be the specific discipline, area of human endeavor, or type of physical object. The application(s) will be cross-referenced with secondary Field/Group assignments that will follow the primary posting(s).

18. **Distribution Statement.** Denote public releasability, for example "Release unlimited", or limitation for reasons other than security. Cite any availability to the public, other than NTIS, with address, order number and price, if known.

19 & 20. **Security Classification.** Do not submit classified reports to the National Technical Information Service.

21. **Number of Pages.** Insert the total number of pages, including introductory pages, but excluding distribution list, if any.

22. **NTIS Price.** Leave blank.

Near-Wall Similarity in a Pressure-Driven
Three-Dimensional Turbulent Boundary Layer

ABSTRACT

Extensive measurements were made to determine the mean velocity field, wall pressure field, and wall shear stress field for a pressure-driven three-dimensional turbulent boundary layer in a forward quadrant of the flow around a cylinder with trailing edge placed normal to a flat plate floor.

The direct force wall shear measurements were made with a unique, omnidirectional floating element mechanical shear meter which sensed both the magnitude and the direction of the local wall shear stress. To establish the credibility of these direct force wall shear measurements, extensive measurements were first made in a two-dimensional turbulent boundary layer over a range of unit Reynolds numbers where generally excellent agreement was obtained with a variety of direct and indirect two-dimensional wall shear diagnostic devices and techniques.

These three-dimensional velocity field, wall pressure field, and wall shear field results were used to test the ability of ten near-wall similarity models proposed in the literature for three-dimensional turbulent boundary layers to describe the near-wall velocity field. Six of these ten models are scalar, treating some form of an equivalent velocity component. Three of the remaining four more complex models are two-component vector models and the last is a scalar model which recognizes the vector nature of the near-wall flow by way of a developed velocity. All of the ten models tested find their origin, directly or indirectly, in an equilibrium boundary layer hypothesis using a mixing length.

For profiles with monotone increasing skew and with skew angles up to about 15-20°, for profiles with an increasing and decreasing skew angle of 10° or less, and for plane of symmetry flow away from separation, any of the six simpler models does a fair job of predicting near-wall similarity in a region of primary focus of $y^+ > 50$ with the qualification that in this study the experimental data tends to ride higher than the theoretical model lines. These (and many other) three-dimensional data show consistently better behavior in a lower y^+ range of secondary focus--the y^+ range where

two-dimensional data is characterized by more scatter and disagreement among even carefully done experiments--and to some extent this better very-near wall behavior compensates for the more rapid departure from similarity in the higher y^+ range of similarity more typical of two-dimensional flows. It would appear that shear velocity magnitudes inferred by Clauser chart type techniques using data in the y^+ range of 10 to about 100 would be within 5-10% of values calculated for the direct force measurements (uncorrected for any possible pressure gradient effects) provided that the similarity law be of the type that reflects the very near-wall departure from the log law-like behavior in this range of smaller y^+ values. The third or fourth order Spalding formula or the two or three formula law of the wall should be adequate to accomodate this lower y^+ range data.

For the above kinds of flows three of the four complex models generally are superior in describing the experimental data for the freestream or principal flow components. For modest transverse velocities two models show some agreement with data but generally not nearly as good as for the freestream or principal flow components. A difficulty with these more complex models lies in the fact that each returns to two-dimensional logarithmic-like law for small y^+ values. Thus, assuming these models could be used to infer local shear velocity magnitude (say to 5-10%), there is the problem of fixing a lower y^+ limit below which data could not be used.

If one were to use these three more complex models in a computational scheme replacing the no slip wall boundary condition at the wall with a match to a similarity model near the wall, then for the flows described above, such a match should be made in a range of about $50 < y^+ < 100$. Practical difficulities will occur since these three more complex models all require an a priori knowledge of the pressure gradient magnitude and direction, and two also require a priori knowledge of at least the wall shear direction.

For the restricted class of three-dimensional flows described above, it appears that the local wall shear stress and nondimensionalizing shear velocity for the various similarity models are related within a modest uncertainty. This implies that at least an approximate magnitude of local wall shear stress would be inferred from such similarity models in a

Clauser chart type of approach. This would also imply that with indirect diagnostic devices which are not strongly sensitive to yaw angles (such as Preston tubes and surface heat meters) would also give a reasonably good approximation to the magnitude of the wall shear stress in such modestly skewed flow as well, using a two-dimensional calibration. Note that without the supporting results of this study with directly measured local wall shear stresses, such use of a two-dimensional calibration in a three-dimensional flow would be speculative at best. The same relative insensitivity to yaw that would allow the use of such indirect devices in a skewed flow would, however, render such devices as relatively poor in indicating the local wall shear stress or limiting wall streamline direction. It would appear that for such modestly skewed flows the combination of say a Preston tube or surface heat meter together with an established wall flow visualization technique could do a reasonably satisfactory job in mapping a wall shear field. The combination of indirect magnitude sensing device and flow visualization for the direction would be significantly easier to use than a direct force sensing three-dimensional wall shear meter such as used in this study.

It appears that for monotone, strongly skewed flows (say 20° and greater) and for flows with increasing-decreasing skew of more than about 10°, none of the ten three-dimensional similarity models tested here seems adequate to describe the near-wall velocity field even approximately.

One additional model found in the literature could not be tested because of the need for turbulent stress gradient data at the wall and such data is exceptionally difficult to measure accurately.

CONTENTS

CONTENTS (CONTINUED)

I. INTRODUCTION

Briefly, near-wall similarity refers to the experimentally determined and demonstrated "sameness" of the velocity profile in the wall region of a broad class of turbulent boundary layer flows when these are plotted in suitably nondimensionalized coordinates. For two-dimensional turbulent boundary layers* the concept of near-wall similarity is well accepted and a brief review of these ideas will facilitate the discussion of near-wall similarity for three-dimensional turbulent boundary layers*.

Near-wall similarity is not to be confused with the rigorous, mathematical similarity type of analysis where for a given physical problem all relevant variables are known and the governing equations can be successfully nondimensionalized to seek out solutions to entire classes of problems. Near-wall similarity is like this but not as rigorous for it is experimental, not analytical; only the strong variables appear known; it is an experimentally based "sameness" of flow with all the usual uncertainties of experimental studies. In the two-dimensional case it does cover large classes of flows. For example, except for extremes in pressure gradient, all turbulent boundary layers appear to be well described by the same similarity law for all flows over hydraulically smooth surfaces without suction or blowing.

For the 2DTBL the generally accepted similarity law is written as

$$u^+ = \frac{1}{\kappa} \ln y^+ + C \qquad 1.1$$

where $u^+ = u/u^*$, $y^+ = yu^*/\upsilon$ and $u^* = \sqrt{\tau_o/\rho}$. Unlike the rigorous mathematical similarity analysis, κ and C are experimentally determined constants (that do change with roughness and suction/blowing) and sometimes appear to have at least a weak but not well defined dependence on

*The short forms 2DTBL and 3DTBL will be used as convenient for the two- and three-dimensional turbulent boundary layer.

other variables. Apparent systematic variations in κ and C are often within the experimental uncertainty of the data itself and this causes difficulty in fixing the universality of these two parameters.

The various regions of flow characterizing a 2DTBL velocity profile with emphasis on those particular to this study are shown in Fig. 1.1. Following the suggestion of Coles (1956) the typical velocity profile for a 2DTBL can be thought of as made of two main regions, a wall region and a wake region. The wake region represents the large majority of the profile and is often identified with velocity defect coordinates. The wall region is a relatively small portion of the profile and is usually identified with the classic logarithmic law of the wall. It is this latter flow region which is the near-wall flow and the subject of this near-wall similarity study.

Multiple designations for portions of the near-wall region have evolved and are reviewed here to avoid ambiguity. This near-wall flow zone is sometimes broken up into three subregions with a viscous sublayer subregion very close to the wall, the logarithmic or law of the wall subregion further from the wall (but well before the wake region of the profile becomes strong), coupled by an intermediate, transition or buffer subregion. One can write equations for the velocity profile in each of these three subregions and this leads to a three formula law of the wall. Alternatively, it is not uncommon to omit the transition, or buffer subregion, with the near-wall similarity zone made up of only the inner viscous sublayer and the more remote logarithmic law of the wall subregion. This leads to a two formula law of the wall. The boundaries between the subregions of the three and two formula law of the wall models are somewhat arbitrary. Finally, in examining a very large volume of experimental data for 2DTBL flows, Coles (1956) shows a lack of consistency in data among experimenters as one approached the wall in the approximate $y^+ \leq 50$ range. It is convenient to designate this zone of flow as the very near-wall zone.

Because the law of the wall designation is often taken to refer to the logarithmic equation which is not valid down to the wall itself, it has sometimes been convenient to refer to the complete near-wall flow region as the region of the extended law of the wall. Spalding (1961)

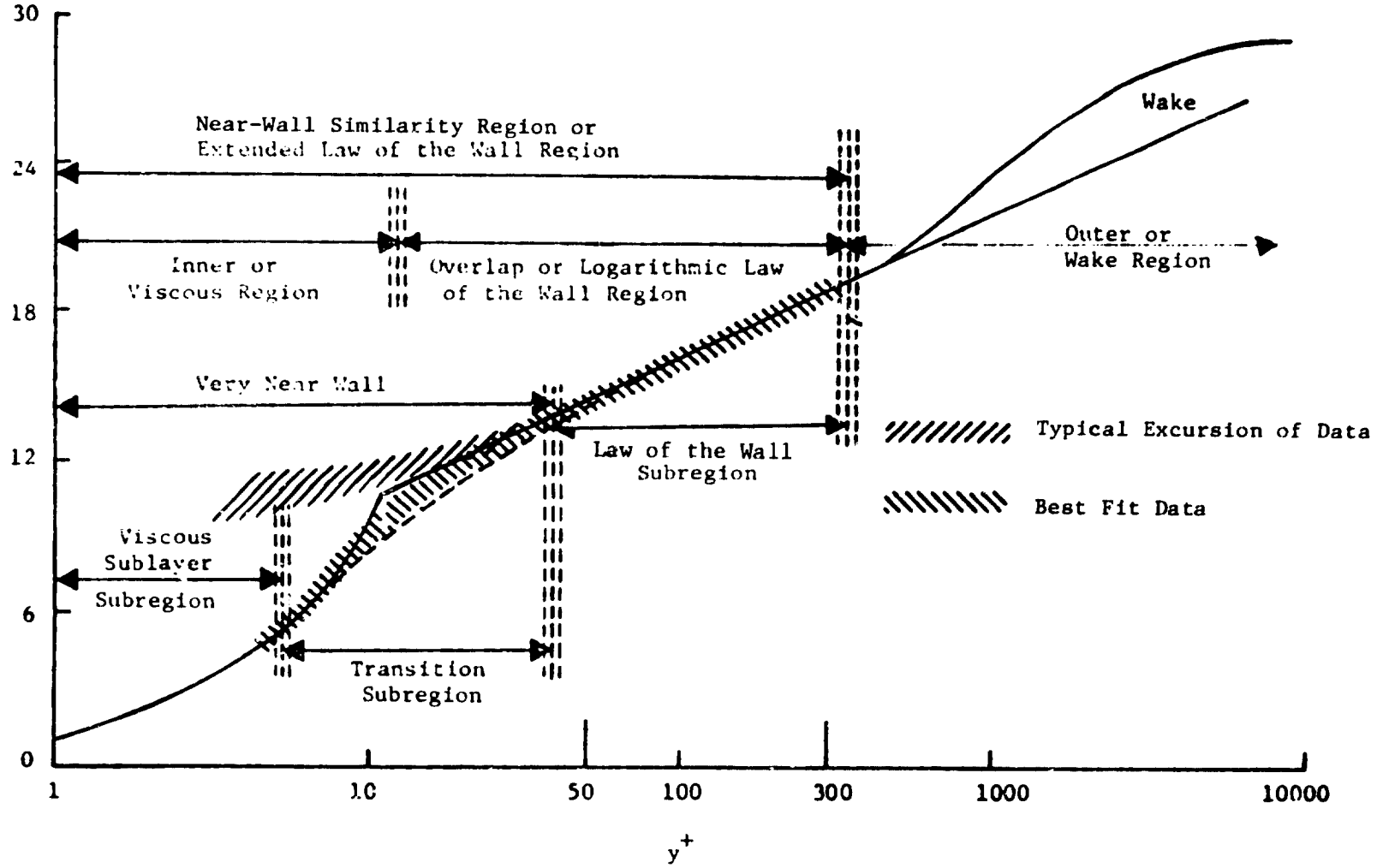

Fig. 1.1. Typical Regions in Two-Dimensional Near-Wall Similarity

and Kleinstein (1967) have proposed a similar, single formula law of the wall to describe the entire near-wall region down to the wall itself.

As a word of caution the reader is reminded that in discussions of the entire velocity profile, particularly in the older literature, it has been common to describe an inner or viscous wall region and an outer or velocity defect (wake) region, which are joined by an overlapping region and from which the original model of the logarithmic law of the wall evolved. It is important not to confuse this overlap region, where the law of the wall in its logarithmic form is valid, with the transition or buffer subregion described in the three formula law of the wall model.

In this work near-wall similarity refers to the usual law of the wall subregion, the transition subregion, and the extreme near-wall viscous subregion or sublayer. These three regions have also been collectively referred to as the extended law of the wall region or simply as the near-wall region.

It is worth noting that in the semi-logarithmic coordinates of Fig. 1.1 the near-wall region appears quite large. In fact, it represents relatively thin layer of flow in the usual case. Based on his extensive and exhaustive study of over 400 velocity profiles Coles (1956, 1968) suggests that logarithmic like behavior begins at a y^+ value of about 50. Even at larger y^+ values there are significant and unresolved questions on the accuracy of velocity measurements in the 2DTBL case with experimental data typically above the logarithmic line. There appears to be no self consistent method or technique to resolve these differences among various sets of data. A frequent explanation is a traditional probe displacement correction but Pierce and Gold (1977) have shown that this does not always resolve such differences. Coles work also suggests that for modest pressure gradients a y^+ upper limit of about 300 is reasonable. Above this value the wake contribution becomes more noticable. This approximate upper limit is affected by pressure gradient, decreasing with increasing adverse pressure gradient. The region of $50 < y^+ < 300$ is more than adequate to define the classic logarithmic law of the wall region. Recognition of the difficulties in very near-wall velocity measurements in the more thoroughly studied and better understood 2DTBL

case, prompts this study in the 3DTBL case to focus on flow generally outside this analogous very near-wall region and in an interval of nominal y^+ values as in the two-dimensional case.

Aside from the fundamental importance of providing basic information of the nature of the near-wall flow in 2DTBL's, this observed similarity also serves (1) to provide a means of inferring the very difficult to measure local wall shear stress from the much easier to measure local velocity profile data, (2) as the basis of the validity of indirect wall shear diagnostic devices such as Preston tubes, rakes, fences, heat meters, etc., and (3) to provide the potential for improving computer solutions to turbulent boundary layer flows by reducing computational steps and computer storage by matching outer computer solutions to accepted inner velocity profiles based on established near-wall similarity models.

The motivation for establishing the existance of and limits on near-wall similarity in the 3DTBL case are much the same as in the 2DTBL case. The importance of local near-wall similarity laws in 3DTBL and channel flows grows when one recognizes that the empirical eddy viscosity and mixing length models often rely on wall similarity information, especially in the near-wall behavior. For example, in the two-dimensional case, the classic van Driest damping factor is designed to return the logarithmic law of the wall-like behavior in the computed velocity profile. Clearly, it is essential to know the nature of this near-wall flow in the three-dimensional case if one is to use such algebraic closure models in the solutions of these kinds of problems. The question is even more critical in current applications of higher order modeling of the Reynolds stresses where in many existing solution techniques only turbulent stresses are included in the motion equations, thus precluding any near-wall calculations where viscous stresses exist. Considerable economies in the computer time and monies can be effected in 3DTBL and channel flow calculations if one replaces the no slip wall boundary condition at the wall with a match to a near-wall similarity law near the wall thereby avoiding the more dense regions of lattice points required by large gradients. A good knowledge of and limits on local three-dimensional near-wall similarity laws are, however, crucial to these solution techniques. It is recognized

that closure of the equations of motion with a turbulent energy model or a turbulent stress transport model or similar higher level models does not require the exclusion of viscous stresses in the motion equations and this is only a consequence of many of these current methods of solution.

It should be noted that in the 2DTBL the near-wall similarity law is a simple scalar law since the velocity profile is always collateral. That is, all the velocity profile vectors are always in the same direction (similarity laws for flow reversal circumstances do not appear to have yet been proposed).

For the three-dimensional case the concept of near-wall similarity is not so well established. To date, 11 models for the velocity profile in the near-wall region have been found in the literature. Six of these models are simpler scaler models, while five of these models recognize in some more elaborate way the vector character of the 3DTBL velocity profile with the vector turning continuously down to the wall.

The resolution of the near-wall similarity question in 3DTBL flows requires the direct force measurement of both the magnitude and direction of the local wall shear stress, the mean velocity field, and the wall pressure field. The wall shear stress is required since a key question in the test of similarity models in three-dimensional flow is whether or not the local wall shear stress is related to some form of a three-dimensional shear velocity as in $q^* = \sqrt{\tau_o/\rho}$, analogous to the two-dimensional case. The test of existing proposed similarity models for the 3DTBL consists of defining a local shear velocity from the directly measured local wall shear stress and plotting the nondimensionalized experimental data in the coordinates of the various proposed models for direct comparison with the various analytical model forms. Some of these models require significant additional experimental data input on wall shear magnitude gradients, wall shear angle gradients, and wall pressure gradients as well.

The direct force measurement of local wall shear stress is an absolute requirement in any serious study of the near-wall similarity question in three-dimensional flows. This is an essential requirement since the several near-wall similarity models proposed in the literature for the 3DTBL case all require the local wall shear stress (or some component of it) in the necessary nondimensionalizing of experimental data. While the

use of indirect wall shear devices has been reported in some 3DTBL flows (e.g., Pierce and Krommenhoek (1968), Prahlad (1968), East and Hoxey (1969), van den Berg (1976), Dechow and Felsch (1977), Higuchi and Peake (1978)) with both Preston tube type devices and miniature surface mounted heat meters, all such devices reported to date have used only two-dimensional calibrations in three-dimensional flows. This, in effect, assumes a priori and without justification, the validity of a two-dimensional near-wall similarity law in three-dimensional flow--and this is wholly unacceptable in any attempt at a definitive study of near-wall similarity in a three-dimensional flow. Up to this point in time no indirect wall shear diagnostic device has been calibrated for wall shear magnitude and direction in a three-dimensional flow for subsequent use in any other three-dimensional flow. The use of a two-dimensional calibration in a three-dimensional flow presumes far more than is acceptable in a near-wall similarity study in 3DTBL flows.

In summary, in the 2DTBL case near-wall similarity concerns itself with the experimentally determined sameness of the flow from the wall itself and through the region where the classic logarithmic law of the wall is valid. This excludes the large outer portion of the velocity profile where the wake character is strong. Practical experimental difficulties in making accurate and repeatable measurements very close to the wall suggests the exclusion of the very near-wall data in two-dimensional near-wall similarity studies. Since all the three-dimensional near-wall similarity models give the two-dimensional logarithmic form of the law of the wall in the limit of vanishing secondary flow and since in the two-dimensional case an approximate y^+ range of 50 to 300 is suggested for modest pressure gradient flows, it would seem reasonable to focus attention on a similar interval in a first look at the existence of near-wall similarity in the three-dimensional case.

II. REVIEW OF SIMILARITY MODELS

Introduction

Two-dimensional near-wall similarity has been studied for over fifty years, while the first three-dimensional similarity model was suggested in 1956 by Coles (1956). Following White's (1974) review, in the 1930's Prandtl, von Karman, and Millikan divided the boundary layer into two distinct regions of flow, an inner or viscous region and an outer region, which were joined in an overlap region characterized by a logarithmic law as shown in Fig. 1.1. Later experimental work by Schultz-Grunow (1940), Ludwieg and Tillmann (1950), Deissler (1955), Clauser (1954), Laufer (1953) and the analytical work by Clauser (1956), van Driest (1956) and Coles (1956, 1957), solidified the near-wall similarity concept for two-dimensional turbulent flows. . .

Coles (1956) suggested the first three-dimensional near-wall similarity model mainly as an extension of the two-dimensional logarithmic similarity law. Johnston (1960) introduced a second model and by 1976 eleven different three-dimensional near-wall similarity models appeared in the literature. It was not until Tennant (1977)* that a preliminary yet fairly extensive comparison of some of these was undertaken. The work reported here is a more detailed and more thorough study of the pressure-driven 3DTBL flow initiated by Tennant.

This review will examine different forms and origins for some of the various smooth wall two-dimensional similarity models since many of the early three-dimensional similarity models assumed forms similar to these two-dimensional models. Subsequently, the three-dimensional models will be examined to see what fundamental differences exist among these models. Since the credibility of the experimental data is critical in verifying any proposed model, a review of Preston tubes is also included since these are a generally accepted method for two-dimensional wall shear inference and Preston tubes were used to help verify the direct wall shear measurements made in two-dimensional flows by the omnidirectional meter in preliminary work to establish credibility of this mechanical meter.

Two-dimensional near-wall similarity is a well accepted concept and a two-dimensional similarity law exists with the understanding that this

---

*See footnote, page 90.

law may be expressed by different equations or models. There is, however, some question surrounding the uniqueness of constants in these equations. In contrast, there is not as yet an established three-dimensional similarity law since, while several models have been proposed, none has been validated by direct local force shear measurements, and such validation is an absolute necessity in establishing the existence of such a law--whatever form or model it may ultimately take.

Two-Dimensional Near-Wall Similarity

Figure 1.1 shows the near-wall or extended law of the wall region which typically composes approximately 10-20% of a two-dimensional turbulent boundary layer. Prandtl (1933) first suggested using the variables in Eq. 1.1. A similarity law for the inner flow or the viscous sublayer followed by assuming that only viscous shear is important in a thin layer immediately adjacent to the wall where

$$\mu \frac{du}{dy} = \tau \approx \tau_o .$$

It follows that

$$u = \tau_o \, y/\mu .$$

It is convenient to define a two-dimensional shear or wall friction velocity as $u^* \equiv \sqrt{\tau_o/\rho}$, in order to nondimensionalize this result with

$$\frac{u}{u^*} = \frac{u^* y}{\upsilon} .$$

If we define

$$u^+ = \frac{u}{u^*}$$

and

$$y^+ = \frac{u^* y}{\upsilon}$$

then for the viscous sublayer,

$$u^+ = y^+. \qquad 2.1$$

There are a number of ways of deriving the relationship that holds in the logarithmic region. Hinze (1975) provides an excellent compilation of these derivations. Two contrasting developments are reviewed briefly here. Historically the outer region was described by a velocity defect or outer law by von Karman as

$$U_\infty - u = f(\tau_o, \rho, y, \delta).$$

It is useful to write the inner law, Eq. 2.1, in functional form as

$$u^+ = f(y^+)$$

and the outer law as

$$\frac{(U_\infty - u)}{u^*} = g(\frac{y}{\delta}).$$

Since the inner and outer laws are both valid in some overlap region, these are combined to give

$$u^+ = f(\frac{\delta u^*}{\upsilon}, \frac{y}{\delta}) = \frac{U_\infty}{u^*} - g(\frac{y}{\delta})$$

For u^+ to exist with both a multiplicative function f and the function g with an additive term, functional analysis requires f and g to be logarithmic. In inner variables this gives the logarithmic law

$$u^+ = \frac{1}{\kappa} \ln y^+ + C \qquad 2.2$$

which describes the flow where the inner and outer regions of Fig. 1.1 join together. This overlap region has come to be designated the law of the wall region or the logarithmic region.

The concept of a constant stress throughout the logarithmic region can also be used with a mixing length or an eddy viscosity to give a logarithmic form. For demonstration purposes Prandtl's mixing-length theory will be reviewed. Since the logarithmic region is fully turbulent,

$$\tau \simeq \rho \, \ell^2 \left|\frac{\partial u}{\partial y}\right| \frac{\partial u}{\partial y}.$$

Prandtl made two important assumptions: (1) that the mixing length in this region is proportional to the distance from the wall, i.e., $\ell = \kappa y$ where κ is usually taken to be von Karman's constant, and (2) that since this inner region is small, τ = constant = τ_o. It follows that

$$\tau_o = \rho \, \kappa^2 y^2 \left(\frac{du}{dy}\right)^2.$$

Introducing the wall friction velocity and separating the variables, one obtains

$$\frac{u^*}{\kappa} \frac{dy}{y} = du.$$

and this can be rewritten as

$$\frac{1}{\kappa} \frac{dy^+}{y^+} = du^+.$$

Integration results in

$$u^+ = \frac{1}{\kappa} \ln y^+ + C \qquad 2.2$$

where κ, often taken as the von Karman's constant, and the constant C are experimentally determined. More about these constants will be discussed later. Townsend (1976) also uses the concept of a constant stress layer to derive the logarithmic form from the turbulent energy equation for channel flow.

Equations 2.1 and 2.2 constitute the classical, two-dimensional similarity law for the near-wall region for smooth walls and this combination is sometimes referred to as the two formula law of the wall. It

is worth noting that the identification of the shear velocity, u^*, with the wall shear stress, with $u^* = \sqrt{\tau_o/\rho}$, comes directly from this kind of analysis. Coles (1968) suggests such developments are not convincing theoretical derivations, with the shear velocity empirically identified with the wall shear stress mainly from pipe flow studies.

Occasionally a relation for the transition subregion shown in Fig. 1.1 is assumed so that a smoother transition takes place between the viscous sublayer and the logarithmic subregions. This relationship can take the form of

$$u^+ = A' \ln y^+ + B' \qquad 2.3$$

where A' and B' are constants different from $1/\kappa$ and C. This three formula law of the wall representation of the near-wall region, Eqs. 2.1, 2.2, and 2.3, may be set aside in favor of a single formula for the entire inner region.

Spalding (1961) and later Kleinstein (1967) independently developed a single formula for the entire near-wall region. Their expression, called a third order equation, is

$$y^+ = u^+ + e^{-\kappa C}\left[e^{\kappa u^+} - 1 - \kappa u^+ - \frac{(\kappa u^+)^2}{2} - \frac{(\kappa u^+)^3}{6}\right]. \qquad 2.4$$

Development of this relation requires the constant shear assumption made previously. This expression also satisfies the requirements that the eddy viscosity is proportional to the cube of the distance from the wall in the viscous sublayer as first noted by Reichardt (1951) and that the eddy viscosity varies as the exponential of the distance from the wall as the similarity law in the logarithmic region requires. In a later study Elrod (1957) concluded that the eddy viscosity varies more closely with the fourth power of the distance from the wall. Spalding presented an alternate equation to satisfy that requirement by adding the term, $(\kappa u^+)^4/4!$, to the bracketed expression in Eq. 2.4. This additional term, which gives a fourth order equation, does little to alter the curve as is shown in Fig. 2.1, yet this small change often enhances fits with experimental data.

Other empirical expressions have been developed by Rotta ,50),

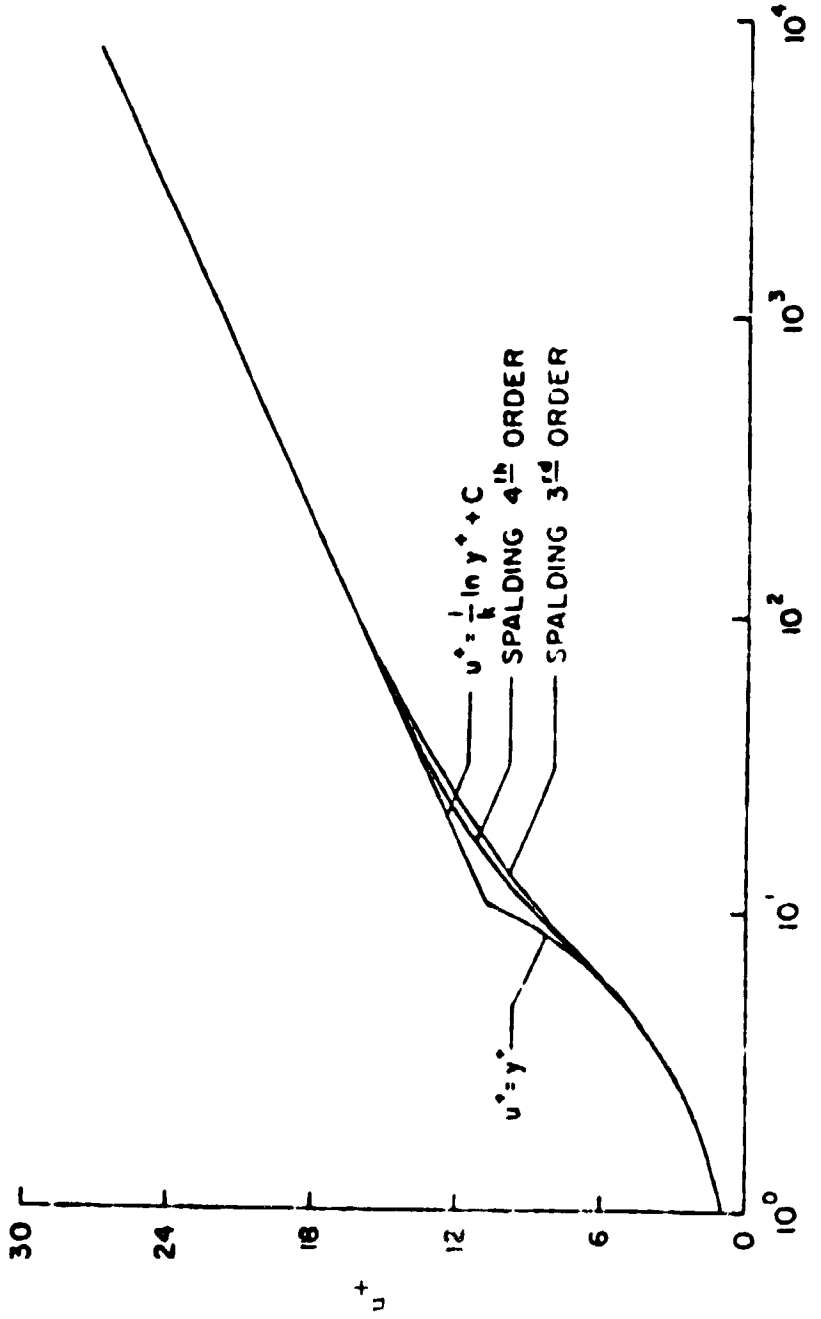

Fig. 2.1 Two-Dimensional Near-Wall Similarity Equations

Reichardt (1951), Deissler (1955), van Driest (1956), and Mellor (1968); however, none of these results in the more useful closed form expression of Spalding. Even more recently, Rasmussen (1975) has developed a single formula expression; however it appears to offer little advantage over Spalding's form. Very recently Dean (1976) has combined Spalding's (1961) inner law with a single polynomial for Coles' (1956) wake function for the outer region as developed by Finley et al., (1966) and later by Granville (1975). The result is a single formula for the whole turbulent boundary layer profile.

Rough walls (Clauser (1956), Hinze (1975), Townsend (1976)), suction/blowing (Kleinstein (1967)), and compressible flow (White and Christoph (1972), East (1972)) generally have different law of the wall forms than those given above but these cases will not be considered in this work.

There is considerable latitude over the choice of the two constants that appear in essentially all forms of the two-dimensional near-wall similarity law and designated κ and C. Table 2.1 lists several of the more popular pairs of constants and several more are available in the literature but are omitted here because of their less frequent usage. Figure 2.2 shows that the choice of constants can have a significant effect on the logarithmic section of the similarity law. The most popular pairs of constants are those of Coles (1968) and Patel (1965), which give nearly identical results, and to a lesser extent those of the N.P.L. (1958) and this group does show reasonably close agreement when plotted in similarity coordinates.

The possible dependence of the similarity constants on Reynolds number is discussed by Kleinstein (1967) who presents an analysis showing a qualitative dependence on Reynolds number, by Patel and Head (1969) who state that the additive constant, C, varies for low Reynolds numbers, Schraub and Kline (1965), who suggest the nonuniversality of these constants for pressure gradient flows, and Huffman and Bradshaw (1972) who also reviewed this question in low Reynolds number flows and suggest that for small shear stress gradients the von Karman constant appears to remain at 0.41 while the additive constant appears Reynolds number dependent.

Figure 2.2 with Table 2.1 shows the kind of disagreement that occurred among careful experiments in the 2DTBL case. This kind of scatter among

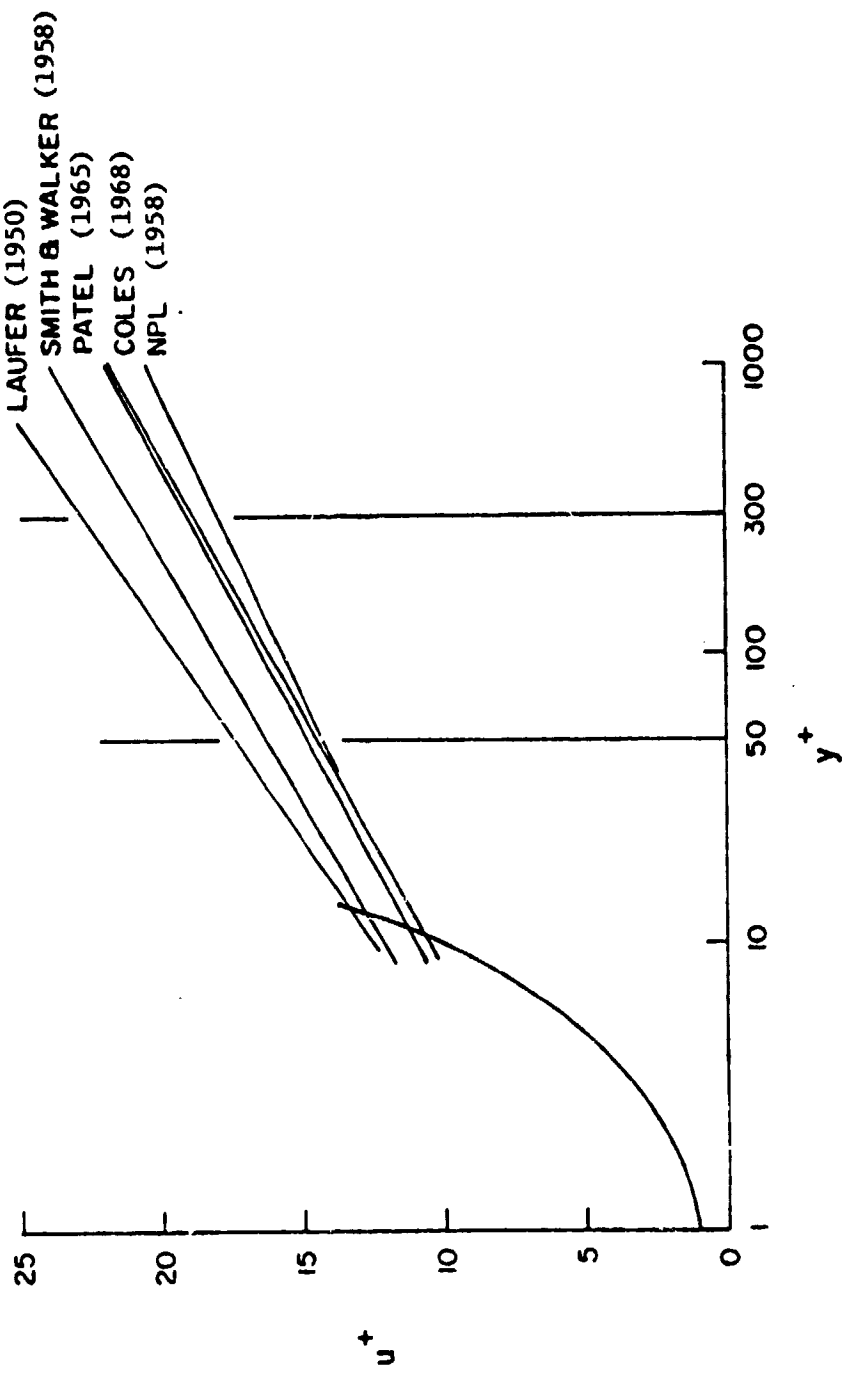

Fig. 2.2 Effect of the Law of the Wall Constants

Table 2.1 Partial Listing of Two-Dimensional Law of the Wall Constants

Investigator	κ	C
Coles (1968)	0.41	5.0
Patel (1965)	0.42	5.45
Clauser (1956)	0.41	4.9
Smith and Walker (1958)	0.46	7.15
N.P.L. Staff (1958)	0.47	5.9
Spalding (1961)	0.40	5.5
Townsend (1976)	0.41	5.61
Coles (1956)	0.40	5.1

careful experiments should be considered in the evaluation of similarity models for the three-dimensional case to be made in Chapter VI.

It would be useful to discuss the effects of pressure gradient and inertial effects on the similarity law for the logarithmic region. Prandtl's constant shear assumption seems adequate for many flows even for moderate pressure gradients or moderately accelerating flows. For cases where these conditions do not exist, the shear stress distribution will vary thoughout the boundary layer. At the wall, the turbulent shear, as well as the velocities parallel and normal to the wall, go to zero so that the momentum equation provides that the viscous shear stress gradient normal to the wall be balanced by the longitudinal pressure gradient:

$$\frac{\partial}{\partial y}\left(\mu \frac{\partial u}{\partial y}\right) = \frac{dp}{dx} .$$

Noting that at the wall $\mu \frac{\partial u}{\partial y} = \tau_o$, one can write

$$\tau = \tau_o + \frac{dp}{dx} y + 0(y^3). \qquad 2.5$$

Ignoring the higher order terms caused by inertial effects for the moment, Eq. 2.5 may be rewritten in the form

$$\frac{\tau}{\tau_o} = 1 + \alpha y^+ \qquad 2.6$$

where

$$\alpha = \frac{\upsilon}{\rho u^{*3}} \frac{dp}{dx} .$$

Utilizing the mixing length assumption as before, it can be shown that,

$$\left(\frac{\tau}{\tau_o}\right)^{1/2} = \kappa y^+ \frac{du^+}{dy^+} . \qquad 2.7$$

By combining Eqs. 2.6 and 2.7 and integrating, one obtains

$$u^+ = \frac{1}{\kappa}\left[\ln y^+ + \kappa C + 2 \ln\left[\frac{2}{(1+\alpha y^+)^{1/2}+1}\right] + 2(1+\alpha y^+)^{1/2} - 2\right]. \qquad 2.8$$

This equation was originally derived by Townsend (1961) and for zero pressure gradient reduces to the near-wall similarity law for the logarithmic region. Van den Berg (1973) points out that for $\alpha y^+ << 1$, Eq. 2.8 may be simplified to:

$$u^+ = \frac{1}{\kappa}[\ln y^+ + \kappa C + \frac{\alpha y^+}{2}]. \qquad 2.9$$

Variations of this analysis have been made by Patel (1973), McDonald (1969), Townsend (1961), and Mellor (1966).

The higher order terms in Eq. 2.5 that have thus far been ignored represent the influence of acceleration of the flow which results from the large velocity gradients near the wall. Van den Berg (1973) estimates that in the logarithmic region, these terms are on the order of half as large as the pressure gradient effects.

Allowance for the inertial terms can be made by multiplying the pressure gradient term by a factor representing the contribution of the inertial terms in the region considered (Bradshaw, et al. (1967)). A constant shear gradient is assumed. Townsend (1956) and van den Berg (1973) suggest that since the shear gradient is essentially not constant, a more satisfying procedure would be to estimate the contribution of the inertial effects as a function of the wall shear stress gradient in the flow direction. If the shear stress varies little with distance from the wall, the velocity profile may be assumed to depend only on the shear stress at the wall. A first approximation of the inertial terms for a given wall shear gradient in the flow direction can therefore be calculated by employing the near-wall similarity law.

Following the derivation of van den Berg (1973), we may write the near-wall similarity law in a more general form:

$$u^+ = f(y^+).$$

It follows that the velocity derivatives may be written as

$$\frac{\partial u}{\partial x} = \frac{du^*}{dx}\left[f + y^+ \frac{df}{dy^+}\right]$$

$$\frac{\partial u}{\partial y} = \frac{u^{*2}}{\upsilon} \frac{df}{dy^+} .$$

Continuity provides that

$$v = - \int_0^y \frac{du}{dx}\, dy = - \frac{du^*}{dx}\, yf.$$

By substituting these velocity gradients into the momentum equation and integrating, one finds that

$$\tau - \tau_o = y \frac{dp}{dx} + \rho \int_0^y \left(u \frac{\partial u}{\partial x} + v \frac{\partial u}{\partial y}\right) dy,$$

or in nondimensional form,

$$\frac{\tau}{\tau_o} = 1 + \alpha y^+ + \beta I_1 \qquad 2.10$$

where

$$\beta = \frac{\upsilon}{u^{*2}} \frac{du^*}{dx}$$

and I_1 is a function of y^+ which appears as the upper limit in the integral

$$I_1 = \int_0^{y^+} f^2\, dy^+.$$

Applying mixing length theory as before, Eqs. 2.7 and 2.10 may be combined to give

$$\frac{\partial u^+}{\partial y^+} = \frac{1}{\kappa y^+} \left(1 + \alpha y^+ + \beta I_1\right)^{1/2}.$$

Assuming that αy^+ and βI_1, are small, this may be approximated as

$$\frac{\partial u^+}{\partial y^+} = \frac{1}{\kappa y^+}\left(1 + \frac{\alpha y^+}{2} + \frac{\beta I_1}{2}\right).$$

and integrated to give

$$u^+ = \frac{1}{\kappa}\left[\ln y^+ + \kappa C + \frac{\alpha y^+}{2} + \frac{\beta I_2}{2}\right]$$

where

$$I_2 = \int_0^{y^+} \frac{I_1}{y^+}\, dy^+.$$

To evaluate the integrals I_1 and I_2, van den Berg suggests the use of the similarity law for the logarithmic region giving

$$I_1 = \frac{y^+}{\kappa^2}\left[\ln y^+ + (\kappa C - 1)\right]^2 + \frac{y^+}{\kappa^2} + \text{constant}.$$

For large values of y^+, the last two terms become small and may be neglected. Substituting I_1 into the expression of I_2 gives

$$I_2 = \frac{y^+}{\kappa^2}(\ln y^+)^2$$

and the near-wall similarity law including pressure and inertial effects takes the form,

$$u^+ = \frac{1}{\kappa}\left[\ln y^+ + \kappa C + \frac{\alpha y^+}{2} + \frac{\beta (\ln y^+)^2 y^+}{2\kappa^2}\right]. \qquad 2.11$$

Three-Dimensional Near-Wall Similarity

Most analytical approaches used in the study of three-dimensional turbulent boundary layers rely heavily on the experience gained in two-dimensional turbulent boundary layers. This section will outline briefly

eleven proposed but unverified models for a suitable similarity model in three-dimensional turbulent boundary layers.

The first six models are scalar models which have approaches centered on finding an equivalent scalar velocity for a three-dimensional turbulent boundary layer which, when inserted into the two-dimensional near-wall similarity law in the logarithmic form of Eq. 2.2, would collapse the velocity profiles, i.e.,

$$q^+ = \frac{q_{equivalent}}{q^*} = \frac{1}{\kappa} \ln \frac{yq^*}{\upsilon} + C. \qquad 2.12$$

where q^* is here arbitrarily identified with the wall shear stress with $q^* = \sqrt{\tau_o/\rho}$ (or some similar form). Note that in these six models there is no convincing theoretical analysis to support this identification. Unlike the two-dimensional case, there is no body of experimental data relating the wall shear stress to the shear velocity to provide an empirical basis for this identification. At this point one simply seeks a suitable nondimensionalizing constant to collapse a velocity profile--that such a nondimensionalizing constant is uniquely identified with the local wall shear stress has not been established. At least for small deviations from two-dimensional flows, this seems to be a reasonable approach, but the assertion by the investigators that $q^* = \sqrt{\tau_o/\rho}$ is without verification, and it should be noted that a parameter q^* might collapse the velocity profiles without being related to the wall shear stress. It is this identification of the nondimensionalizing shear velocity with the wall shear stress which is the critical assumption in near-wall similarity in the 3DTBL. This identification is empirical and it must be experimentally demonstrated that the local wall shear stress is in fact identified with the nondimensionalizing shear velocity. In the following the symbol q^* will be used to distinguish the shear velocity in the 3DTBL from its u^* counterpart in the 2DTBL case. It is noted once again that only the direct measurement of wall shear stress can verify the relationship between wall shear stress and q^* because indirect wall shear stress measurement techniques using devices calibrated in 2DTBL flows presume a priori that the scalar two-dimensional near-wall similarity model describes adequately the vector character of a three-dimensional near-wall flow.

Figure 2.3 shows a sketch of a three-dimensional turbulent boundary layer velocity profile skewed in one direction only and Fig. 2.4 shows a typical polar plot of such a velocity profile. Both notation and the coordinate systems used in the first six models are also shown. It should be noted that the approximate triangular shape of the polar plot is valid only for the profiles where the boundary layer skew is unilateral or in one direction only. For flows where there is recurvature of the freestream streamlines bilateral skewing may occur. Figures 2.5 and 2.6 show a bilaterally skewed three-dimensional profile and a typical polar plot which no longer can be characterized as having a triangular shape.

The first of the simple, scalar models was introduced by Coles (1956) who suggested that the velocity vector, $\vec{q} = \vec{u} + \vec{w}$, could be expressed as the sum of a wall, $\vec{q}_w$, and a wake, $\vec{q}_{wake}$, component. He reasoned that: (1) near the wall the wake component would be small, (2) that the direction of the mean flow near the surface is also the direction of the wall shear, τ_o, as well as the direction of the wall velocity component, and (3) that the wall velocity component in the direction of the wall shear stress could be described by the two-dimensional logarithmic similarity law. Assuming one can identify a nondimensionalizing shear velocity q^* as

$$q^* = \sqrt{\tau_o/\rho} \qquad 2.13$$

then with $q_{equivalent} = q_w$ and $q_w = q \cos \gamma$ one can write

$$q^+ = \frac{q_w}{q^*} = \frac{q \cos \gamma}{q^*} \qquad 2.14$$

with

$$y^+ = \frac{y q^*}{\upsilon} . \qquad 2.15$$

The Coles model becomes a scalar model in the wall shear direction with

$$\frac{q \cos \gamma}{q^*} = \frac{1}{\kappa} \ln \frac{q^* y}{\upsilon} + C. \qquad 2.16$$

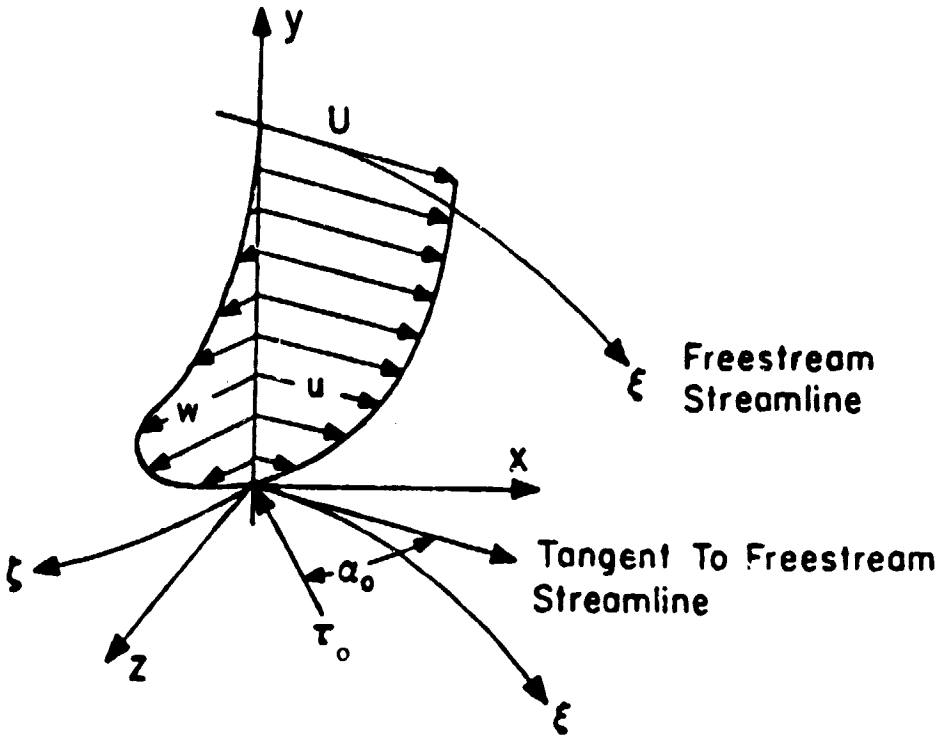

Fig. 2.3 Typical Pressure-Driven Three-Dimensional Boundary Layer

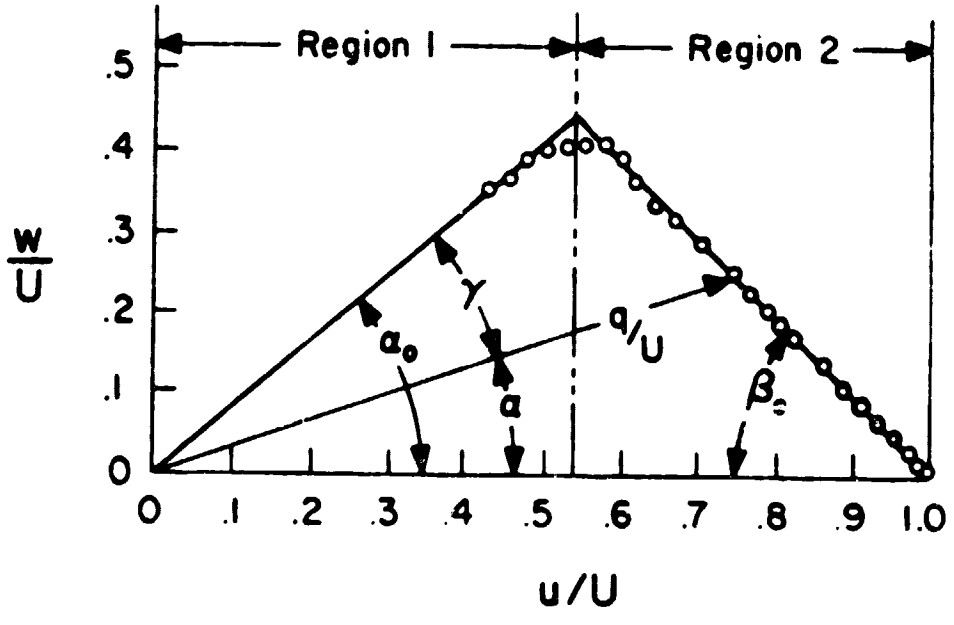

Fig. 2.4 Polar Plot for a Typical Pressure-Driven Three-Dimensional Boundary Layer

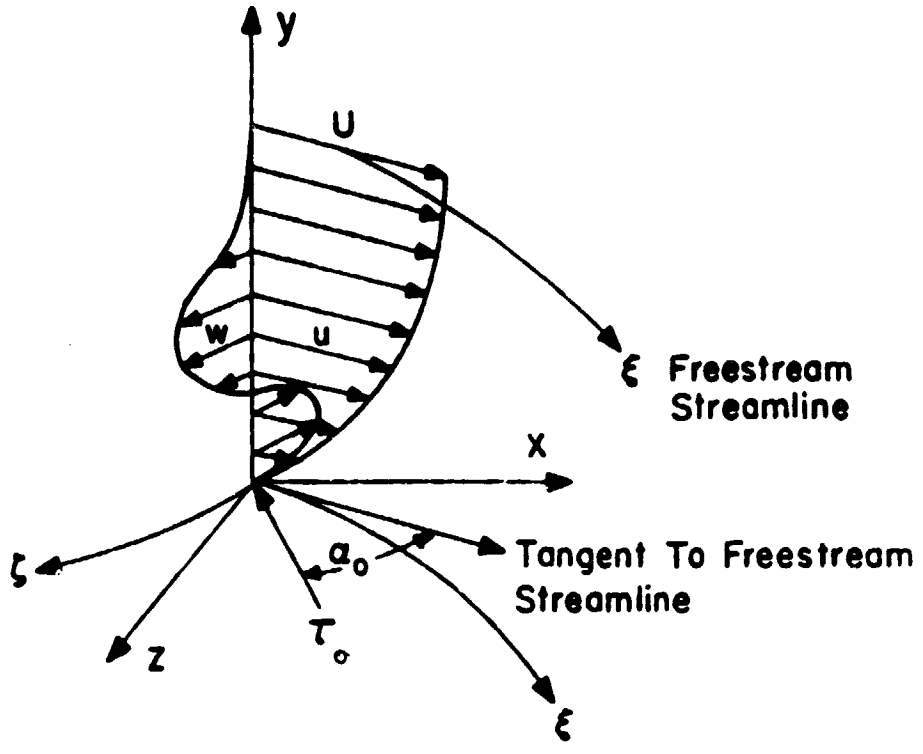

Fig. 2.5 Bilaterally Skewed or S-Shaped Three-Dimensional Boundary Layer

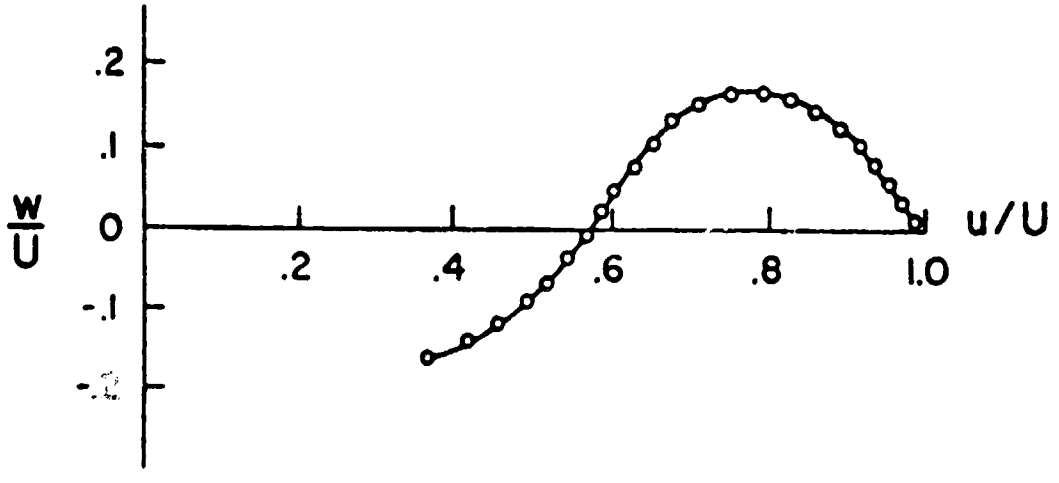

Fig. 2.6 Polar Plot of Bilaterally Skewed or S-Shaped Three-Dimensional Boundary Layer

Coles used the data of Kuethe, McKee, and Curry (1949) on a swept airfoil to test his model. Coles pointed out that large angles of skew were noted throughout the boundary layer, but that sudden changes in flow direction within the sublayer were assumed to be fictitious. The airfoil used was an elliptical planform with the major axis swept back at an angle of 25.0°. Though the velocity profiles seemed to be fairly well represented by Coles' model, no direct or indirect measurements of wall shear stress were included. No y^+ range was suggested for this three-dimensional model but a range similar to the two-dimensional log law would seem a reasonable first estimate.

It was later shown that the vector model proposed for the complete velocity profile did not accommodate certain 3DTBL profile data. This observation did not necessarily invalidate the proposed near-wall similarity model since the shortcomings of the overall vector profile model were not identified with the near-wall region of flow.

Four years later, Johnston (1960) introduced a second similarity model by noting the existence of an apparently collateral region very near the wall. He proposed that the angle which the near-wall velocity vector has with respect to the freestream approaches the angle α_o in the collateral region, where α_o is the limiting wall streamline angle and coincident with the wall shear direction with

$$\lim_{y \to 0} \frac{w}{u} = \tan \alpha_o .$$

He proposed that the two-dimensional similarity law for the logarithmic region be used for local velocities in the direction of α_o, where he defined his equivalent scalar velocity as

$$q_{equivalent} = \frac{u}{\cos \alpha_o} .$$

Nondimensionalizing with the shear velocity q^* as in Eqs. 2.13 for

$$q^+ = \frac{q_{equivalent}}{q^*} = \frac{u/\cos \alpha_o}{q^*} \qquad 2.17$$

gave the Johnston scalar model

$$\frac{u/\cos \alpha_o}{q^*} = \frac{1}{\kappa} \ln \frac{q^* y}{\upsilon} + C \qquad 2.18$$

When q is along α_o, $u/\cos \alpha_o$ is equal to the physically real q. When q is not along α_o, $u/\cos \alpha_o$ gives a fictitious velocity. Johnston based his model on the experimental measurements of Kuethe, et al. (1949) discussed previously, Gruschwitz (1935) who gave data in a turning passage of a rectangular duct, and his own study (Johnston (1960)) over a flat wall bounding a two-dimensional air jet impinging against a perpendicular back wall. He noted from his data that the applicability of Eq. 2.18 would be from the outer portion of Region I into the inner portion of Region II of the polar plot in Fig. 2.4. It is difficult to specify a specific y^+ range for this model since Johnston's data suggested Region I was within the viscous sublayer while Hornung and Joubert (1963) showed Region I to have y^+ ranges which were well outside the viscous sublayer.

Both Cole's and Johnston's models assume that the mean flow near the surface is in the same direction as the wall shear stress. The dangers in such an assumption should be recognized. Much of the early data plotted in the coordinates of Fig. 2.4 show two, three, or more velocity points in the very near-wall region which appear to have the same direction, suggesting the existence of a collateral near-wall flow. The very careful measurements of Rogers and Head (1969) and Hebbar and Melnick (1976) using very small instrumentation and emphasizing spatial resolution showed no region of near-wall collateral flow. In addition, Pierce and East (1972) and Klinksiek and Pierce (1973) have demonstrated with a finite difference solution to a three-dimensional turbulent boundary where the viscous stresses were retained in the motion equations that no near-wall collateral flow was predicted in a computer solution. Since only the viscous equations were being solved in the very near-wall region where the turbulent stresses vanish, the Reynolds stress model used is immaterial and the existence of a collateral region appears to be inconsistent with the governing equations. Prahlad (1973) also presented work supporting these computer results where he noted local streamline turning in the immediate neighborhood of the wall which "suggests the

ossibility of a fairly large variation in the flow direction within the viscous sublayer." These results cloud the question of the accurate measurement of the limiting wall streamline direction. It is therefore especially important to note that when three-dimensional experimental measurements are made of velocity profiles, typically with y^+ over 10, the direction of the velocity vector nearest to the wall is probably not the limiting wall streamline direction or the direction of the wall shear. It is perhaps unfortunate that the polar plot shown in Fig. 2.4 gained such extensive early use since such a plot tends to obscure angle changes near the wall and suggests support of the false assumption of near-wall collateral flow.

In 1963 Hornung and Joubert (1963) presented the results of a study of the flow around a circular cylinder with trailing edge standing on a plate. Their measurements seemed to confirm Johnston's polar plot, but in contrast to Johnston's assumption, they found the polar plot peak did not necessarily lie within the viscous sublayer. Hornung and Joubert suggested that the freestream profile follows the two-dimensional logarithmic similarity law, nondimensionalizing with a shear velocity based on the local wall shear stress as in Eq. 2.13. From their work (their Fig. 15) it appears that the equivalent velocity is the streamwise component

$$q_{equivalent} = u$$

and the nondimensionalized velocity is

$$q^+ = \frac{u}{q^*} \qquad 2.19$$

so that their similarity model is written as

$$\frac{u}{q^*} = \frac{1}{\kappa} \ln \frac{q^* y}{\upsilon} + C \qquad 2.20$$

They indicated that their model applied "up to the point where the boundary layer becomes yawed," usually to $y^+ < 150$. No direct measurements of wall shear were reported with inferred values determined by the Clauser (1954) chart technique which assumes the two-dimensional logarithmic law of the wall. They noted that this technique based on the

two-dimensional similarity law would at most "deduce whether a correlating quantity u_τ, say, exists or not. It is not possible to deduce that this quantity u_τ is equal to $(\tau_o/\rho)^{\frac{1}{2}}$ but it will be assumed below that it is, generalizing from two-dimensional flow."

The fourth model is a similar model of unknown origin first reported by Pierce and Krommenhoek (1968). In this case the freestream component of the three-dimensional velocity profile was assumed to follow the two-dimensional similarity law so that the equivalent velocity is the free-stream component

$$q_{equivalent} = u$$

but in this case a shear velocity was defined from a component of the wall shear stress in the freestream direction with

$$\tau_{o\xi} = \tau_o \cos \alpha_o$$

giving

$$q^*_\xi = q^* \sqrt{\cos \alpha_o}$$

Thus the nondimensional velocity is

$$q^+ = \frac{u \sqrt{\cos \alpha_o}}{q^*} \qquad 2.21$$

and Eq. 2.15 is modified to correspond to this with

$$y^+ = yq^*_\xi/\upsilon \qquad 2.22$$

so that this fourth similarity model is

$$\frac{u\sqrt{\cos \alpha_o}}{q^*} = \frac{1}{\kappa} \ln \frac{yq^*_\xi}{\upsilon} + C \qquad 2.23$$

Prahlad* (1968) introduced a fifth scalar similarity model based on studies of flow around a circular cylinder and an inclined flat plate

*It was recently pointed out to the authors that H. G. Hornung used this model as early as 1962 in his M.E. Sc. thesis at the University of Melbourne.

placed normal to the tunnel wall. Prahlad assumes that the equivalent velocity is the magnitude of the skewed velocity vector $\bar{q}$ hence

$$q_{equivalent} = |\bar{q}| = q$$

with the shear velocity taken as $\sqrt{\tau_o/\rho}$ as in Eq. 2.13. The Prahlad similarity model is then

$$\frac{q}{q^*} = \frac{1}{\kappa} \ln \frac{yq^*}{\upsilon} + C. \qquad 2.24$$

Prahlad (1968) used his own data to verify his model and found good agreement in a two-dimensional law of the wall coordinate system. For adverse or positive pressure gradients the y^+ range of similarity was approximately 20→300, while for highly favorable or negative pressure gradients the upper limit of the y^+ range was reduced considerably, depending on the gradient magnitude. No mention of any other three-dimensional model was made.

Indirect wall shear measurements were made with Preston tubes which used the two-dimensional Patel (1965) calibration. Prahlad noted that larger Preston tubes give smaller values of wall shear than smaller Preston tubes. He concludes that "This deviation implies departures from wall similarity and consequent errors in the use of the Preston tube technique in these flows."

Based on their own experiments in a pressure-driven 3DTBL, East and Hoxey (1969) proposed yet another similarity model based on the Johnston triangular polar plot. They noted Hornung and Joubert's (1963) work which disputed Johnston's finding that Region I of Fig. 2.4 was within the viscous sublayer and cited their own experimental results showing the triangle apex taking on large and widely varying y^+ values.

In summary, the East and Hoxey similarity model uses an equivalent near-wall velocity defined as

$$q_{equivalent} = q/\cos \alpha_1$$

where

$$\alpha_1 = \sin^{-1} \{(K_1 q^*/U_o)^{-1} \sin \beta_1\} - \beta_1$$

$$\beta_1 = -\tan^{-1} \frac{\delta_2}{\delta_1}$$

$$K_1 = 19.45$$

and U_o is an imprecisely defined "working section reference velocity" with δ_1 and δ_2 the freestream and transverse displacement thickness.

In the development of this model, α_1 was initially identified with the angle α_o of the polar plot in Fig. 2.4 and the constant K_1 was defined through a relationship relating the value of the velocity ratio at the apex to the shear velocity with

$$K_1 \, q^*/Q = u/Q_{apex}.$$

In order to better fit some of their experimental data, the constant K_1 was assigned a fixed value and the freestream velocity Q was replaced by the imprecisely defined reference velocity. With these changes α_1 no longer is identified with the polar plot angle α_o.

The nondimensionalized velocity is then

$$q^+ = \frac{q/\cos \alpha_1}{q^*} \qquad 2.25$$

and the similarity model is written as

$$\frac{q/\cos \alpha_1}{q^*} = \frac{1}{\kappa} \ln \frac{yq^*}{\upsilon} + C \qquad 2.26$$

To generate a three-dimensional flowfield East and Hoxey used a teardrop body, geometrically similar in appearance to the ones used by Hornung and Joubert and in this study. Indirect wall shear measurements were made using a Preston tube and razor blades with difficulties reported. The angle of the velocity vector closest to the wall at 0.0254 cm (0.010 in.) was taken as the direction to orient the Preston tube and razor blades assuming collateral flow to the wall. In their discussion of wall

shear measuring techniques, they indicate that in spite of the problems associated with using floating element devices, such use would be preferred assuming that such instrumentation was available.

In general specific y^+ ranges of applicability of these six models are not given. In the case of the Johnston model subsequent measurements have shown his upper limit of $y^+ = 50$ might well be raised significantly. As a generalization, since these six models are all variations of the logarithmic form of the two-dimensional law of the wall, a first look for similarity in the three-dimensional case would focus on the range of y^+ from approximately 50 to 300, with the upper limit expected to be sensitive to pressure gradient magnitude (Patel (1965), Patel and Head (1968)), with the effect of pressure gradient direction in general not predictable. In the comparison of models with experimental data to follow, the analytical two-dimensional similarity law used will be the third-order Spalding formula, Eq. 2.4. This choice offers the advantage of allowing focus on a secondary y^+ range--that below y^+ of 50. This is desirable since in some of the earlier work (Prahlad (1968), Pierce and Zimmerman (1973), Ezekwe (1974)) on similarity in three-dimensions, where only indirect wall shear diagnostics were used, suggests that the very near-wall data are more consistent in their behavior than in the two-dimensional case.

The last five models tend to become quite complicated and while not all in vector form, they all explicitly treat or at least recognize the vector nature of the 3DTBL velocity profile, this in contrast to the first six models which are in essence scalar models. Each of these models will be discussed briefly in order of ascending complexity. The complications encountered in these last models come about through consideration of some or all of the following: (1) separate consideration of velocity components, (2) pressure gradients, (3) wall shear gradients, and (4) wall shear angle gradients.

Chandrashekhar and Swamy (1976) proposed a model characterized by separate, two-dimensional-like logarithmic equations for the freestream and transverse velocity components. Examining the data of East and Hoxey (1969) for a pressure-driven 3DTBL Chandrashekhar and Swamy observed that logarithmic functions could be applied separately to the freestream and crossflow components of velocity with

$$u_\xi^+ = \frac{u_\xi}{u_\xi^*} = A \log_{10} \frac{y u_\xi^*}{\upsilon} + B \qquad 2.27$$

where A = 5.4 and B = 4.9, and

$$w_\zeta^+ = \frac{w_\zeta}{w_\zeta^*} = C \log_{10} \frac{y w_\zeta^*}{\upsilon} + D \qquad 2.28$$

where C = 1.0 and D = 11.8. The values of A, B, C, and D were determined from the East and Hoxey data.

The nondimensionalizing shear velocities u_ξ^* and u_ζ^* are from the components of the wall shear stress where

$$\tau_{o\xi} = \tau_o \cos \alpha_o = \rho u_\xi^{*2}$$

with

$$u_\xi^* = \sqrt{\tau_{o\xi}/\rho} = \sqrt{\tau_o \cos \alpha_o/\rho}$$

or

$$u_\xi^* = q^* \sqrt{\cos \alpha_o}$$

and similarly

$$w_\zeta^* = q^* \sqrt{\sin \alpha_o}$$

The components of this model are shown in Fig. 2.7.

Note that the streamwise similarity law is essentially identical to the scalar Pierce and Krommenhoek (1968) freestream model cited earlier since Eq. 2.27 can be written as

$$\frac{u}{u_\xi^*} = \frac{1}{\kappa_1} \ln \frac{y u_\xi^*}{\upsilon} + B$$

where the Chandrashekhar and Swamy value of κ_1 is approximately 0.426.

Chandrashekhar and Swamy show similarity results for the freestream equation with data in the approximate region of $9 \leq y^+ \leq 900$. For $y^+ \geq 300$

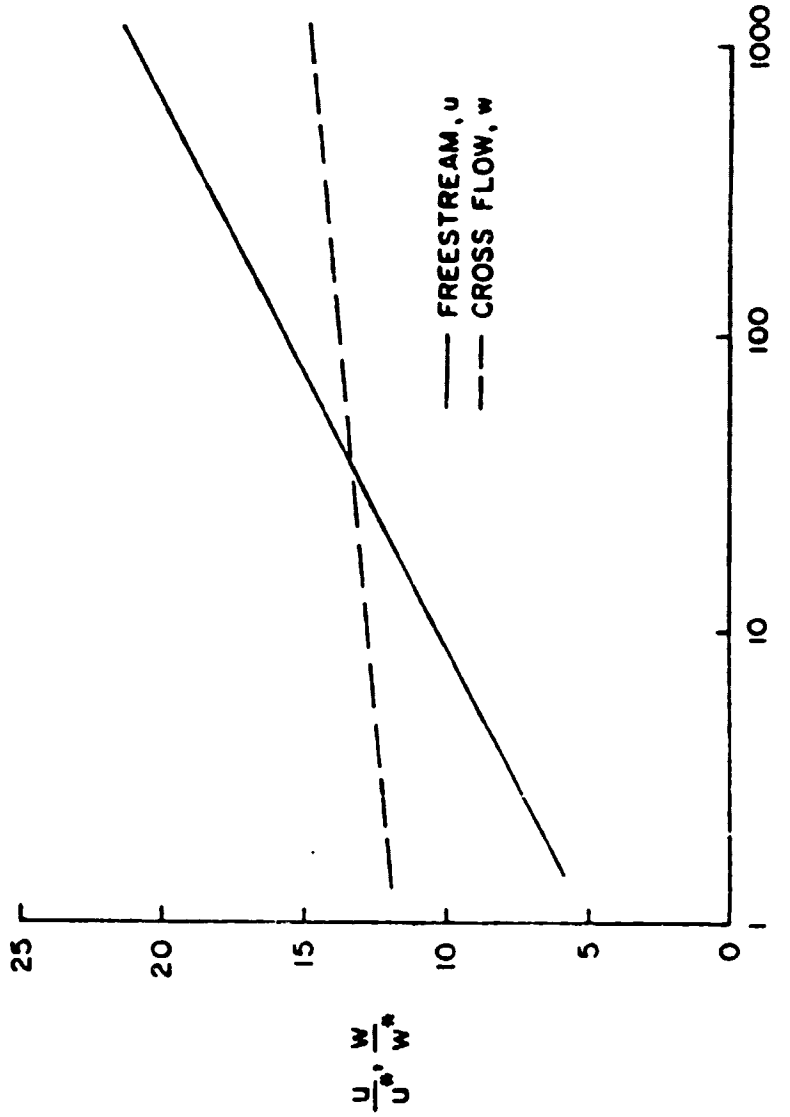

Fig. 2.7 Three-Dimensional Near-Wall Similarity Model as Given by Chandrashekhar and Swamy (1976)

(an approximate value) the data exhibits a two-dimensional wake behavior and for $y^+ \leq 9$ the agreement is poor so that a y^+ range of approximately $9 \leq y^+ \leq 300$ would be reasonable from their work.

Data for the transverse equation was found to have a very small slope hence the constants C and D were difficult to evaluate. To alleviate this problem, the w_ζ^+ and y^+ coordinates in Eq. 2.28 were modified with

$$\frac{w_\zeta}{w_m} = a \log_{10} \frac{y}{\Delta} + b$$

where w_m = maximum value of w_ζ in the crossflow profile

Δ = y distance corresponding to $w_m/2$ (with this y the furthest from the wall)

The constants C, D, a, and b are easily related with

$$C = a \frac{w_m}{w_\zeta^*}$$

and

$$\frac{D}{C} = \frac{b}{a} + \log_{10} \frac{w_m}{w_\zeta^*} - \log_{10} \frac{w_m \Delta}{\upsilon}$$

with East and Hoxey data giving values of C = 1 and D = 11.8. The y^+ range for Eq. 2.28 was not specified but an examination of the transverse similarity plots showed data in the range $1 \leq y^+ \leq 60$, with the best fit appearing in the $1 \leq y^+ \leq 15$ range. For $y^+ \geq 15$ the data points fell consistently below the analytical model line.

The second of the complex similarity models was proposed by White, Lessmann, and Christoph (1975) to provide a velocity profile expression for use in their integral boundary layer analysis. This model uses a freestream streamline coordinate system and the freestream profile $u_\xi(y)$ is related to the pressure gradient using the mixing length theory to obtain

$$\tau = \tau_o + \frac{1}{h_1}\frac{\partial p}{\partial \xi}\, y = \rho\kappa^2 y^2 \left|\frac{\partial u_\xi}{\partial y}\right| \frac{\partial u_\xi}{\partial y}$$

Introducing a freestream shear velocity based on the freestream component of the wall shear with $u_\xi^* = \sqrt{\tau_{o\xi}/\rho}$, then $u_\xi^+ = u_\xi/u_\xi^*$, and the above can be written as

$$\frac{du^+}{dy^+} = \frac{(1 + \alpha_\xi y^+)^{1/2}}{\kappa y^+}$$

where

$$y^+ = \frac{y u_\xi^*}{\upsilon}$$

and

$$\alpha_\xi = \frac{\upsilon}{\rho u_\xi^{*3}} \frac{1}{h_1}\frac{\partial p}{\partial \xi}$$

Integrating,

$$u_\xi^+ = \frac{1}{\kappa}\{2(S - S_o) + \ln\left(\frac{S-1}{S+1}\frac{S_o+1}{S_o-1}\right)\} \qquad 2.29$$

where $S = (1 + \alpha_\xi y^+)^{1/2}$

$S_o = (1 + e^{-\kappa C y^+})^{1/2}$

White, et al., mentioned attempts at developing a crossflow profile with the same logic as for the u_ξ^+ expression but without success. Based on the unilateral hodograph model of Mager (1951) they ultimately suggested the form

$$w_\zeta^+ = u_\xi^+ \Theta\,(1 - y^+/\delta^+)^2 \qquad 2.30$$

where $\Theta = \tan \alpha_o$

δ^+ = nondimensional boundary layer thickness

It was noted that this form does not accommodate bilateral crossflow profiles as shown in Fig. 2.5.

No similarity plots were given by White, et al., for this two-component model as it was developed as part of a larger computational study not aimed specifically at near-wall similarity. The approximate y^+ range of Eq. 2.29 was inferred by White, et al., when they defined S_o such that for zero pressure gradient the two-dimensional logarithmic law of the wall would result. This suggests a y^+ range of approximately 50 to 300. There is no simple way to estimate the y^+ range for the transverse similarity model.

Perry and Joubert (1965) developed a near-wall model using similarity arguments and treating the near-wall region as an equilibrium layer. While not a vector model this model relates the mean velocity distribution with the pressure gradient and the wall shear directions. The theory was compared with the data of Hornung and Joubert cited earlier; however, the results were inconclusive due to a lack of sufficient data. No direct or indirect measurements of wall shear were reported. The details of the analysis by Perry and Joubert are quite lengthy, and only a brief outline of the development of their model will follow.

Considering a prismatic element with sides dx, dy, and dz at a small distance y from the wall and neglecting inertia terms, a force balance on the element in terms of a double subscript on the stresses after Perry and Joubert gives,

$$\frac{\partial p}{\partial x} + \frac{\partial \tau_{xy}}{\partial y} + \frac{\partial \tau_{xz}}{\partial z} = 0$$

$$\frac{\partial p}{\partial y} + \frac{\partial \tau_{yx}}{\partial x} + \frac{\partial \tau_{yz}}{\partial z} = 0$$

$$\frac{\partial p}{\partial z} + \frac{\partial \tau_{zx}}{\partial x} + \frac{\partial \tau_{zy}}{\partial y} = 0.$$

Townsend's (1961) equilibrium layer concept led Perry and Joubert to an eddy viscosity model by which the shear stresses and strain rates are related with

$$\tau_{xy} = \rho\ \varepsilon_1\ [\frac{\partial u}{\partial y} + \frac{\partial v}{\partial x}]$$

$$\tau_{xz} = \rho\ \varepsilon_2\ [\frac{\partial u}{\partial z} + \frac{\partial w}{\partial x}]$$

$$\tau_{yz} = \rho\ \varepsilon_3\ [\frac{\partial v}{\partial z} + \frac{\partial w}{\partial y}]$$

where ε_1, ε_2, and ε_3 are the three components of the eddy viscosity expression.

Close to the wall the velocity derivatives $\frac{\partial}{\partial x}$ and $\frac{\partial}{\partial z}$ are much smaller than $\frac{\partial}{\partial y}$, hence

$$\tau_{xy} = \varepsilon_1\ \rho\ \frac{\partial u}{\partial y}$$

$$\tau_{xz} = 0$$

$$\tau_{zy} = \varepsilon_3\ \rho\ \frac{\partial w}{\partial y}$$

and the force balance becomes

$$\frac{\partial p}{\partial x} = -\ \frac{\partial \tau_{xy}}{\partial y}$$

$$\frac{\partial p}{\partial y} = 0$$

$$\frac{\partial p}{\partial z} = -\ \frac{\partial \tau_{zy}}{\partial y},$$

Integration of these gives

$$\tau_{xy} = \tau_{xy_o} - y\ \frac{\partial p}{\partial x}$$

$$\tau_{zy} = \tau_{zy_o} - y\ \frac{\partial p}{\partial z}$$

Perry and Joubert assumed that the eddy viscosity is isotropic and that the maximum shear stress acts in the same direction as the maximum strain rate. They suggest that

$$[\tau_{xy}^2 + \tau_{zy}^2]^{\frac{1}{2}} = \rho\varepsilon[(\frac{du}{dy})^2+(\frac{dw}{dy})^2]^{\frac{1}{2}}, \qquad 2.31$$

and by dimensional reasoning that

$$\varepsilon = \kappa\rho^{-\frac{1}{2}}[\tau_{xy}^2 + \tau_{zy}^2]^{\frac{1}{4}}y.$$

Substitution of the stress and eddy viscosity expressions into Eq. 2.31 gives, after simplification,

$$[\tau_o^2 - 2y\,\tau_o\,\rho\alpha\cos\Theta + y^2\alpha^2]^{\frac{1}{4}} = \rho^{\frac{1}{2}}\,\kappa y[(\frac{du}{dy})^2 + (\frac{dw}{dy})^2]^{\frac{1}{2}} \qquad 2.32$$

where

$$\tau_o = [\tau_{xy_o}^2 + \tau_{zy_o}^2]^{\frac{1}{2}}$$

$$\alpha = \frac{1}{\rho}[(\frac{\partial p}{\partial x})^2 + (\frac{\partial p}{\partial z})^2]^{\frac{1}{2}}$$

and

$$\tau_o\,\rho\alpha\cos\Theta = \tau_{xy_o}(\frac{\partial p}{\partial x}) + \tau_{zy_o}(\frac{\partial p}{\partial z})$$

is the scalar product of the wall shear and pressure gradient vectors with Θ the angle between these two vectors. Integration of Eq. 2.32 gives

$$\frac{u_o}{q^*} = \frac{\int_0^{y^+}[1 + (\frac{dw}{du})^2]^{\frac{1}{2}}\,du}{q^*}$$

$$= \frac{1}{\kappa}\int_0^{y^+}\frac{1}{y^+}(1-2\omega\cos\Theta + \omega^2)^{\frac{1}{4}}\,dy^+ \qquad 2.33$$

where $\omega = y^+ \alpha\upsilon/q^{*3}$, $q^* = \sqrt{\tau_o/\rho}$, and $y^+ = yq^*/\upsilon$. The first integral of Eq. 2.33 represents a developed velocity profile and is equal to the length of the arc on a polar plot beginning at the origin. In the limit for small values of y^+ within the logarithmic region,

$$\frac{u_o}{q^*} = \frac{1}{\kappa} \ln y^+ + C,$$

so that Eq. 2.33 can be altered to read

$$\frac{u_o}{q^*} = \frac{1}{\kappa} \int_1^{y^+} \frac{1}{y^+} [1-2\omega\cos\Theta + \omega^2]^{\frac{1}{4}} \, dy^+ + C. \qquad 2.34$$

Equation 2.34 is plotted in Fig. 2.8 for various values of Θ. The effect of the pressure gradient parameter, $\alpha\upsilon/q^{*3}$, is to cause the deviations from the simple logarithmic line to shift bodily up and down along the line. A value of $\Theta = 0$ corresponds to the two-dimensional favorable pressure gradient case. A value of $\Theta = 180°$ corresponds to the adverse pressure gradient case. It should be noted that Θ depends on an a priori knowledge of the direction of wall shear.

The upper y^+ limit for this model is identified with the apex of the Johnston polar plot. While Johnston (1960) originally set the apex of the polar model as $y^+ \simeq 15$, Hornung and Joubert (1963) subsequently found this apex to approach $y^+ \simeq 150$ and still later Perry and Joubert show three-dimensional similarity plots with this apex as high as $y^+ \simeq 2000$. All this suggests a relatively large possible y^+ range for this similarity model, from as low as about 10 to 2000 or more.

Following the same general method as outlined for the two-dimensional case, van den Berg (1973, 1975, 1976) developed a similarity model that includes both pressure gradient and inertial effects. His theory was compared with a limited number of measurements by van den Berg and Elsenaar (1972) and Vermeulen (1971) where wall shear was indirectly measured by the Stanton tube and sublayer fence methods respectively.

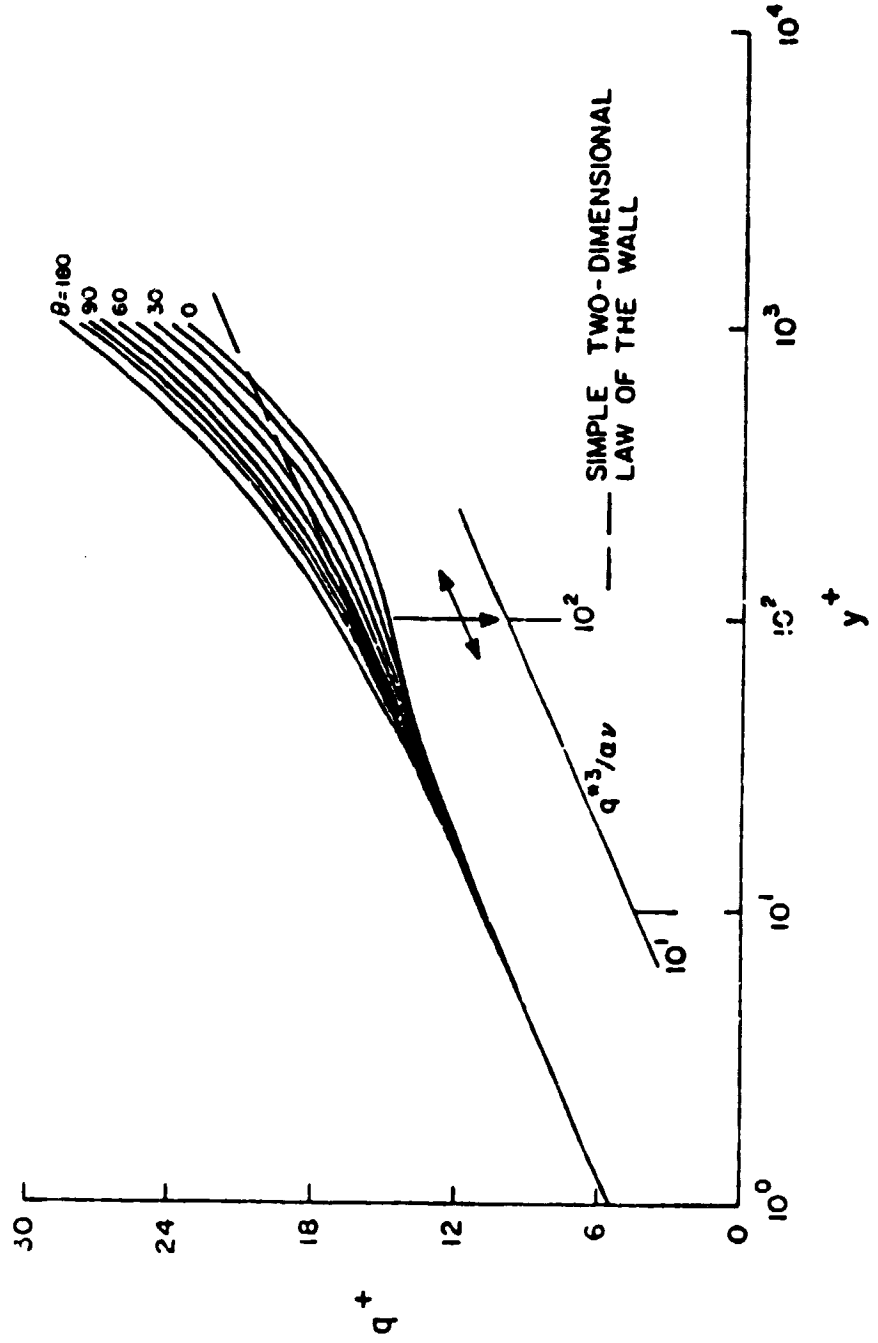

Fig. 2.8 Three-Dimensional Near-Wall Similarity Model as Given by Perry and Joubert (1965)

boundary layer of a curved duct. Van den Berg emphasizes that his model is not valid for large pressure gradients or for large changes of shear stress from the wall value, and the restriction that his shear have a small transverse component in the boundary layer presumes small skewing as well, so that the model would be valid for only modest skewing.

Beginning as in his two-dimensional case reviewed earlier, similarity in the near-wall region for the three-dimensional case can be expressed as

$$q^+ = f(y^+)$$

Starting with the 3DTBL motion equations in Cartesian coordinates and using a single subscript on the stress terms after van den Berg gives

$$\rho u\frac{\partial u}{\partial x} + \rho v\frac{\partial u}{\partial y} + \rho w\frac{\partial u}{\partial z} = -\frac{\partial p}{\partial x} + \frac{\partial \tau_x}{\partial y} \qquad 2.35$$

$$\rho u\frac{\partial w}{\partial x} + \rho v\frac{\partial w}{\partial y} + \rho w\frac{\partial w}{\partial z} = -\frac{\partial p}{\partial z} + \frac{\partial \tau_z}{\partial y}. \qquad 2.36$$

The acceleration terms were written in terms of components of a similarity law where $u = u^* f(y^+)$ and $w = w^* f(y^+)$ and u^* and w^* are components of the shear velocity $q^* = \sqrt{\tau_o/\rho}$ in the direction of τ_o. Van den Berg noted that a considerable simplification of these acceleration terms and in the subsequent mathematics occurs if the similarity models are developed for components of velocity along and normal to the local wall shear stress directions which can be designated ξ and ζ. These are in effect rotated Cartesian coordinates not to be confused with frequent usage as orthogonal curvilinear coordinates identified with the freestream flow. The corresponding velocity components would be u_ξ, v, and w_ζ with shear velocity componants u^*_ξ and w^*_ζ and while at a particular location w^*_ζ is zero, its derivatives in the local Cartesian directions ξ and ζ are not necessarily zero. This choice of coordinate system requires the <u>a priori</u> knowledge of the local wall shear direction.

In these local directions the acceleration terms were written as

$$u_\xi \frac{\partial u_\xi}{\partial \xi} + v \frac{\partial u_\xi}{\partial y} + w_\zeta \frac{\partial u_\xi}{\partial \zeta} = q^* f^2 \frac{\partial q^*}{\partial \xi} + q^* \frac{\partial w_\zeta^*}{\partial \zeta} \frac{df}{dy^+} \int_0^{y^+} f dy^+$$

$$u_\xi \frac{\partial w_\zeta}{\partial \xi} + v \frac{\partial w_\zeta}{\partial y} + w_\zeta \frac{\partial w_\zeta}{\partial \zeta} = q^* \frac{\partial w_\zeta^*}{\partial \xi} f^2$$

This form of the acceleration terms is combined with the continuity equation and substituted into Eqs. 2.35 and 2.36 and integrated for stress distributions in y^+ along the ξ and ζ directions, giving

$$\frac{\tau_\xi}{\tau_o} = 1 + \alpha_\xi y^+ + \beta_\xi I_1 + \gamma_\xi I_3 \qquad 2.37$$

and

$$\frac{\tau_\zeta}{\tau_o} = \alpha_\zeta y^+ + \beta_\zeta I_1 \qquad 2.38$$

where

$$\alpha_\xi = \frac{\upsilon}{\rho q^{*3}} \frac{\partial p}{\partial \xi}$$

$$\alpha_\zeta = \frac{\upsilon}{\rho q^{*3}} \frac{\partial p}{\partial \zeta}$$

$$\beta_\xi = \frac{\upsilon}{q^{*2}} \frac{\partial q^*}{\partial \xi}$$

$$\beta_\zeta = \frac{\upsilon}{q^*} \frac{\partial \phi}{\partial \xi}$$

$$\gamma_\xi = \frac{\upsilon}{q^*} \frac{\partial \phi}{\partial \zeta}$$

and ϕ is the wall shear stress angle with

$$I_1 = \int_0^{y^+} f^2 dy^+$$

$$I_3 = f\int_0^{y^+} f dy^+ - I_1$$

Values for I_1 and I_3 were obtained by numerical integration using data tabulated from Coles (1955) and the two-dimensional similarity law, and the I_3 term was omitted as it was found to be significantly smaller than I_1.

These shear distributions, Eqs. 2.37 and 2.38, were substituted into the mixing length relations simplified for small variations near the wall with

$$\frac{du_\xi^+}{dy^+} = \frac{1}{\kappa y^+}\frac{\tau_\xi^{1/2}}{\tau_o^{1/2}} \qquad 2.39$$

$$\frac{dw_\zeta^+}{dy^+} = \frac{1}{\kappa y^+}\frac{\tau_\zeta}{\tau_o} \qquad 2.40$$

where both u_ξ^+ and w_ζ^+ are nondimensionalized by $q^* = \sqrt{\tau_o/\rho}$. These are integrated from $0 \to y^+$ to obtain

$$u_\xi^+ = \frac{1}{\kappa}\{\ln y^+ + A + \frac{1}{2}\alpha_\xi y^+ + \frac{1}{2}\beta_\xi I_2\}$$

$$w_\zeta^+ = \frac{1}{\kappa}(\alpha_\zeta y^+ + \beta_\zeta I_2 + B)$$

The integral I_2 was evaluated using his two-dimensional simple similarity model and the constants A and B evaluated to give the two-component three-dimensional similarity model as

$$u_\xi^+ = \frac{1}{\kappa}[\ln y^+ + \kappa C + \frac{1}{2}\alpha_\xi y^+ + \frac{1}{2}\beta_\xi \frac{(\ln y^+)^2 y^+}{\kappa^2}] \qquad 2.41$$

$$w_\zeta^+ = \frac{1}{\kappa}[\alpha_\zeta (y^+ + b) + \beta_\zeta \frac{(\ln y^+)^2 y^+}{\kappa^2}] \qquad 2.42$$

where $u_\xi^+ = u_\xi/q^*$ and $w_\zeta^+ = w_\zeta/q^*$ and $b = 13$. Recall that these components are along and normal to the local wall shear directions, and for simplicity the subscripts ξ and ζ will occasionally be omitted in future use as convenient.

When only the pressure gradient effects are considered, the van den Berg model reduces to a model similar to that of Perry and Joubert. Figure 2.9 shows the effect of various θ-values on the u_ξ^+ component of velocity. The angle parametric values have been changed to conform to that of Perry and Joubert for convenience in comparison and the qualitative results are similar to those of Perry and Joubert. For this plot, all the inertial terms have been set to zero. Figure 2.10 shows a similar plot on a linear scale for the w_ζ^+ component of velocity. Finally Fig. 2.11 shows a typical similarity plot by van den Berg showing data comparison with the two-dimensional similarity law, van den Berg's model with inertial terms set to zero, and with the inertial terms included. It should be noted that the inclusion of the inertial terms in the three-dimensional case requires a priori knowledge of the magnitude and direction of wall shear.

It is worth noting that the functional form of this similarity law may be expressed as

$$u_\xi^+ = f(y^+, \frac{\partial p}{\partial \xi}, \frac{\partial q^*}{\partial \xi})$$

$$w_\zeta^+ = g(y^+, \frac{\partial p}{\partial \zeta}, \frac{\partial \phi}{\partial \xi})$$

which is more complex than was initially assumed with different functions for the two components. Some caution is noted over the use of the two-dimensional similarity law in the evaluation of the integrals I_1, I_2, and I_3, especially as these may appear in the transverse model development, although van den Berg does restrict the model to small skewing and small shear variations near the wall. Somewhat arbitrarily the y^+ range of the u^+ and w^+ models will be taken as approximately 10 to 300.

East (1972) proposed the most complex three-dimensional similarity model for compressible flows which requires shear stress distribution information through the boundary layer and takes into account the non-alignment of the velocity gradient and shear stress. This feature

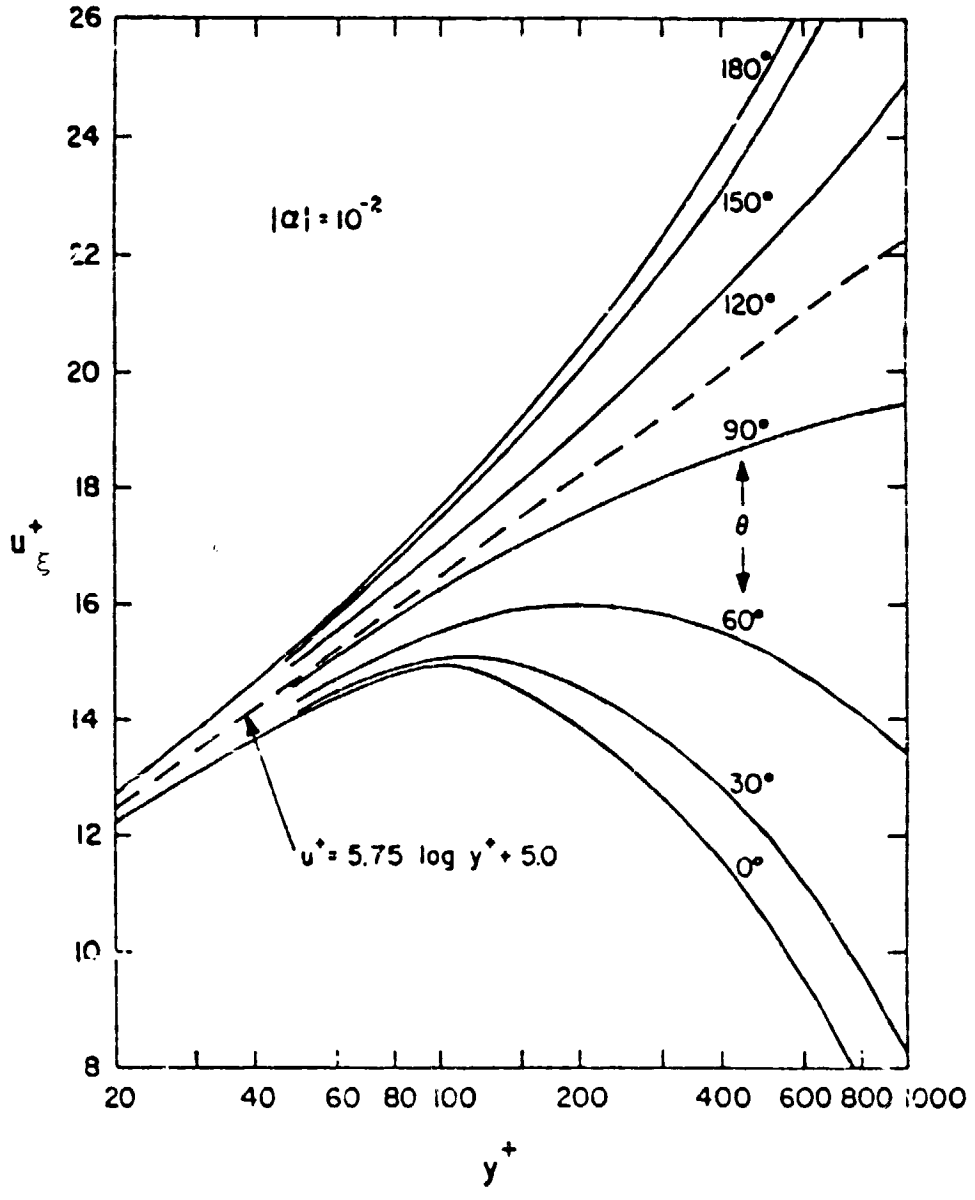

Fig. 2.9 The Velocity in the Direction of the Wall Shear Stress at Various θ and $|\alpha| = 10^{-2}$ as Given by van den Berg (1973)

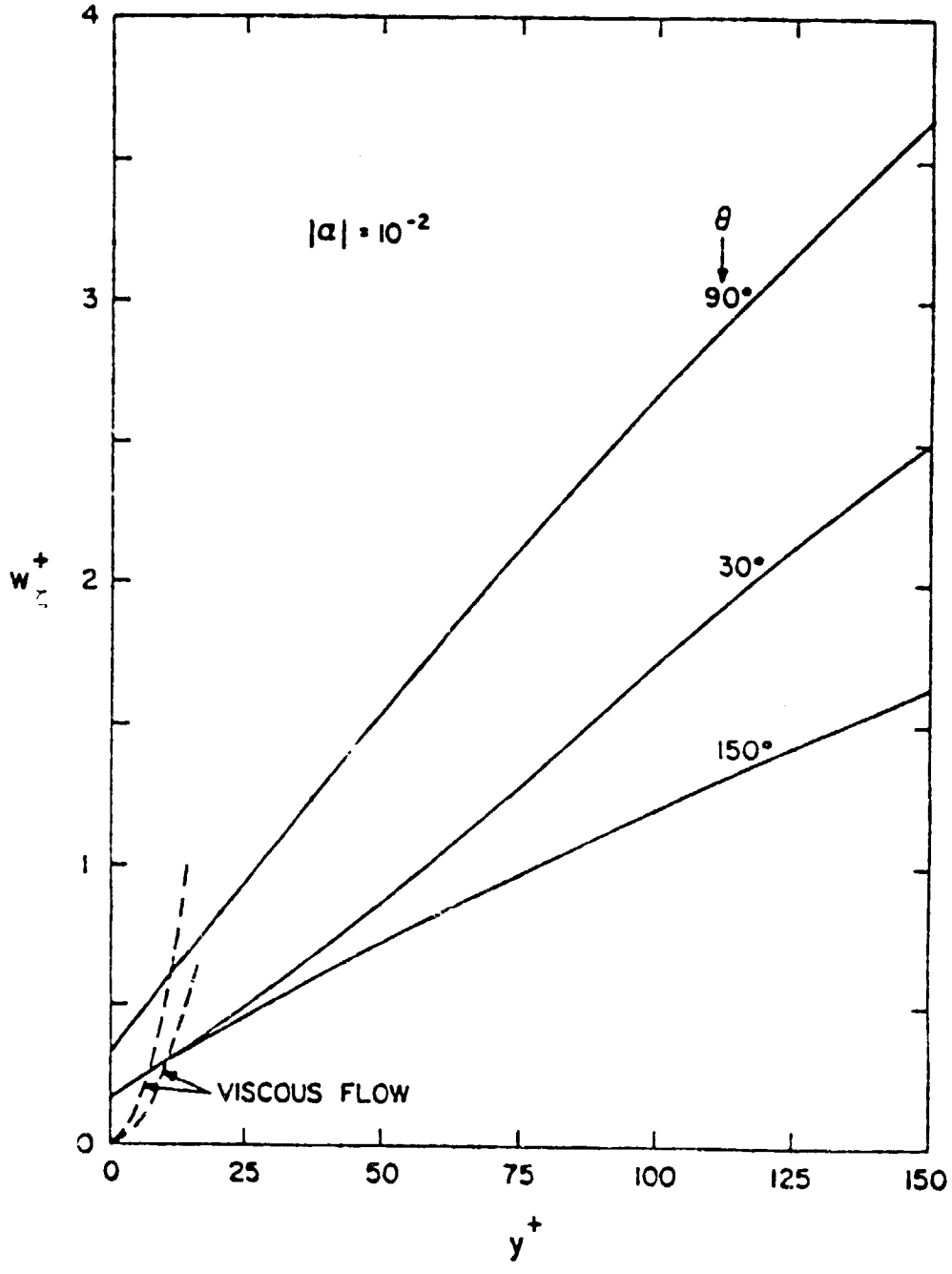

Fig. 2.10 The Velocity Normal to the Wall Shear Stress at Various Θ and $|\alpha| = 10^{-2}$, b = 13, as Given by van den Berg (1973)

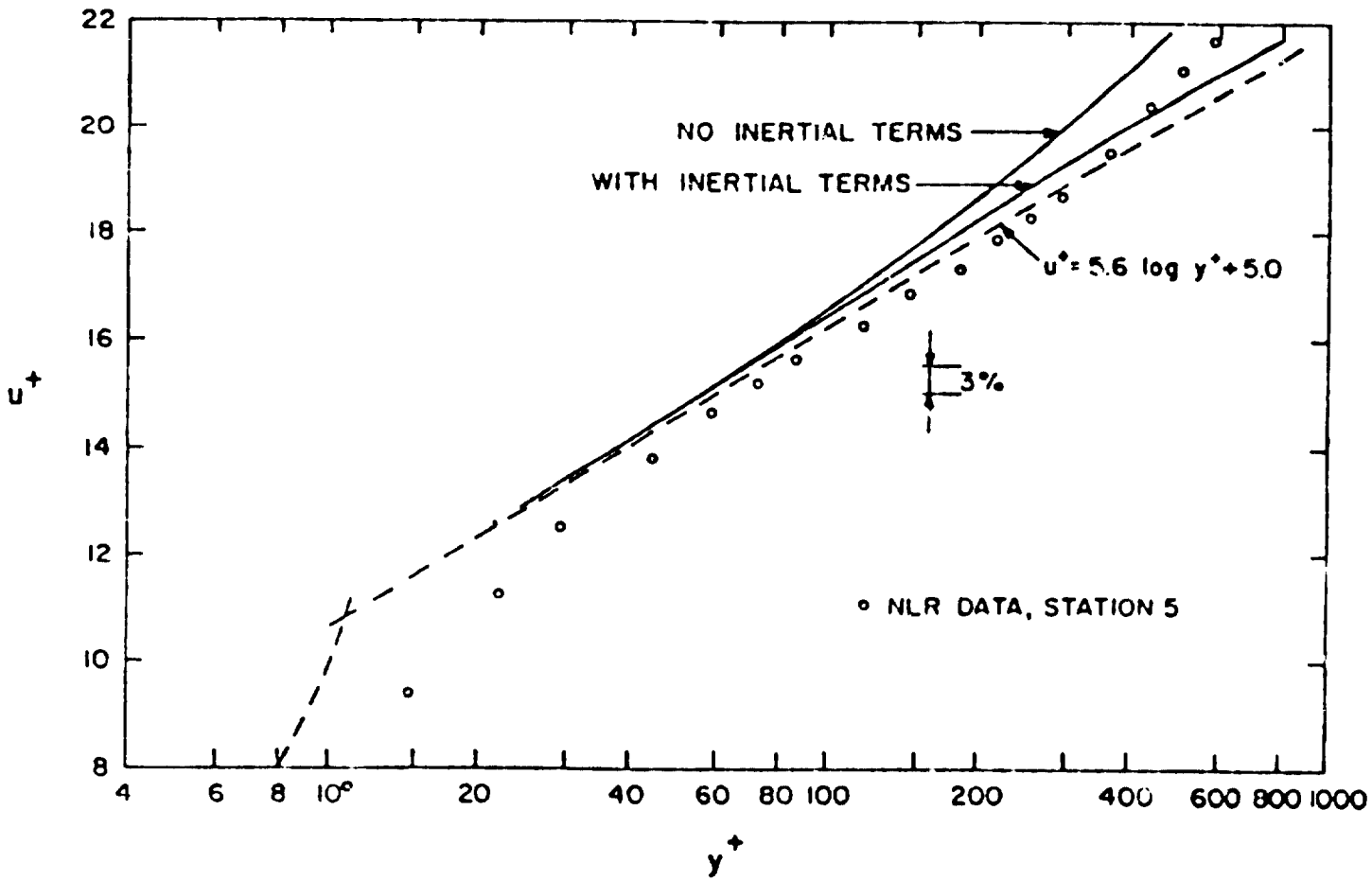

Fig. 2.11 Comparison of van den Berg's Three-Dimensional Similarity Model (1973) for small αy^+ with Experimental Data of van den Berg and Elsenaar (1972). $\alpha_x = -3.0 \times 10^{-3}$, $\beta_x = -10.0 \times 10^{-6}$

appears to have been built into the model so that it would fit into Bradshaw's (1971) computational scheme which also treats this nonalignment. Because the experimental program reported on here did not include turbulence data in the flow field, comparisons of experimental data with this model were not made. The model is reviewed here for completeness in the survey of similarity models.

The East model consists of six partial differential equations and two algebraic equations. Two of the partial differential equations were derived by taking into account the variation in the orientation of the shear stress vector, two were derived by relating the velocity vector magnitude and magnitude of the velocity gradient, and the remaining two were modifications to Bradshaw's (1971) turbulent stress transport equations. These equations can only be solved numerically.

The first two equations take into account the variation in the orientation of the shear stress vector. East made the first order approximation

$$\left|\tau_t\right| = \left|\tau_o\right|$$

$$\psi = y\left(\frac{\partial \psi}{\partial y}\right)_o$$

where ψ is the rotation of the total shear stress vector, $\vec{\tau}_t$, relative to the wall shear stress vector, $\vec{\tau}_o$. Note that this assumes a constant stress near the wall. This stress is composed of a laminar and turbulent component whose orientation is shown in Fig. 2.12. The relationship between the shear stress components is given by

$$\tau_t^2 = \mu^2\left(\frac{\partial q}{\partial y}\right)^2 + \tau^2 + 2\mu\left|\frac{\partial q}{\partial y}\right|\left|\tau\right|\cos(\alpha-\beta)$$

$$\frac{\left|\tau\right|}{\sin(\alpha-\psi)} = \frac{\left|\tau_t\right|}{\sin(\alpha-\beta)}$$

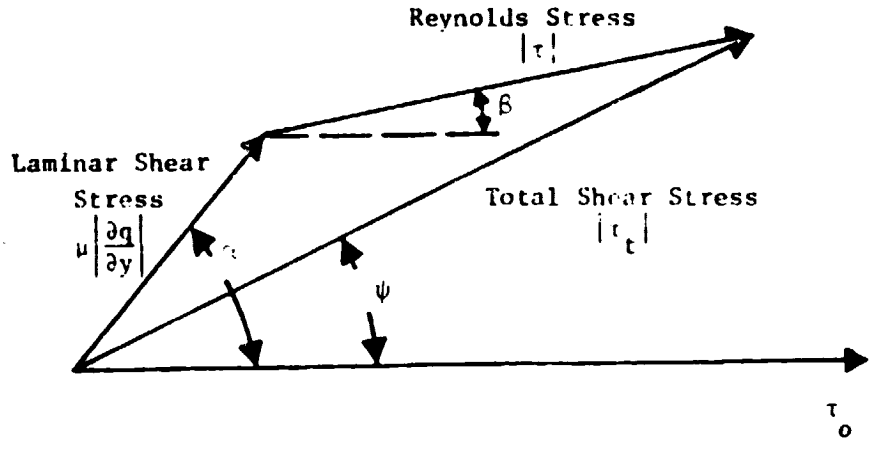

Fig. 2.12 Laminar and Reynolds Stress Orientation for the East (1972) Model

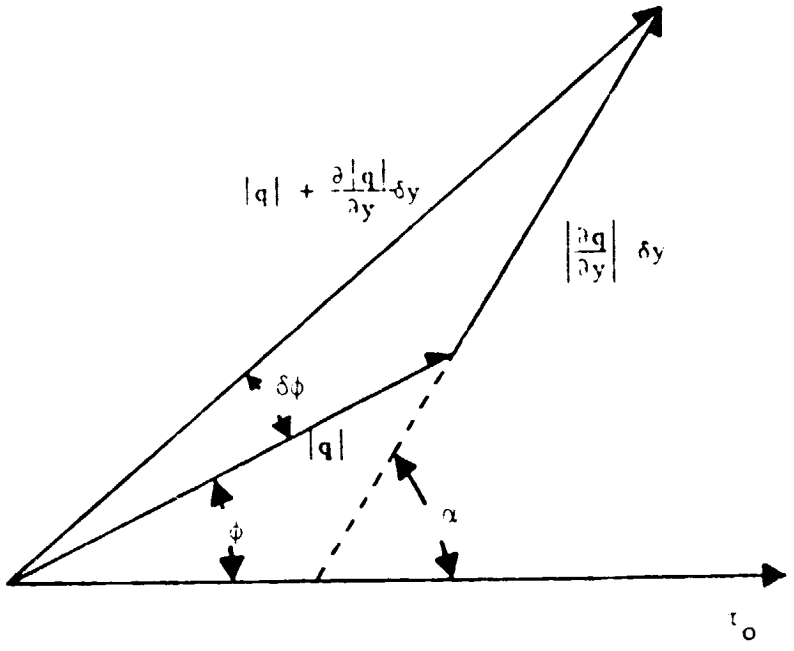

Fig. 2.13 Velocity and Velocity Gradient Orientation for the East (1972) Model

Nondimensionalizing and rearranging gives

$$\mu^+\left|\frac{\partial q^+}{\partial y^+}\right| = \pm\{1-\tau^{+2}\sin^2(y^+(\frac{\partial\psi}{\partial y^+})_o(\alpha^+-\beta^+))\}^{1/2} - \tau^+\cos(y^+(\frac{\partial\psi}{\partial y^+})_o(a^+-b^+) \quad 2.43$$

where the negative square root is taken if

$$\cos\,(y^+(\partial\psi/\partial y^+)_o(\alpha^+-1)) < 0$$

and

$$\alpha^+ y^+(\frac{\partial\psi}{\partial y^+})_o = \tan^{-1}\{\frac{\sin(y^+(\partial\psi/\partial y^+)_o)-\tau^+\sin(y^+\beta^+(\partial\psi/\partial y^+)_o)}{\cos(y^+(\partial\psi/\partial y^+)_o)-\tau^+\cos(y^+\beta^+(\partial\psi/\partial y^+)_o)} \quad 2.44$$

where in the following the zero subscript refers to wall values and not freestream stagnation values

$$\mu^+ = \mu/\mu_o$$

$$\tau^+ = \tau/\tau_o$$

$$\alpha^+ = \alpha/(y^+(\partial\psi/\partial y^+)_o)$$

$$\beta^+ = \beta/(y^+(\partial\psi/\partial y^+)_o)$$

$$\psi^+ = \psi/(y^+(\partial\psi/\partial y^+)_o)$$

East obtained two more equations by relating the gradient of the velocity vector magnitude $|q|$ and the magnitude of the velocity gradient $|\partial q/\partial y|$. Using the notation in Fig. 2.13 these relationships are

$$\frac{\partial|q|}{\partial y} = \left|\frac{\partial\underline{\imath}}{\partial y}\right|\cos\,(\alpha-\phi)$$

$$\frac{\partial\phi}{\partial y} = \frac{|\partial q/\partial y|}{|q|}\sin(\alpha-\phi)$$

which when nondimensionalized become

$$\frac{\partial |q^+|}{\partial y^+} = \left|\frac{\partial q^+}{\partial y^+}\right| \cos\left(y^+ \left(\frac{\partial \psi}{\partial y^+}\right)_o (\alpha^+ - \phi^+)\right) \qquad 2.45$$

$$\frac{\partial (y^+ (\partial \psi / \partial y^+)_o \phi^+)}{\partial y^+} = \frac{|\partial q^+ / \partial y^+|}{|q^+|} \sin\left(y^+ \left(\frac{\partial \psi}{\partial y^+}\right)_o (\alpha^+ - \phi^+)\right). \qquad 2.46$$

For compressible flow it was necessary to provide for density and viscosity distributions in the boundary layer. East assumed Crocco's law,

$$c_p T + \frac{r q^2}{2} = \text{constant} = c_p T_o$$

and the nondimensional temperature is

$$T^+ = \frac{T}{T_o} = 1 - F^2 q^{+2}$$

where F is a compressibility factor given by

$$F = M_\infty \sqrt{r(k-1)C_f/4} = M^+ \sqrt{r(k-1)/2}$$

and M^+ is the shear velocity q^* divided by the sound speed at the wall. This temperature expression allows the density ratio to be written as

$$\rho^+ = \frac{\rho}{\rho_o} = (1 - F^2 q^{+2})^{-1} \qquad 2.47$$

and the nondimensional viscosity as

$$\mu^+ = \frac{\mu}{\mu_o} = (1 - F^2 q^{+2})^n \qquad 2.48$$

where

$n \approx 0.76$ at sea level.

East modified Bradshaw's (1971) transport equations in the wall region to include the pressure diffusion term in order to obtain the last two equations in his model. The Poisson equation for the fluctuating pressure shows it is partially related to the mean velocity vector and because of this East assumed the fluctuating pressure could be modeled by

$$p' = A\rho v'|q|$$

The pressure diffusion terms were written in the x direction as

$$\frac{1}{\rho}\frac{\partial}{\partial y}(\overline{p'u'}) = \frac{1}{\rho}\frac{\partial}{\partial y}(A\rho|q|\,\overline{u'v'}) = \frac{A}{\rho}\frac{\partial}{\partial y}(\tau_x|q|)$$

$$= -\frac{A}{\rho}\left(\tau_x\frac{\partial|q|}{\partial y} + |q|\frac{\partial\tau_x}{\partial y}\right)$$

and in the z direction

$$\frac{1}{\rho}\frac{\partial}{\partial y}(\overline{p'w'}) = -\frac{C}{\rho}\left(\tau_z\frac{\partial|q|}{\partial y} + |q|\frac{\partial\tau_z}{\partial y}\right)$$

With the above, Bradshaw's shear stress equations in East's coordinate system are

$$0 = \frac{|\tau|}{\rho}\left|\frac{\partial q}{\partial y}\right|\{\cos(\alpha-\beta) - A\cos(\alpha-\phi)\} - \left(\frac{\tau}{\rho}\right)^{3/2}\frac{1}{\ell} - \frac{A|q|}{\rho}\frac{\partial\tau}{\partial y} \qquad 2.49$$

$$0 = -\left|\frac{\partial q}{\partial y}\right|\sin(\alpha-\beta) + A|q|\frac{\partial\beta}{\partial y} \qquad 2.50$$

In a two-dimensional boundary layer where the τ gradient is small, East reduced Eq. 2.49 to obtain

$$\tau = \rho(1-A)^2\ell^2\left(\frac{\partial q}{\partial y}\right)^2$$

where $(1-A)\ell$ is the effective mixing length and $A = 0.283$. East then replaced the mixing length, ℓ, in Eq. 2.49 with the effective mixing length and nondimensionalized Eqs. 2.49 and 2.50 to obtain

$$\frac{\partial \tau^+}{\partial y^+} = (\tau^+ \left|\frac{\partial q^+}{\partial y^+}\right| \{\cos(y^+ (\frac{\partial \psi}{\partial y^+})_o(\alpha^+ - \beta^+)) - A \cos(y^+ (\frac{\partial \psi}{\partial y^+})_o(\alpha^+ - \phi^+))\}$$

$$- \frac{\tau^{+3/2}(1-A)}{\kappa y^+ \sqrt{\rho^+}}) / A|q^+| \qquad 2.51$$

$$\frac{\partial (y^+ (\partial \psi / \partial y^+)_o \beta^+)}{\partial y^+} = \{\left|\frac{\partial q^+}{\partial y^+}\right| \sin(y^+ (\frac{\partial \psi}{\partial y^+})_o(\alpha^+ - \beta^+))\} / A|q^+| \; . \qquad 2.52$$

Summarizing, Eqs. 2.43-2.48, 2.51, and 2.52 form the system of equations for East's model. The equations were numerically solved by East as part of Bradshaw's (1971) program in the range $0 \leq y^+ \leq 10{,}000$. No comparisons with experimental data was presented for these calculations.

East presents results in q^+ and y^+ coordinates for his model for the incompressible 2DTBL case and shows excellent agreement with well accepted results for this case, noting that the closeness of fit of other results to his is dependent on the choice of law of the wall constants κ and C. As an alternative to the similarity equations for two-dimensional flows presented earlier in this report, East cites the results of Green* where q^+ is more properly designated u^+ and

$$u^+ = \frac{1}{2\kappa} \ln(y^{+2} \frac{\kappa}{D} + 1) - D(1 - \exp(-\frac{y^+}{D})) \qquad 2.53$$

with recommended values of $\kappa = 0.40$ and $D = 9.0$.

East also presents graphical results for the incompressible three-dimensional case with strong cross flow and these are shown in Fig. 2.14. These results are in terms of two parameters, α, the direction of the viscous shear and $(\partial \psi / \partial y^+)_o$, the gradient value at the wall of the total shear vector angle.

---

*This reference is given in East as a 1971 unpublished RAE report by J. E. Green entitled "A Note on the Turbulent Boundary Layer at Low Reynolds Number in Incompressible Flow at Constant Pressure." The library of the RAE was unable to provide any copy of this report.

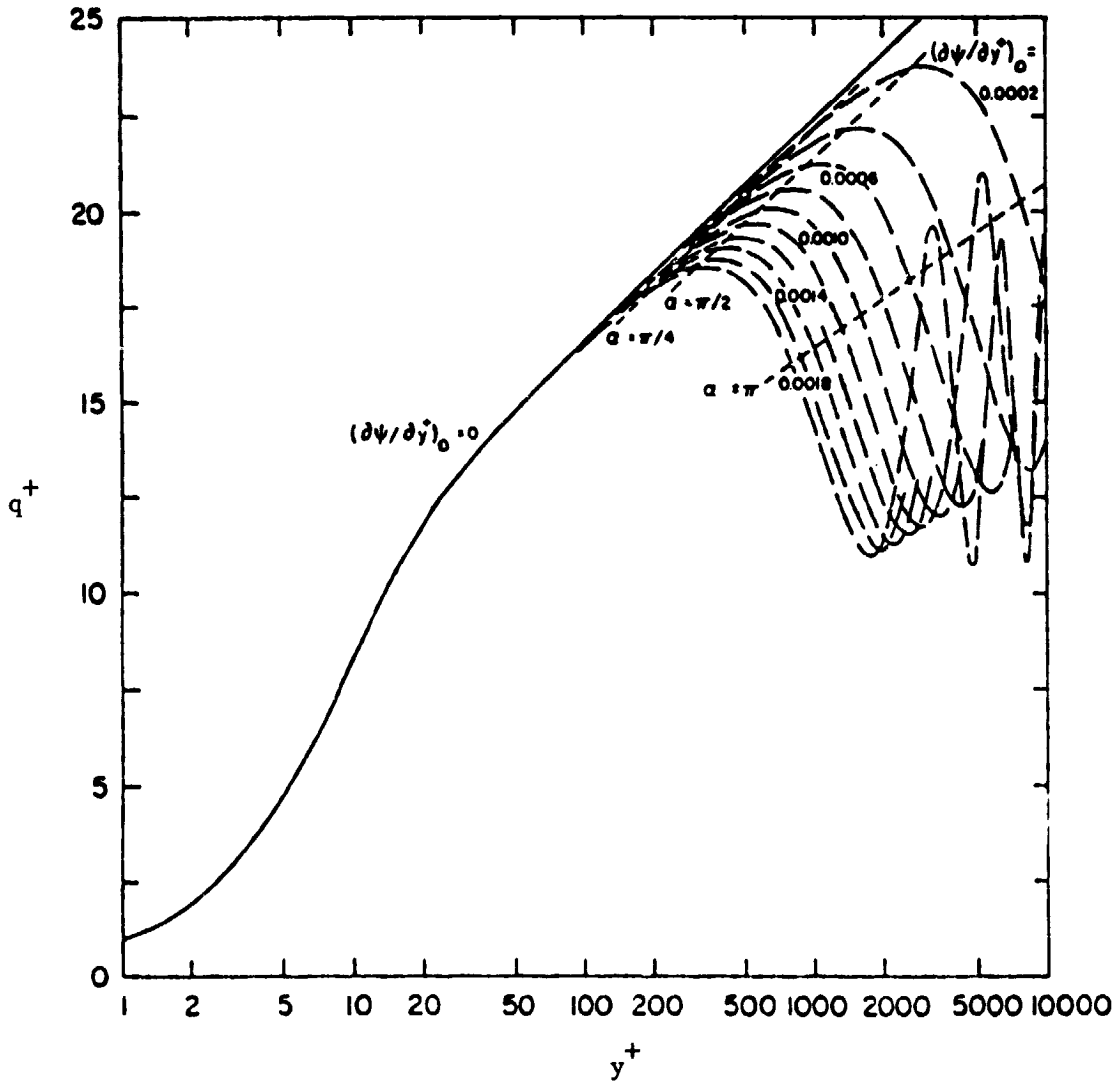

Fig. 2.14 Three-Dimensional Near-Wall Similarity Model for Large Cross Flows in Incompressible Flows as Given by East (1972)

Two points should be noted: (1) that no effect on the similarity law for the logarithmic region is seen until values of $y^+ > 200$ which is nearly outside the expected limit of logarithmic region, and (2) that the gradient of the angle of rotation of the total shear stress vector at the wall is a most difficult parameter to measure.

Based on his own usage the y^+ range for East's model would be estimated at from 0 to almost 10,000. No experimental data was used to verify the full or approximate model and no mention was made of any other three-dimensional similarity models.

III. EXPERIMENTAL PROGRAM - INSTRUMENTATION AND WALL SHEAR DIAGNOSTICS

Introduction

The testing of the validity of the several proposed models for near-wall similarity in three-dimensional flows requires careful measurements of (1) the velocity field - magnitude and direction, (2) both the magnitude and direction of local wall shear stress by direct force measurement, and (3) the wall pressure field which would be presumed to be the pressure field through the boundary layer except in the immediate neighborhood of separation. These measured values would allow calculation of gradients in the wall pressure field, the wall shear stress magnitude and direction, and the mean flow velocity direction, some of which are required in some of the more complex similarity models. One proposed similarity model also requires the gradient in the total shear angle at the wall and since such measurements were not attempted in this program the last of the 11 three-dimensional similarity models reviewed was not tested.

There is an absolute need for direct force wall shear measurements in the validation of any proposed similarity model in a three-dimensional flow. This is an essential requirement since the several near-wall similarity models proposed in the literature for 3DTBL flows all require the local wall shear stress--or some component of it--in the necessary nondimensionalizing of experimental data. While the use of indirect wall shear devices has been reported for 3DTBL flows (e.g., Prahlad (1968), van den Berg (1973), Higuchi and Peake (1978)) with both Preston tube type devices and miniature surface mounted heat meters, all such devices reported on to date have used only two-dimensional calibrations in three-dimensional flows. This, in effect, assumes a priori and without justification, the validity of a two-dimensional near-wall similarity law in a three-dimensional flow--and this is wholly unacceptable in any attempt at a definitive study of near-wall similarity in a three-dimensional flow. Up to this point in time no indirect wall shear diagnostic device has been calibrated for wall shear magnitude and direction in a three-dimensional flow for subsequent use in any other three-dimensional flow. The use of a two-dimensional calibration in a three-dimensional flow

presumes far more than is acceptable in a near-wall similarity study in 3DTBL flows. It should be clear that in any attempt at a definitive study of near-wall similarity in a three-dimensional turbulent flow, the need for local direct force wall shear measurements of both magnitude and direction is essential and absolute, the degree of difficulty required by such a measurement notwithstanding. While such direct force measurements carry with them specific experimental uncertainties, some of which are difficult to quantify at this point in time, such direct force measurements are judged far more desirable than the use of indirect diagnostic devices which in effect presume a two-dimensional-like near-wall similarity behavior.

Flow Tunnel

A large scale, low speed, modest turbulence level wind tunnel shown schematically in Fig. 3.1 was used in this study. Room air enters a 3.66 x 2.44 m (12 x 8 ft) inlet section, passes through a filter pad, a matrix of nominally 2.54 cm (1 in.) diameter by 15.2 cm (6 in.) mailing tubes, four 14 x 18 mesh screens (open area approximately 70%), and a 16 to 1 contraction nozzle designed for zero exit acceleration passing into a 0.91 x 0.61 m (3 x 2 ft) tunnel section where boundary layer trips of 3.2 mm (0.125 in.) circular rods are used. The tunnel length to the test section is nominally 4.88 m. (16 ft). The freestream flow field at the test section is flat to nominally plus or minus 1% of the mean value and the freestream turbulence was measured at 0.6%. The principal instrumentation was contained in a test section of approximately 0.61 m (2 ft) length which was followed by an additional 1.22 m (4 ft) tunnel, finally passing into a rectangular to round 3.44 m (8 ft) transition piece which led to the centrifugal fan inlet. Two rows of flow straightness were placed at the fan entrance to minimize any possible inlet whirl propagating into the test section and the fan itself was isolated from the tunnel. Air speeds up to about 25.0 m/sec (82 ft/sec) where possible, varied by adjustable louvers at the fan exit. The test section itself could accommodate a variety of velocity and pressure traversing probes and traverses mounted on its roof, and the floor pieces were interchangeable providing for wall pressure field measurements and for wall shear stress

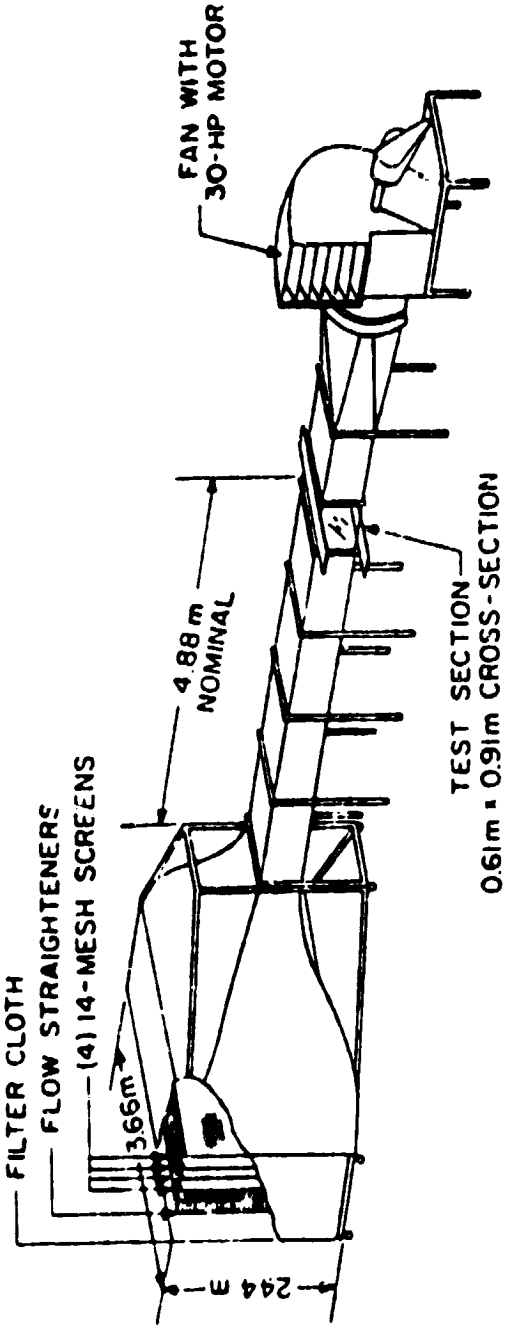

Fig. 3.1 Wind Tunnel

measuring devices such as the direct force sensing mechanical shear meters, Preston tubes, or heat meters.

Generally, it was not possible to obtain all data simultaneously and tunnel similitude was maintained by holding the unit Reynolds number, Re/L, at the tunnel inlet nominally constant for similar flow conditions. In addition essentially all of the data was taken at a nominally constant room temperature with the day to day barometric variations generally modest as well.

Three-Dimensional Flow Geometry

The pressure-driven 3DTBL flow was generated by a cylinder with a trailing edge place normal to the floor of the tunnel as shown in Fig. 3.2. This configuration provided a wide range of skewing conditions, a wide variation of pressure gradient and wall shear orientations, and represents conditions encountered in a variety of real world circumstances. The cylinder itself has a diameter of 12.7 cm (5 in.), is 25.4 cm (10 in.) high and has a tapered end that trails to a sharp edge with an overall length of 29.2 cm (11.5 in.). The body is positioned in the tunnel by a sting secured well downstream of the test section.

Velocity Measurements

Velocity measurements were made with a specially designed goose neck, cobra, stagnation pressure probe consisting of three 0.51 mm (0.020 in.) OD tubes with sensing face on the vertical axis of rotation. The outside tubes were used to determine the flow direction and the stagnation pressure was measured with the center tube. The static pressure was sensed with an 0.40 mm (0.0156 in.) diameter pressure tap located 0.653 cm (0.25 in.) off the tunnel centerline at the probe's axis of rotation. Velocity measurements in the two- and three-dimensional flow configurations range from 0.254 mm (0.010 in.) to approximately 18 cm (7 in.) off the tunnel floor.

The probe was held in place and positioned by a specially designed traversing mechanism located on the roof of the tunnel. A Unislide translational screw provided for adjustment of the vertical position, while mating worm and spur gears allowed for rotation of the probe around the vertical axis. Wall contact was determined by electrical

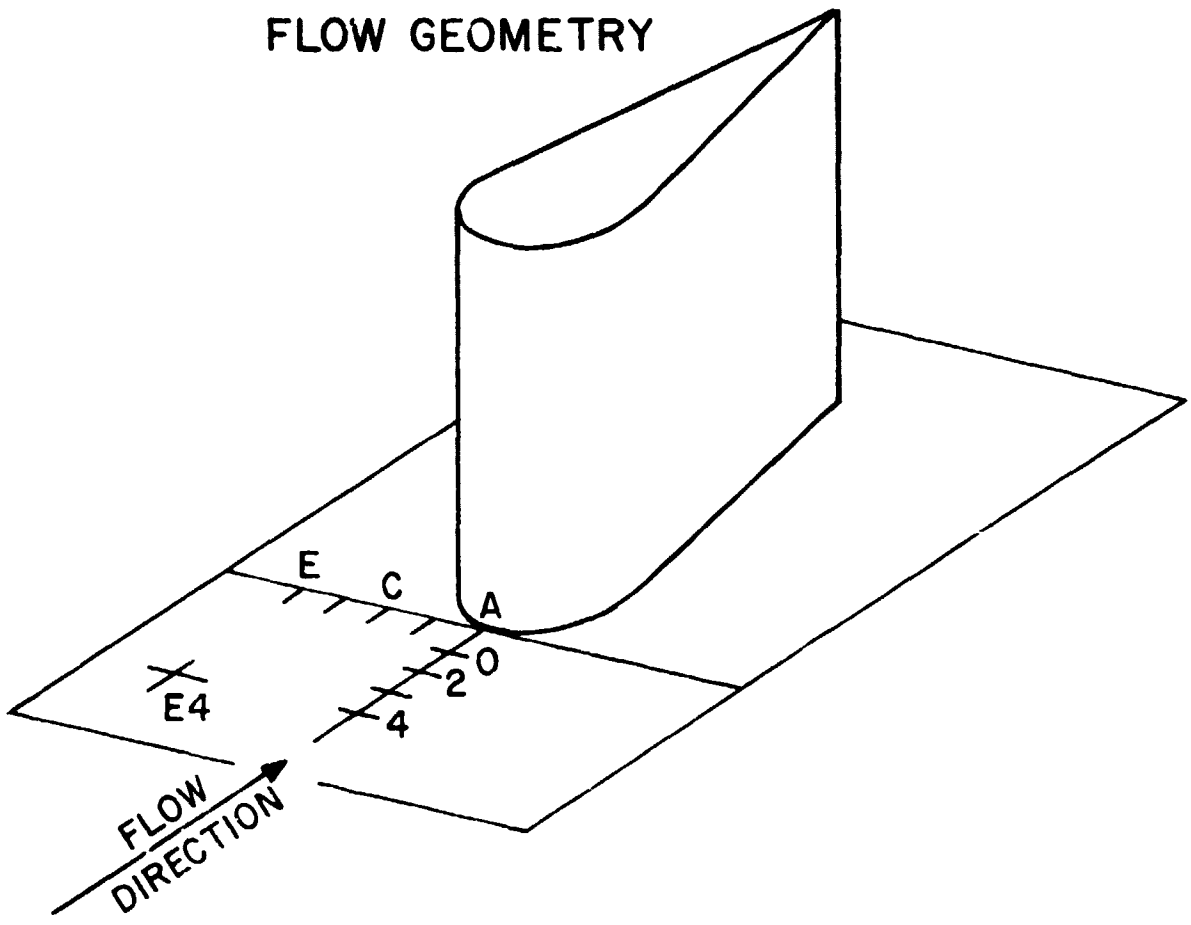

Fig. 3.2 Teardrop Body Used to Generate the Pressure Driven Flow

contact and the probe position could be determined by a Starrett long travel dial gauge, the calibrated Unislide assembly, or a Gaertner Horizontal-Vertical cathetometer. The uncertainty in the probe position was taken to be 0.0254 mm (0.001 in.). Backlash problems in the vertical movement of the transverse were essentially eliminated by one directional motion in all profiles.

The claw probe was nulled for flow direction using a Celesco Model P90D differential pressure transducer and a companion CD25 transducer indicator. While the dial vernier used for angular measurements had a least count of 0.2°, repeated measurements suggested an angular measurement uncertainty of 0.5° for two-dimensional velocity profiles and 1.0° for three-dimensional velocity profiles.

The dynamic pressure was sensed by a Datametrics model 1400 electronic manometer with a Gould type 590 D-10 W-2P1-V1-4D transducer reading 2.54 microns (0.0001 in.) of water on its lowest range. Essentially all of the data was taken with a least count of 25.4 microns (0.001 in.) of water. The sensitivity and fast response time of the manometer required either viscous dampers in the pressure lines or electronic averaging to facilitate reading. For velocity readings less than 2.5 cm (1.0 in.) of water the uncertainty was estimated at 0.076 mm (0.003 in.) of water while at higher readings an uncertainty of 0.127 mm (0.005 in.) of water. The uncertainties in probe position, flow direction, and dynamic pressure are estimated from instrument least counts, differences in data repeated in similar flow conditions, and differences in data taken by different individuals in similar flow conditions.

In addition to the uncertainties in the physical position of the probe, the angular measurement, and the dynamic pressure measurement, there is the question of viscous, turbulence, velocity gradient, pressure gradient, and wall proximity effects which all contribute to possible errors in two-dimensional flows while transverse velocity, pressure, and shear gradients would also contribute to possible errors in three-dimensional measurements. For the two-dimensional case, Dean (1958), MacMillan (1956), Davies (1958), Young and Maas (1936), MacMillan (1954), and Livesey (1956) have studied the effects of different combinations of these problems with no uniform agreement. The most popular correction

seems to be a displacement correction due to the velocity gradient across the probe face. Coles (1968) in analyzing the 1968 Stanford Conference data chose to ignore very near-wall data because of the uncertainty over choice of corrections to apply. The data presented in this study was not corrected because of the uncertainty of such corrections.

Static Pressure System

For static pressure measurements the floor of the test section can be replaced by an aluminum plate containing 52 static pressure taps in a 15.2 x 61.0 cm (6 x 24 in.) grid on 5.1 cm (2 in.) centers. The static pressure taps are 0.40 mm (0.0156 in.) diameter fabricated to insure that all edges were sharp. Pressures were measured by a Systems bi-directional differential capacitance type pressure transducer used with a 48-port Scanivalve sampling valve which sequentially sampled 44 static pressure in from 0.1 to 1 second intervals. Figure 3.3 is a schematic of the static pressure measuring system. Four ports on the Scanivalve system were reserved for calibration purposes. The voltage signal of the central transducer was fed into a Vidar model 240 voltage to frequency converter and then to a Hewlett Packard model 5326A counter and read out on a Hewlett Packard model 5050A printer. The counter provided a means of averaging the signal from the VFC and triggered the Solenoid Controller which in turn determined the sampling rate of the Scanivalve.

The pressure measuring system was calibrated against the Datametrics model 1400 electronic manometer by connecting these to a constant low pressure source. Figure 3.4 shows a calibration curve for the Setra transducer. Several calibrations were made and the linear curve shown was demonstrated to be repeatable. Uncertainties from this system were estimated from repeatability of data to be 3.45 Pa (0.0005 psi).

Omnidirectional Floating Element Device

The omnidirectional floating element device developed by Tennant (1977) was used to measure wall shear in both the two- and three-dimensional flows. A schematic of this floating element device is shown in Fig. 3.5. The primary difference between this device and all other two-dimensional

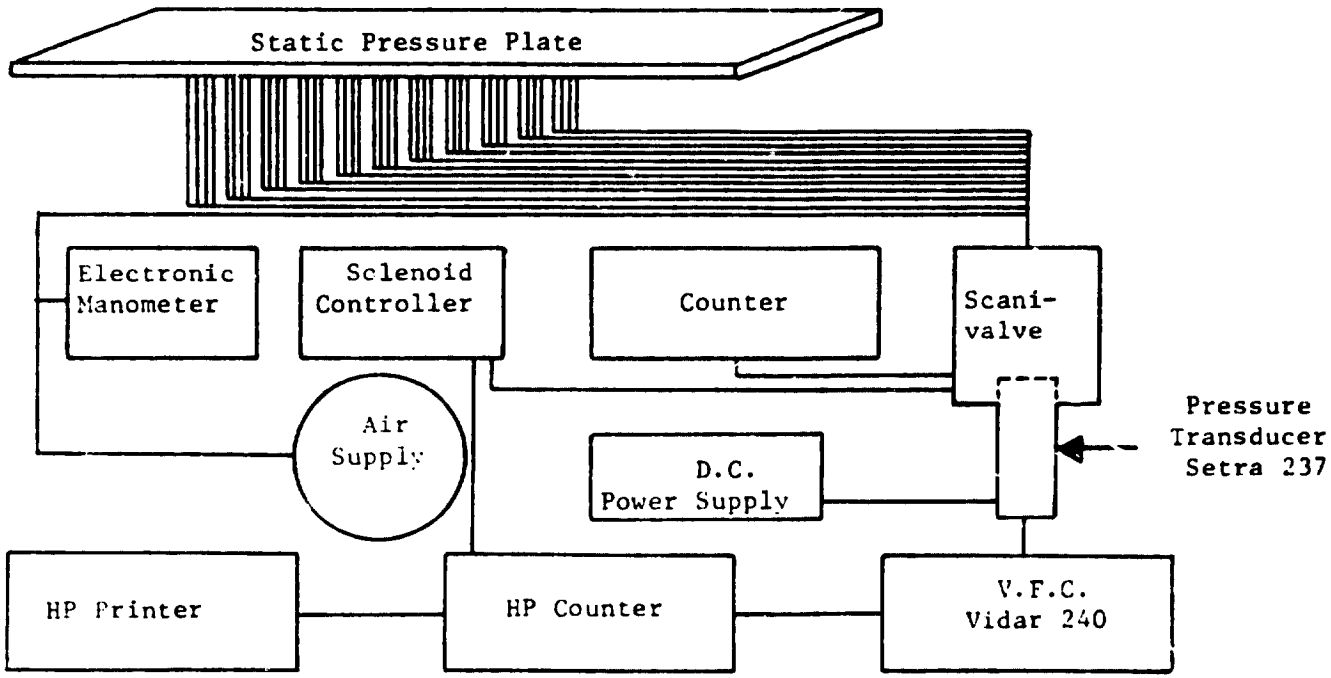

Fig. 3.3 Schematic for the Static Pressure Measurement System.

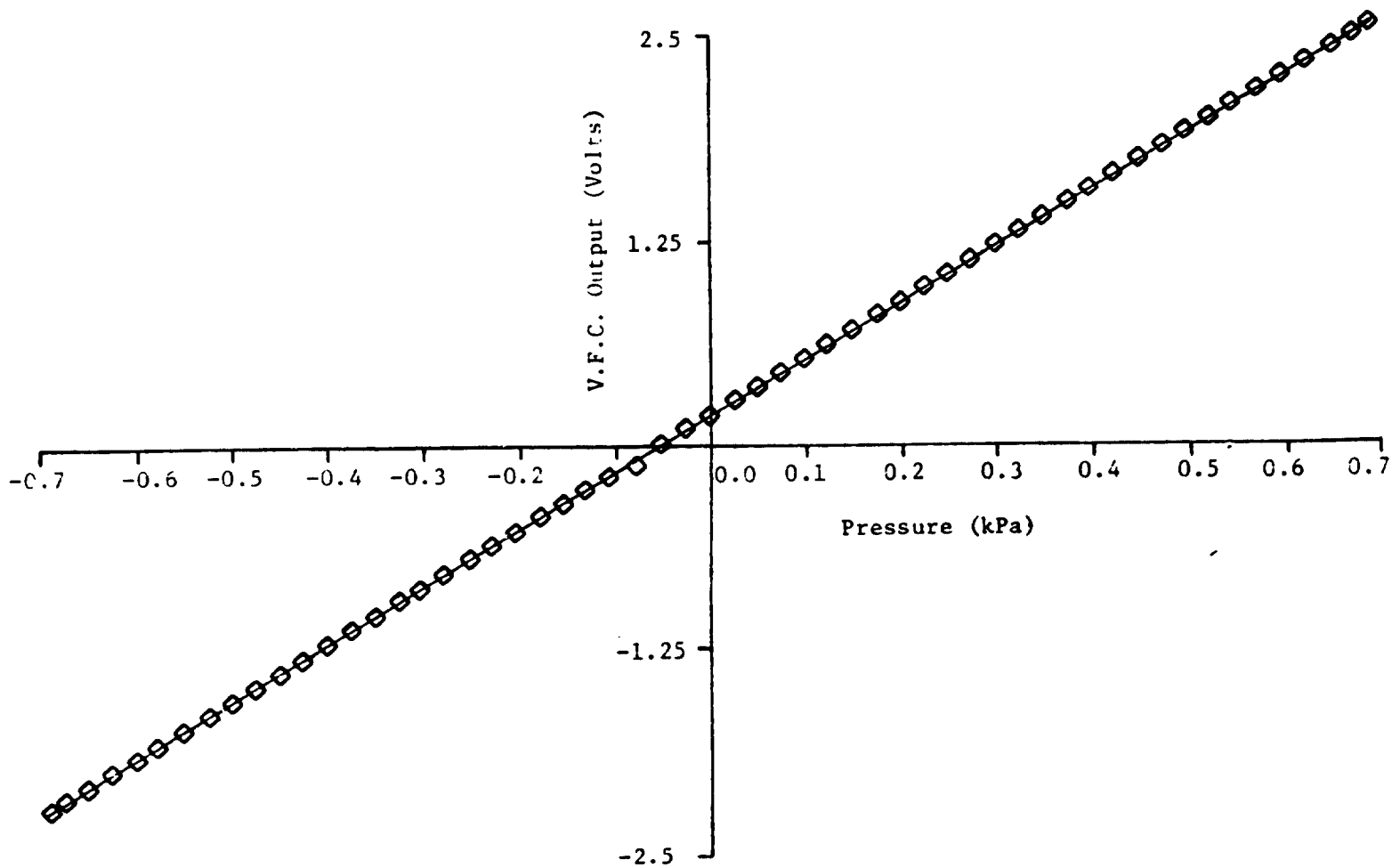

Fig. 3.4 Calibration Curve for the Setra 237 Pressure Transducer

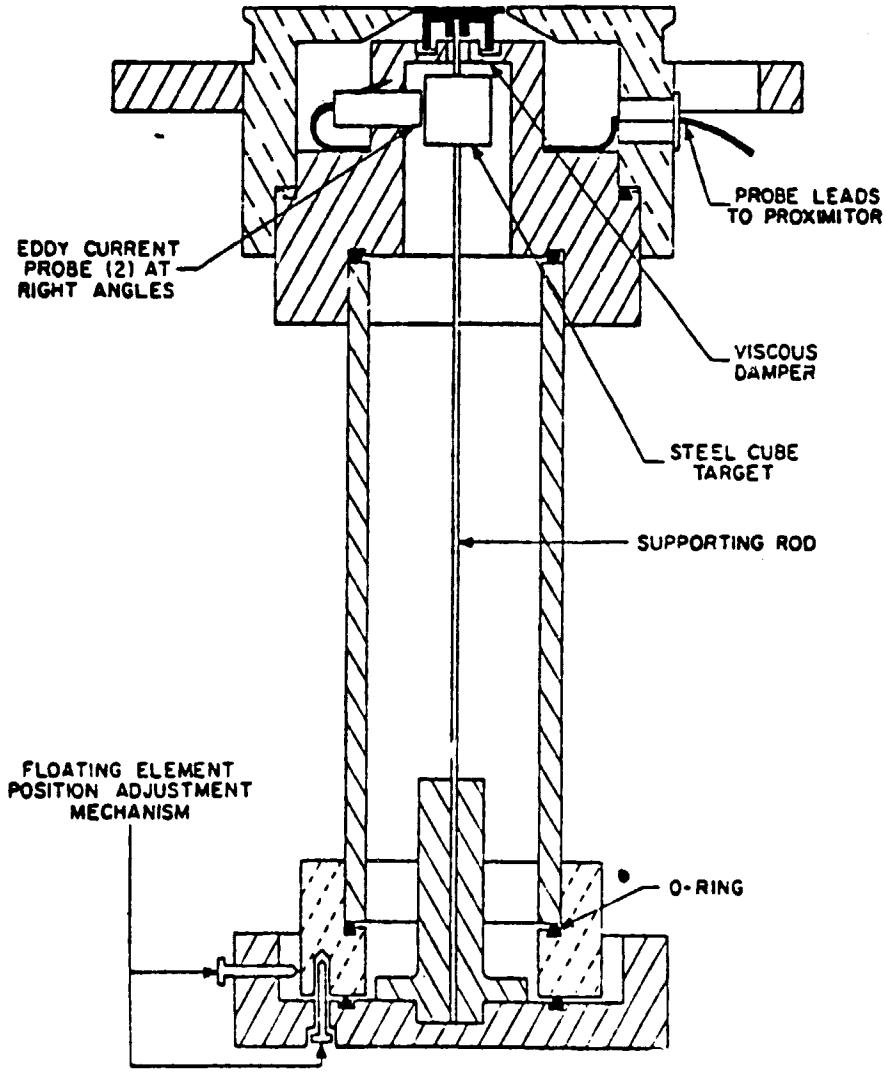

Fig. 3.5 Sectional View of the Omnidirectional Meter

floating element devices is its ability to simultaneously measure the magnitude and direction of the wall shear force.

The button (disk) has a 2.86 cm (1.125 in.) diameter, a lip thickness of 0.635 mm (0.025 in.), and the uniform gap between the button and housing is 0.127 mm (0.005 in.). The button is supported by a 2.16 cm (8.5 in.) long, 1.59 mm (0.0625 in.) diameter steel rod. Vertical misalignment between the button and housing was measured using shims to be less than 0.0126 mm (0.0005 in.) and this was maintained each time the meter was taken apart and reassembled. The lower section of the button is immersed in a 10,000 centistoke fluid to dampen tunnel vibrations while taking experimental data. To prohibit air leakage while taking data the shear meter was sealed at all points of electrical entry and a plastic enclosure was placed around the lower section of the meter.

Two Bently Nevada model 2388-3000 series eddy current proximitors and model 300 probes, designated channels A and B, are placed at right angles to each other and sense the movement of the steel target cube on the rod holding the button. Manufacturer's specifications indicate a resolution of 1.27 μm (50 μin.) displacement, less than 1% nonlinearity of full scale, and a temperature sensitivity of 0.0264 μm/°C (1.88 μin./°F). The drift was measured at constant temperature to be 0.028 μm/5 min and 0.070 μm/5 min and this drift corresponds to a change in the sensed load of less than 0.03 and 0.08 dynes/5 min for channels A and B. Temperature effects were considered negligible since the calibrations and 96% of the data were within a 2.2°C (4°F) temperature range. The wall shear magnitude and direction was determined by resolving the output signals from the two probes.

Figure 3.6 is a schematic of the omnidirectional meter measuring system. Two Hewlett Packard power supplies were used to provide minus 18 volts d.c. to the proximitors and two Racal Dana model 5100-16 multimeters were used to read each proximitor's output. The probes were operated in their linear -5 to -8 volt range.

The floating element was calibrated before being installed and on removal from the tunnel and calibration curves for each channel before and after being in the tunnel were usually within 1%.

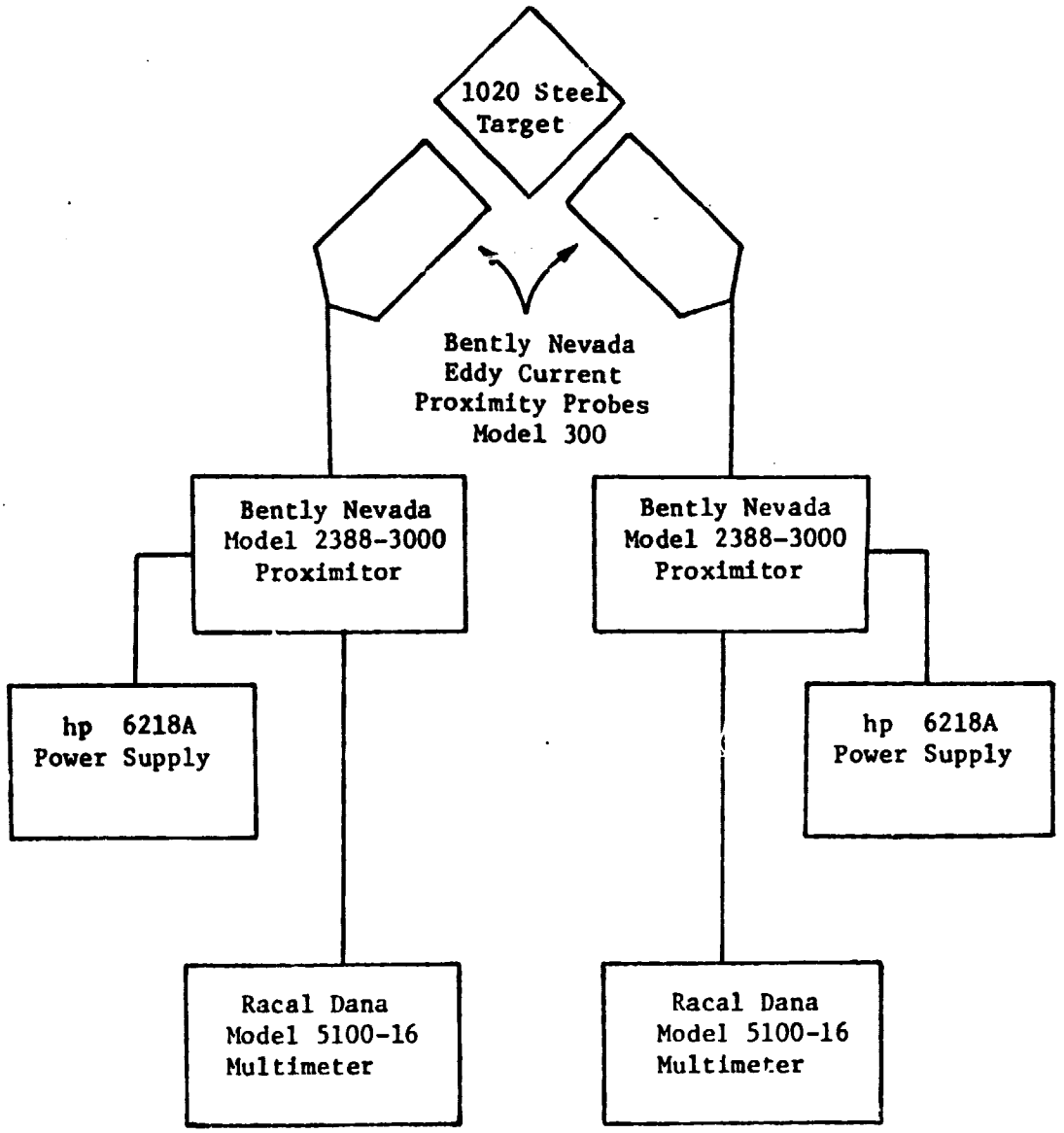

Fig. 3.6 Block Diagram for the Omnidirectional Meter System

The meter was calibrated by weights on a calibration stand. A strand of human hair was aligned at 45° with each Bently Nevada probe, attached to a removable pin at the disk center, and placed over a small, jeweled pulley. The angle formed by the hair and calibration stand top was nearly zero so the entire load placed in the calibration pan would act on the disk. Two vibrators were used to minimize dry friction effects in the jeweled pulley and, to a lesser extent to simulate tunnel vibrations as encountered during tunnel operations. After putting the human hair in place, the calibration stand was leveled so that the button was centered in its space in the top of the meter housing. A typical calibration curved voltage output versus loading is shown in Fig. 3.7. A more informative way to plot the calibration data is to show the sensitivities for each load. Such a figure emphasizes the scatter for the lower loadings which is most likely due to dry friction forces in the jeweled pulley where such secondary forces become large with respect to the small loads. The individual load sensitivities for the results in Fig. 3.7 are shown in Fig. 3.8 with the greatest scatter at the lower loadings.

Tennant (1977) modeled the supporting rod and its load with a computer program called Line Solution Developer (LSD) which is based on transfer matrix or initial parameter theory. These results indicated

1) that the ideal system is linear over a larger range than which the system is operated,
2) that eccentric moments due to weight imbalances in the target or floating disk would have no effect on the linearity or sensitivity, and
3) that any initial bend in the supporting beam would have no effect on the linearity or sensitivity

and these results support the experimentally obtained linear calibration curves. Calibration data were obtained well beyond the design data range showing linearity well beyond the design movement.

Uncertainty estimates for the three-dimensional shear measurements included contributions from possible errors in the

1) physical area of the floating element
2) voltage output of the transducers
3) sensitivity values from the calibration procedure

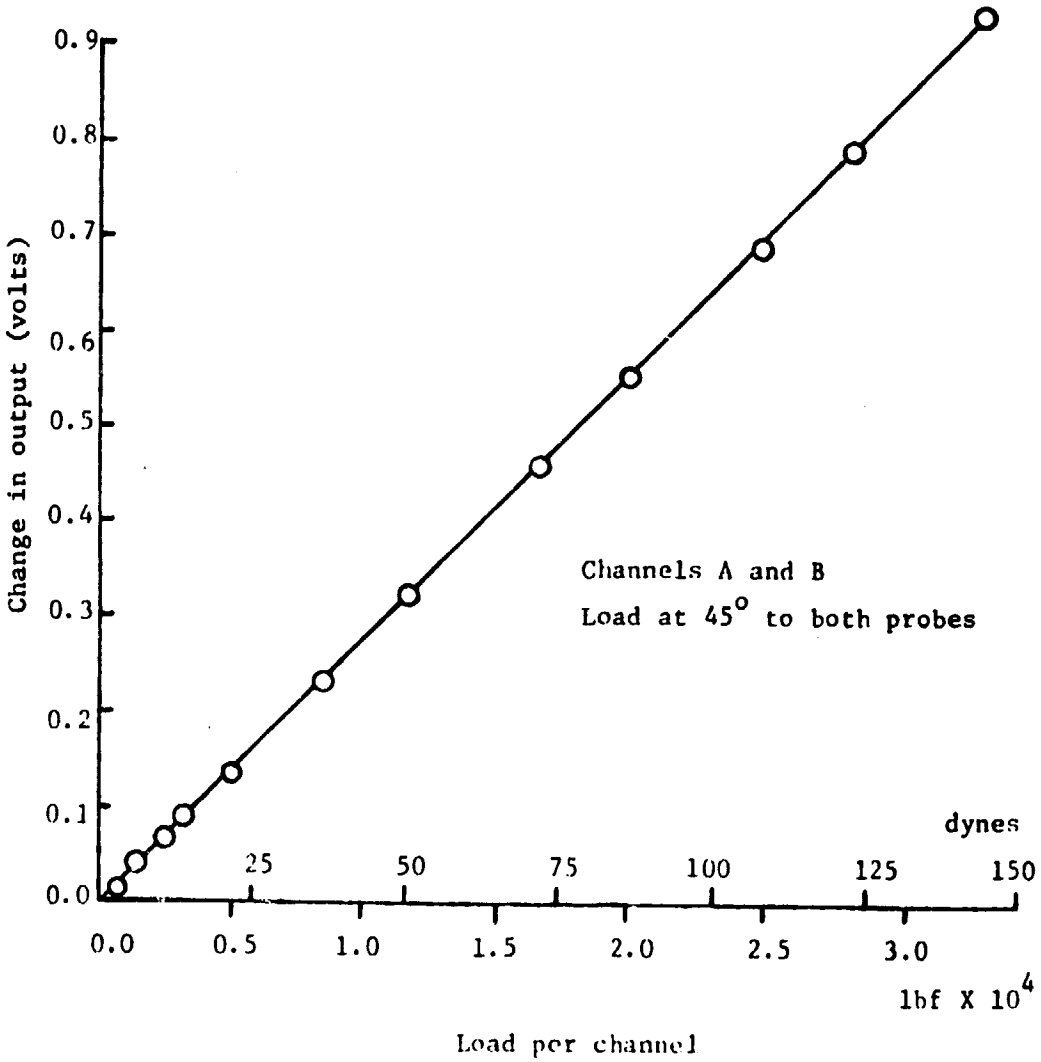

Fig. 3.7 Calibration Curves for the Omnidirectional Meter

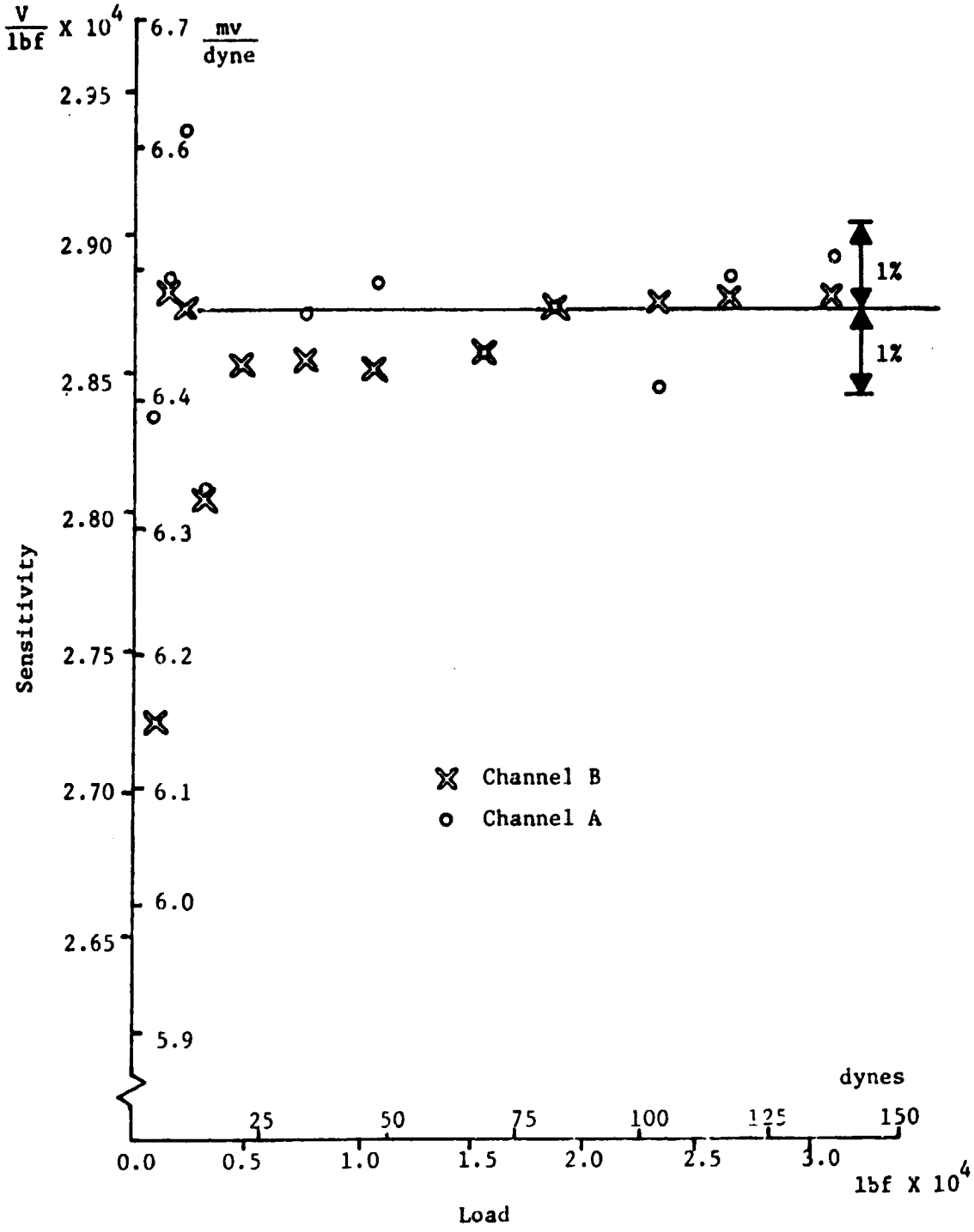

Fig. 3.8 Individual Load Sensitivities for the Omnidirectional Meter Calibration Curves

4) misalignment of the shear meter with respect to the reference tunnel centerline

5) vertical misalignment of the floating element with respect to the meter surface, and

6) transducer drift.

These uncertainties were combined in a Kline-McClintock (1953) type procedure and an overall uncertainty is estimated for each shear data point reported. The inclusion of these several possible sources of error was made in an attempt to have this overall uncertainty approach an Nth order uncertainty estimate as described in Moffat (1980).

In an effort to establish a high degree of credibility to the three-dimensional meter, a substantial number of measurements was taken in two-dimensional flow conditions for comparison with a two-dimensional direct force sensing shear meter and a series of Preston tubes over a modest range of unit Reynolds members. Such two-dimensional measurements were judged to be a valid test of the three-dimensional meter since it was required to measure a force magnitude and a force direction (albeit the nominal tunnel centerline direction) in the two-dimensional flows.

Two-Dimensional Floating Element Device

The two-dimensional floating element device developed by Pierce and Krommenhoek (1968) and shown schematically in Fig. 3.9 was used to measure wall shear in two-dimensional flows. In this device, the circular disk is free to move in only one direction and this movement is detected by a linear variable differential transformer (LVDT). Since Pierce and Krommenhoek reported on this meter, the original LVDT and associated power supply with accompanying electronics has been replaced (Rule (1976) and Pierce, Tennant, and Rule (1976)) by a Schaevitz 025MHR LVDT with an LPM-205 signal conditioning module.

The disk in Fig. 3.9 has a 2.858 cm (1.125 in.) diameter and the equally spaced gap between the button and meter housing is 0.127 mm (0.005 in.). The button is supported by a pinless four-bar linkage of two brass reinforced copper-beryllium fixtures while the lower part of the button rests in a well filled with 30,000 centistoke methylsilozane oil. The oil serves to damp out external vibrations from the tunnel

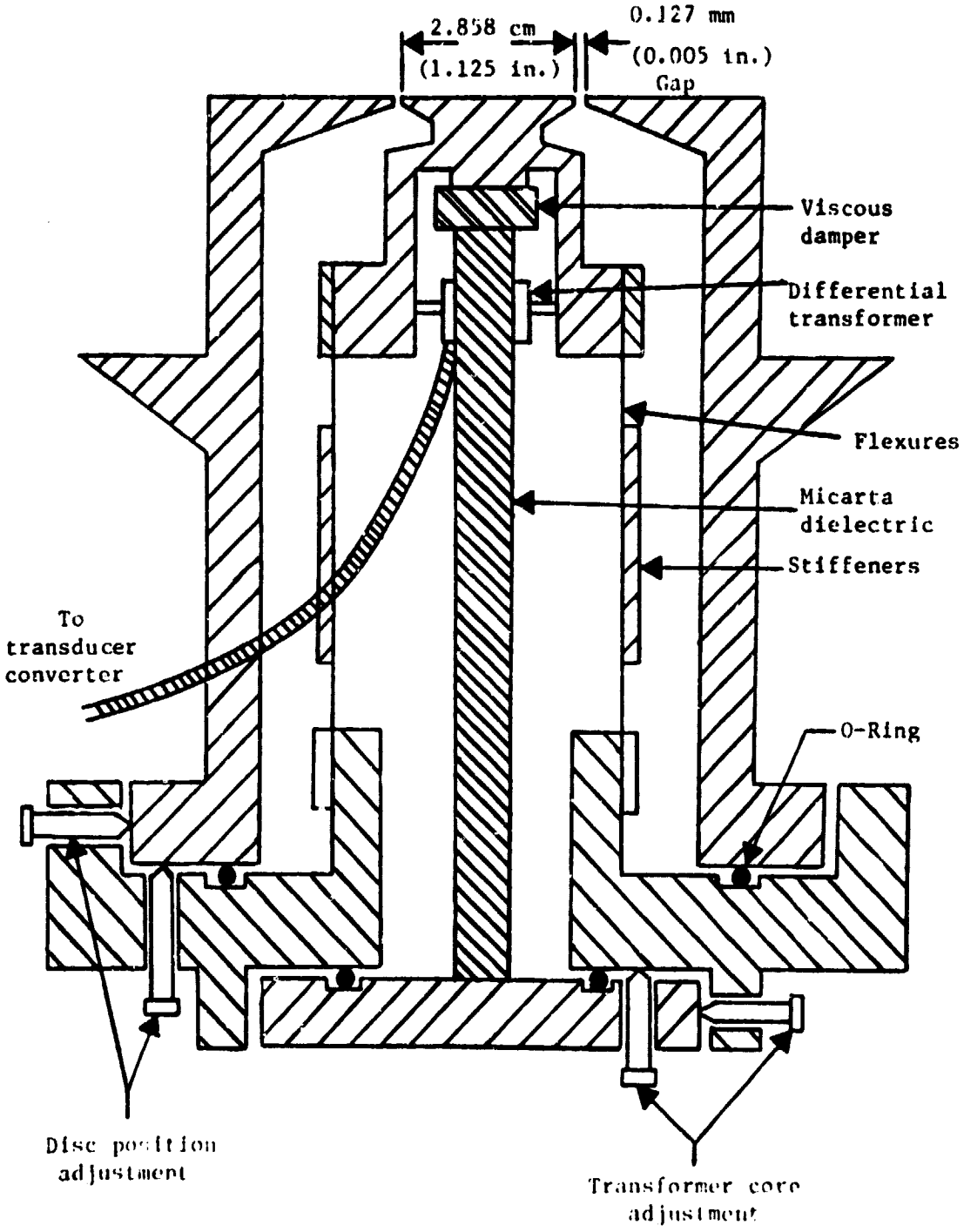

Fig. 3.9 Sectional View of the Two-Dimensional Floating Element

while measurements are being taken. Additionally, the meter is sealed to prevent any air flow between the atmosphere and the tunnel. A static pressure tap in the surface of the meter was used in combination with the claw probe previously described to take freestream velocity data to construct C_f values. The overall two-dimensional floating element system can be represented by the block diagram shown in Fig. 3.10.

The meter was calibrated in the same device and in the same manner as the three-dimensional meter but with the line of action of the calibrating weights aligned with the meter displacement direction. One typical set of calibration results is shown in Fig. 3.11. The calibration curve was fitted from a first order least squares fit of the calibration data. The coefficient of determination (Burr(1974)), r^2, was generally 0.99990 to 0.99999 for the calibration runs indicating excellent linearity. As before, it is instructive to show the sensitivities for each load and data of Fig. 3.11 is shown this way in Fig. 3.12 where large scatter is also shown for the lower loadings.

For reliable wall shear readings the two-dimensional floating element was calibrated before being installed in and after removal from the tunnel. If two calibrations differed by 1.5% the calibration after removal was considered the more accurate since the floating meter was subjected to less handling in removal than in installation.

Preston Tubes

The Preston tubes were individually mounted on 12.7 cm (5 in.) diameter aluminum disks with the tube opening centered on the disk. The opening of each stainless steel tube was hand crafted in order to insure a smooth, round entrance free of burrs. The tubes were approximately 3.81 cm (1.5 in.) long and they were epoxied to the aluminum disk. Tubes with outside diameters of 0.46 (0.018), 0.71 (0.028), 0.91 (0.036), and 2.11 mm (0.083 in.) were used. The inside diameters were 0.241 (0.0095), 0.394 (0.0155), 0.584 (0.023), and 1.60 mm (0.063 in.) respectively. Except for the largest tube, the static pressure taps were located 1.27 cm (0.5 in.) from the tube opening in a line transverse to the direction defined by the tube axis. In preliminary testing of the three smaller tubes, static pressure tap locations as close as 0.64 cm (0.25 in.) to

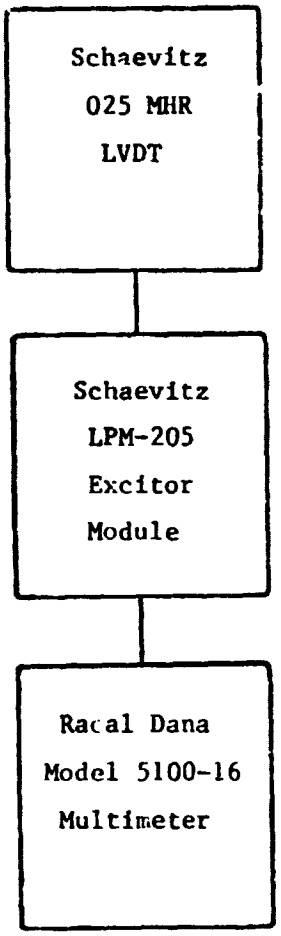

Fig. 3.10 Block Diagram for the Two-Dimensional Floating Element System

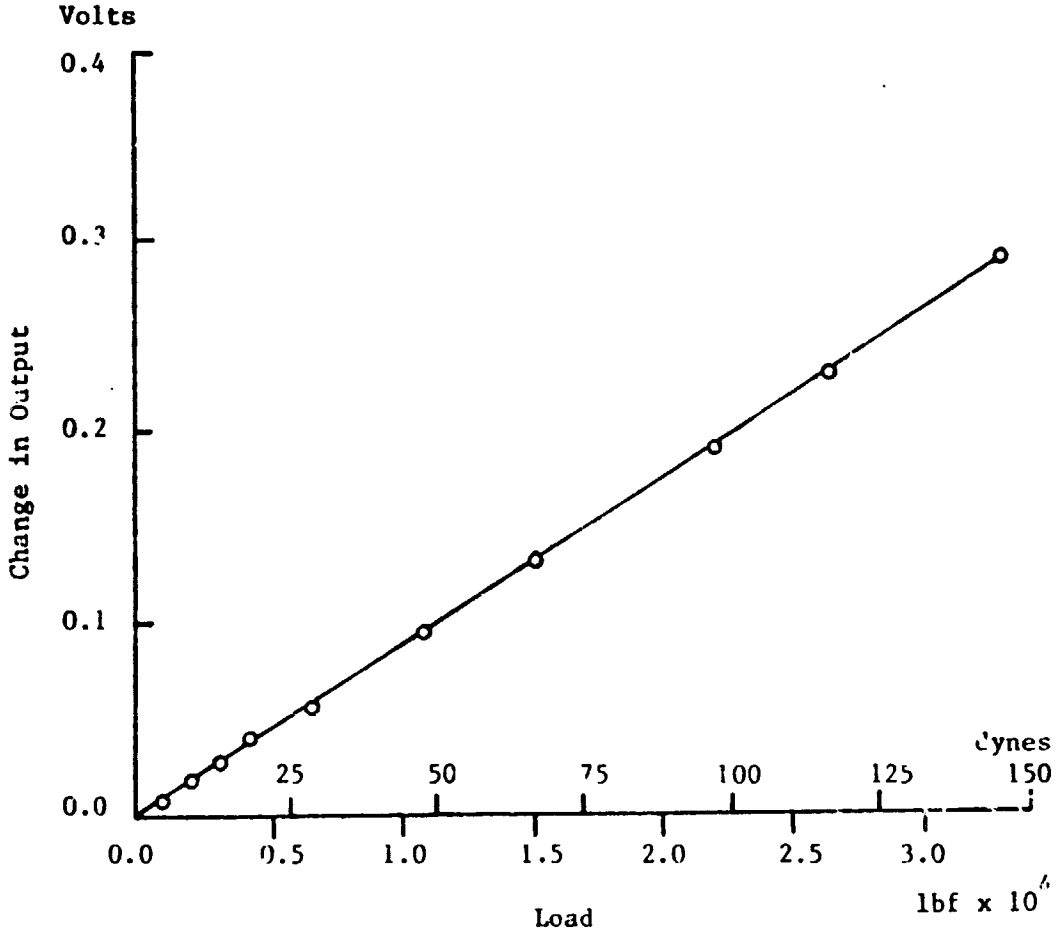

Fig. 3.11 Calibration Curve for the Two-Dimensional Floating Element

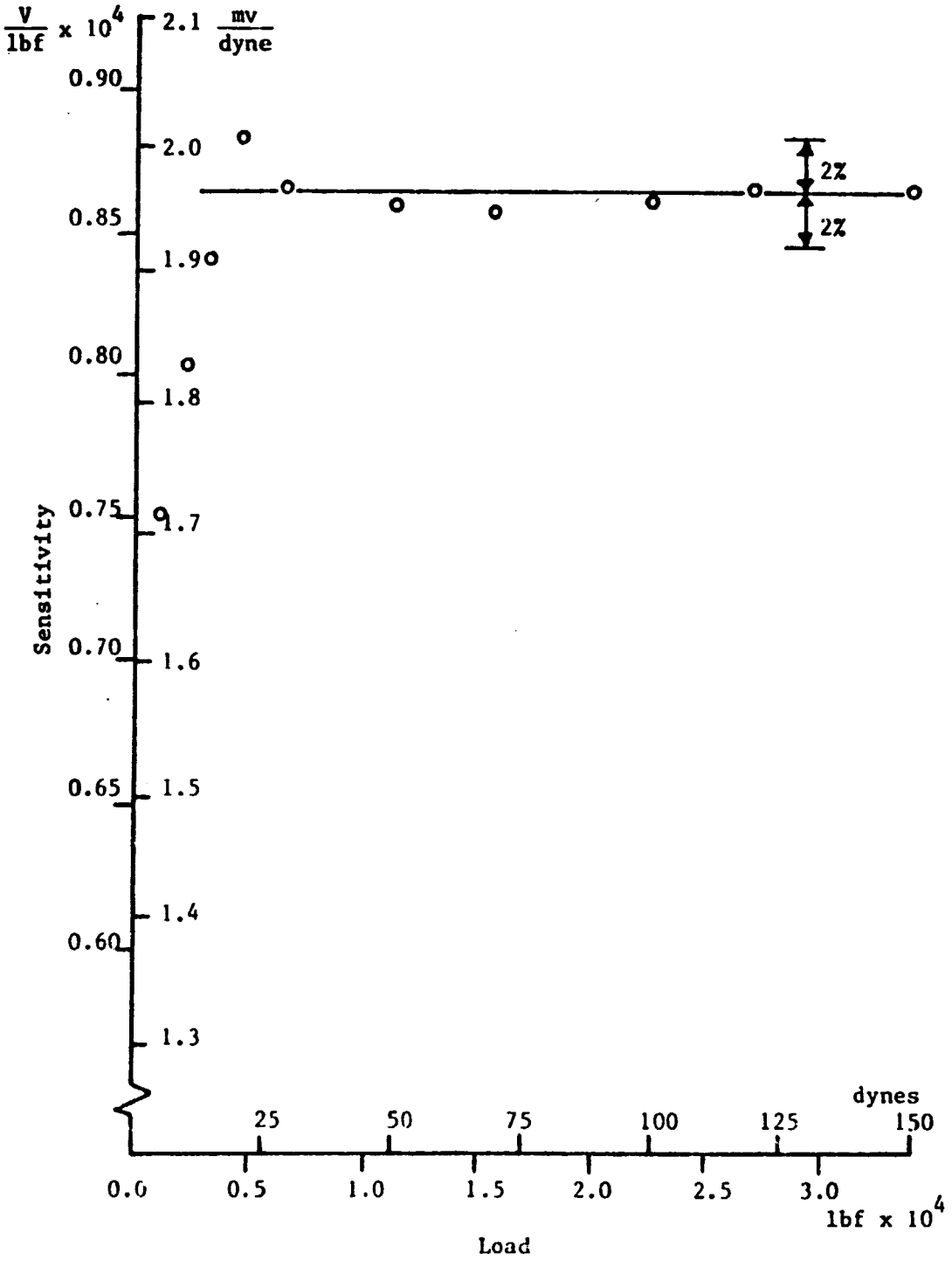

Fig. 3.12 Individual Load Sensitivities for the Two-Dimensional Floating Element Calibration Curve

the Preston tube produced the same results as the taps located at the 1.27 cm (0.5 in.) distance. For the largest diameter Preston tube, the static pressure tap was 2.54 cm (1.0 in.) from the Preston tube opening. Static pressure taps closer than 1.27 cm (0.5 in.) gave readings dependent on this separation distance, while readings with the static pressure taps located from 1.6 cm (0.75 in.) up to 3.2 cm (1.25 in.) gave identical results. The Preston tube measurements were made with the electronic digital pressure measuring system described earlier.

Experimental Procedure

The experimental program was completed in two phases--the first involving measurements in a two-dimensional nominally zero pressure gradient boundary layer over a modest range of unit Reynolds numbers, and the second phase in a pressure-driven three-dimensional turbulent boundary layer at a nominally constant unit Reynolds number. The first phase required measurements of static pressure field, velocity field, wall shear stress by the three-dimensional shear meter, by the two-dimensional shear meter, and by the series of Preston tubes. The second phase involved measurements of the wall pressure field, velocity field, and wall shear measurements with the three-dimensional shear meter. The measurements of each phase were not necessarily made in the order listed above. Instrumentation system requirements were such that these measurements could not be made simultaneously. In order to insure dynamically similar flow conditions for any particular measurements, the tunnel unit Reynolds number based on freestream velocity and fluid properties at the tunnel entrance was held nominally constant. This was accomplished by maintaining the laboratory temperature within small temperature variations and making minor changes in the tunnel speed as required for barometric changes.

It would have been preferable to keep the flow body stationary while moving the measurement sensors. This was practical for the pressure field and velocity field measurements, but the mechanical shear meter required extensive leveling whenever the movable floor of the test section was repositioned. Following the example of Prahlad (1968), it was decided to keep the measurement location stationary and to move the body around that location. Every effort was made to insure the accurate placement of the

body at each location and attempts were made to obtain different wall shear measurements by slightly misaligning the body. These attempts showed that slight misalignments did not result in measurable changes in wall shear stress. Velocity measurements made after the body was removed and then replaced proved to be repeatable also indicating that body placement was not a problem. Wall pressure field measurements made with the body moved to a new position showed consistent and repeatable values within experimental uncertainties.

The two-dimensional data were taken over a tunnel inlet unit Reynolds number range from 0.71 to 1.33 x 10^6/m. The three-dimensional data were taken at a reference unit Reynolds number of 1.322 x 10^6/m $\pm$ 1%.

Wall Shear Stress Measurement Techniques

In the last 100 years a large number of investigators have attempted to measure wall shear in incompressible turbulent boundary layers. All but a small and recent number of these investigations have dealt with two-dimensional flows.

For two-dimensional flows the techniques found in this review included floating element devices used in channel flows by Tennant (1977), Pierce, Tennant and McAllister (1980), Brown and Joubert (1969), Smith and Walker (1958), Vinh (1973), Allen (1977), Fowke (1969), Everett (1958), Boyce and Blick (1971), Boyce and Blick (1969), Waltrup (1971), Miller (1972); in annular shapes by Franklin (1961), White and Franklin (1964), Smith, Lawn and Hamlin (1968), on a cylinder by Morsey (1974), and on flat plates by Depooter, Brundrett and Strong (1977), Hakkinen (1955), Dhawan (1952), Dershin, Leonard and Gallaher (1967), Shutts, Hartwig and Weiler (1955) and Furuya, Nakamura, Osaka and Honda (1975); Preston tubes used by Preston (1954), Smith and Walker (1958), the NPL Staff (1958), Rechenberg (1963), Ferriss (1965), Head and Rechenberg (1962), Patel (1965), Brown and Joubert (1969), Miller (1972), and Samuel and Joubert (1974); Stanton tubes used by Stanton, Marshall and Bryant (1920), Konstantinov and Dragnysh (1960), and Bradshaw and Gregory (1961); sublayer fences used by Wills (1963), Nash-Weber and Oates (1971), Wanschkuhn and Vasanta Ram (1975); razor blades used by East (1968), Wyatt and East (1968), Pai and Whitelaw (1969), Miller (1972); heated elements used by Fage and Falkner (1931), Ludwieg (1950), Owen (1970), Ludwieg and Tillmann (1950), Liepmann and Skinner

(1954), Drinkuth & Pierce (1966), Bellhouse & Schultz (1966, 1968), Brown (1967), Armistead & Keyes (1968); and electrochemical devices used by Mitchell and Hanratty (1966), Kashinskiy, Kutateladze, and Mukhin (1974). Winter (1977) provides a more detailed review of some of these and other works, as do Tennant (1977) and McAllister (1979).

Figure 3.13 lists most of these techniques/methods. The floating element technique is difficult to use, but only it can provide a direct measurement of wall shear stress. Except for the less direct momentum balance calculations and liquid film movement measurements, all other techniques that have been reviewed rely on the assumed existence and form of near-wall similarity to infer wall shear stress.

The indirect similarity techniques listed above may generally be divided into two groups: (1) those which infer wall shear stress through pressure measurements and (2) those which infer wall shear stress through heat or mass transfer rate measurements near the wall. Both groups rely in one form or another on the assumed existence of near-wall similarity, i.e.

$$u^+ = f(y^+).$$

For instance Preston tubes are simply pitot tubes laid on the wall and are used to measure dynamic pressure which is correlated with the local wall shear stress. Stanton tubes and the razor blade technique are similar to Preston tubes but are smaller and may even be confined to the viscous sublayer. Heat and mass transfer techniques utilize near-wall similarity through Reynolds' analogy. These methods sense flow conditions in the thin thermal or concentration layers above the wall. These layers must usually remain within the viscous sublayer for accurate calibration. Miller (1972), Rechenberg (1963), Pierce and Krommenhoek (1968), and Rubesin et al., (1975) provide more detailed discussions of these techniques.

The only technique that directly measures the wall shear stress is the floating element technique. In essence a small area of the wall is isolated and the force acting on that area is measured. This technique would appear to be the only one capable of resolving the question of near-wall similarity in three-dimensional flow. However floating element measurements can be very difficult due to a number of possible error sources.

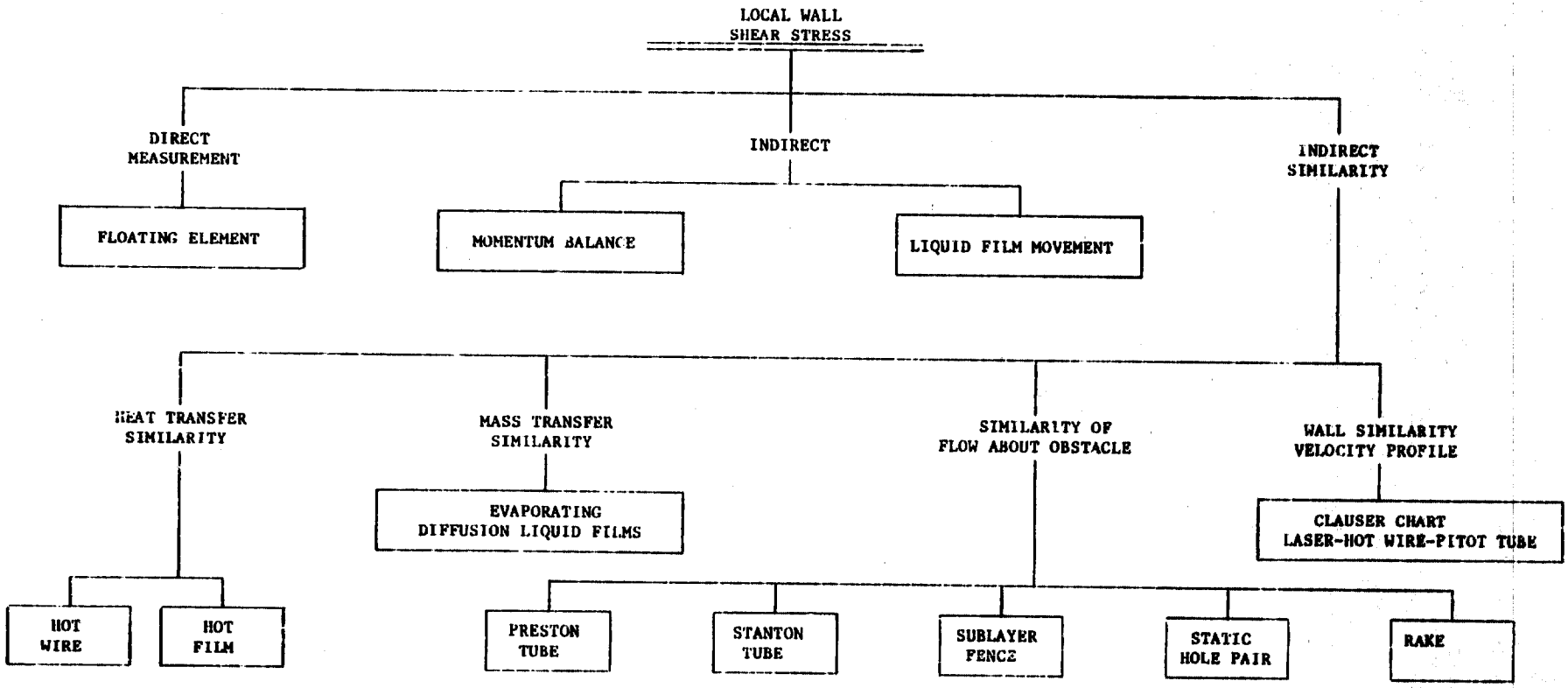

Fig. 3.13. Local Wall Shear Stress Diagnostic Techniques

Errors in the measurement of wall shear with a floating element device in two-dimensional flows have been attributed to a number of different effects as noted in Brown & Joubert (1969), Pierce and Krommenhoek (1968), Everett (1958) and Allen (1977), and typically can include:

1) Misalignment of the floating disk with the surrounding wall can cause significant errors though these errors can be minimized through careful installation.

2) Secondary forces may be imposed on the edge or lip of the floating disk by penetration of the freestream pressure into the air gap. It is usually suggested that these errors can be minimized by minimizing the lip thickness, thereby decreasing the area over which the pressure may act but Everett's (1958) results suggest that a thicker lip will result in reducing the error. Regardless of how these errors may be minimized, they can remain significant when the wall shear approaches zero. Vinh (1973) suggests these errors are unique to the floating element design itself.

3) The pressure gradient will cause a pressure difference between the boundary layer above any point in the air gap and cause flow through it. These errors can be minimized but not entirely eliminated by sealing the floating element casing from the surroundings.

Of possible less importance, Brown and Joubert (1969) include:

4) The air gap will act as a roughness element in the smooth wall. Everett (1958) suggests that the gap be reduced in size to minimize errors as is the usual practice. Allen (1977) suggests that less error is encountered for larger gaps.

5) The shear stress measured is the mean shear stress over the area of the floating disk. If the flow geometry is large in comparison to the floating disk, this effect can be minimized.

6) The floating element can alter the geometry of the device according to its position and thus cause changes in the flow pattern through the air gap. It would appear to be advantageous if the floating element device were of the nulling type.

7) Even when the disturbance caused by the gap is ignored, there will be a shear stress transmitted through the shear layer.

Hakkinen (1955) suggests that a part of the gap area be considered as an effective floating element area.

8) An imposed pressure gradient can result in a normal force acting on the floating element some distance from the disk's center. This normal force can thus cause a moment that can introduce errors for large pressure gradients.

From the preceding list it can generally be concluded that the largest errors for the floating element technique are derived from two sources: (1) element misalignment and (2) the pressure gradient imposed on the element.

Three experimental studies have been made concerning errors induced by floating element misalignment. The supersonic studies of Allen (1977) and O'Donnell (1964) appear to be the most comprehensive on disk misalignment and they indicate varying effects of element protrusion on the measured wall shear as shown in Fig. 3.14. Supporting these results are the low speed studies by (1) Furuya, et al. (1975) which indicated that negative protrusions from 0→15 μm (0→0.0006 in.) have no effect, negative protrusions from 15→30 μm (0.0006→0.0012 in.) have a slight effect, and positive protrusions of only 3 to 5 μm (0.0001 to 0.0002 in.) have a noticable effect on τ_o, (2) Smith and Walker (1957) who state negative protrusions up to 0.0127 mm (0.0005 in.) have no effect and any positive projections caused intolerable errors in τ_o values, and (3) Morsy's (1974) statement positive 0.125 mm (0.005 in.) misalignment of the disk with its solid boundary gives unacceptable τ_o values. From these studies it would appear that negative disk projections of 0.0127 mm (0.0005 in.) to 0.0254 mm (0.001 in.) are tolerable. O'Donnell points out that on a smooth surface a misalignment error of 0.005 mm (0.0002 in.) can be felt by hand and that an error of 0.013 mm (0.0005 in.) can be often seen. Thus it should be possible to keep these errors below ± 3% of the flush reading.

Everett (1958), Pierce and Krommenhoek (1968), Brown and Joubert (1969), and Miller (1972) have made experimental studies of pressure gradient effects on floating elements. These studies were made in small subsonic wind tunnels. Both Pierce and Krommenhoek, and Brown and Joubert

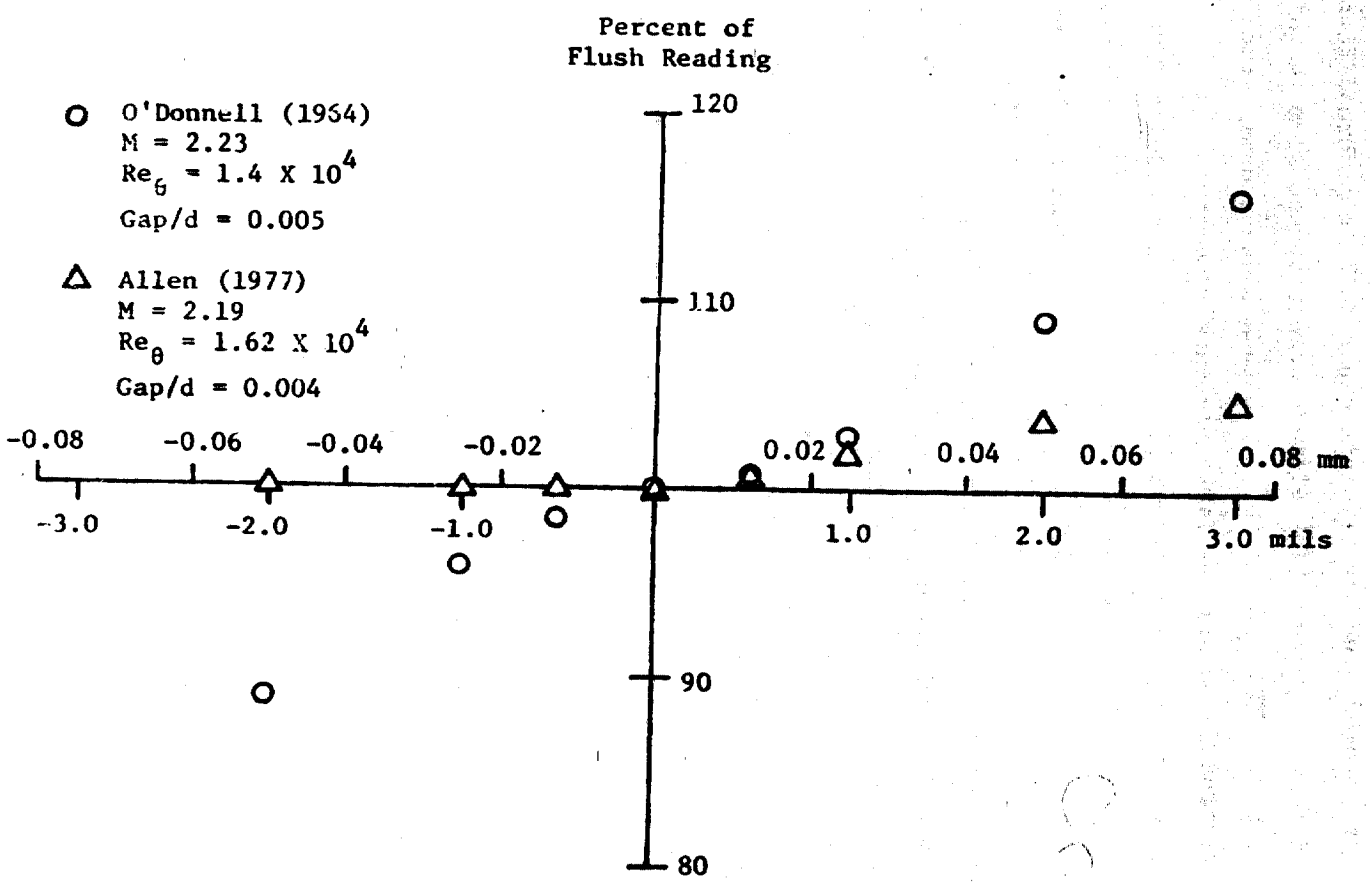

Fig. 3.14 Effects of Disk Misalignment

studied the effects of adverse pressure gradients. Miller studied both adverse and favorable pressure gradients, and Everett's work was in a favorable pressure gradient. Figure 3.15 shows their results. The results of Pierce and Krommenhoek are based on 28 data points where the wall shear stress was inferred from Clauser charts with Coles' (1962) constants and compared with a floating element device that could not be nulled. Brown and Joubert's results are based on more than 120 data points where the wall shear was inferred from Preston tubes using Patel's (1965) calibration and compared with a floating element device that was nulled by tipping the device. Miller's results for favorable pressure gradients were based on 9 data points. Miller used fully developed flow between two plates and calculated the wall shear stress with a momentum balance, i.e.,

$$\tau_o = \frac{d_p}{2} \frac{dp}{dx}$$

where the distance between plates, d_p was 0.318 cm (0.125 in.) and 1.27 cm (0.5 in.). Miller's floating element was of the nulling type. Miller used a different tunnel for his adverse pressure gradient studies. There he compared wall shears using a Preston tube with Patel's calibration, a near-wall similarity plot for the logarithmic region using Patel's constants, and his floating element device corrected by + 10% using Brown and Joubert's results. Compared with the floating element results, the Preston tube measurements were reported to be 2 to 4% low, while the similarity plot gave results that were high by as much as 5%. The poorest agreement was in accelerated flow regions. In addition, Fig. 3.15 shows the pressure correction suggested by Everett which takes the form

$$\tau_o - \tau_{meter} = \frac{t}{2} \frac{dp}{dx}$$

where t is the thickness of the floating element lip. The gap-to-disk diameter ratio was 0.0044 for the Pierce and Krommenhoek study, 0.004 for the Brown and Joubert study, and 0.0035 for Miller's work. A significant question in Fig. 3.15 concerns the nominally correct or reference τ_o used to derive the correction factors for the wall shear reading, τ_{meter}, from a floating element device.

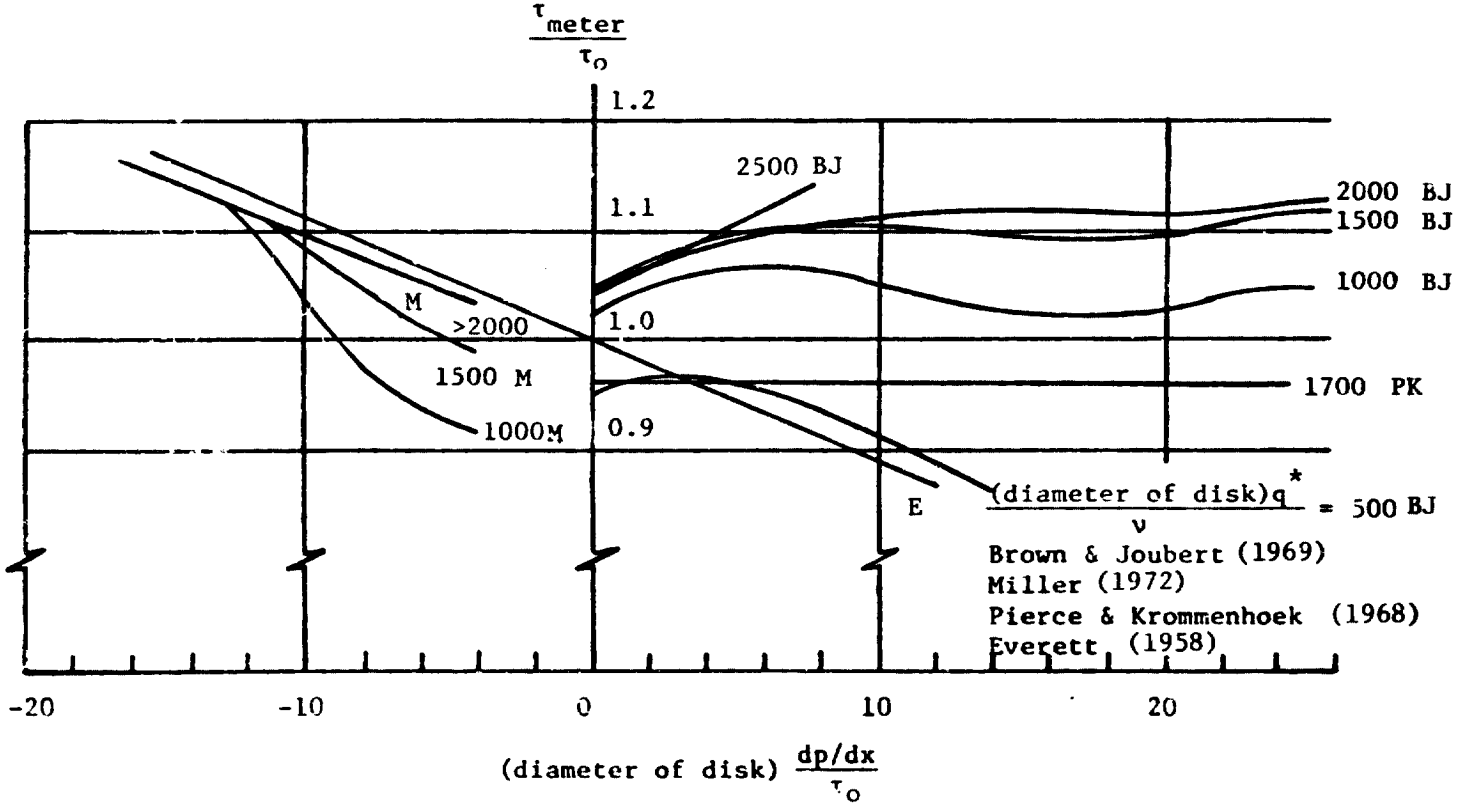

Fig. 3.15 Proposed Pressure Gradient Corrections for Two-Dimensional Floating Element Devices

Everett's (1958) work was completed in a high aspect ratio channel and he assumed fully developed flow to equate the wall shear and pressure gradient forces. The existence of nonuniform wall shear around the channel perimeter can be considered as such effects have been noted in some more recent studies but in the case of undeveloped flows. In their pipe studies Head and Rechenberg (1962) encountered wall shear differences of up to 20% around a pipe circumference, and Furuya, et al. (1975) and Bradshaw (1965) both reported flat surface spanwise wall shear differences of up to 10%, and de Bray (1965) discussed the spanwise nonuniformity of a nominally two-dimensional turbulent boundary layer on a flat surface. Additionally, the effect of a possible channel height nonuniformity must be considered. Ferriss (1965) presents an analysis for pipe flow showing tapers of 0.001 d_p (d_p = pipe diameter) in an axial distance of one diameter can cause the measured wall shear to deviate by 13% from the theoretical wall shear for his flow rates. Similar effects could occur in nearly parallel channel flows.

In the proposed Pierce and Krommenhoek (1968) floating element pressure gradient correction factors the reference wall shear was determined by taking a velocity profile over the floating element flow station for arbitrary pressure gradient and inferring the wall shear stress with a Clauser chart using Coles' (1962) law of the wall constants. Here it should be noted that the variation in inferred wall shear from different law at the wall constants is sufficient to alter the Pierce and Krommenhoek's pressure gradient correction. Additionally, the particular form of the near-wall similarity law used also can alter the inferred wall shear value in any such method.

Brown and Joubert (1969) used Preston tube wall shear readings as their reference wall shear using Patel's (1965) calibration curve. They reported their floating element wall shear values as consistent and generally 4-5% higher than the Preston tube results for a zero pressure gradient flow for a unit Reynolds number range of about 2×10^5 to 12×10^5/ft with this difference attributed to slight secondary forces on the floating element disk. In this study a comparison was made between 113 direct force shear measurements with 75 Preston tube shear values from a series of four different size Preston tubes for an essentially zero pressure gradient

flow over a similar but narrower unit Reynolds number range of about 2.4 x 10^6 to 4.4 x 10^6/ft. A statistical analysis for a second order fit to these two sets of data showed that the direct force shears also exceeded the Preston tube data, here by about 4% for the lower half of the Re/L interval with the difference decreasing nearly monotonically to about 0.4% at the upper end of this interval.

Miller's (1972) favorable pressure gradient results were the most recent of such studies and perhaps the most thorough. He was careful to maintain a uniform tunnel height ranging from 3.18→12.7 mm (0.125→0.5 in.) and to eliminate flow nonuniformity in the spanwise direction.

For the adverse pressure gradient corrections, Brown and Joubert arrived at correction curves from a multiple curvilinear regression surface using the variables of Fig. 3.15. Examining Fig. 3.15 several observations can be made. Firstly, the studies of Pierce and Krommenhoek and of Brown and Joubert are apparently in conflict for equal values of $d_m u^*/\upsilon$. One suggests positive corrections associated with adverse pressure gradients while the other suggests negative corrections. Although not shown in the figure Pierce and Krommenhoek's results show a nearly constant +3 to +5% correction required up to a value of the parameter $d_m \frac{dp/dx}{\tau_o} \simeq 33$. The correction from there out to a parameter value of 51 increases to +17%. Everett's simple correction formula seems to support Pierce and Krommenhoek's results qualitatively. However, Miller's studies in adverse pressure gradients appear to support Brown and Joubert's results but it should be recalled that Miller used the proposed Brown and Joubert corrections in his own results. In contradiction however, Miller's studies in favorable pressure gradients appear to be supported by Everett's formula. Winter (1977) joins the Miller favorable pressure gradient curves with those of Brown and Joubert for adverse pressure gradients and this requires a complete reversal of the direction of these curves, with no evidence of this kind of behavior reported by Miller.

For the zero pressure gradient case, Pierce and Krommenhoek's device read consistantly low by 3 to 5% when compared to wall shear determined from Clauser charts. Brown and Joubert's instrument read consistently high by 4 to 5% when compared to Preston tube measurements. These can be compared with Allen's instrument which read consistently low by 6% when

compared to Preston tube measurements. Miller does not report any data for his device in a zero pressure gradient flow. It should be noted that: (1) these errors are calculated under the assumption that the near-wall similarity laws, the law of the wall constants, and the instruments that depend on them can provide exact wall shear values, and (2) an approximate nominal ±5% uncertainty can exist between very carefully designed and constructed floating element devices reported on up to this time.

It is important to note that all such corrections are unique to the geometric details of the particular mechanical meter for which they were determined. Vinh (1973) shows experimental results comparing direct force shear values with Preston tube results for two geometrically different floating element buttons or discs. His results show strongly different pressure gradient effects on the nominal wall shear values suggesting a strong button geometry dependence. Generalization of any of the results in Fig. 3.15 to shear meters in general would not seem warranted in view of Vinh's results.

The edge thickness of the movable disk would appear related to possible errors in floating element results. Intuitively one would expect to minimize a pressure force by minimizing the element lip thickness. This is recommended and confirmed in the modeling of this effect by Brown and Joubert (1969). Yet contradicting this are the experimental results of Everett which show that a thicker lip minimizes pressure gradient corrections. The latter experiments were in favorable pressure gradients but the Brown and Joubert modeling of this effect does not appear to be restricted by the gradient direction. If in fact the pressure gradient effects appear as both direct pressure forces and as residual secondary forces attributable to secondary flows induced around and through the floating element clearance gap, as modeled by Brown and Joubert, it may well be that a thicker lip reduces the pressure gradient induced flow around the element thereby reducing these residual secondary forces. Supporting this hypothesis in Everett's recommendation to minimize the clearance to element lip thickness ratio.

Null type floating element designs have a uniform gap around the element and were used by Franklin (1961), Paros (1970), Allen (1977), Smith and Walker (1957), Boyce and Blick (1971), Miller (1972), and

Depooter, Brundrett, and Strong (1977). Nonuniform gap widths have been presumed to contribute some type of error but there is no quantitative estimate or analysis to suggest the possible error magnitude. The advantages of not having to null a displaced floating element are generally substantial.

The gap size has been considered as a roughness element exposed to the flow and varying solutions have been suggested to reduce this effect. Everett (1958) suggested a small gap size (minimizing the clearance to edge thickness ratio) while Allen (1977) recommended a larger gap as more desirable. Portions of the gap area have been treated as disk area assuming a shear stress is transmitted through the gap shear layer. Hakkinen's (1955) transonic flow studies used half the gap area as adding to the disk area while the transpiration study of Depooter, et al. (1977) used from 0.0 to 0.365 of the gap area, depending on the transpiration rate. Waltrup (1971) and Dershin, et al., (1967) reduced the gap effect by using an elliptic shaped disk. In contrast to these investigations is Dhawan's (1952) conclusion after using spark Schlieren photos and attempts at measuring the pressure disturbance caused by the gaps that no gap effect was present. White and Franklin (1964) also concluded the gap effect was negligible in their annulus work but their element size (a 10.16 cm (4.0 in.) diameter tube with a length of 10.16 cm (4.0 in.)) was large compared to the 0.0762 mm (0.003 in.) gap width.

No discussions of possible errors in direct force wall shear stress measurements in three-dimensional flows were found in the literature*. Clearly possible errors similar to those for single line of action meters used in 2DTBL flows can occur for unrestricted line of action devices as required in 3DTBL flows.

---

*As this report was going to press, Prof. Peter Joubert provided the authors with a copy of the doctoral dissertation of K. C. Brown entitled "Three-Dimensional Turbulent Boundary Layers," University of Melbourne, 1971. Portions of this thesis dealing with two-dimensional wall shear measurements with a direct force sensing single line of action device and pressure gradient corrections are published as Brown and Joubert (1969) and are discussed in this report. Regrettably, some very thorough work dealing with direct force wall shear measurements and an examination of the suitability of four similarity models in pressure driven 3DTBL flows contained in the thesis were not published and hence unknown to the authors for inclusion in the body of this report. Footnote references to this work appear in the text.

For three-dimensional flows the techniques employed for measurement of wall shear have been similar to those used in the two-dimensional case. The techniques employed include: Preston tube type probes by Pierce and Krommenhoek (1968), East and Hoxey (1969), Prahlad (1968, 1972, 1973), Power (1973), Hebbar and Melnik (1976), Dechow (1976); Stanton tubes by van den Berg and Elsenaar (1972); sublayer fences by Hebbar and Melnick (1976) and Vagt and Fernholz (1973); razor blades by East and Hozey (1969) and heated elements by Pierce and Krommenhoek (1968), McCrosky and Durbin (1972) and Higuchi and Peake (1978). All the above are indirect measurement techniques and were calibrated in two-dimensional flows. Only the work of Pierce and Krommenhoek (1968) includes three-dimensional measurements with a floating element device.

The direct force measurements by Pierce and Krommenhoek (1968) totaled only five data points. Their test flow was the boundary layer confining a jet impinging on a back wall. They compared their results with wall shear values inferred from a directionally sensitive heat meter, a Preston tube, and a yaw probe calibrated as a Preston tube. All the indirect devices were calibrated in a two-dimensional flow, and agreement between these devices and the floating element was within $\pm$10%. This would tend to indicate that the nondimensionalizing wall friction velocity is, for the limited flow studied, at least approximately related to wall shear in the same manner for both two- and three-dimensional flows. Regrettably, their experiment lacked a sufficient number of direct wall shear measurements, lacked companion velocity profiles, lacked static pressure data in the neighborhood of the measuring location, and used a floating element device unable to discern the direction of the wall shear vector.

On this last point, some further discussion is required, since the 3DTBL is seriously clouded by the question of limiting wall streamline direction and its accurate measurement. Most of the experiments noted earlier show two, three, or more velocity points in the very near-wall region which have the same direction when displayed as in Fig. 2.4, suggesting the existence of a collateral near-wall flow. The very careful measurements of Rogers and Head (1969) and Hebbar and Melnik (1976) using very small instrumentation and emphasizing spatial resolution show no region of near-wall collateral flow. Additionally, Pierce and East (1972)

and Klinksiek and Pierce (1973) have demonstrated in finite difference solutions to a 3DTBL flow where viscous stresses are retained in the motion equations that no near-wall collateral flow is predicted by the analysis. The question of modeling of the Reynolds stresses might be raised but is irrelevant since the turbulence modeling was suppressed in the very near-wall region (viscous sublayer) and made no contribution to the solution. In effect, in the extreme near-wall region the viscous boundary layer equations for the three-dimensional case were solved and in this viscous extreme near-wall region the solution indicated that the existence of a collateral boundary layer is inconsistent with the governing equations. Prahlad (1973) also presented work supporting these computer results which revealed local streamline turning in the immediate neighborhood of the wall. These results cloud the question of accurate measurement of limiting wall streamline direction. Preston tubes and similar devices have relatively poor spatial resolution and would be expected to respond to some average flow direction over their faces. The agreement found by Pierce and Krommenhoek between Preston tube and yaw probe directions and those obtained by a directionally sensitive surface-mounted heat meter suggests that the heat meter device also responds to thermal diffusion over a thin near-wall region through which velocity direction is varying, and hence the heat meter also appears to respond to an average near-wall flow direction. Unfortunately, in that experiment the determination of limiting wall streamline direction by the floating element device was not made because of the good agreement noted among the Preston tube, yaw probe, and heat meter. More recent work suggests that while indirect devices may sometimes give reasonable estimates of wall shear magnitude in 3DTBLs, surface-mounted indirect devices generally give erroneous information on wall shear direction.

More recently, the flush mounted type heat meter of the Pierce and Drinkuth (1966) type has been modified and miniaturized for use in three-dimensional flows. McCroskey and Durbin (1972) designed a two-element foil for direct application to the flow surface, and Higuchi and Peake (1978) modified the Rubesin et al. (1975) flush buried wire gage to include two wires for use in three-dimensional flows. The Higuchi and Peake two-wire meter is extremely small (typically 1/8" in diameter) and has the

potential to make measurements over very small local areas. It is essential to note that neither of these indirect devices has ever been calibrated in a three-dimensional flow. Only limited use has been reported for the McCroskey and Durbin gage and recent contact with one of its developers did not encourage use. Higuchi and Peake have reported on the use of two of the two-wire heat meters in a three-dimensional flow. Their report clearly shows that each element of the meter was calibrated only in a two-dimensional flow using a Preston tube as the 'primary' standard. Since the calibration of a Preston tube is in effect dependent on the two-dimensional near-wall similarity law, use of heat meters calibrated in a two-dimensional flow with a Preston tube in effect assumes a priori the validity of the two-dimensional near-wall similarity law in a three-dimensional flow. Such an assumption is unacceptable in any experiment designed to identify a near-wall similarity law in three-dimensional flows. Higuchi and Peak also calibrated the directional sensitivity of the two-element heat meters in a two-dimensional flow as well. Using these heat meters in a three-dimensional flow, they reported flow angle measurements differing typically by 5-15°, with occasional larger differences, when compared to standard wall flow visualization techniques. While shear magnitude data were reported for the heat meters for the three-dimensional flow, there were no other data available to validate the two-dimensional calibration of these two-element heat meters for use in a three-dimensional flow. It would seem unnecessary to emphasize that simply using such a device in a three-dimensional flow does not validate its two-dimensional calibration for use in a three-dimensional flow. Concerns over the use of two-dimensional calibrations of heat meters in three-dimensional flows were noted as early as 1966 by Pierce and Drinkuth (1966) when they suggested this technique for flush mounted wire type sensors.

Rubesin, et al. (1975) note that in a two-dimensional flow the calibration of a very fine wire heat meter in a laminar flow can be used in a turbulent flow. However, those authors note that the analysis itself which indicates this universality of calibration would introduce a nominal 10% error in such a universal calibration for two-dimensional turbulent flow. Combining this magnitude error with the other probable experimental errors of drift, meter resolution, etc., would likely result in an excessively

large uncertainty in using such a universal calibration in two-dimensional work. The possibility of such a universal calibration existing in a three-dimensional case has not been demonstrated and the simple extension of the two-dimensional model into a three-dimensional flow is highly suspect since this would appear to ignore the vector character of the near-wall flow in the three-dimensional case (e.g., Rogers and Head (1969), Hebbar and Melnik (1976), East and Pierce (1972) and Klinksiek and Pierce (1973)).

It should be clear that in any attempt at a definitive study of near-wall similarity in a three-dimensional turbulent flow, the need for local direct force wall shear measurement of both magnitude and direction is essential and absolute, the degree of difficulty required by such a measurement not withstanding.

Other than the work by Pierce and Krommenhoek (1968), only Prahlad (1968, 1972) appears to have sought to address the question of wall shear in near-wall similarity in three-dimensional flows. Prahlad used Preston tubes calibrated in two-dimensional flows to infer wall shear in the limiting wall streamline direction as determined by yaw probes. The objection to yaw probes to determine wall shear direction would be even stronger than cited above for the heat meter. Prahlad studied the flow around a cylinder and an inclined plate. His results for small skews suggest that a nondimensionalizing kind of wall friction velocity correlates his data. Since his measurement technique was indirect, it is impossible to conclude any direct relationship between the wall friction velocity and wall shear. Prahlad also noted two other results: (1) the effects of pressure gradients in three-dimensional flows appear to be qualitatively similar to those in two-dimensional flows, and (2) the larger Preston tubes give smaller values of wall shear than smaller Preston tubes. With regard to this last point, Prahlad notes, "This deviation implies departures from wall similarity and consequent errors in the use of the Preston tube technique in these flows."

In establishing the credibility of the omnidirectional shear meter used in this study, substantial measurements were made in a 2DTBL flow for comparison with the generally well accepted Preston tube method. A brief review of Preston tubes particularly as regards calibration equations

follows. The Preston tubes were chosen because then have been broadly studied in recent years and are considered reliable in two-dimensional flows, with reasonably well defined pressure gradient restrictions. For the interested reader Bertelrud (1974) and Allen (1973) contain bibliographies of Preston tube usage in high speed flows while Simpson and Whitten (1968) and Depooter, Brundrett, and Strong (1978) discuss Preston tube applicability in transpired turbulent boundary layers.

Since Preston (1954) first reported the technique of laying a Pitot tube on a solid boundary to indirectly measure the wall shear stress, many investigators have published their own calibration curves. Table 3.1 lists a number of calibration formulas for Preston tubes with round, open ends. Not included are the calibration results for rectangular Preston tubes by Quarmby and Das (1969). The calibration results in Table 3.1 were obtained under different conditions which are outlined in Table 3.2. Preston's (1954) calibration results are generally considered inaccurate and this prompted several studies before Patel's (1965) comprehensive results appeared. Patel's work is the most thorough as it is the only investigation to actually set usage limits depending on the type and severity of pressure gradient present in the flow. For adverse pressure gradients, Patel set as a rough guide a Preston tube operating range as

maximum 3% error $0 < \alpha < 0.01$, $q^*D/\upsilon \leq 200$

maximum 6% error $0 < \alpha < 0.015$, $q^*D/\upsilon \leq 250$

and for favorable pressure gradients

maximum 3% error $0 < \alpha < -0.005$, $q^*D/\upsilon \leq 200$ $d\alpha/dx < 0$

maximum 6% error $0 < \alpha < -0.007$, $q^*D/\upsilon \leq 200$ $d\alpha/dx < 0$

where

$$\alpha = \frac{y}{\rho u^{*3}} \frac{dp}{dx}$$

A subsequent study by Brown and Joubert (1969) suggest that 6% limits given above "are slightly optimistic."

It has been noted that Patel's three calibration equations do not match at the endpoints and one equation is transcendental in τ_o (the y^* variable). Head and Ram (1971) presented tabulated results for Patel's

Table 3.1 Preston Tube Calibration Equations

Investigator	Calibration Equations[#]	
Preston (1954)	$y^* = 0.1505 + 0.5x^*$	$2 \leq x^* \cdot 4.1$
	$y^* = -1.396 + 0.875x^*$	$4.1 \leq x^* \leq 6.5$
Head and Rechenberg (1962)	$y^* = -1.467 + 0.889x^*$	$5.14 \leq x \leq 6.94$
Ferriss (1965)	$y^* = -1.422 + 0.881x^*$	$4.79 \leq x^* \leq 6.38$
Smith and Walker (1958)	$y^* = -1.366 + 0.877x^*$	$5.0 \leq x^* \leq 7.5$
N.P.L. Staff (1958)	$y^* = -1.353 + 0.875x^*$	$5.25 \leq x^* \leq 7.20$
Patel (1965)	$y^* = 0.5x^* + 0.037$	$x^* < 2.90$
	$y^* = 0.8287 - 0.1381x^* + 0.1437x^{*2} - 0.006x^{*3}$	$2.9 \leq x^* < 5.60$
	$x^* = y^* + 21\log_{10}(1.95y^* + 4.10)$	$5.6 \leq x^* < 7.6$
Bertelrud (1976A)	$\frac{p_t - p}{\tau_o} = 38.85x^* - 88.53$	$4.80 < x^* < 7.72$

[#]Symbol Definitions

$$x^* = \log_{10}\left(\frac{\Delta p_p D^2}{4\rho\nu^2}\right) \qquad y^* = \log_{10}\left(\frac{\tau_o D^2}{4\rho\nu^2}\right)$$

D = Preston tube outer diameter

$\Delta p_p = p_t - p$

Table 3.2 Conditions Under Which the Preston Tube Calibration Equations Were Obtained

Investigator	Flow Type	Standard Used	Pressure Gradients Present	Tube Sizes (diameter)
Preston (1954)	Pipe	Pipe pressure dr[illegible]	$\frac{dP}{dx} > 0, < 0$	0.740 to 3.084 mm (0.02915 to 0.1214 in.)
Head and Rechenberg (1962)	Pipe	Sublayer fence	$\frac{dP}{dx} = 0, > 0, < 0$	0.597 to 9.520 mm (0.0235 to 0.3748 in.)
Ferris (1965)	Channel	Sublayer fence	$\frac{dP}{dx} = 0, > 0$	0.914 to 2.870 mm (0.036 to 0.113 in.)
Smith and Walker (1958)	Flat Plate	Floating element device	$\frac{dP}{dx} = 0$	0.762 and 3.091 mm (0.0300 and 0.1217 in.)
N.P.L. Staff (1958)	Flat Plate	Wake-traverse method and Stanton tubes	$\frac{dP}{dx} = 0$	1.194 to 3.175 mm (0.047 to 0.125 in.)
Patel (1965)	Pipe	Pipe pressure drop	$\frac{dP}{dx} = 0, > 0, < 0$	0.597 to 12.649 mm (0.0235 to 0.498 in.)
Bertelrud (1976A)	Pipe	Pipe pressure drop	no mention	0.599 to 18.999 mm (0.0236 to 0.748 in.)

calibration equations and Bertelrud (1976A) used the new variable instead of the y^* variable previously used in Preston tube calibrations. The Bertelrud calibration equation agrees well with Patel's results but the x^* range is limited with respect to the equivalent Patel range.

The relative ease in constructing and using Preston tubes has lead to their widespread usage and the basic Preston tube or variations of it have been used in attempts to measure wall shear stress in three-dimensional flows by Pierce and Krommenhoek (1968) Prahlad (1968, 1972, 1973), East and Hoxey (1969), Power (1973), Hebbar and Melnik (1976) and Dechow (1977). Without exception, these two-and three-dimensional studies used a two-dimensional calibration equation, usually Patel's (1965) calibration results.

The use of Preston tubes in three-dimensional flows requires the alignment of the Preston tube axis and the wall shear stress vector since misalignment can result in erroneous readings. Pierce and Krommenhoek used a heat meter to determine the wall shear stress direction and then aligned the Preston tube accordingly. In general, the other three-dimensional studies aligned the Preston tubes with the direction of the velocity vector nearest the wall as measured by a yaw type probe. This assumes the existence of collateral flow at the wall and the error of this assumption has already been discussed. Power (1973) using 1.651 mm (0.065 in.) and a 3.188 mm (0.1255 in.) diameter Preston tubes, reported C_f differences of 2% between the two different tube sizes. Differences of this magnitude could very well be caused by uncertainty in taking the data but Power believed the difference indicated "a possible effect of cross flow skew across a Preston tube diameter." Contrasting these remarks is Prahlad's (1972) work showing Preston tubes aligned with the local flow to be relatively insensitive for a misalignment of up to 20° between the tube axis and estimated wall shear stress direction.

The relative insensitivity of Preston tubes as reported by Prahlad (1972) can in part be solved by variations in the Preston tube design. Prahlad tested two variations of the regular Preston tube design, the single chamfered and Conrad probes shown in Fig. 3.16 each of which demonstrated greater yaw sensitivity than a regular Preston tube.

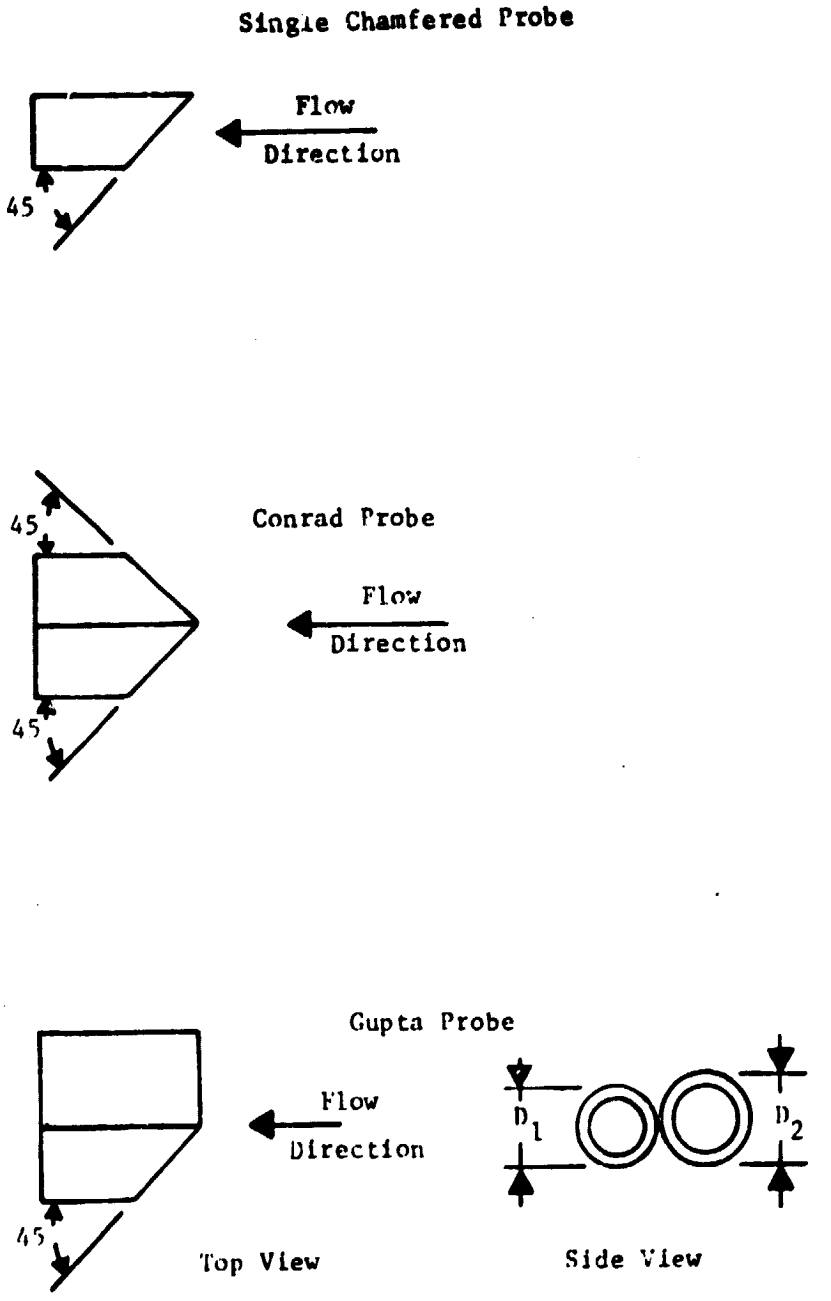

Fig. 3.16 Variations of the Preston Tube Design

The placement of the static pressure tap needed in Preston tube work can also cause errors in the measured wall shear stress. The readings from static pressure taps too close to the Preston tube opening are affected by the tube while taps located too far from the tube will give erroneous readings if pressure gradients exist, and the existence of transverse pressure gradients becomes important in three-dimensional flows. Gupta (1975) devised a variation of the Preston tube design also shown in Fig. 3.16 which does not use a static pressure tap. This design was only tested in a two-dimensional flow and its applicability to three-dimensional flows has not been determined but its geometry does offer some possibility of flow alignment by prior calibration in a uniform flow for possible use in a three-dimensional flow. Bertelrud (1976B, 1977) designed a probe which measures a modified static pressure with the tube itself as well as the total pressure. This device was only tested in a two-dimensional flow and while the geometry offers a more local pressure measurement, the probe is necessarily larger and does not appear to offer any convenient means of flow alignment in three-dimensional use.

IV. TWO-DIMENSIONAL MEASUREMENTS

Introduction

The principal purpose for taking two-dimensional measurements was to develop credibility in the omnidirectional meter and confidence estimates in the data acquisition techniques.

Static Pressure Field

The static pressure field was obtained over a 15.24 by 50.8 cm (6.0 by 20.0 in.) area for the tunnel speeds used. Very small spanwise variations were detected and overall the static pressure decreased in the flow direction showing approximately the same magnitude favorable pressure gradient of -13.57 Pa/m (-0.006 psi/ft) for all flow conditions.

Velocity Profiles

Velocity profiles were taken on the tunnel centerline over the Re/L range of 0.66 to 1.33 x 10^6/m. Velocity profiles were taken off the tunnel centerline at $\pm$5.08 cm (2.0 in) and $\pm$10.16 cm (4.0 in.) at nominal tunnel Re/L numbers of 1.12 x 10^6/m and 1.33 x 10^6/m. Table 4.1 lists the nominal Re/L numbers which were identified with letter designations for convenience in later use.

Different notation was used to identify tunnel centerline and off centerline two-dimensional velocity profiles. Centerline profiles are labeled as 2D X Y where X denotes the profile number and Y the particular tunnel Re/L as given in Table 4.1. Off centerline profiles are labeled as 2D$\pm$Z Y X where X and Y are interchanged but defined as before and Z is the distance in inches off the centerline with the sign convention shown in Fig. 4.1. For example, 2D 10 D indicates the tenth two-dimensional velocity profile run at the D tunnel speed while 2D+2 C 1 indicates the first two-dimensional velocity profile located two inches off the tunnel centerline at the C tunnel speed.

Data from 26 velocity profiles generally show small skewing is present in all cases, increasing in a monotone fashion toward the wall.

Table 4.1 Nominal Re/L by Letter Designation

Nominal Re/L(10^6/m)	Letter Designation
1.33	D
1.30	E
1.21	I
1.12	C
1.04	B
0.95	G
0.84	H
0.71	A

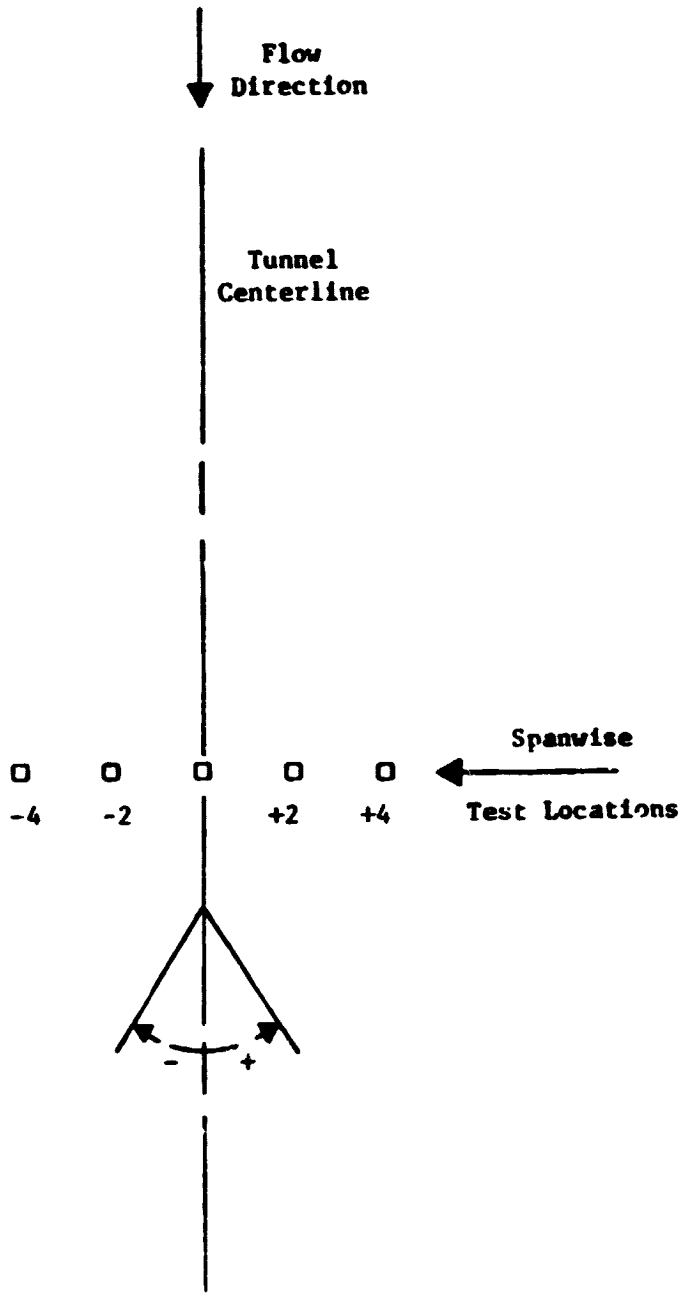

Fig. 4.1 Two-Dimensional Test Stations

This skewing ranges from 0° to a maximum of 1.6° with an average of 1.0° at the wall and is always positive as noted in Fig. 4.1, showing the same variability and extent on 18 centerline and 8 off centerline profiles and for the full range of tunnel flow conditions. Table 4.2 summarizes the range of this skewing.

Six representative velocity profiles are shown in the nondimensional form in Fig 4.2 showing excellent repeatability. Profiles taken by four individuals showed similar repeatability indicating that the velocity data acquisition system was not dependent on any one operator for repeatable measurements. Excellent repeatability is also shown in Fig. 4.3 for three other tunnel speeds. Figures 4.4 and 4.5 both show similar and anomolous spanwise nonuniformity at the tunnel test section for two different tunnel speeds. The centerline and left of centerline profiles at +2 and +4 inches show a very small spanwise variation of less than approximately 3% and this variation tends to be consistent with a very slight flattening of the profile away from the centerline. The profiles to the right of the centerline show a more dramatic but repeatable transverse variation that is difficult to explain. At the -2 inch position there is a clear flattening of the profile of the order of 5%, while at -4 inches off the centerline there is an opposite steepening of the profile, also of about 5%. No explanation could be found for these relatively large right of center variations but their existence is confirmed by their repeatability. Transverse measurements made on four inch centers 1.9 m upstream of the test section show no such variations with all profiles coincident within experimental uncertainties. Similar transverse measurements made 1. m upstream show an acceleration in the lower portion of the profile at the -4 in. station similar to but slightly less than that of the test section shown for profiles 2D-4C1 and 2D-4D1 in Figs. 4.4 and 4.5.

Bradshaw (1965) and de Bray (1965) have studied spanwise non-uniformity using Preston tube data while Furuya and Osaka (1975) looked at freestream velocity and turbulence intensity. Furuya, et al. (1975) have also studied spanwise non-uniformity through Preston tube and boundary layer velocity profile measurements which also showed similar skewing trends as the two-dimensional velocity profile data in this study. These investigators have generally concluded that these non-uniformities are due to screens with small open areas well upstream of

Table 4.2 Summary of 2D Profile Angle Variations

Nominal Speed	Re/L(10^6/m)	Angle Range
A	0.71	0.2 to 0.4
H	0.84	0. to 1.4
G	0.95	0. to 1.0
B	1.04	0. to 1.2
B	1.04	0. to 1.4
C	1.12	0. to 0.6
C	1.12	0.1 to 0.8
C+2	1.12	0. to 1.0
C+4	1.12	0. to 1.0
C-2	1.12	0. to 0.6
C-4	1.12	0. to 1.4
I	1.21	0. to 0.4
I	1.21	0. to 0.4
E	1.30	0. to 1.0
E	1.30	0. to 0.6
D	1.33	0. to 1.4
D	1.33	0. to 1.0
D	1.33	0. to 0.8
D	1.33	0. to 1.0
D	1.33	-0.2 to 1.0
D	1.33	-0.2 to 1.6
D	1.33	0.2 to 0.6
D+2	1.33	0. to 0.8
D+4	1.33	0. to 1.2
D-2	1.33	0. to 1.6
D-4	1.33	0. to 1.6

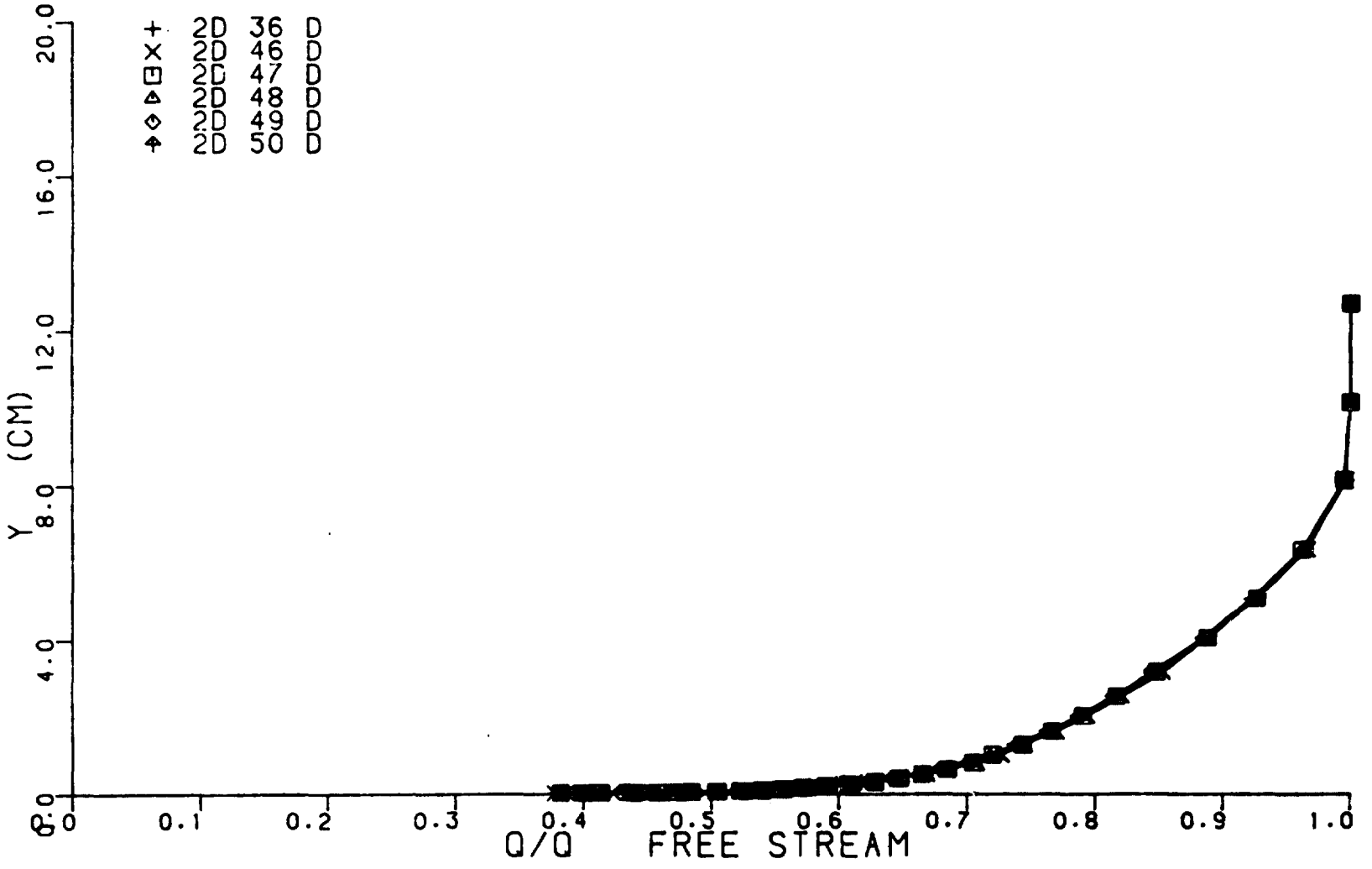

FIG. 4.2 VELOCITY PROFILES FOR CENTERLINE D RUNS.

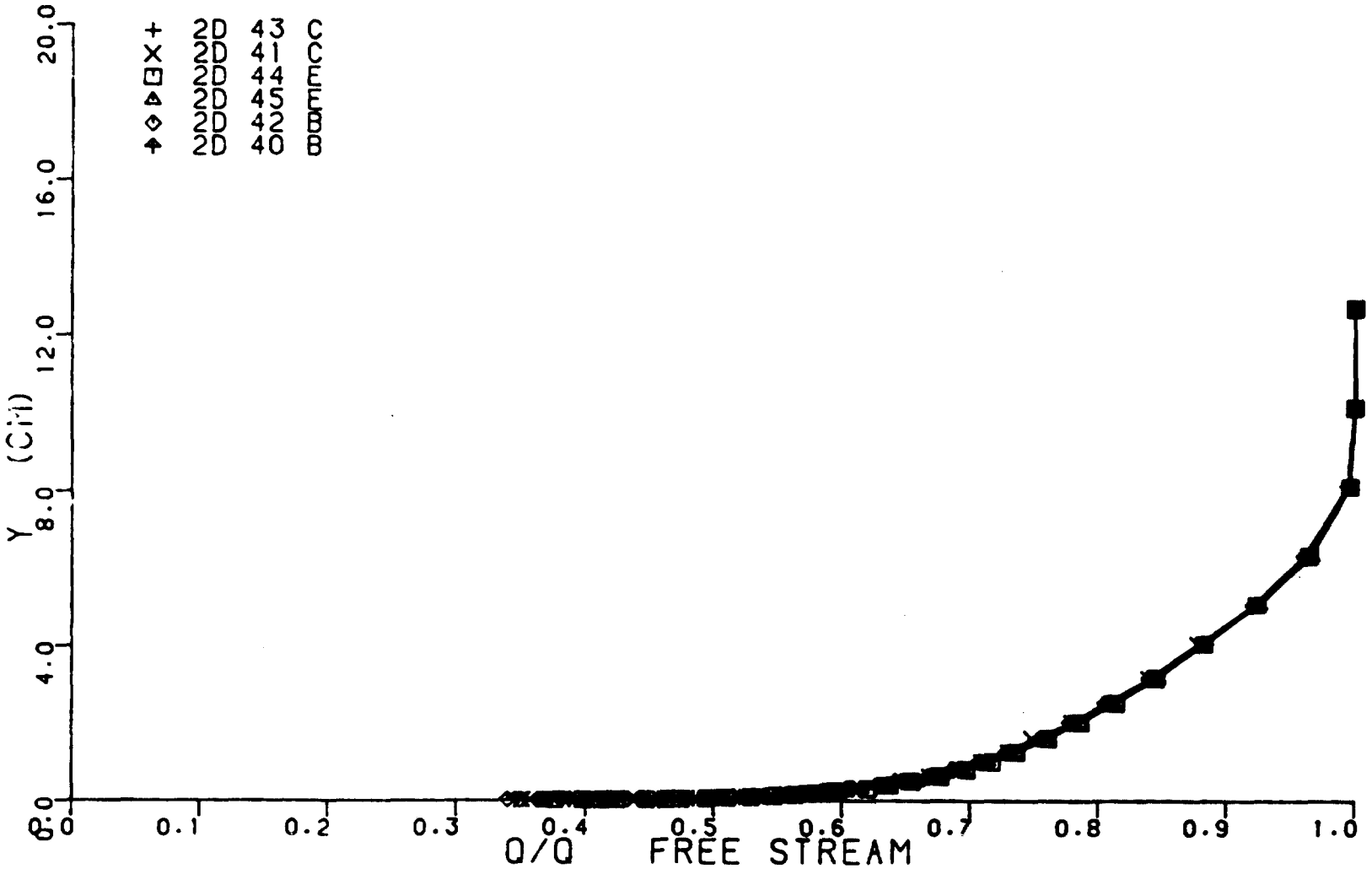

FIG. 4.3. VELOCITY PROFILES FOR CENTERLINE C.B. AND E RUNS.

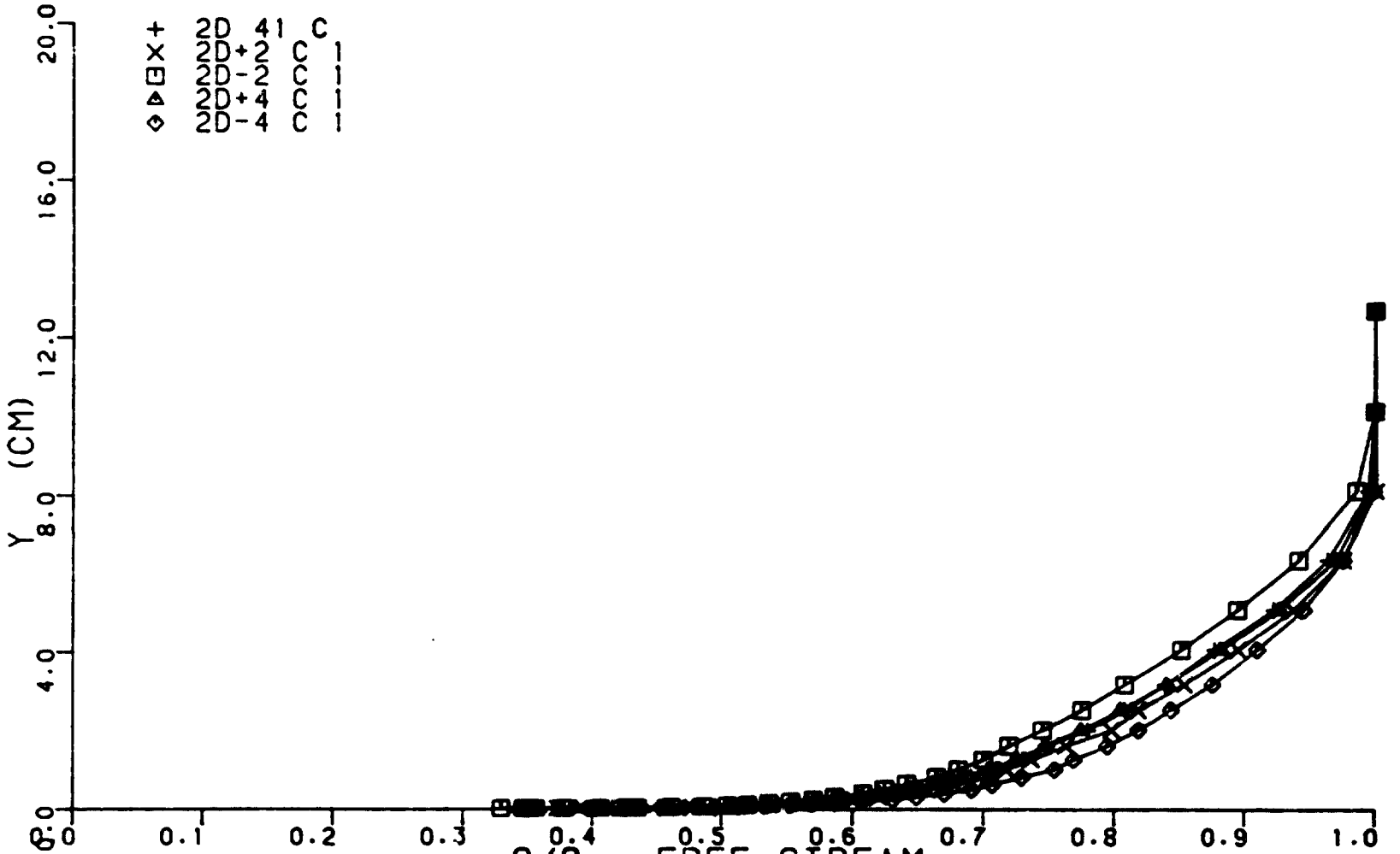

FIG. 4.4. VELOCITY PROFILES FOR SPANWISE C RUNS.

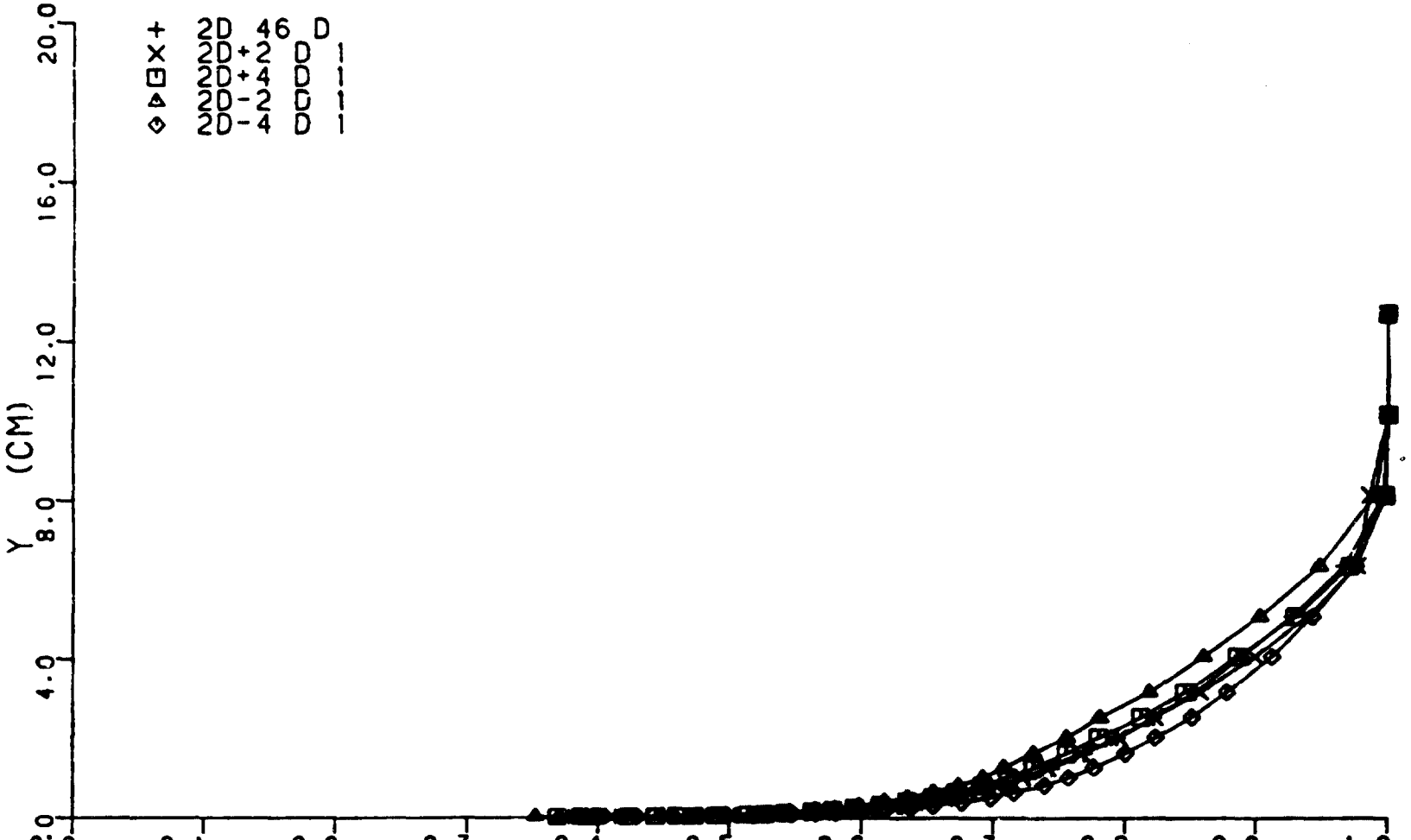

FIG. 4.5. VELOCITY PROFILES FOR SPANWISE D RUNS.

the data stations. An open area of 57% was suggested by Bradshaw, Furuya and Osaka, and de Bray as the lowest open area which could be used to insure minimal spanwise variations. Furuya, et al. made no recommendations on reducing spanwise variations. Bradshaw further stated that the 57% should only be taken as representative until other studies were conducted in other wind tunnels. De Bray's results showed that even when using screens with 60% open area the C_f spanwise variations were $\pm$8% which would suggest that the selection of the minimum screen open area of 57% does not always preclude sizeable spanwise variations in two-dimensional flow fields. The four screens at the entrance to the nozzle section of the tunnel used for this experiment each had an open area of 70% which is well above the value suggested by these various studies.

De Bray's (1965) work indicated that spanwise variations are less important for three-dimensional situations which "generally have large pressure gradients." The three-dimensional pressure-driven flow studied in the present experiment would fall into this category. All three-dimensional measurements were made with the body on the minus side of the text section as shown in Fig. 4.1, with the more uniform upstream flow in the region of measurements.

Direct Wall Shear Measurements

Direct wall shear measurements by the two-dimensional and omni-directional wall shear meters were taken over the tunnel Re/L range and representative data points are shown in Fig. 4.6. The results by Rule (1976) and Tennant (1977) are included because they were taken in the same tunnel several months before the present measurements and during this period both floating element meters were disassembled, inspected, and realigned, and the method of eddy current output measurement and LVDT output measurement was changed.

The repeatability in Fig. 4.6 demonstrates the ability to obtain data independent of personnel. Those readers interested in using Tennant's (1977) two-dimensional wall shear values (his Table A4) are advised of a computational error in his Re/L values.

The two-dimensional floating element wall shear results for the tunnel centerline are given in Tables 4.3 through 4.7. For the data

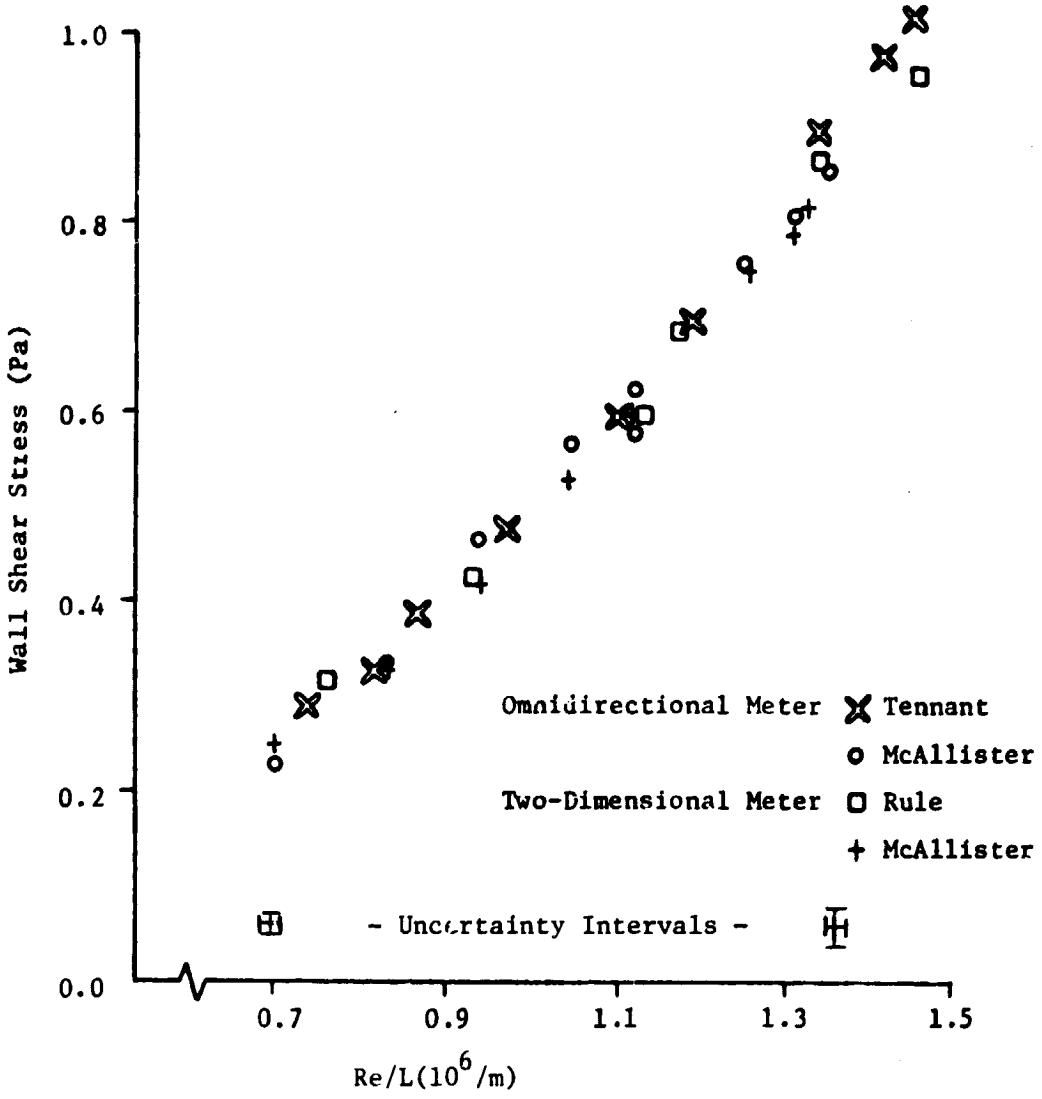

Fig. 4.6 Two-Dimensional Direct Wall Shear Measurements

TABLE 4.3 SET 1 OMNIDIRECTIONAL METER WALL SHEAR DATA.

TEMPERATURE (DEGREES C)	BAROMETRIC PRESSURE (MM OF HG)	INLET DELTA H (CM OF H20)	WALL SHEAR (PA)	WALL SHEAR UNCERTAINTY (PA)	ANGLE (DEGREES)	ANGLE UNCERTAINTY (DEGREES)	STATION	RE UNIT (1/M X 10**6)
26.1	709.7	2.888	0.85	0.021	-0.5	1.6	2D D	1.355
26.1	709.7	2.888	0.85	0.021	-0.7	1.7	2D D	1.355
26.1	709.7	2.888	0.85	0.020	-0.0	1.6	2D D	1.355
26.7	709.7	2.888	0.86	0.021	0.3	1.6	2D D	1.351
26.7	709.7	2.888	0.85	0.021	0.0	1.7	2D D	1.351
26.7	709.7	2.888	0.85	0.021	-0.1	1.6	2D D	1.351
26.7	709.7	2.734	0.81	0.020	0.3	1.7	2D E	1.315
26.7	709.7	2.729	0.81	0.020	0.2	1.7	2D E	1.314
26.7	709.7	2.729	0.81	0.020	0.4	1.7	2D E	1.314
26.7	709.2	2.489	0.76	0.020	-0.1	1.7	2D F	1.254
26.7	709.2	2.489	0.76	0.020	-0.1	1.7	2D F	1.254
26.7	709.2	2.489	0.75	0.019	0.1	1.7	2D F	1.254
26.7	709.2	1.996	0.63	0.017	0.9	1.8	2D C	1.123
26.7	709.2	1.996	0.63	0.017	0.7	1.8	2D C	1.123
26.7	709.2	1.996	0.63	0.017	0.4	1.8	2D C	1.123
26.7	709.2	1.753	0.57	0.017	1.0	1.9	2D B	1.052
26.7	709.2	1.753	0.58	0.016	0.8	1.8	2D B	1.052
26.7	709.2	1.753	0.57	0.016	1.1	1.8	2D B	1.052
26.7	709.2	1.400	0.47	0.014	1.1	1.9	2D G	0.940
26.7	709.2	1.400	0.48	0.014	1.7	1.8	2D G	0.940
26.7	709.2	1.407	0.48	0.014	1.0	1.9	2D G	0.943

TABLE 4.4 SET 2 OMNIDIRECTIONAL METER WALL SHEAR DATA.

TEMPERATURE (DEGREES C)	BAROMETRIC PRESSURE (MM OF HG)	INLET DELTA H (CM OF H2O)	WALL SHEAR (PA)	WALL SHEAR UNCERTAINTY (PA)	ANGLE (DEGREES)	ANGLE UNCERTAINTY (DEGREES)	STATION	RE UNIT (1/M X 10**6)
26.7	709.7	2.786	0.85	0.021	-0.4	1.7	2D D	1.327
26.7	709.7	2.789	0.85	0.021	-1.0	1.6	2D D	1.328
26.7	709.7	2.670	0.83	0.021	-1.4	1.7	2D E	1.299
26.7	709.7	2.720	0.82	0.021	-1.1	1.7	2D E	1.311
26.7	709.7	2.602	0.58	0.016	-0.0	1.8	2D C	1.125
26.7	709.4	1.994	0.57	0.015	-0.1	1.8	2D C	1.123
26.7	709.4	0.782	0.23	0.011	2.0	2.8	2D A	0.703
26.7	709.4	0.782	0.23	0.011	2.4	2.9	2D A	0.703
26.7	709.4	2.769	0.82	0.020	0.5	1.6	2D D	1.323
26.1	712.7	2.794	0.86	0.020	-0.6	1.6	2D D	1.335
26.7	712.7	2.794	0.84	0.020	-1.0	1.6	2D D	1.332
26.7	712.5	2.794	0.82	0.020	-0.5	1.6	2D D	1.332
26.7	712.5	2.791	0.83	0.020	-1.5	1.6	2D D	1.331
27.2	712.0	2.784	0.81	0.021	-1.3	1.7	2D D	1.325
27.2	712.0	2.786	0.81	0.020	-1.5	1.7	2D D	1.326
27.2	712.2	2.786	0.82	0.020	-1.7	1.6	2D D	1.326
28.3	712.2	2.776	0.79	0.020	-1.8	1.7	2D D	1.318
28.3	711.7	2.784	0.78	0.020	-0.7	1.7	2D D	1.320
28.3	711.5	2.774	0.78	0.021	-1.4	1.8	2D D	1.317
28.9	707.4	2.769	0.79	0.020	-0.9	1.7	2D D	1.309
27.2	710.2	2.771	0.81	0.021	-0.4	1.7	2D D	1.321
27.2	710.9	2.784	0.80	0.021	-1.2	1.7	2D D	1.325
27.2	711.5	2.774	0.79	0.021	-0.6	1.7	2D D	1.323
26.7	711.5	2.766	0.80	0.021	-0.9	1.7	2D D	1.324
26.7	710.7	2.776	0.81	0.019	-0.4	1.6	2D D	1.326
26.7	709.9	2.774	0.82	0.021	-1.4	1.7	2D D	1.324
26.1	708.7	2.776	0.79	0.020	0.1	1.6	2D D	1.327
26.7	708.7	2.776	0.80	0.021	-0.6	1.7	2D D	1.324
26.7	709.2	2.764	0.78	0.021	-1.3	1.8	2D D	1.321
25.6	709.4	2.771	0.84	0.021	-0.0	1.7	2D D	1.330

TABLE 4.5 SET 2 OMNIDIRECTIONAL METER WALL SHEAR DATA.

TEMPERATURE (DEGREES C)	BAROMETRIC PRESSURE (MM OF HG)	INLET DELTA H (CM OF H20)	WALL SHEAR (PA)	WALL SHEAR UNCERTAINTY (PA)	ANGLE (DEGREES)	ANGLE UNCERTAINTY (DEGREES)	STATION	RE UNIT (1/M X 10**6)
26.1	710.2	2.771	0.82	0.022	-0.8	1.7	2D D	1.327
26.1	710.2	2.771	0.80	0.022	-0.6	1.8	2D D	1.327
26.1	710.2	2.784	0.81	0.020	-0.7	1.6	2D D	1.331
27.2	709.9	2.766	0.82	0.022	-1.2	1.7	2D D	1.319
27.2	705.4	2.756	0.79	0.021	0.2	1.8	2D D	1.313
27.2	705.1	2.743	0.77	0.020	-0.5	1.7	2D D	1.309
25.6	708.7	2.779	0.82	0.019	1.6	1.6	2D D	1.331
26.1	710.2	2.779	0.83	0.021	0.3	1.6	2D D	1.329
26.1	710.2	2.779	0.80	0.019	-0.6	1.6	2D D	1.329
26.7	709.9	2.769	0.86	0.021	0.8	1.6	2D D	1.323
26.7	709.7	2.766	0.85	0.022	0.6	1.7	2D D	1.322
26.7	709.7	2.766	0.83	0.021	-1.1	1.7	2D D	1.322
26.7	709.7	2.774	0.83	0.021	-0.1	1.7	2D D	1.324
26.7	710.2	2.776	0.84	0.021	-1.6	1.7	2D D	1.325
26.7	710.4	2.776	0.84	0.020	-1.0	1.6	2D D	1.326
26.1	712.2	2.781	0.85	0.020	-1.3	1.6	2D D	1.332
26.7	712.2	2.781	0.82	0.029	-1.1	2.2	2D D	1.328
26.7	714.8	2.799	0.84	0.023	-1.8	1.8	2D D	1.335
26.7	715.0	2.794	0.83	0.022	-1.7	1.7	2D D	1.334
26.7	714.8	2.791	0.83	0.021	-0.5	1.7	2D D	1.333
26.7	714.5	2.791	0.80	0.019	-1.4	1.6	2D D	1.333
26.7	714.5	2.791	0.82	0.031	-1.5	2.3	2D D	1.333
26.7	714.5	2.791	0.80	0.020	-1.6	1.7	2D D	1.333
26.7	718.8	2.809	0.85	0.021	-0.4	1.6	2D D	1.341
26.7	719.3	2.812	0.83	0.020	-0.6	1.7	2D D	1.342
27.8	713.5	2.781	0.84	0.022	-1.6	1.7	2D D	1.323
27.8	713.5	2.771	0.85	0.020	-0.6	1.6	2D D	1.320
28.9	713.5	1.110	0.34	0.011	2.8	2.0	2D M	0.832
28.9	713.5	1.110	0.33	0.012	2.3	2.2	2D M	0.832

TABLE 4.6 SET 3 OMNIDIRECTIONAL METER WALL SHEAR DATA.

TEMPERATURE (DEGREES C)	BAROMETRIC PRESSURE (MM OF HG)	INLET DELTA H (CM OF H20)	WALL SHEAR (PA)	WALL SHEAR UNCERTAINTY (PA)	ANGLE (DEGREES)	ANGLE UNCERTAINTY (DEGREES)	STATION	RE UNIT (1/M X 10**6)
26.7	707.4	2.779	0.83	0.020	1.5	1.6	2D D	1.323
26.1	707.4	2.779	0.83	0.021	1.2	1.7	2D D	1.327
26.1	707.6	2.700	0.81	0.020	1.2	1.7	2D E	1.308
26.1	708.2	2.779	0.84	0.021	1.8	1.7	2D D	1.327
26.1	708.4	2.779	0.84	0.022	1.5	1.7	2D D	1.328
26.1	708.7	2.779	0.84	0.021	1.5	1.7	2D D	1.328
26.1	708.7	2.703	0.80	0.022	1.3	1.8	2D E	1.310
26.1	708.7	2.705	0.81	0.022	0.4	1.8	2D E	1.310
26.1	708.7	2.349	0.71	0.019	1.2	1.8	2D I	1.221
26.7	708.7	2.344	0.72	0.020	1.3	1.8	2D I	1.217
26.7	708.7	1.979	0.60	0.017	1.1	1.8	2D C	1.118
26.7	703.9	1.979	0.61	0.018	1.6	1.9	2D C	1.118
26.7	708.9	2.779	0.83	0.020	1.5	1.7	2D D	1.325
26.7	708.9	1.737	0.54	0.015	1.6	1.8	2D B	1.048
26.7	708.9	1.737	0.54	0.016	1.3	1.9	2D B	1.048
26.7	708.9	1.417	0.46	0.016	1.0	2.2	2D G	0.946
26.7	709.2	2.779	0.85	0.021	1.5	1.7	2D D	1.325
26.7	709.2	1.389	0.46	0.015	1.9	2.0	2D G	0.937
26.7	709.2	1.110	0.38	0.013	1.4	2.2	2D H	0.837
26.7	709.2	1.092	0.38	0.013	1.2	2.1	2D H	0.831
26.7	709.2	0.787	0.28	0.013	-1.1	2.8	2D A	0.705
26.7	709.2	0.787	0.28	0.012	0.6	2.7	2D A	0.705
26.7	709.2	1.427	0.46	0.017	0.7	2.3	2D G	0.950
26.7	709.2	1.966	0.61	0.016	1.8	1.7	2D C	1.120
26.7	709.2	2.784	0.83	0.022	1.0	1.8	2D D	1.325
26.7	707.4	2.769	0.83	0.021	1.8	1.7	2D D	1.321
26.7	706.9	2.771	0.83	0.021	1.0	1.7	2D D	1.321
26.1	709.9	2.791	0.85	0.031	1.7	2.2	2D D	1.332
26.7	715.3	2.802	0.80	0.020	1.3	1.7	2D D	1.336
26.7	715.3	2.804	0.82	0.020	1.5	1.7	2D D	1.337

TABLE 4.7 SET 3 OMNIDIRECTIONAL METER WALL SHEAR DATA.

TEMPERATURE (DEGREES C)	BAROMETRIC PRESSURE (MM OF HG)	INLET DELTA H (CM OF H2O)	WALL SHEAR (PA)	WALL SHEAR UNCERTAINTY (PA)	ANGLE (DEGREES)	ANGLE UNCERTAINTY (DEGREES)	STATION	RE UNIT (1/M X 10**6)
26.7	715.3	1.974	0.58	0.018	1.2	1.9	2D C	1.121
26.7	715.3	1.974	0.59	0.017	1.2	1.8	2D C	1.121
26.7	714.2	2.799	0.83	0.022	2.2	1.7	2D D	1.335
26.7	714.5	2.799	0.81	0.020	1.9	1.7	2D D	1.335
26.7	714.5	2.819	0.80	0.021	1.0	1.7	2D-2 D	1.340
26.7	714.5	2.819	0.78	0.022	1.6	1.8	2D-2 D	1.340
26.7	714.2	2.807	0.75	0.019	1.5	1.7	2D-2 D	1.336
26.7	714.2	2.807	0.76	0.021	1.3	1.8	2D-2 D	1.336
26.7	714.0	1.986	0.53	0.016	1.7	2.0	2D-2 C	1.124
26.7	714.0	1.986	0.56	0.016	2.0	2.0	2D-2 C	1.124
26.7	711.5	2.779	0.79	0.022	2.5	1.8	2D-2 D	1.327
26.7	709.7	2.776	0.78	0.018	2.1	1.6	2D-2 D	1.325
27.2	708.7	2.776	0.87	0.021	3.0	1.7	2D+2 D	1.321
27.2	708.7	2.776	0.86	0.021	3.0	1.6	2D+2 D	1.321
27.2	708.7	2.776	0.86	0.023	2.7	1.7	2D+2 D	1.321
27.2	708.7	1.958	0.61	0.018	2.6	1.9	2D+2 C	1.109
27.2	708.7	1.958	0.60	0.015	2.7	1.7	2D+2 C	1.109
26.7	708.9	2.774	0.87	0.021	3.8	1.6	2D+2 D	1.324
27.2	707.1	2.753	0.84	0.021	2.9	1.7	2D+2 D	1.314
27.2	707.1	2.753	0.85	0.021	3.4	1.7	2D+4 D	1.314
27.2	707.1	2.753	0.85	0.021	3.2	1.7	2D+4 D	1.314
27.2	707.1	1.989	0.60	0.016	3.1	1.7	2D+4 C	1.117
27.2	707.1	1.989	0.62	0.018	3.4	1.9	2D+4 C	1.117
27.8	707.1	1.989	0.64	0.017	0.9	1.7	2D-4 C	1.114
27.8	709.7	1.989	0.64	0.018	0.7	1.8	2D-4 C	1.116
27.2	709.7	2.753	0.86	0.021	0.5	1.6	2D-4 D	1.316
27.8	709.7	2.753	0.87	0.021	0.2	1.6	2D-4 D	1.313

in Tables 4.6 and 4.7 the freestream velocity was measured simultaneously with the wall shear for C_f calculations. These C_f values are compared with those calculated for the Ludwieg-Tillmann formula

$$C_f = 0.246 Re_\theta^{-0.268} 10^{-0.678H}$$

and easily overlap when the uncertainties are considered as shown in Fig. 4.7.

The wall shear uncertainties were determined from the Kline-McClintock (1953) propagation method with contributions from drift, vertical misalignment, angular misalignment, calibration sensitivity, area uncertainty, and voltage readout and are intended to at least approach an Nth order uncertainty estimate as described in Moffat (1980).

Two-dimensional omnidirectional wall shear stress data were taken in three sequences and the data in Fig. 4.6 are representative of these three sequences. Figure 4.8 shows the repeatability among the three data sets and Tables 4.3-4.7 contain all the two-dimensional tabulated data. Station identification is as follows. For centerline values 2D Y is a two-dimensional run where Y indicates the tunnel Re/L. For off-centerline values 2D$\pm$Z Y is a two-dimensional run where Y again indicates the tunnel Re/L and Z is the distance in inches off the tunnel centerline after Fig. 4.1.

While the uncertainty was uniquely dependent on the individual wall shear conditions, representative omnidirectional meter uncertainty characteristics are presented in Fig. 4.9 and 4.10 as a constant magnitude value shear typical of the D series unit Reynolds number was rotated off the tunnel centerline to determine the directional sensitivity of the meter. In these figures a 0.86 Pa wall shear stress was rotated 180° off the tunnel centerline to show the effects of a given wall shear stress orientation. It is noted that these figures would change somewhat, generally showing larger uncertainties for smaller shear values.

The larger number of two-dimensional wall shear values at Re/L = 1.327×10^6/m for data Sets 2 and 3 allowed Figs. 4.11 and 4.12 to be constructed. In Fig. 4.11 for data Set 2 the average τ_o was 0.82 $\pm$ 0.02 Pa. The estimated uncertainties encompassed all but four of the twenty-four shear values. In Fig. 4.12 for data Set 3 the average τ_o was 0.83 $\pm$ 0.02 Pa and fourteen of fifteen data points fell within the uncertainty

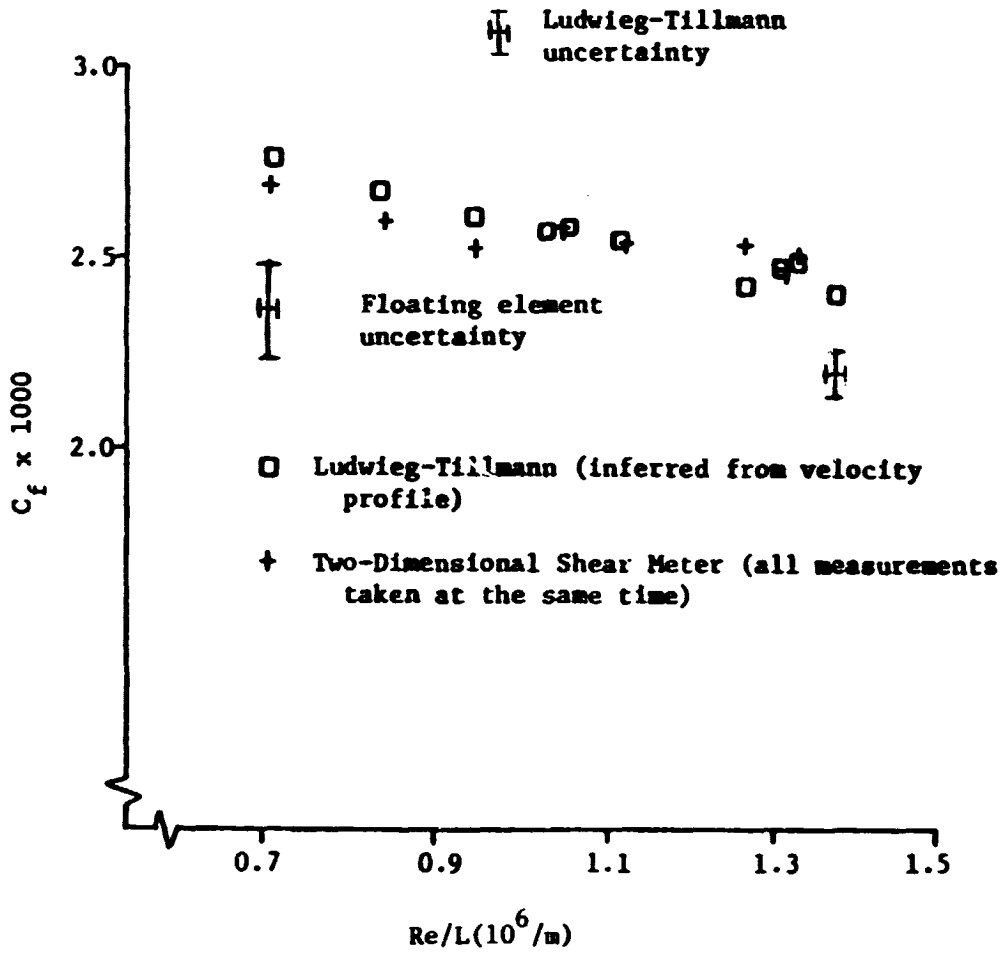

Fig. 4.7 C_f Results for the Two-Dimensional Floating Element and Velocity Profiles

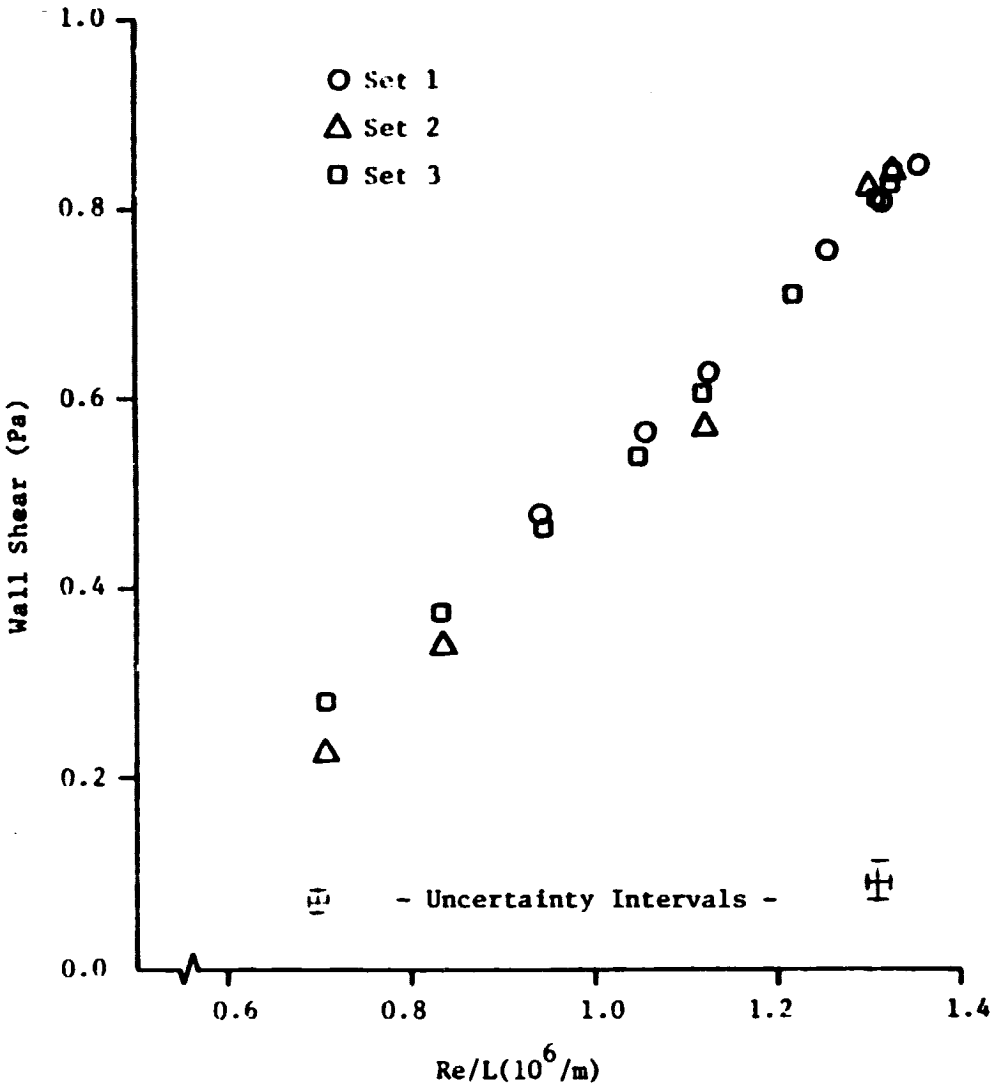

Fig. 4.8 Two-Dimensional Wall Shear Data Taken With the Omnidirectional Floating Element.

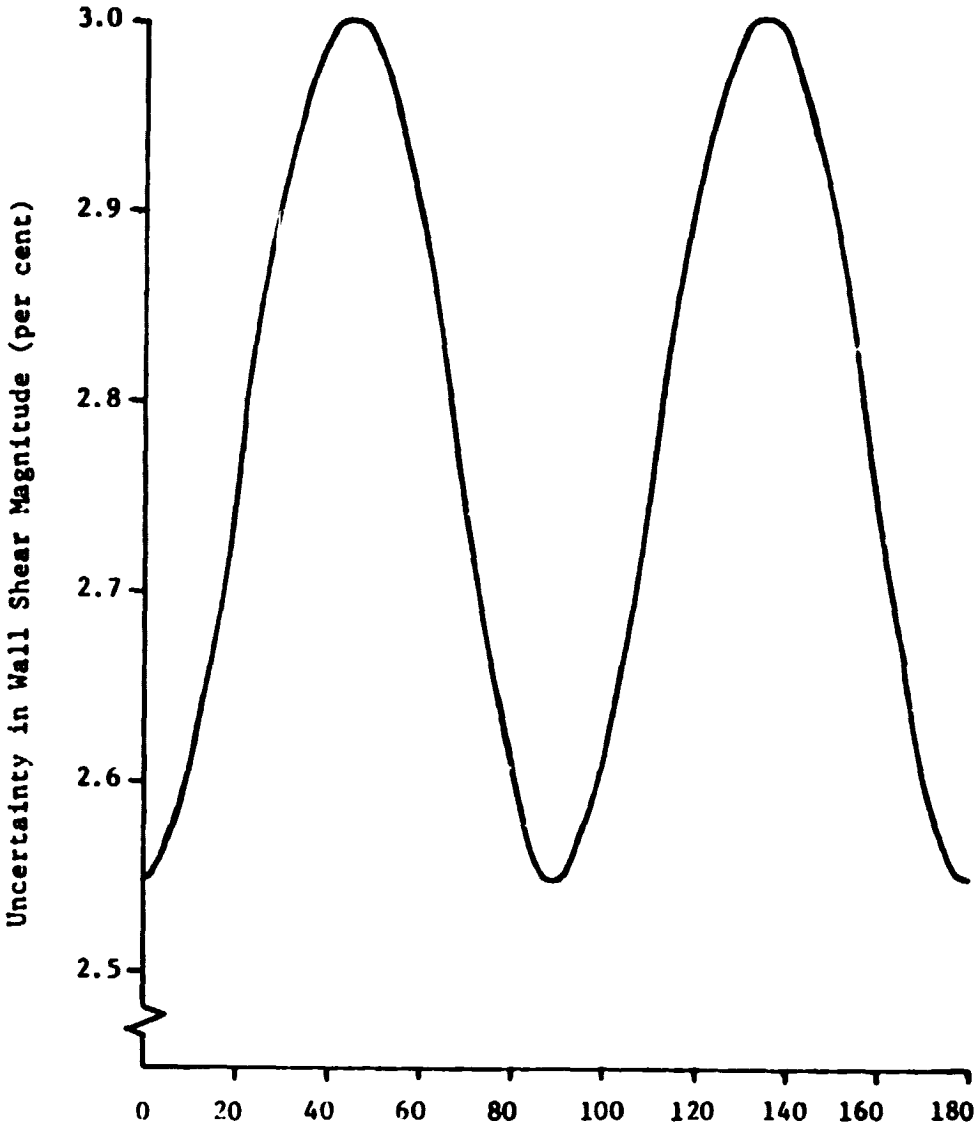

Fig. 4.9 Variation in Wall Shear Magnitude Uncertainty as a Constant Magnitude Shear Stress is Rotated off the Tunnel Centerline

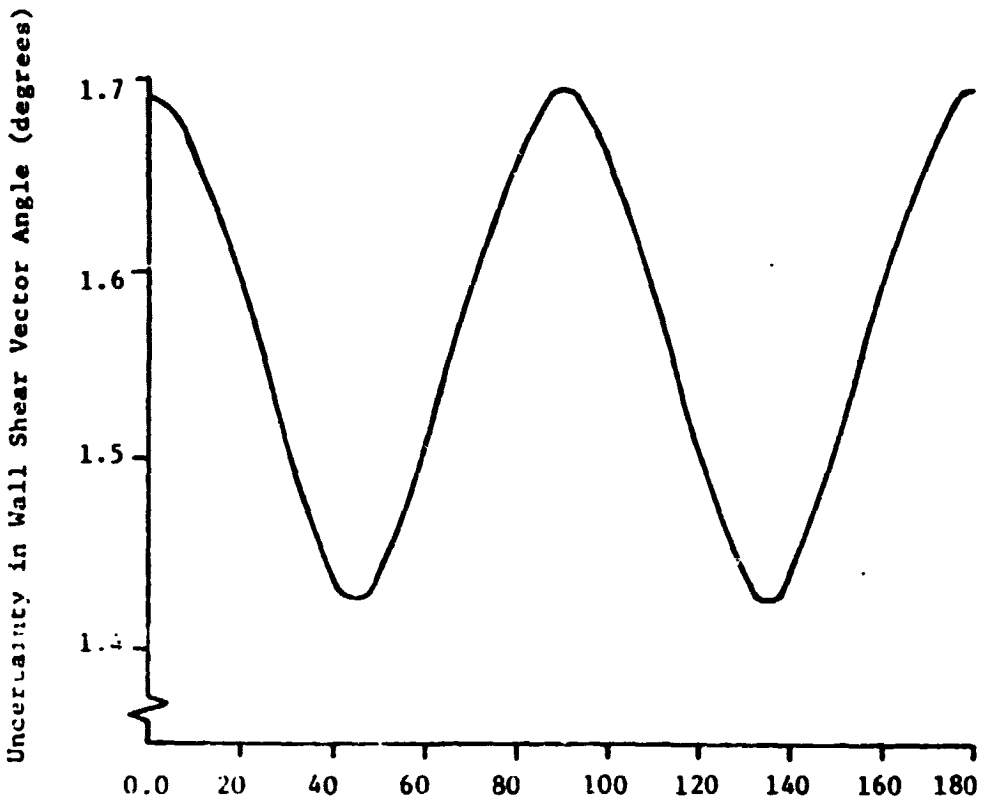

Fig. 4.10 Variation in Wall Shear Angular Uncertainty as a Constant Magnitude Shear Stress is Rotated off the Tunnel Centerline

$Re/L = 1.327 \pm 0.004 \times 10^6/m$

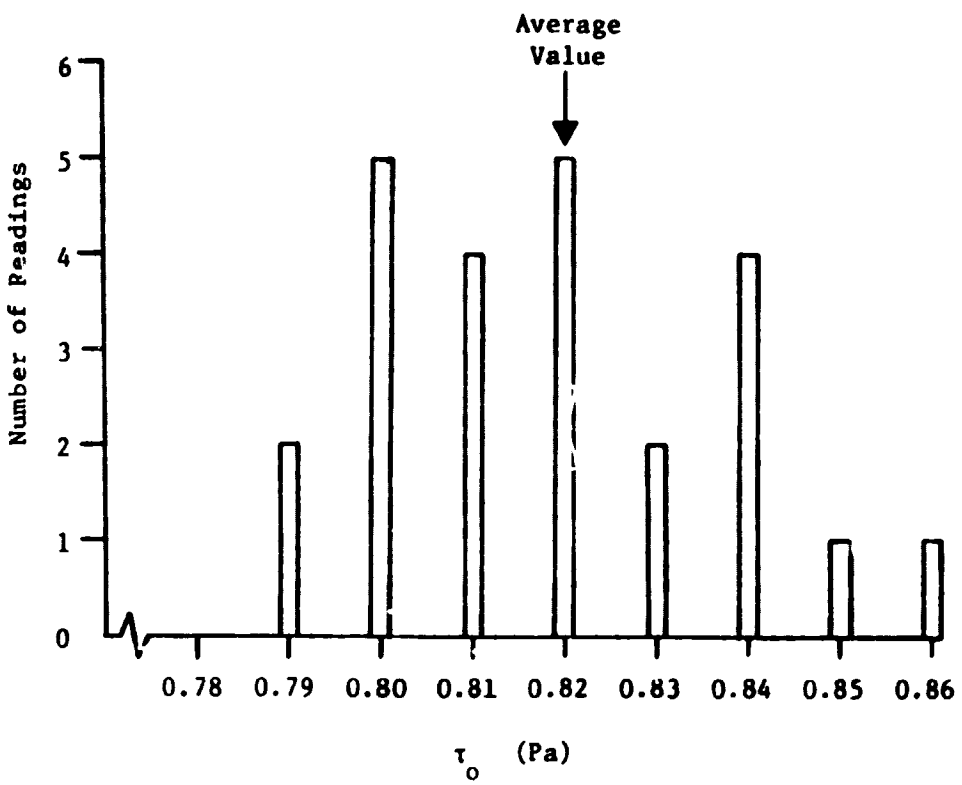

Fig. 4.11 Set 2 Omnidirectional Meter Results for $Re/L = 1.327 \times 10^6/m$

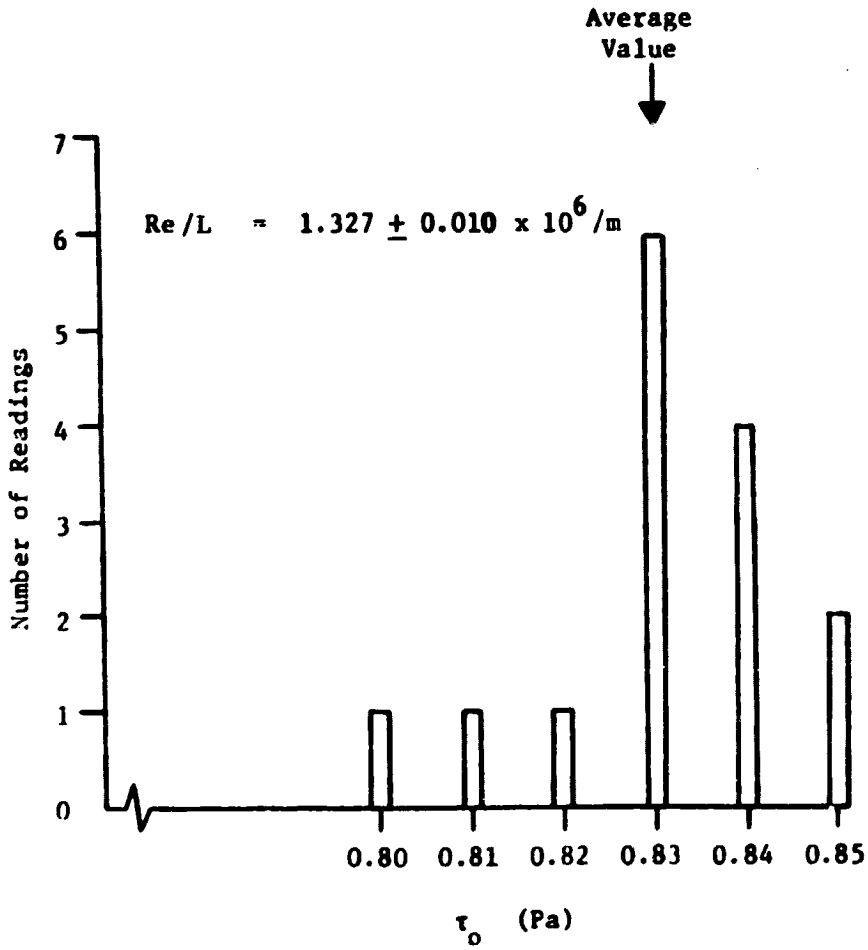

Fig. 4.12 Set 3 Omnidirectional Meter Results for Re/L = 1.327×10^6/m

range. Examining Fig. 4.8, the data of Set 3 is taken to be the most consistent when comparing these results to an imagined line through all the data points. The slight tendency for the Set 2 results to vary from this mean is reflected in the four poor data points noted above. The additional care and experience which went into the Set 3 results indicates a greater degree of repeatability. Overall, the uncertainty values used in these shear data are estimated to be valid at 15:1 odds since this reflects the added experience and improved techniques that were acquired through these three data sets and these odds are suggested by the third data set. In the various comparisons made among these two-dimensional shear stress values odds of 20:1 are assumed so that the tabulated uncertainties in Tables 4.3-4.7 were increased by 6% in such comparisons.

In examining the wall shear data in Sets 1, 2, and 3 in Tables 4.3-4.7 the small variations in the angular orientation of the wall shear vector exhibits an interesting pattern. In Sets 1 and 3 the wall shear vector angle while small is positive for all but one data point while the Set 2 angles are small but predominantly negative. Since all the data in Sets 1, 2, and 3 were taken in the same tunnel facility, the angular differences were judged to result from two sources. First, small differences in the alignment of the movable element with the omnidirectional meter housing (vertical disk misalignment) could cause small changes in the τ_o direction. This misalignment was measured at eight equally spaced points on the disk circumference for each data set with only one point no more than 0.0127 mm (0.0005 in.) above the meter housing, and at most only one point no lower than 0.0127 mm (0.0005 in.) below the meter housing. This small misalignment is estimated to have had a minimal effect on the τ_o magnitude and is supported by the agreement in τ_o values for the different data sets at similar Re/L values. The second source of angular uncertainty could result from the misalignment of the tunnel centerline and a line bisecting the 90° angle between the two proximitor probes. This is considered the most likely source for the angular differences because of the difficulty in precisely making this alignment. The line of action for all the τ_o vectors at similar tunnel Re/L are contained within the angle uncertainty calculated for that Re/L.

Representative values of skin friction coefficient are shown in Fig 4.13 for data from Set 3 where wall shear and freestream velocity were measured simultaneously and compared to Ludwieg-Tillmann values. Agreement is considered good for all Re/L values since the Ludwieg-Tillmann and direct wall shear stress C_f values overlap when the uncertainty bands are considered. It is important to point out that the uncertainty estimated in the reported calculated C_f values for the Ludwieg-Tillmann formula reflect only probable errors in the calculation of input data to the formula from laboratory measurements. No probable error is assigned to the formula itself and this is not realistic since the formula is not likely to be absolutely correct in its predictions. As noted by White (1974), an uncertainty as high as $\pm$10% can be assigned to the Ludwieg-Tillmann formula itself. Including such an added probable error in the estimated uncertainties shown for the Ludwieg-Tillmann formula would increase these significantly and place all the data in good agreement within such combined uncertainty bands.

Preston Tube Measurements

Four different Preston tubes were used to indirectly measure the wall shear stress using the calibration equations in Table 3.2 with data obtained over an Re/L range of 0.7 to 1.35 x 10^6/m. The tunnel inlet unit Reynolds number was again used to insure similar tunnel flow conditions between the Preston tube and direct force measurements. Freestream velocities over the measuring station ranged from 12.9 to 24.4 m/sec. An essentially constant magnitude, small favorable pressure gradient of -13.57 Pa/m existed for all tunnel flow conditions.

Wall shear stresses calculated from the various Preston tube calibration equations reviewed in Chapter III and compared to the direct force measurements are shown in Figs. 4.14-4.17. Figure 4.14 compares the four different sizes of Preston tubes to the original Preston tube calibration equations. It is clear that the tube size is not properly accounted for in these calibration equations. Figure 4.15 compares the N.P.L. (1958), the Ferris (1965), the Bertelrud (1974), and the Smith and Walker (1958) calibration equation results to the direct force measurements. Figure 4.16 shows the results of the Patel (1965) intermediate range formula for

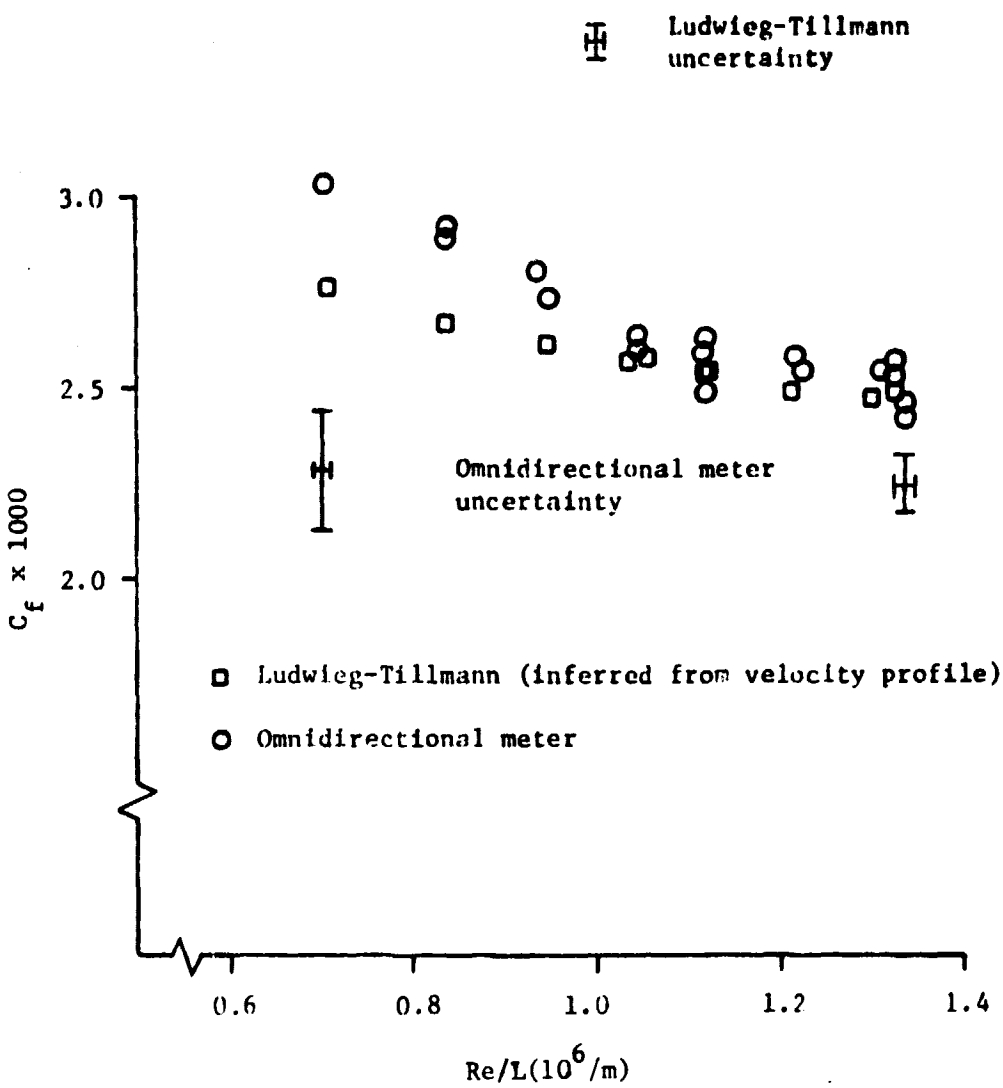

Fig. 4.13 C_f Results from Simultaneous τ_o and Q_∞ Measurements

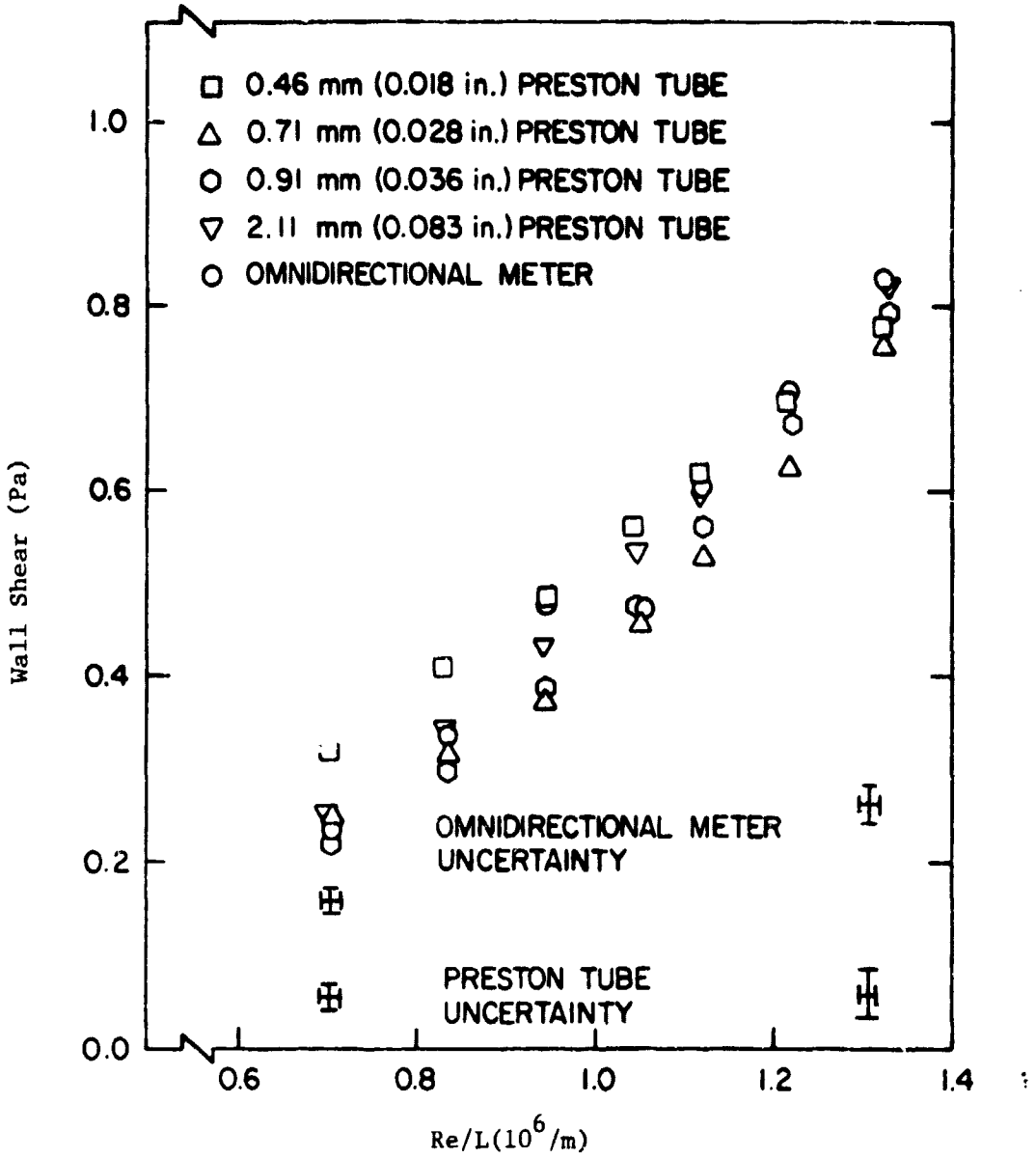

Fig. 4.14 Preston Tube Results Using the Preston Calibration Equations

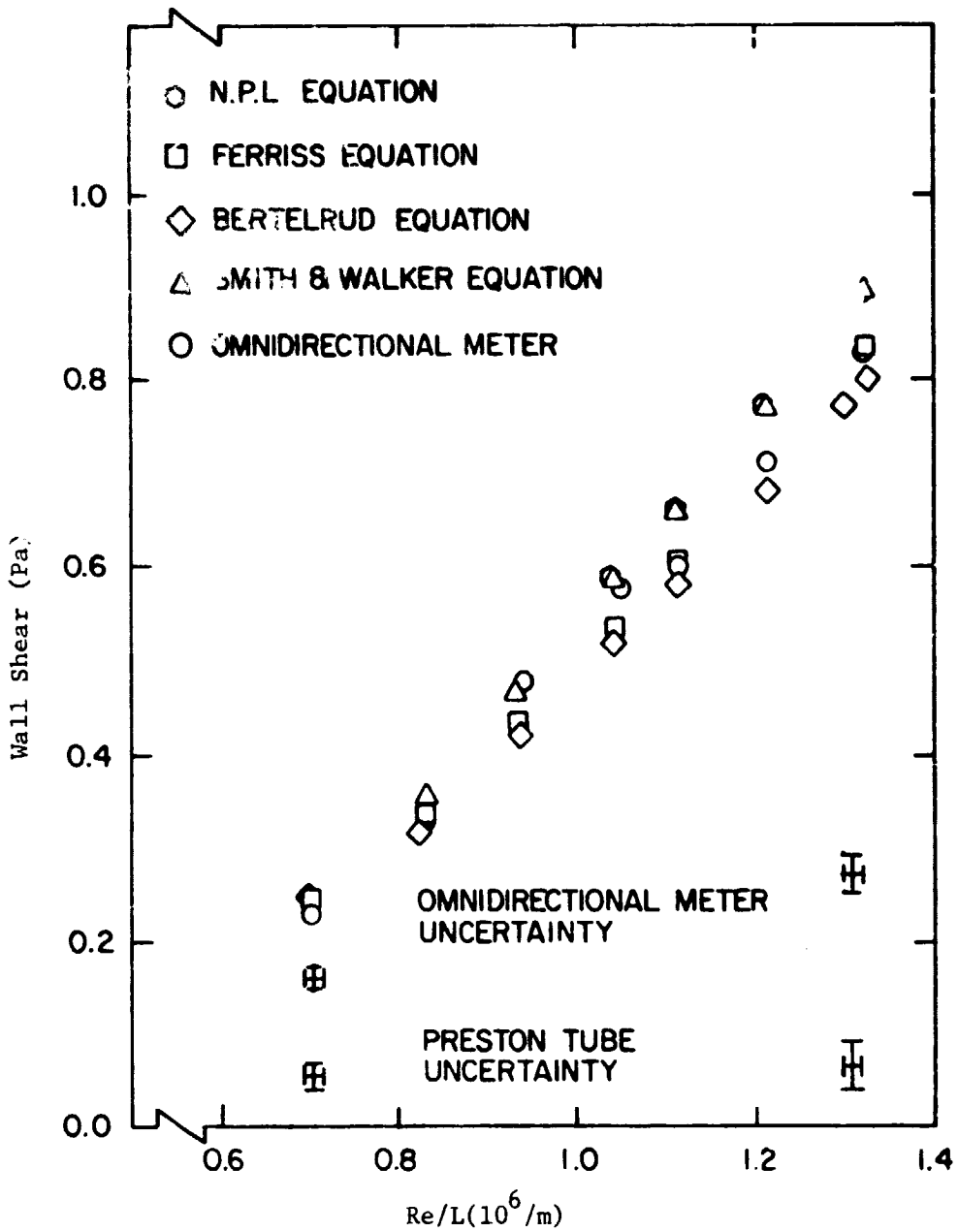

Fig. 4.15 2.11 mm (0.083 in.) Preston Tube Results Using the N.P.L., Ferriss, Bertelrud, and Smith and Walker Calibration Equations

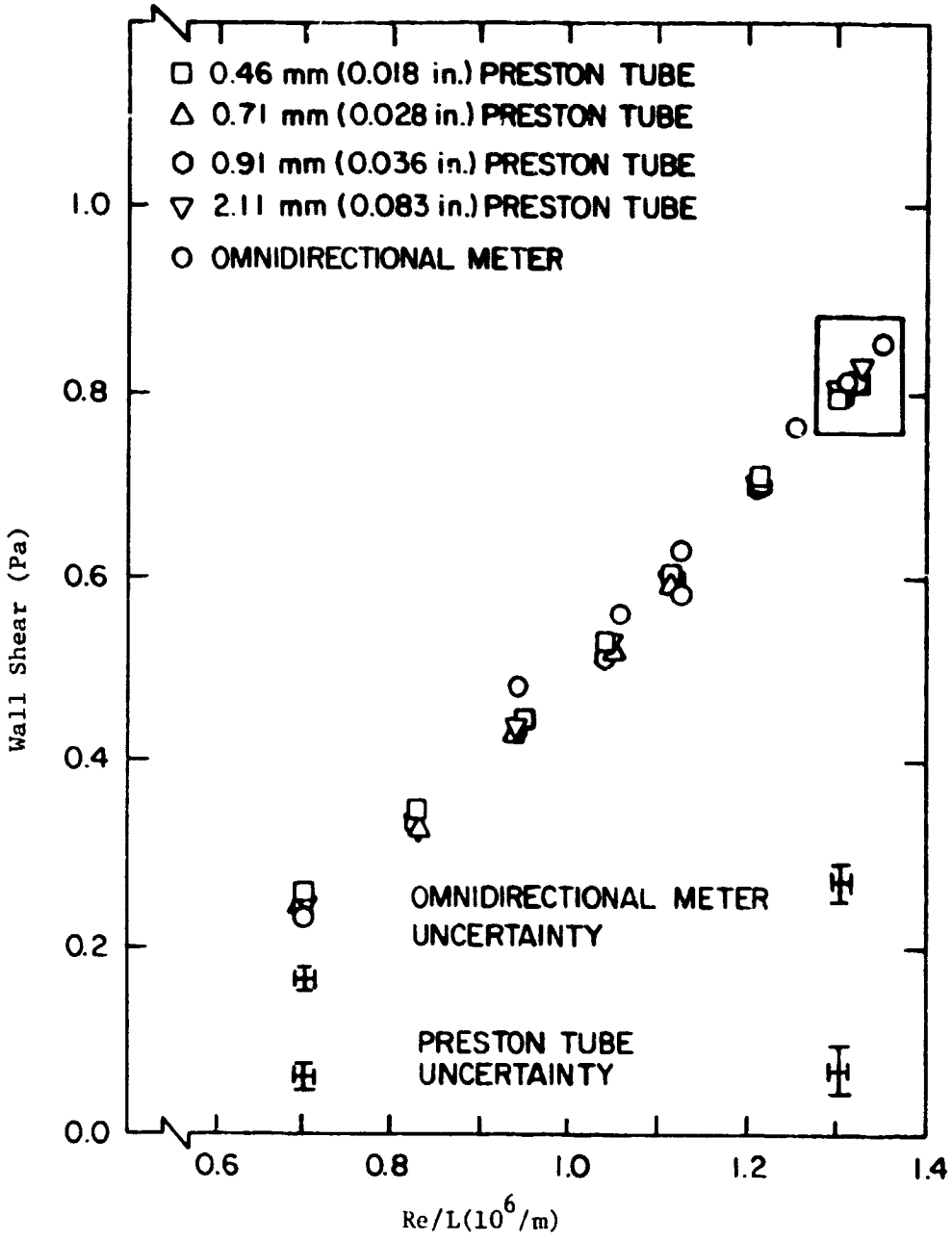

Fig. 4.16 Preston Tube Results Using the Patel Calibration Equations

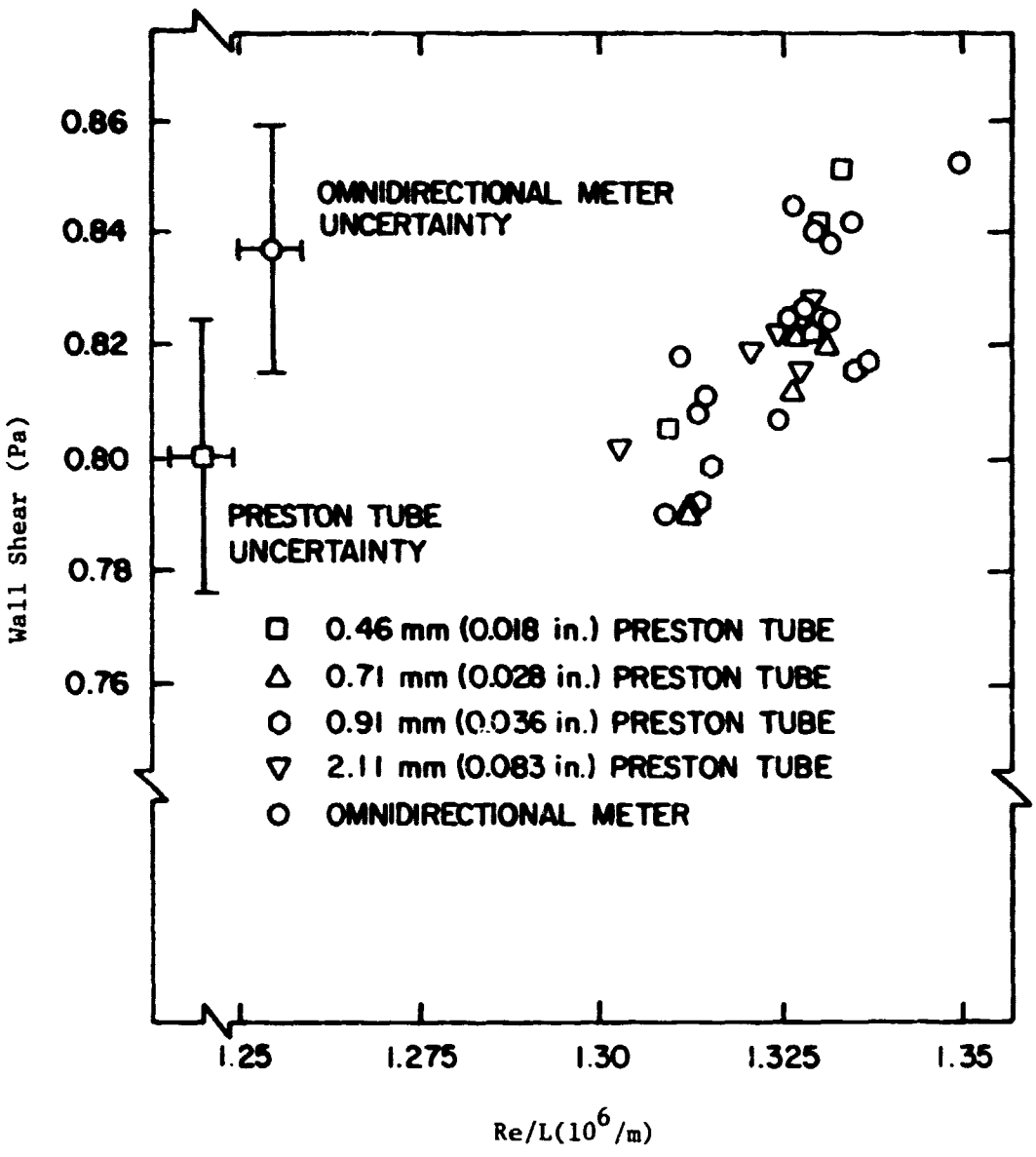

Fig. 4.17 Expanded Scale Showing Preston Tube and Omnidirectional Wall Shear Data

the range of unit Reynolds numbers of this study. There was substantially more data available, especially at the higher unit Reynolds numbers than could be shown in Fig. 4.16, and more of these data in the range of the boxed area in Fig. 4.16 are shown in Fig. 4.17 on an expanded scale. From these figures it is evident that the intermediate range Patel calibration equation gives better agreement with the direct force wall shear measurements than the Preston, N.P.L., Bertelrud, and Smith and Walker calibration equations. The Ferriss formula appears to offer the same level of agreement with the direct wall shear data as the Patel equations but the Ferriss formula is somewhat limited in its applicable range. The N.P.L. and the Smith and Walker wall shear values are generally higher than the direct force wall shear values. While the Bertelrud results are generally lower, the choice of dependent variable in this equation leads to overall wall shear uncertainties for this calibration equation that are smaller than for the other equations. Bertelrud purposely used different variables for his calibration equation given in Table 3.2 because Head and Ram (1971) showed these variables to be less sensitive to the Preston tube data inputs than the x* and y* variables used by most other investigators. A close examination of the Patel and Bertelrud results in Figs. 4.15 and 4.16 indicates that although both agreed with the direct wall shear data within experimental uncertainty, the Patel calibration gives overall better agreement. As in Depooter, Brundrett, and Strong (1978), all the Preston tube data in this study also fell into the x* range covered by the intermediate Patel calibration formula so that results from the remaining two Patel formulas are not represented in Figs. 4.16 and 4.17.

Representative C_f values using the results of Fig. 4.16 are shown in Fig. 4.18 where agreement with the inferred C_f results using the Ludwieg-Tillmann formula is good. As with Fig. 4.7 the wall shear and freestream data needed for Fig. 4.18 were taken simultaneously avoiding any possible problems in matching data from different tunnel runs.

A actual number of data represented in Fig. 4.16 includes 75 Preston tube shear values and 113 direct free shear measurements. A second order statistical fit to these two sets of data indicated the direct force shear values were nominally 4% higher then the Preston tube data over the lower half of the Re/L interval shown with this difference decreasing

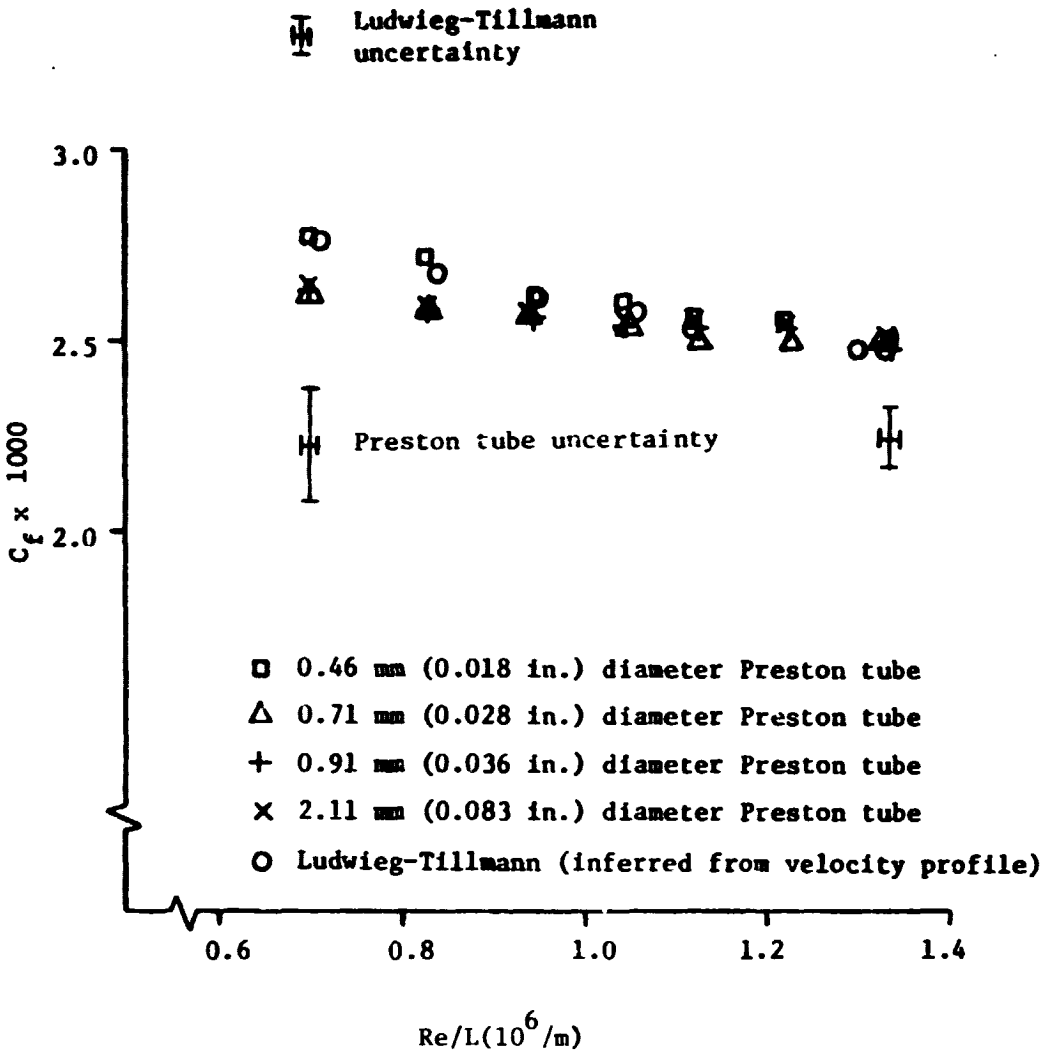

Fig. 4.18 C_f Results For the Preston Tube Data Using the Patel Calibration Equations

nearly monotonically to about 0.4% at the upper end of this interval. It is worth noting that these curve fits are heavily biased in that the bulk of both data sets occured at the higher Re/L values and the agreement between these two sets of data is well within 1% in this region.

Two-Dimensional Near-Wall Similarity Results

Repeatability in the velocity profiles, and the indirect and direct wall shear values for these two-dimensional measurements establishes a high degree of credibility for the following two-dimensional near-wall similarity plots and the subsequent three-dimensional wall shear measurements.

Twenty-six two-dimensional velocity profiles were plotted in similarity variables. These included eighteen profiles taken on the centerline of the tunnel over the full range of Reynolds numbers studied and eight profiles taken at two- and four-inch distances off the tunnel centerline in both directions at two of the nominally higher Reynolds number values. Table 4.8 lists the profiles, wall shear values, and corresponding unit Reynolds numbers for these profiles and shear data.

It is informative to compare the measured velocity and wall shear data to proposed near-wall similarity laws for the two-dimensional case but two questions should be considered first. First, there is considerable latitude over the choice of the two constants that appear in essentially all forms of the two-dimensional near-wall similarity law and designated κ and C. This question is reviewed in Chapter II where Table 2 shows several of the more popular pairs of constants in the literature. Figure 2.2 shows that the choice of constants can have s significant effect on the logarithmic section of the similarity law. The Patel and N.P.L. constants are used in the comparisons to follow. The second question concerns itself with the exact form of a similarity law that will be used. As noted in the review of these models, a two-dimensional near-wall similarity law for small y^+ values to include very near-wall data can be written in various forms. Three forms will be shown in the following; the two formula law of the wall (the logarithmic form combined with a sublayer form), the third order Spalding and the fourth order Spalding forms. These are shown in Fig. 2.1 for one set of law of the wall constants.

Table 4.8 Matched Wall Shear and Velocity Profile Re_{unit} Numbers

Velocity Profile	Velocity Profile Re_{unit} $(\frac{1}{m} \times 10^6)$	Wall Shear Re_{unit} $(\frac{1}{m} \times 10^6)$	Wall Shear (Pa)
2D 36 D	1.328	nominal 1.328	0.82*
2D 37 H	0.837	0.832	0.34
2D 38 A	0.710	0.705	0.28
2D 39 G	0.949	0.943	0.48
2D 40 B	1.055	1.052	0.58
2D 41 C	1.116	nominal 1.120	0.60**
2D 42 B	1.033	1.052	0.57
2D 43 C	1.122	nominal 1.120	0.60**
2D 44 E	1.312	1.314	0.81
2D 45 E	1.299	1.299	0.83
2D 46 D	1.334	1.335	0.83
2D 47 D	1.331	1.332	0.85
2D 48 D	1.328	1.328	0.84
2D 49 D	1.330	1.326	0.83
2D 50 D	1.330	1.326	0.83
2D 51 D	1.321	1.323	0.83
2D 52 I	1.211	1.217	0.72
2D 53 I	1.211	1.217	0.72
2D+2 D 1	1.329	1.324	0.87
2D+4 D 1	1.323	1.314	0.85
2D-2 D 1	1.326	1.327	0.79
2D-4 D 1	1.323	1.316	0.88
2D+2 C 1	1.119	1.109	0.60
2D-2 C 1	1.125	1.124	0.56
2D+4 C 1	1.124	1.117	0.62
2D-4 C 1	1.124	1.116	0.64

*Average of 24 values from the Set 2 omnidirectional meter results.

**Average of 10 values from the Set 1, Set 2, and Set 3 omnidirectional meter results.

Calculated uncertainties can be identified with the plotted experimental data points and these uncertainties vary according to the wall shear value and distance from the wall. The largest percent uncertainties occur for the low unit Reynolds number runs with the smallest occurring for the highest tunnel speeds. The percent uncertainties also decrease as one moves away from the wall and they also decrease at a given wall distance as the tunnel speed increases. This behavior exists because the wall shear stress has a larger uncertainty at lower tunnel speeds and the velocity magnitude uncertainty increases in the wall direction. Figures 4.19 and 4.20 show the typical uncertainties for a high and low unit Reynolds number run at the extremes of the data. The similarity law shown is the Spalding third order formula for the Patel and N.P.L. constants.

Figure 4.21 shows mainly D series velocity profiles both on and off the tunnel centerline and compares these to the Spalding third order similarity formula for both the Patel and N.P.L. constants. This figure suggests that the Patel constants would represent these data well. Figure 4.22 shows the same data compared to the Spalding fourth order similarity formula and the difference is seen in the low y^+ value data fitting better with the fuller curve. Figure 4.23 shows the same D series data fitted to the two-formula law of the wall similarity law. It appears that in the y^+ range of 50 to 300 all three of these models fit the data very well and if one includes the very near wall data (y^+ values less than 50) the Spalding fourth order similarity model would be preferred slightly over the third order model in terms of fit, and over the two-formula law of the wall in terms of the convenience of a single formula model. If the choice of y^+ as independent variable is important, then the two-formula law of the wall could be selected. Clearly, the three-formula law of the wall could be manipulated to include a logarithmic buffer region formula to better fit the buffer region data.

Thirteen profiles taken over the range of Reynolds numbers of the twodimensional data, with the exception of any D sequence data, are shown in Fig. 4.24 for comparison with the Spalding third order similarity model for both the Patel and N.P.L. constants. The data generally lie well within the uncertainty intervals and the interval defined by the

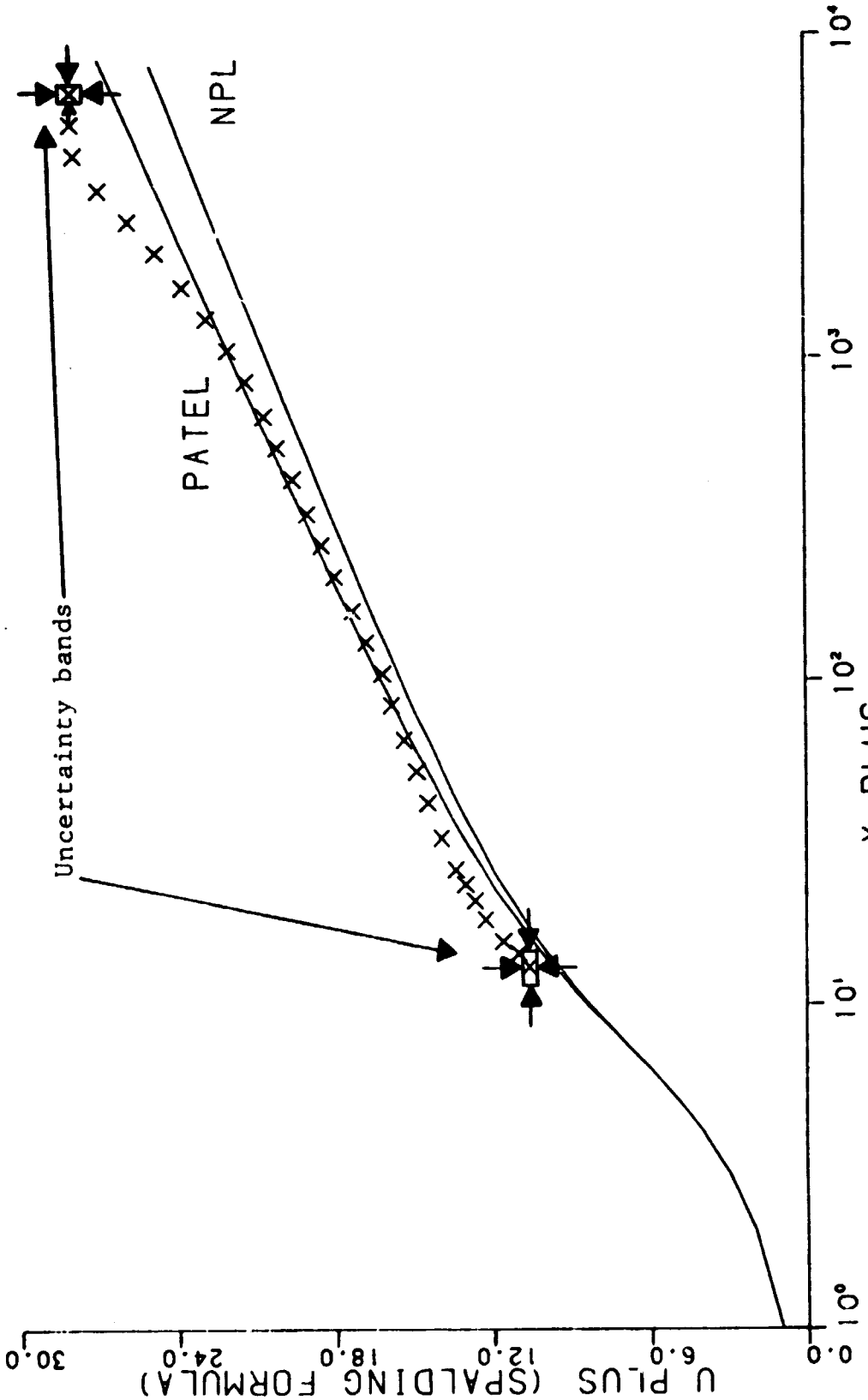

FIG. 4.19 TWO-DIMENSIONAL SIMILARITY PLOT FOR RUN 2D 36 D.

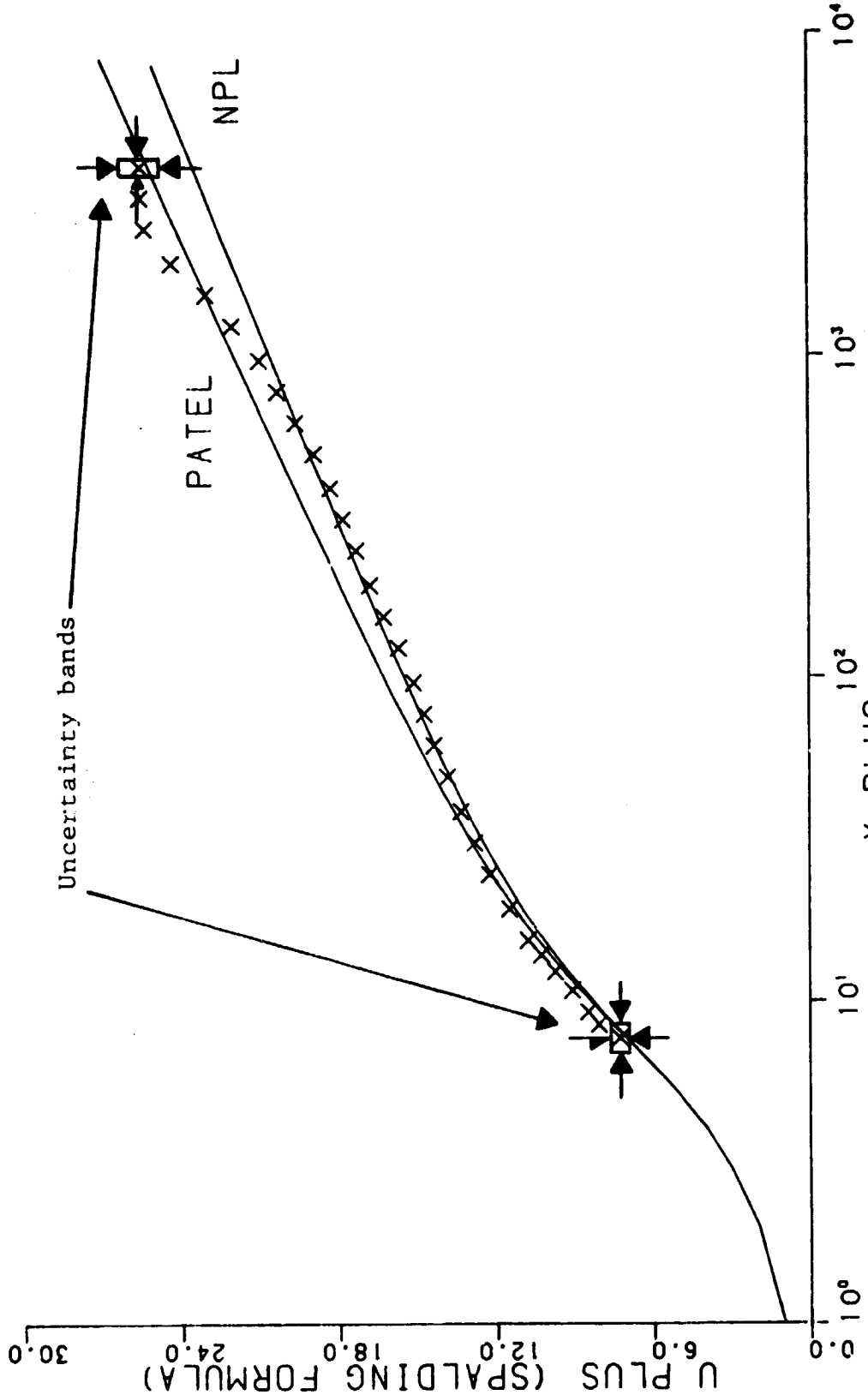

FIG. 4.20 TWO-DIMENSIONAL SIMILARITY PLOT FOR RUN 2D 38 A.

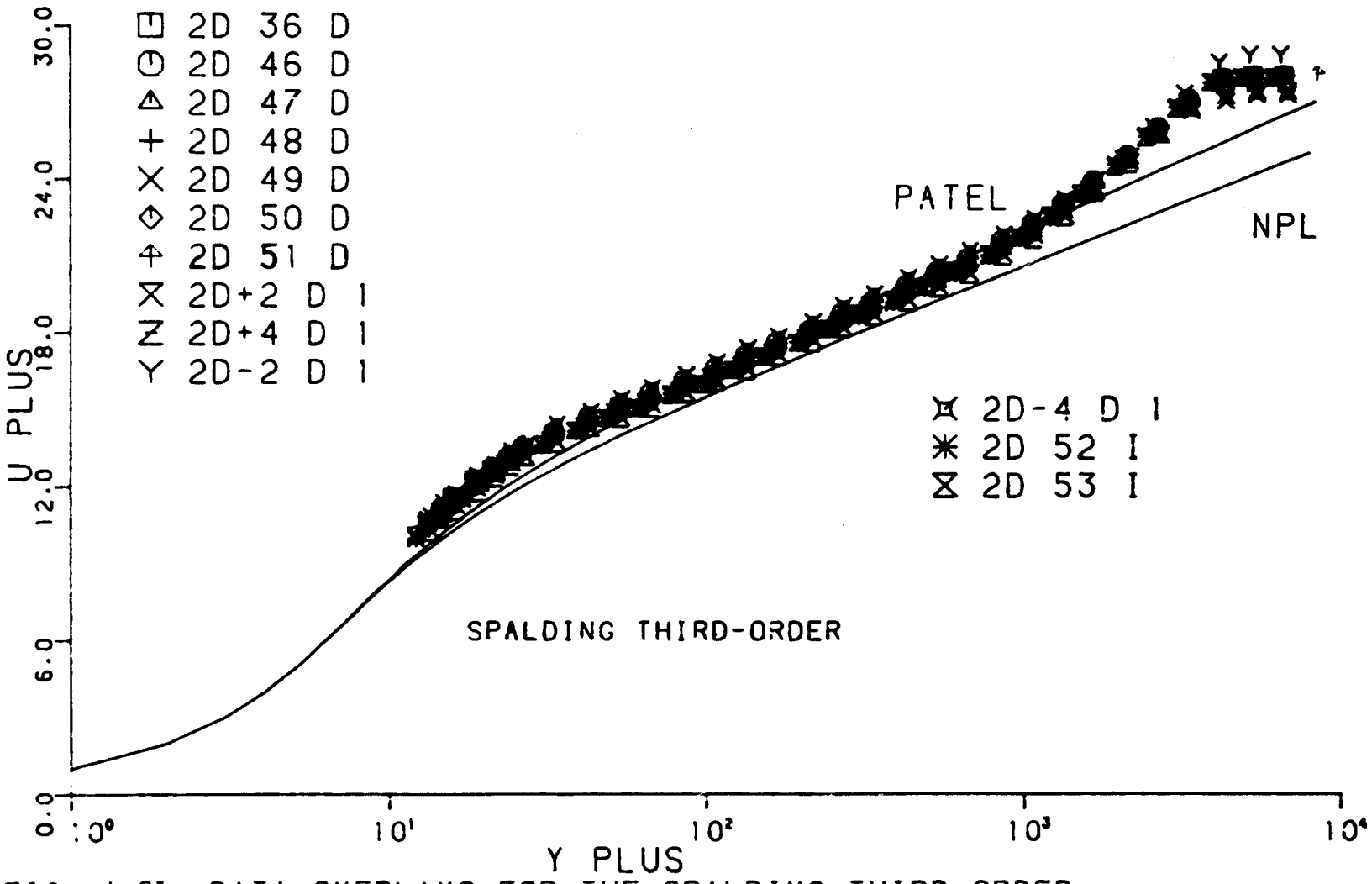

FIG. 4.21 DATA OVERLAYS FOR THE SPALDING THIRD-ORDER.

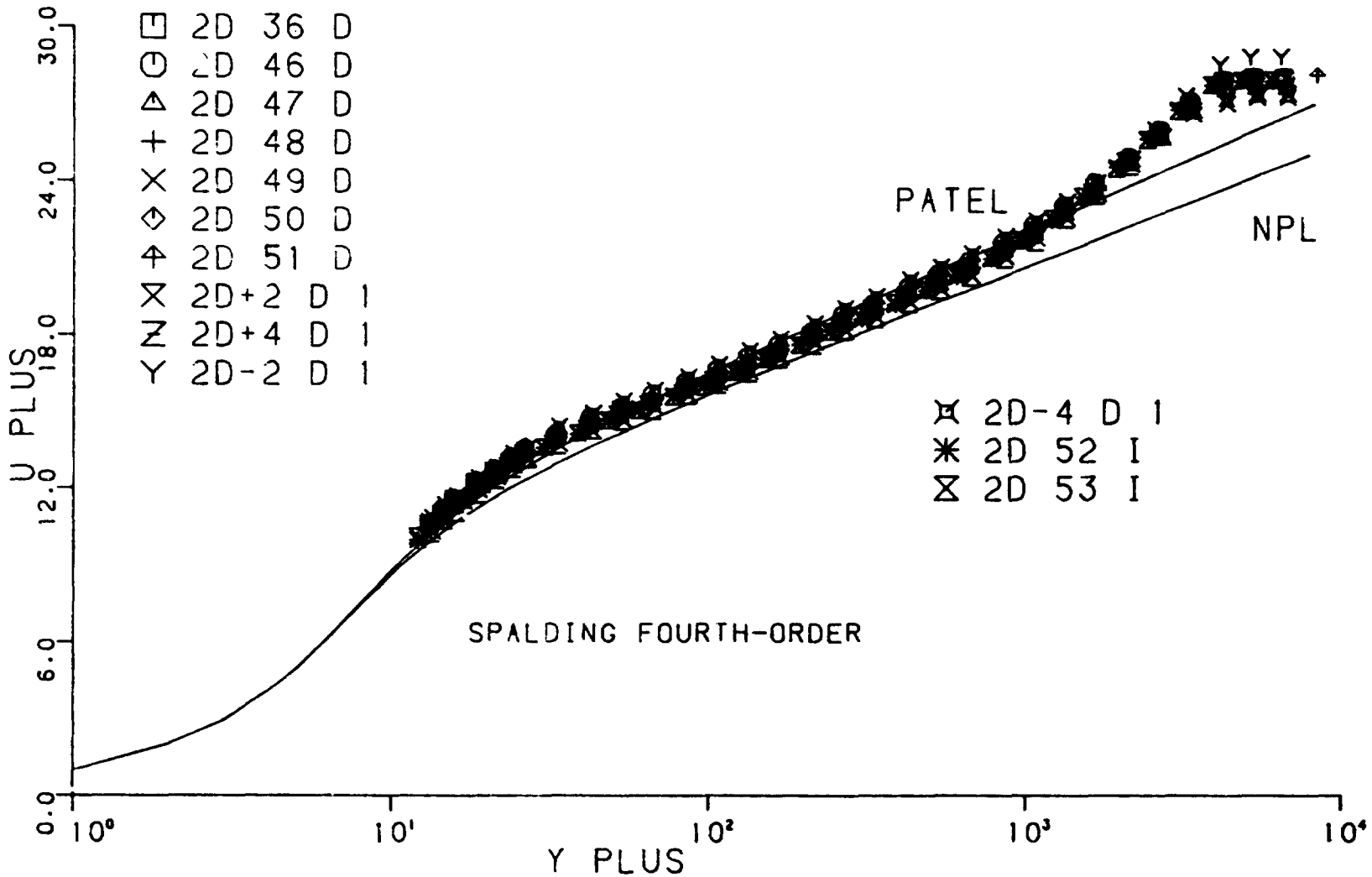

FIG. 4.22 DATA OVERLAYS FOR THE SPALDING FOURTH-ORDER.

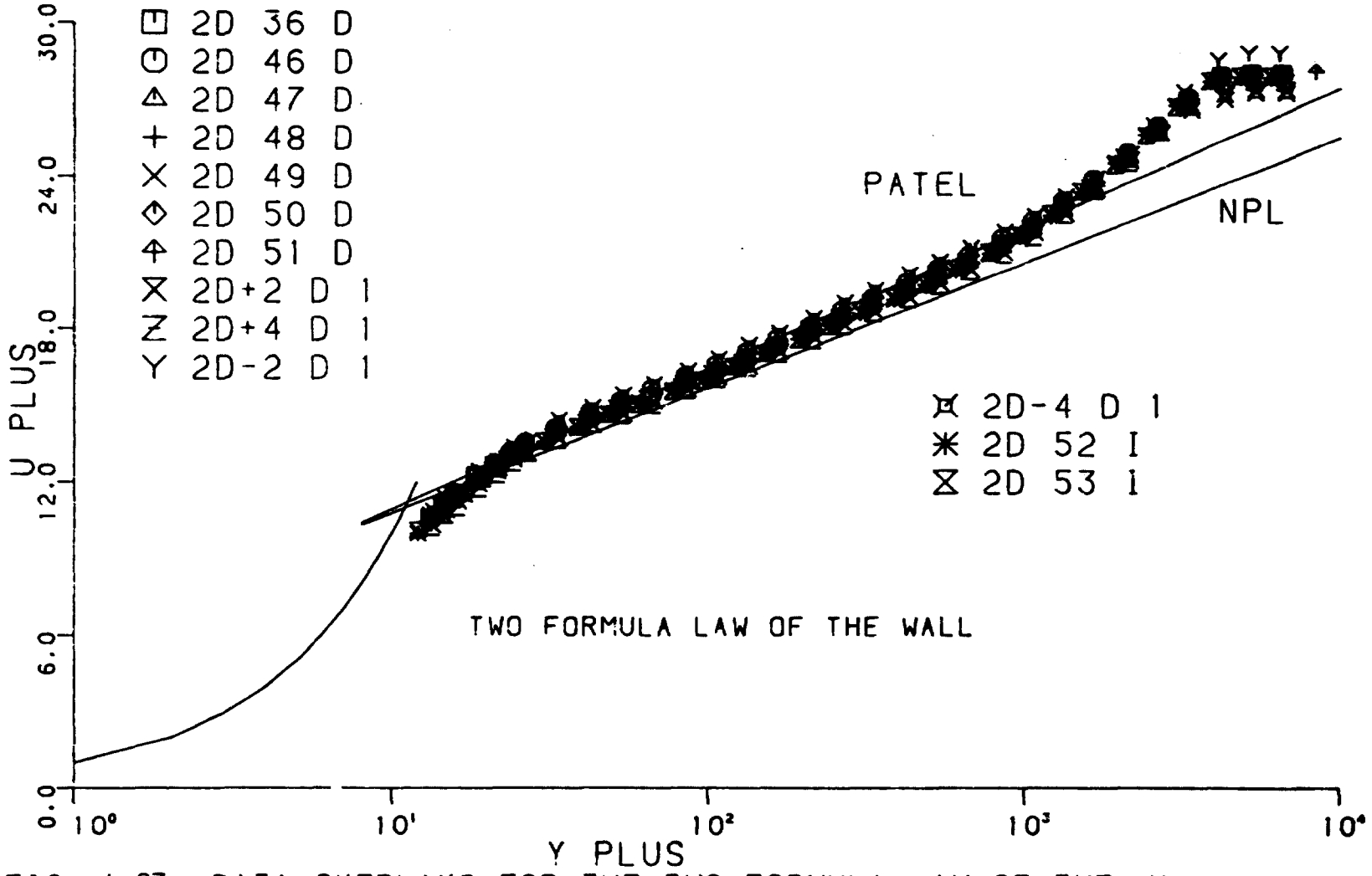

FIG. 4.23 DATA OVERLAYS FOR THE TWO FORMULA LAW OF THE WALL.

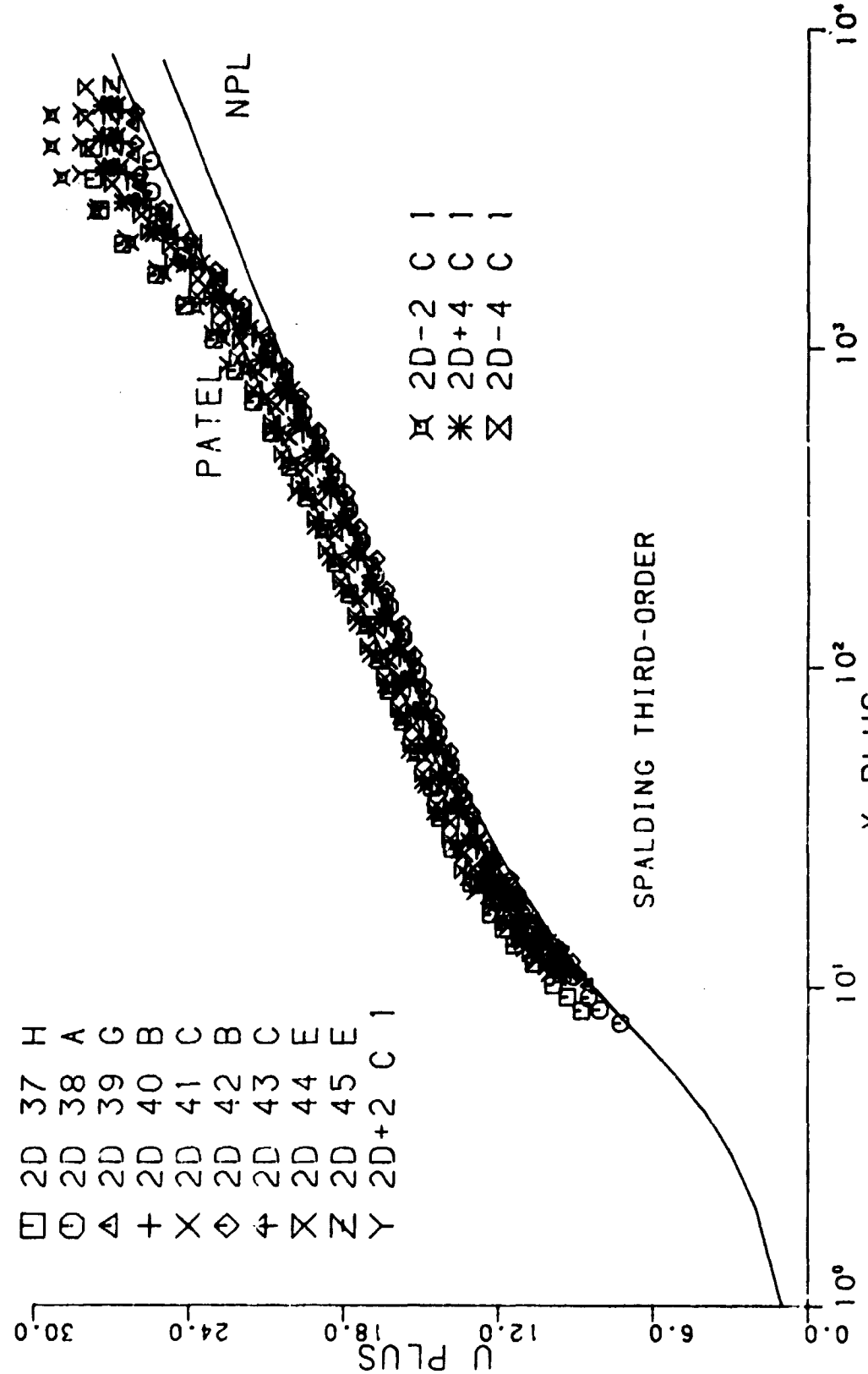

FIG. 4.24 DATA OVERLAYS FOR THE SPALDING THIRD-ORDER.

two curves for each of the two sets of constants. The suggestion of a Reynolds number dependence on the similarity constants is strong. A careful look at the individual profiles shows that in general the lower unit Reynolds number flows favor the N.P.L. constants and the higher unit Reynolds number flows favor the Patel constants, but exceptions to this trend are noted so that any stronger generalization is not warrented. Thus, should one define a modest Reynolds number dependence of these constants over the Reynolds number range of this two-dimensional, near zero pressure gradient data, the uncertainty limits identify with this variation would have to be generous. As noted in Chapter II the possible deperdence of the similarity constants on Reynolds number is discussed by Kleinstein (1967), Patel and Head (1964), Schraub and Kline (1965), and Huffman and Bradshaw (1972).

As with the D sequence data, Figs. 4.25 and 4.26 show the variable Re/L data in comparison with the Spalding fourth order similarity formula and the two formula law of the wall, again, for the same two sets of constants. And as in the earlier case, it is clear that the inclusion of a buffer region formula as in the three formula law of the wall would show an even better agreement than the two formula models.

The design and development of the flow tunnel, instrumentation, and especially the three-dimensional shear meter is described more fully in Tennant (1977). He also reports the results of preliminary data taken with this system. The two-dimensional Tennant data is very similar to that shown for this study but a close examination of his similarity plots shows slghtly better overall agreement with the N.P.L. constants. A careful evaluation of both this and the Tennant data indicates that for the unit Reynolds number over which the subsequent three-dimensional measurements were made the Patel constants best represent the two-dimensional data. The margin of choice is not large. Additionally, the three-dimensional flow conditions in this same test section will obviously be different than for the two-dimensional case even at the same tunnel inlet unit Reynolds number. The subsequent three-dimensional similarity models will be presented for comparison with the Patel constants in the similarity models, but some limited comparisons will be made for both sets of constants.

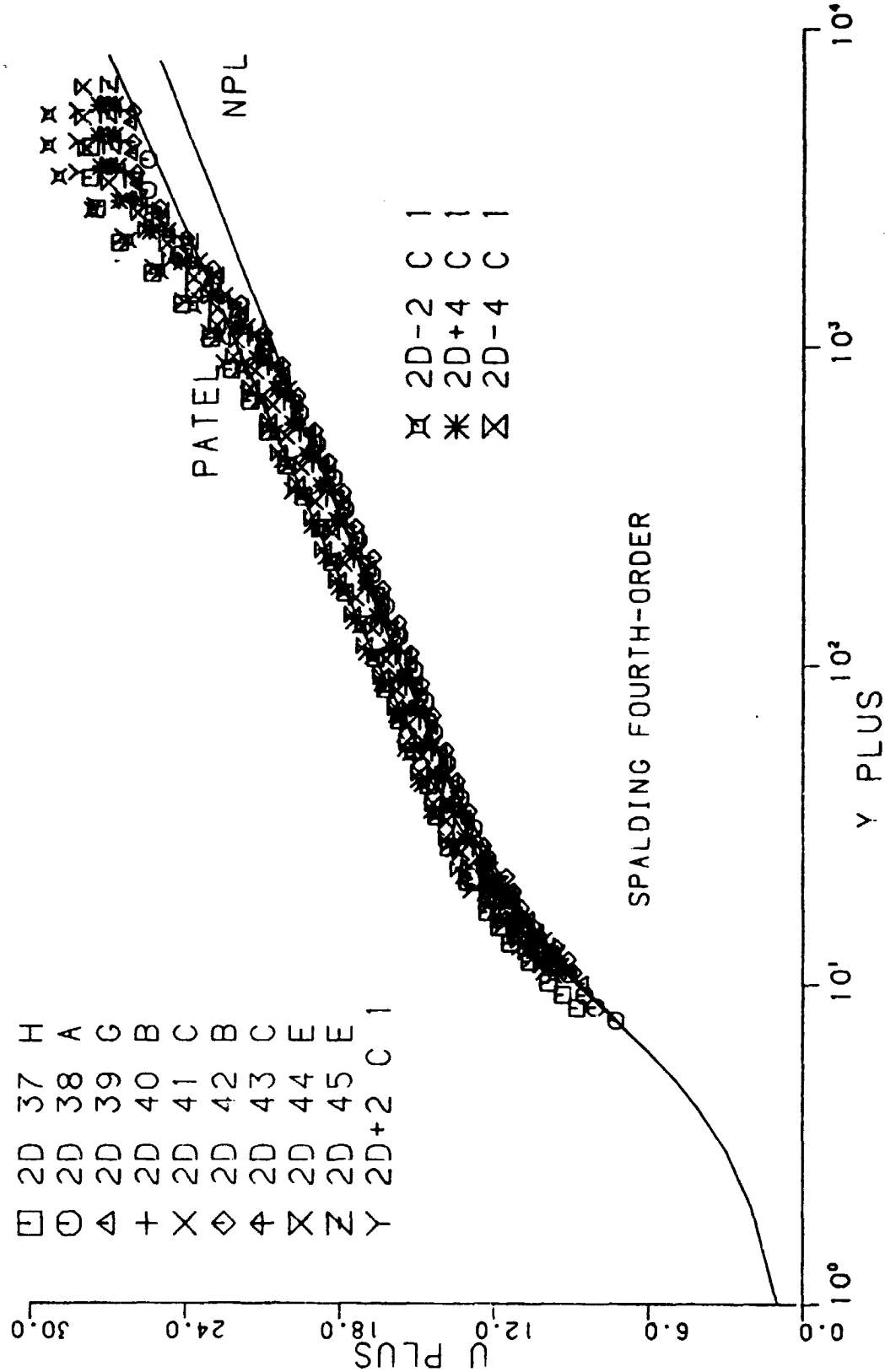

FIG. 4.25 DATA OVERLAYS FOR THE SPALDING FOURTH-ORDER.

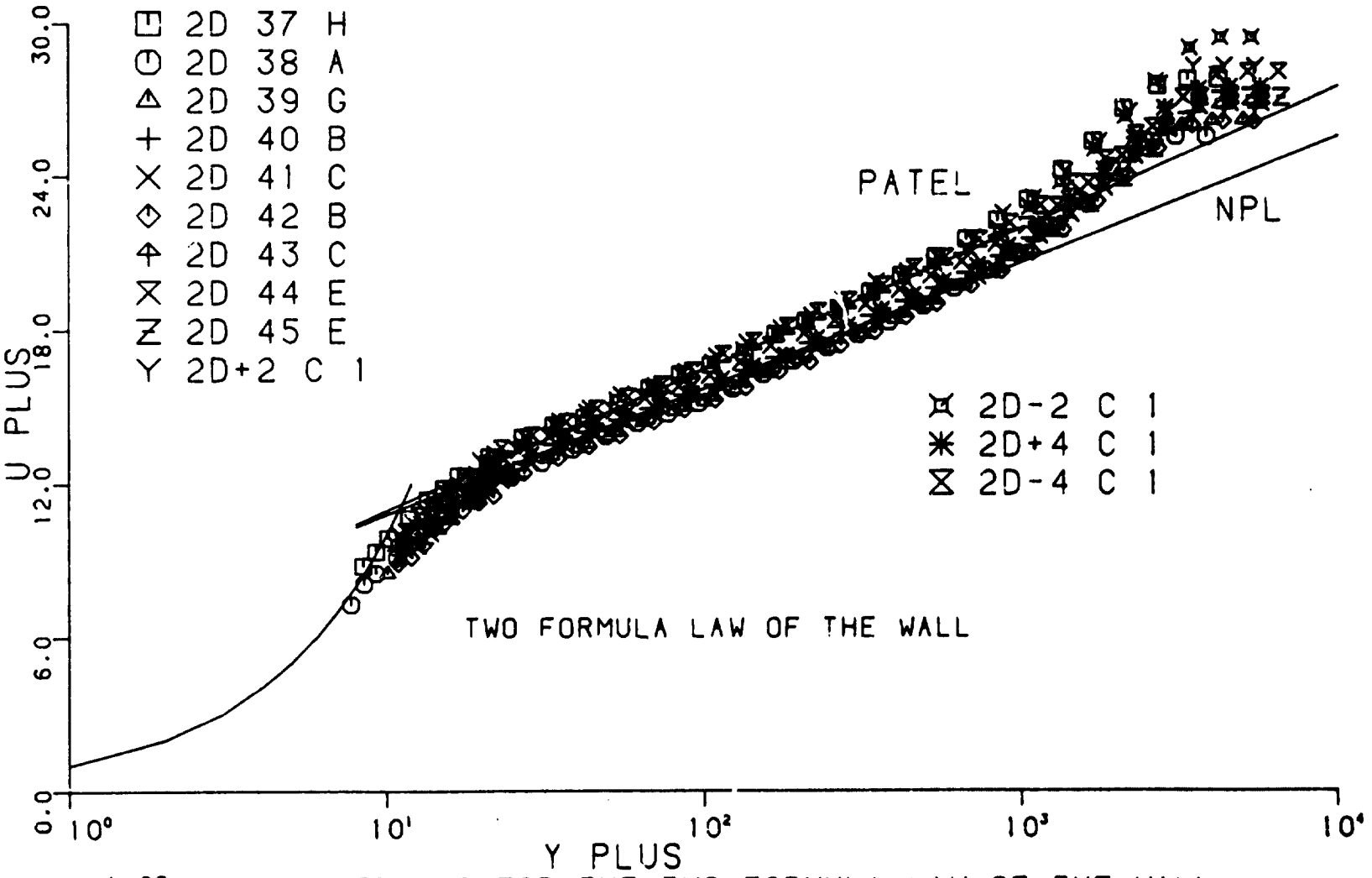

FIG. 4.26 DATA OVERLAYS FOR THE TWO FORMULA LAW OF THE WALL.

It should be noted that no tube displacement or other corrections were used for the velocity probe data reported either in this work or the earlier work of Tennant (1977). In analyzing an extensive quantity of two-dimensional near-wall data, Coles (1968) elected to ignore very near wall data for y^+ values less than 50 because of the wide scatter among different sets of data in this low y^+ range. The reasons for such scatter have not been precisely determined with a variety of possible error often mentioned (low Reynolds number effects, displacement corrections, wall proximity effects, etc.). Note that the data in this study and the preliminary data of Tennant (1977) do not exhibit wide scatter for the very near-wall region and follow the predictions of the third and especially the fourth order Spalding similarity model well. Pierce and Gold (1977) undertook a systematic study of such very near-wall data in a smaller tunnel for 2DTBL flow and considered different impact probes, hot films, gooseneck probes, straight probes, slight flow convergence and divergence, and favorable and adverse pressure gradients. While for some of these variations in instrumentation and flow conditions small systematic changes in the very near-wall data were consistently noted, none of the variations explored were adequate to move the very near-wall data as often required for better agreement with the presumed behavior suggested by models such as the third or fourth order Spalding formula. The MacMillan (1956) tube displacement corrections for distance from the wall were tried but the changes were not adequate.

In most of these figures the data for y^+ less than 50 fall slightly above theoretical predictions for either set of constants when using the Spalding third order formula model and the agreement is improved with the fourth order Spalding formula or the two formula law of the wall for either sets of constants. The overall agreement of the data in this study with any of these three models used in the y^+ range of 50-300 suggests that either set of constants and any of the three similarity models used (clearly, the three formula law of the wall can be included in this group) gives generally good agreement with the experimental results. Overall, the Patel constants are favored because of their good agreement with the extensive D series unit Reynolds number.

V. THREE-DIMENSIONAL MEASUREMENTS

Introduction

Velocity field, wall pressure field, and direct force local wall shear stress measurements were made in the pressure driven 3DTBL generated by the teardrop body with axis placed normal to the floor shown in Fig. 3.2. Figure 5.1 shows the data stations on a 5.1 cm (2 in.) grid where velocity field and wall shear data are reported here. Station designations are made up of a letter and number with sign. The letter represents the row of the data station with A being the centerline of body and moving rightward in one-inch increments. The number represents the distance forward of the body nose measured in inches with the zero being the leading edge. Positive numbers are forward of the body and the sign is omitted. Negative numbers represent stations behind the leading edge. Velocity profiles are designated by an additional number indicating the number of the profile. For example, profile C5 02 is the second profile taken at the C5 location shown in Fig. 5.1.

The required static pressure field, wall shear field, and velocity field were obtained separately. The unit Reynolds number of the tunnel at inlet was maintained at an essentially constant value ($1.322 \times 10^6/m \pm 1\%$) to insure dynamically similar conditions during data acquisition. At least two wall shear data points were taken at each point shown in Fig. 5.1. After repeatibility was established for the three-dimensional profile data acquisition, generally one velocity profile was taken at each of the data stations except for A1, C1, E-3, and E-5. Close proximity to the separation region resulted in very large velocity fluctuations at these stations. Static pressure distributions were obtained on 1.27 cm (0.50 in.) grid because of the larger number of data points required to obtain reasonable polynomial curve fits to these pressure data for the prediction of wall pressure gradients required in some of the three-dimensional similarity models.

Velocity Profiles

Figures 5.2 through 5.11 show the velocity magnitude and angle variation profiles along the various rows. The A column on the plane of

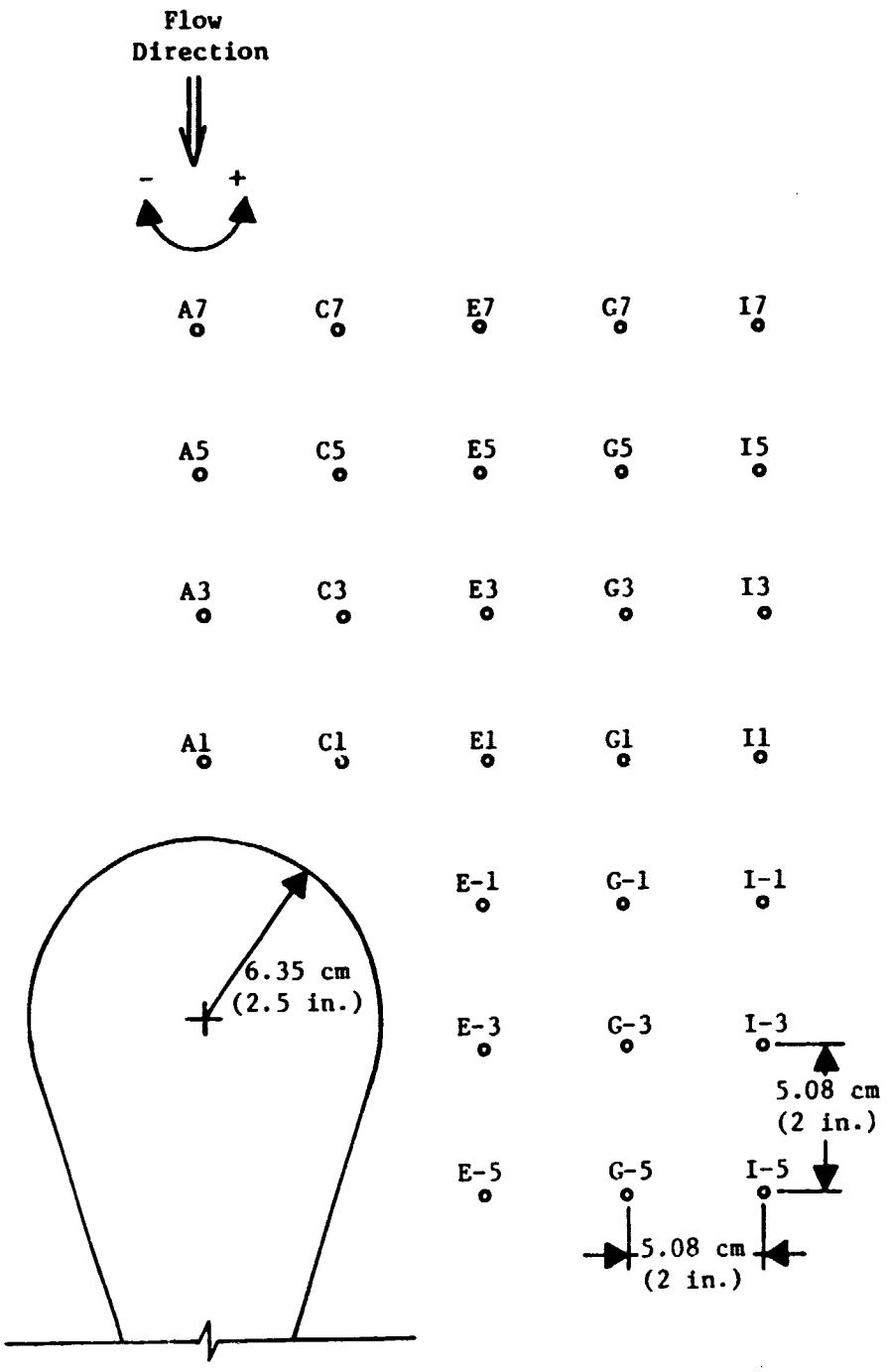

Fig 5.1 Diagram Showing the Data Stations for the Teardrop Flow

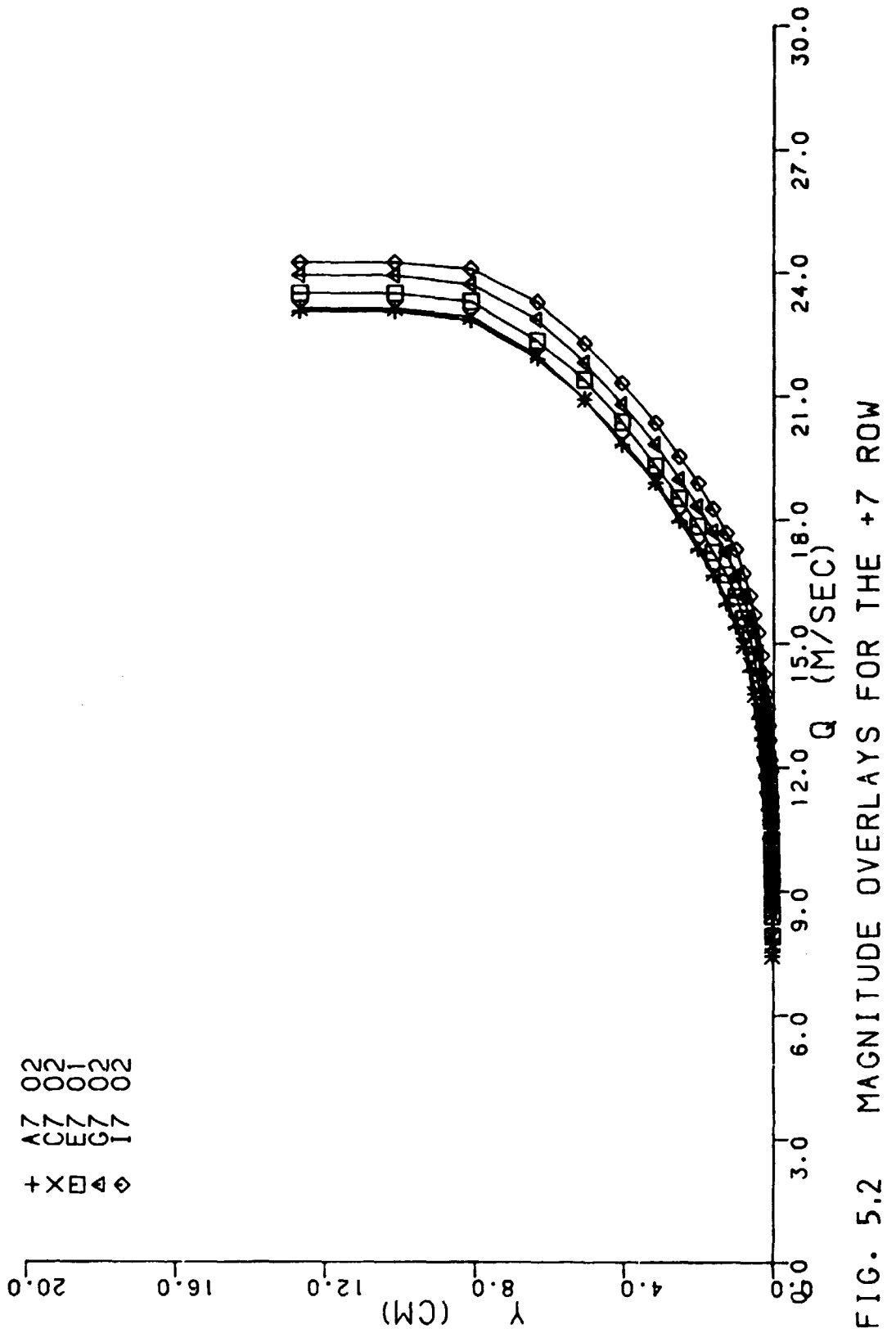

FIG. 5.2 MAGNITUDE OVERLAYS FOR THE +7 ROW

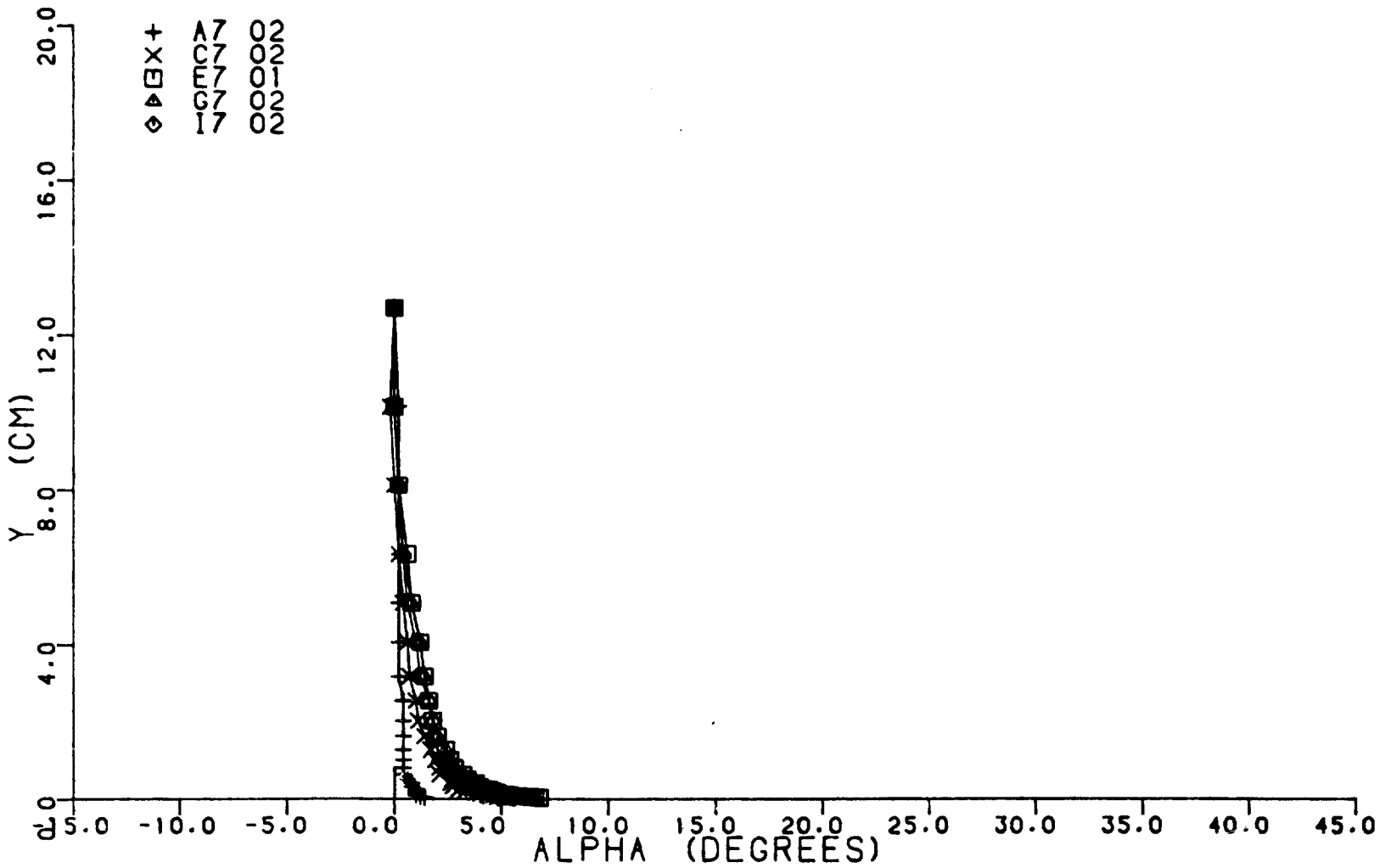

FIG. 5.3 ANGULAR OVERLAYS FOR THE +7 ROW

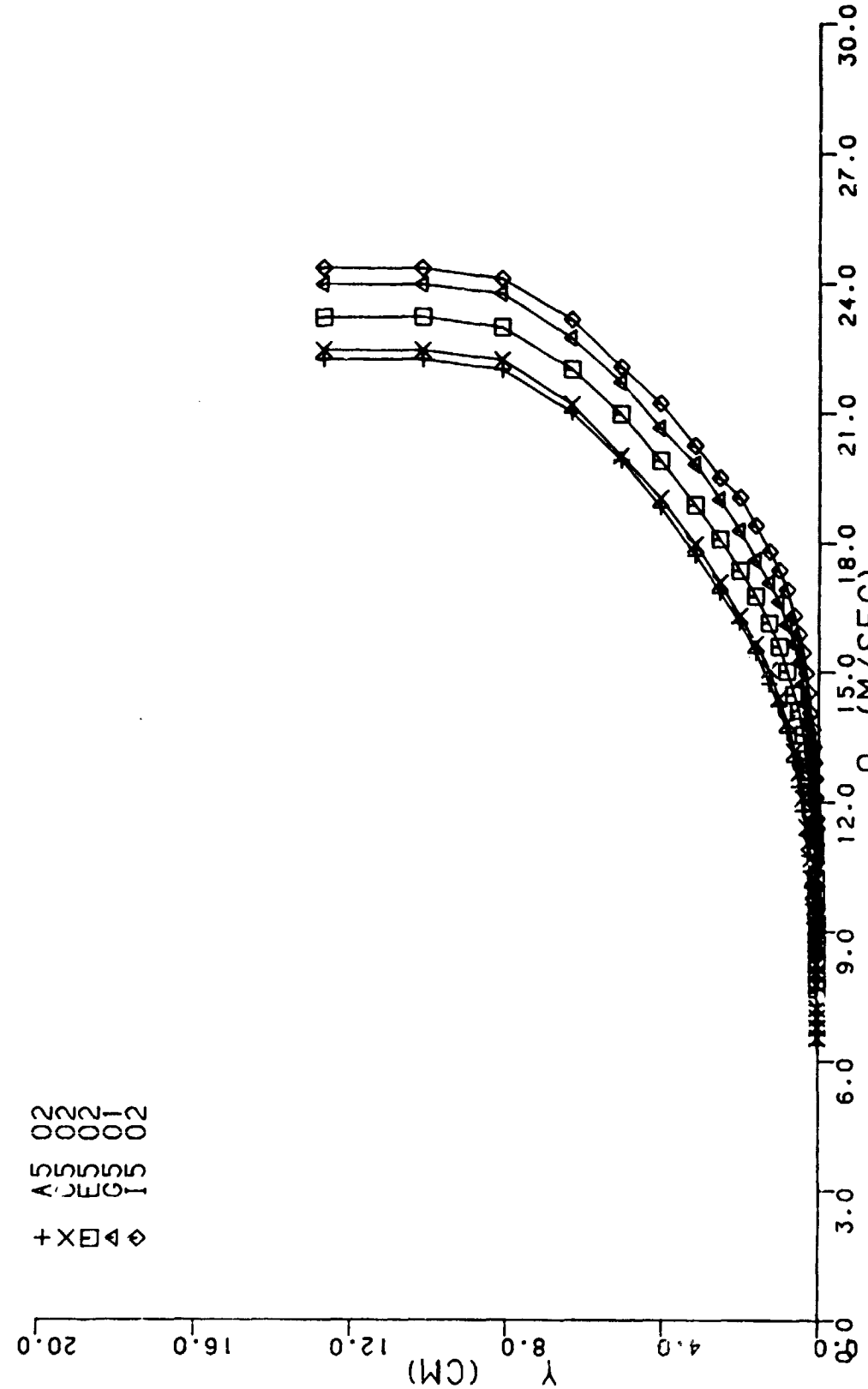

FIG. 5.4 MAGNITUDE OVERLAYS FOR THE +5 ROW

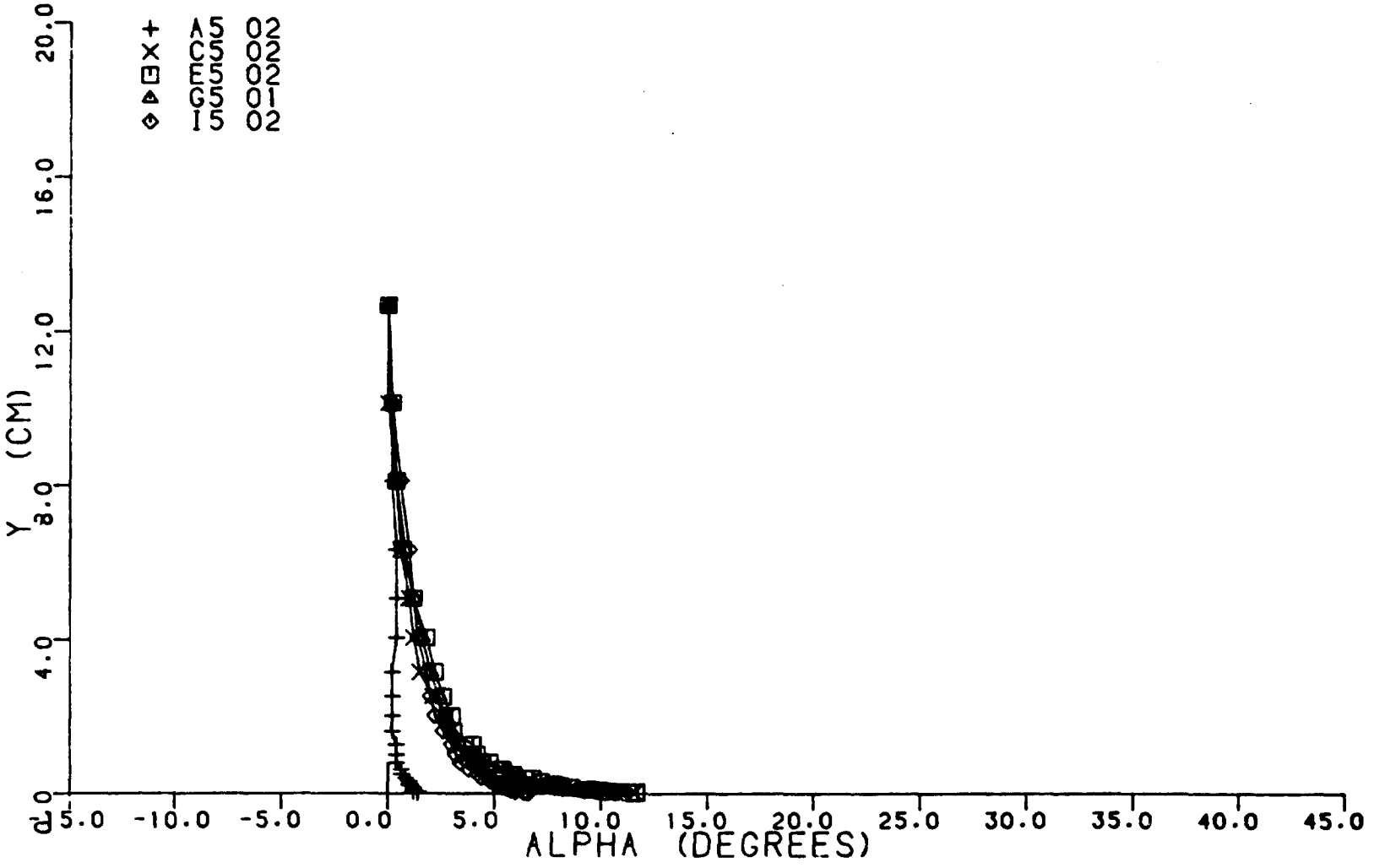

FIG. 5.5 ANGULAR OVERLAYS FOR THE +5 ROW

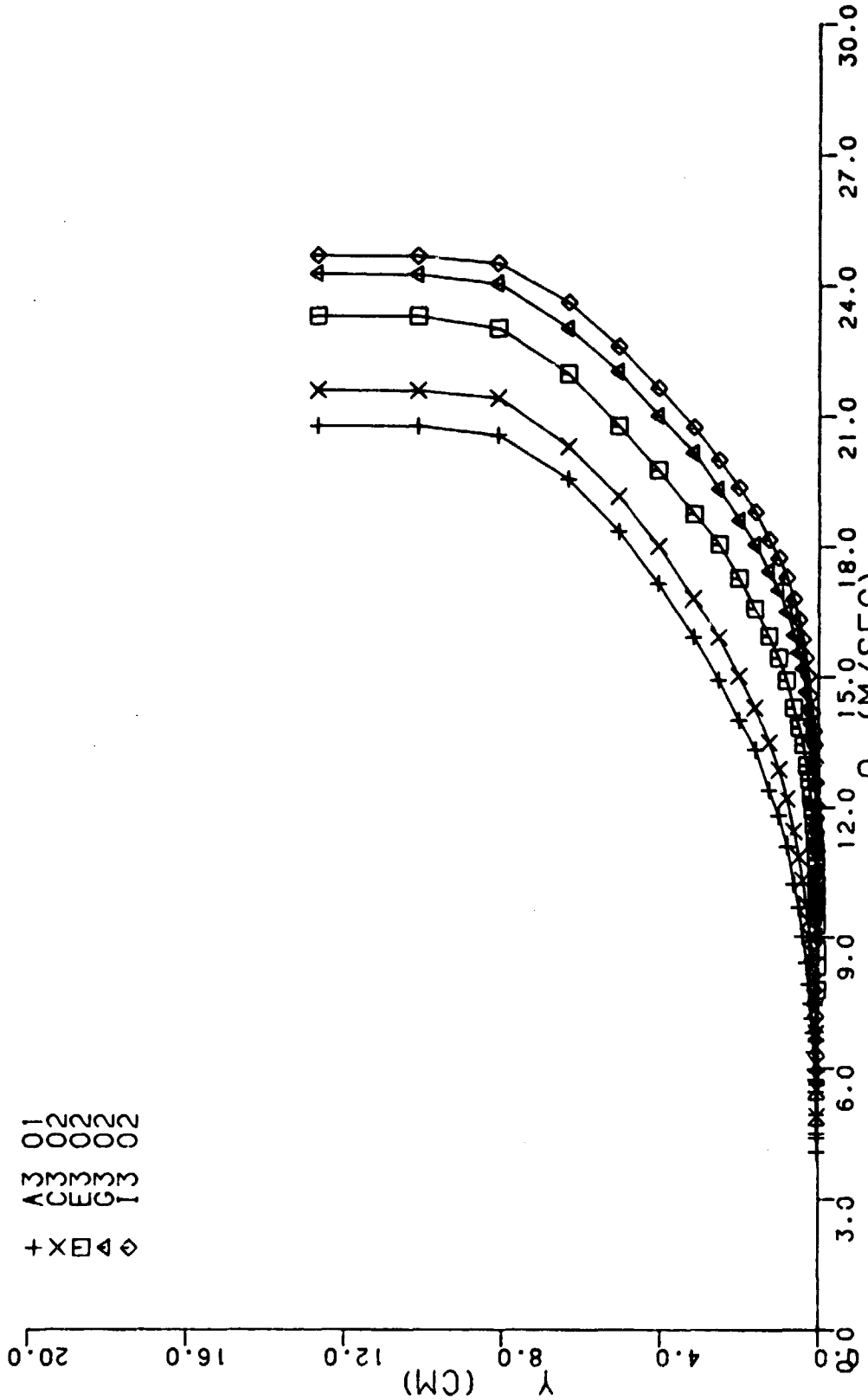

FIG. 5.6 MAGNITUDE OVERLAYS FOR THE +3 ROW

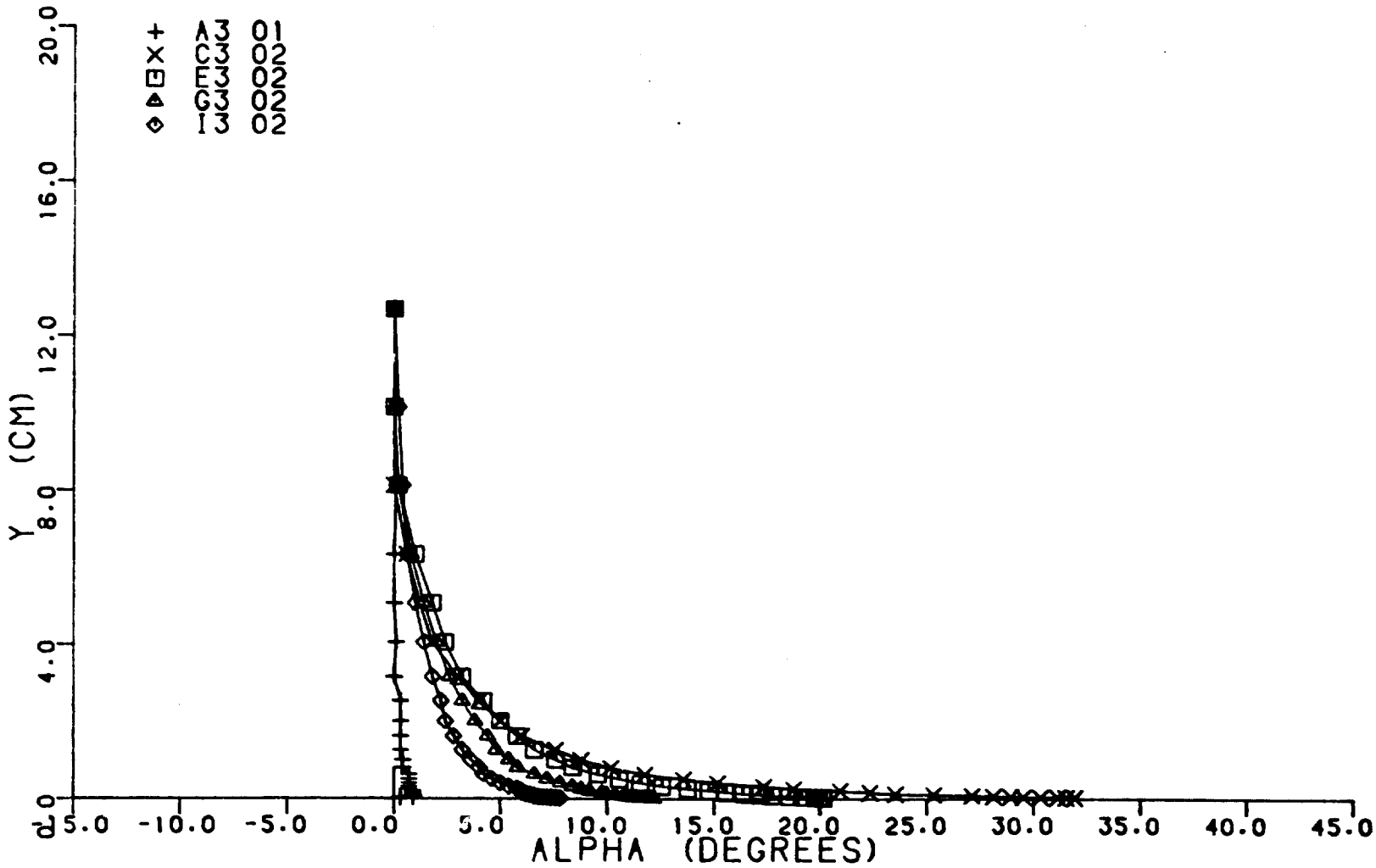

FIG. 5.7 ANGULAR OVERLAYS FOR THE +3 ROW

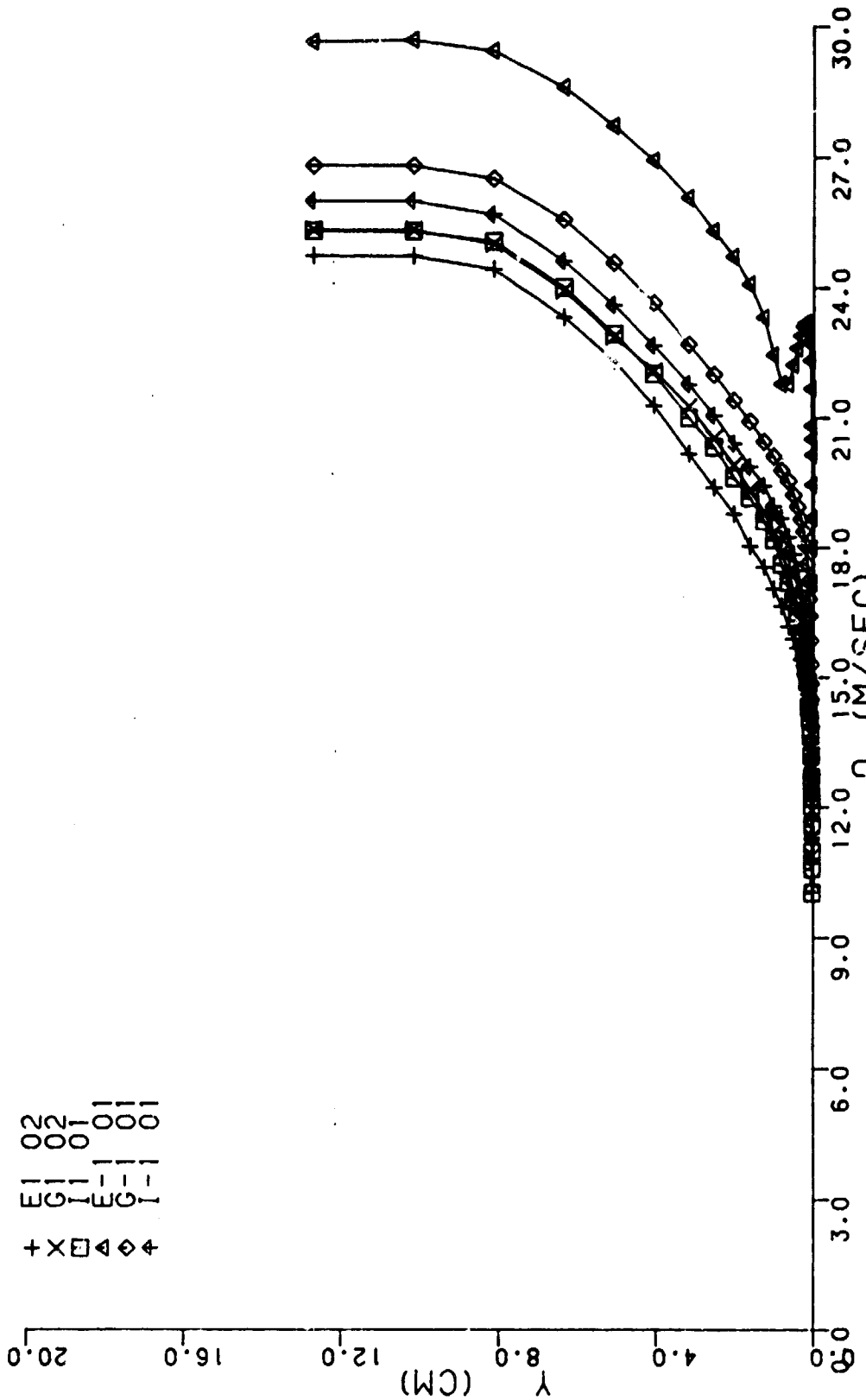

FIG. 5.8 MAGNITUDE OVERLAYS FOR THE +1 AND -1 ROWS.

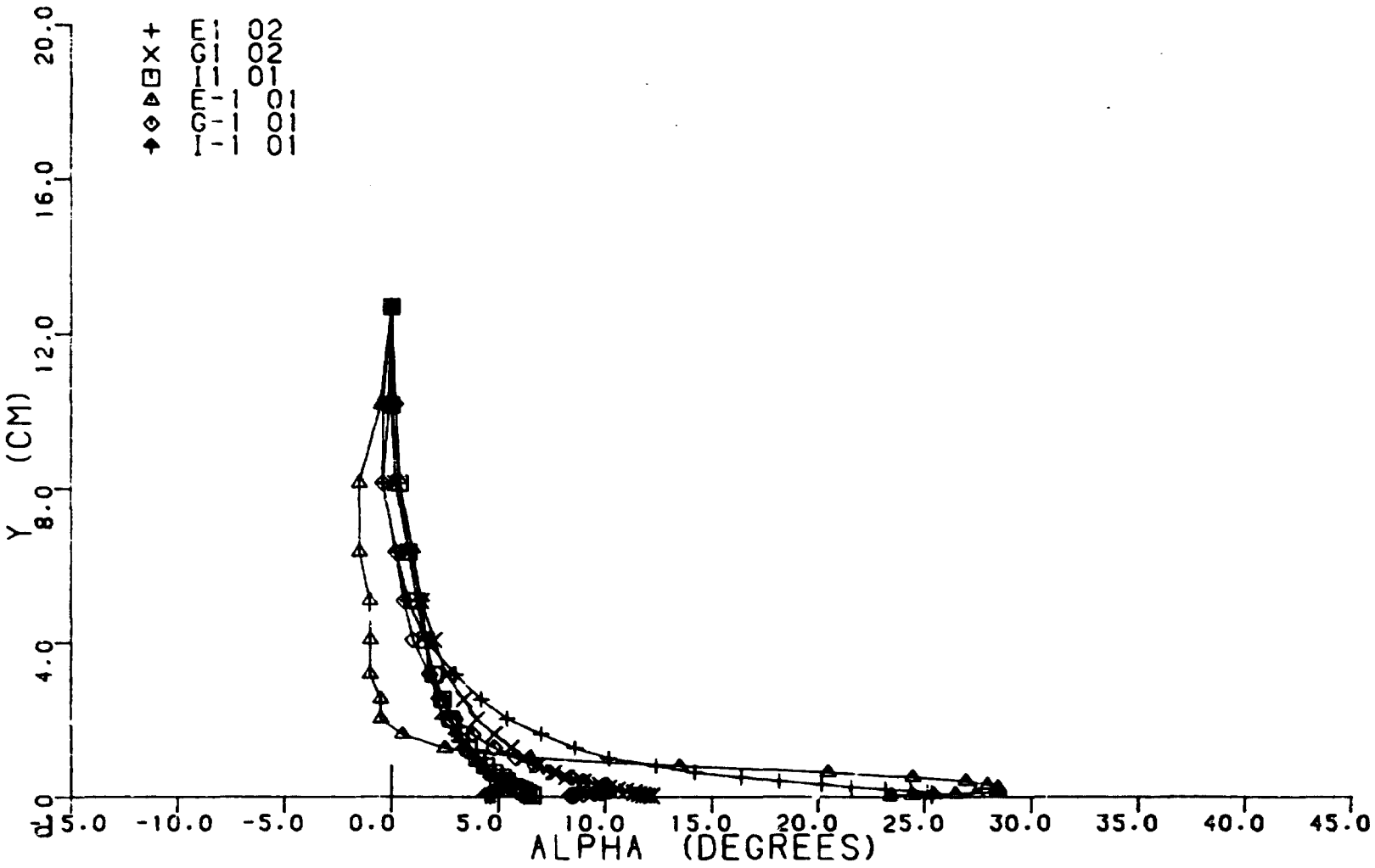

FIG. 5.9 ANGULAR OVERLAYS FOR THE +1 AND -1 ROWS

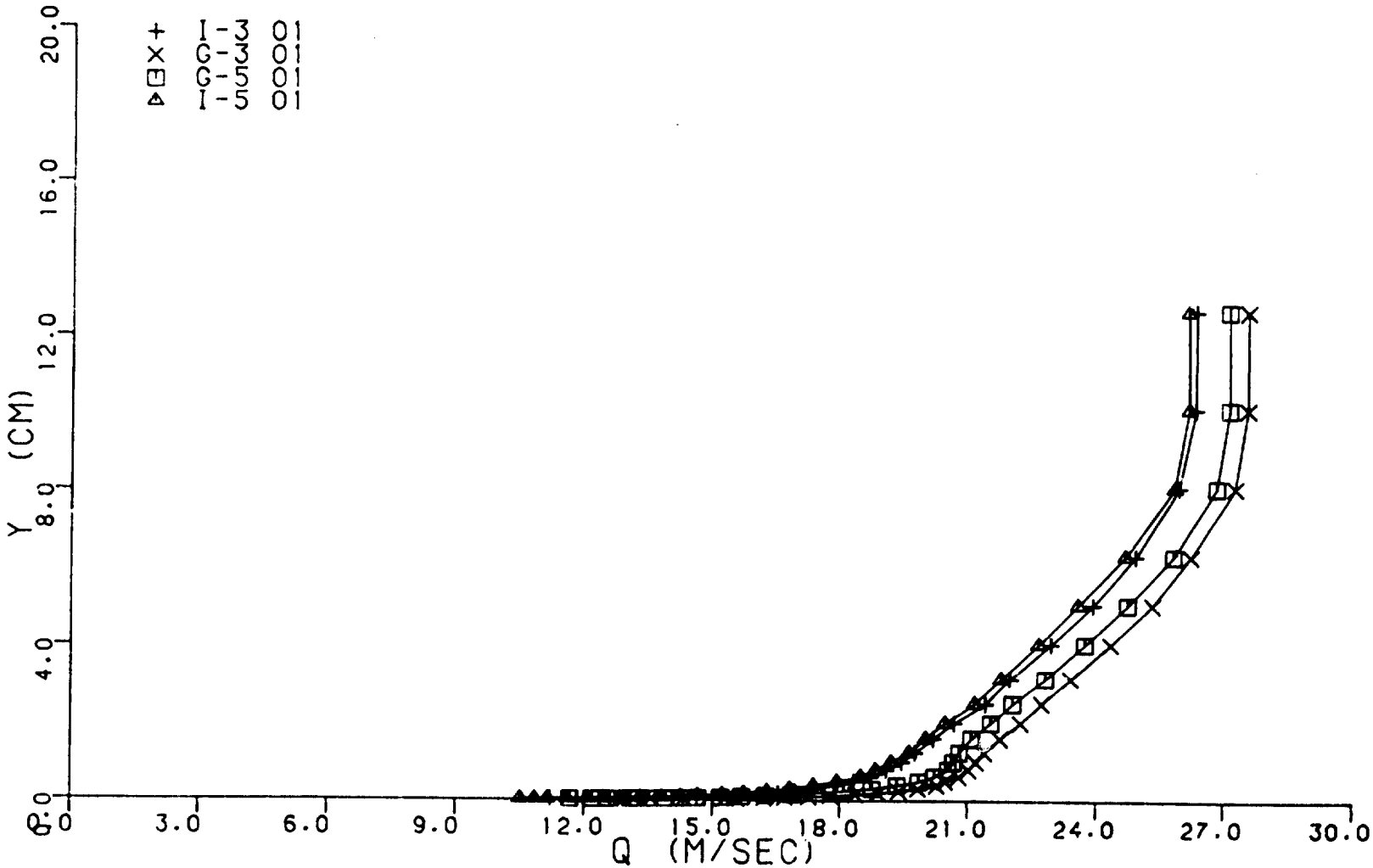

FIG. 5.10 MAGNITUDE OVERLAYS FOR THE -3 AND -5 ROWS

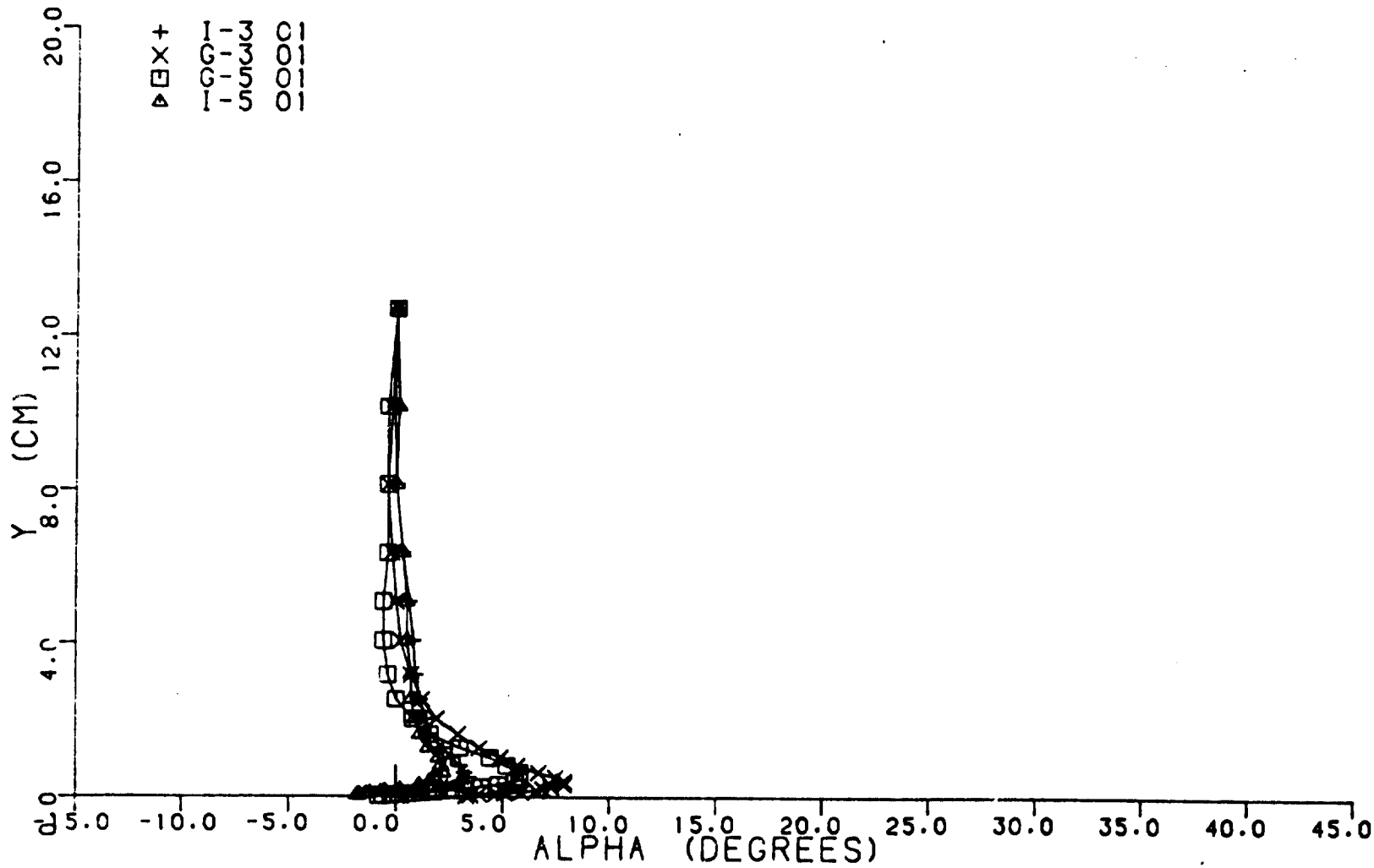

FIG. 5.11 ANGULAR OVERLAYS FOR THE -3 AND -5 ROWS

symmetry shows two-dimensional behavior except that a very small amount of skewing occurs very close to the wall--nominally two degrees or less--but the trend is clear. This small skew is similar to that identified with the two-dimensional profiles taken with the body removed and discussed earlier. Skewing along column C reaches over 30° as the body is approached. Station E-1 shows an interesting velocity magnitude reversal near the wall after the body leading edge has been passed with a corresponding reversal in the skew angle as well. Columns G and I show substantially less skewing though the nature of the skewed profile and the magnitude of the skewing depends on the position along the particular column.

In general the minimum velocity magnitudes and maximum skewing occurs for those flow stations closest to the teardrop. If one could imagine a control volume enclosing the stations and body in Fig. 5.1, conservation of mass suggests the flow velocities downstream of the teardrop will be larger than those in row 7 because of the reduced flow area available downstream in the body. This is the general case but the increase in velocity is not uniform. As the flow sweeps past the teardrop body there is a tendency toward returning to a two-dimensional-like profile.

Static Pressure Field

Omitting the singular zero pressure gradient case, the pressure gradient-wall shear vector orientations in two-dimensional flows are limited. These vectors may be directed in the same sense or in the opposite sense, but they are always collinear and may be treated in a scalar sense. The three-dimensional case is more complex. Wall static pressure measurements were made on a 1.27 cm (0.50 in.) grid to provide a large number of data points to obtain reasonable polynomial curve fits to the pressure data for the prediction of wall pressure gradients required in some of the three-dimensional similarity models. As is well known, the prediction of accurate gradients from experimental data requires special care. The wall pressure readings for each row and column were curve fit to a family of polynomial curves from second through eighth order with graphical output. Each figure was individually examined and in some instances the data was re-fitted through the same range of polynomials in a piecewise manner--that is, polynomial representations were obtained for

two or three segments with data overlap in all cases. This procedure was usually required where large variations in wall pressure occurred close to the body. Derivatives along the longitudinal and transverse directions were computed for these families of polynomial curves for each row and column, again with graphical output. For each row and column the choice of derivative values was obtained by "consensus" from the three polynomial representations which gave the closest agreement in the predicted derivatives. While this procedure involved considerable personal attention to a large quantity of data, it yielded the most consistant results and allowed for an estimate in the uncertainty of the predicted derivative results. Details of the instrumentation and method of estimates are given in Nelson (1979). Figure 5.12 shows the pressure gradient vectors for a forward quadrant of the body and Fig. 5.13 shows the pressure gradient vector map for the forward half of the body. Figure 5.13 was constructed to determine if the side wall boundary layers affected the body flow field as the body was moved about to take the necessary data. The results in this figure show excellent symmetry and are a good indication that the overall flow field was not noticeably changed by moving the body since only the most remote data on the far sides show modest differences.

This same computer software was used to predict gradients in the wall shear magnitude and in the wall shear direction which were required by some of the models tested. A lower degree of accuracy is identified with these two sets of gradients because of the smaller amount of data points for each row or column in the array over which gradients were calculated.

Wall Shear Field

The direct wall shear measurements by the omnidirectional meter for the tear drop flow are tabulated in Tables 5.1 - 5.5. The wall shear magnitude and angular uncertainties were determined after a Kline-McClintock error analysis as for the two-dimensional omnidirectional wall shear uncertainties and here again an attempt was made to approach an Nth order uncertainty estimate as discussed by Moffot (1980). No corrections of any type have been applied to the data in these tables. At least two wall shear readings were obtained on a 2.54 cm (1 in.) grid for the quadrant shown in Fig. 5.1 except for the I column where a 5.08 cm (2 in.) spacing

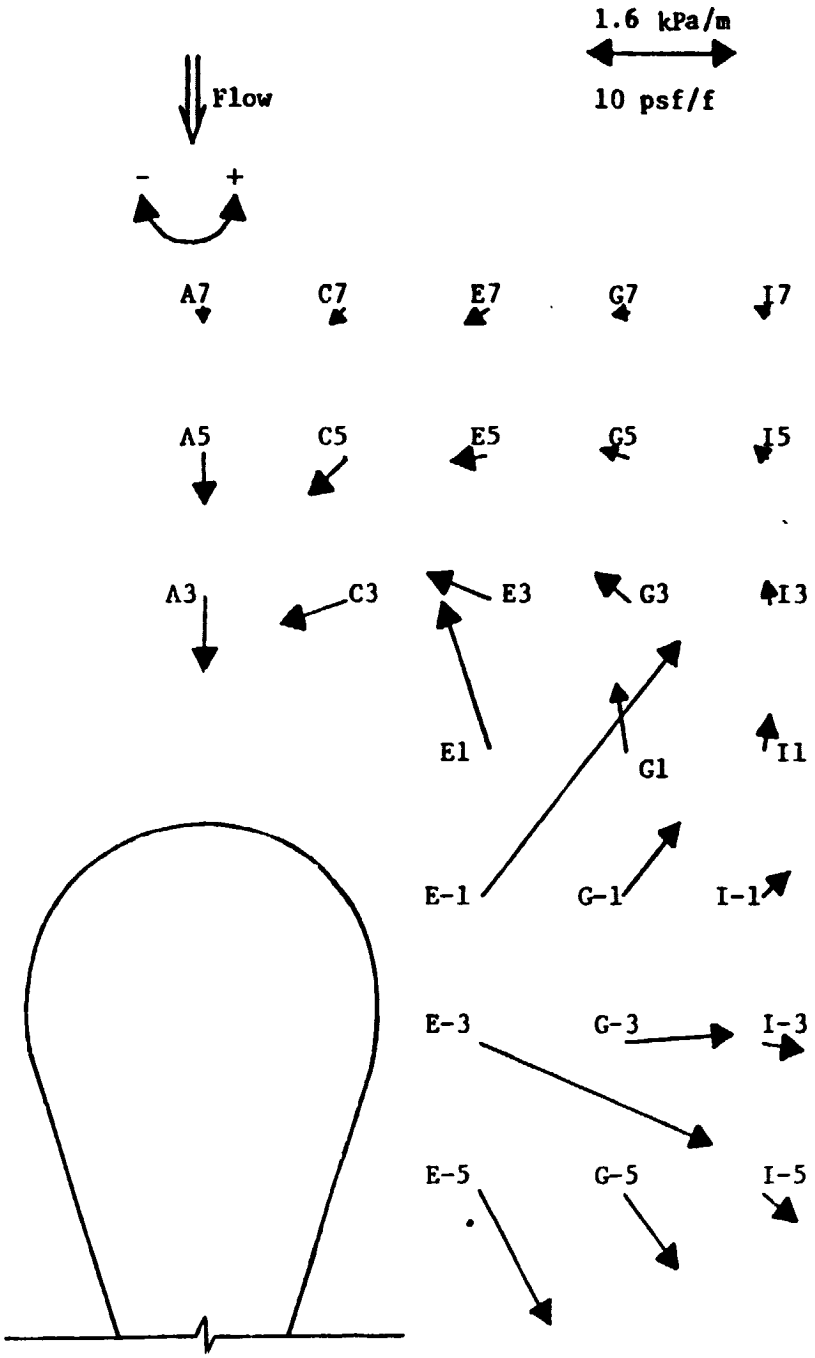

Fig. 5.12 Pressure Gradient Map for One Quadrant of the Teardrop Body

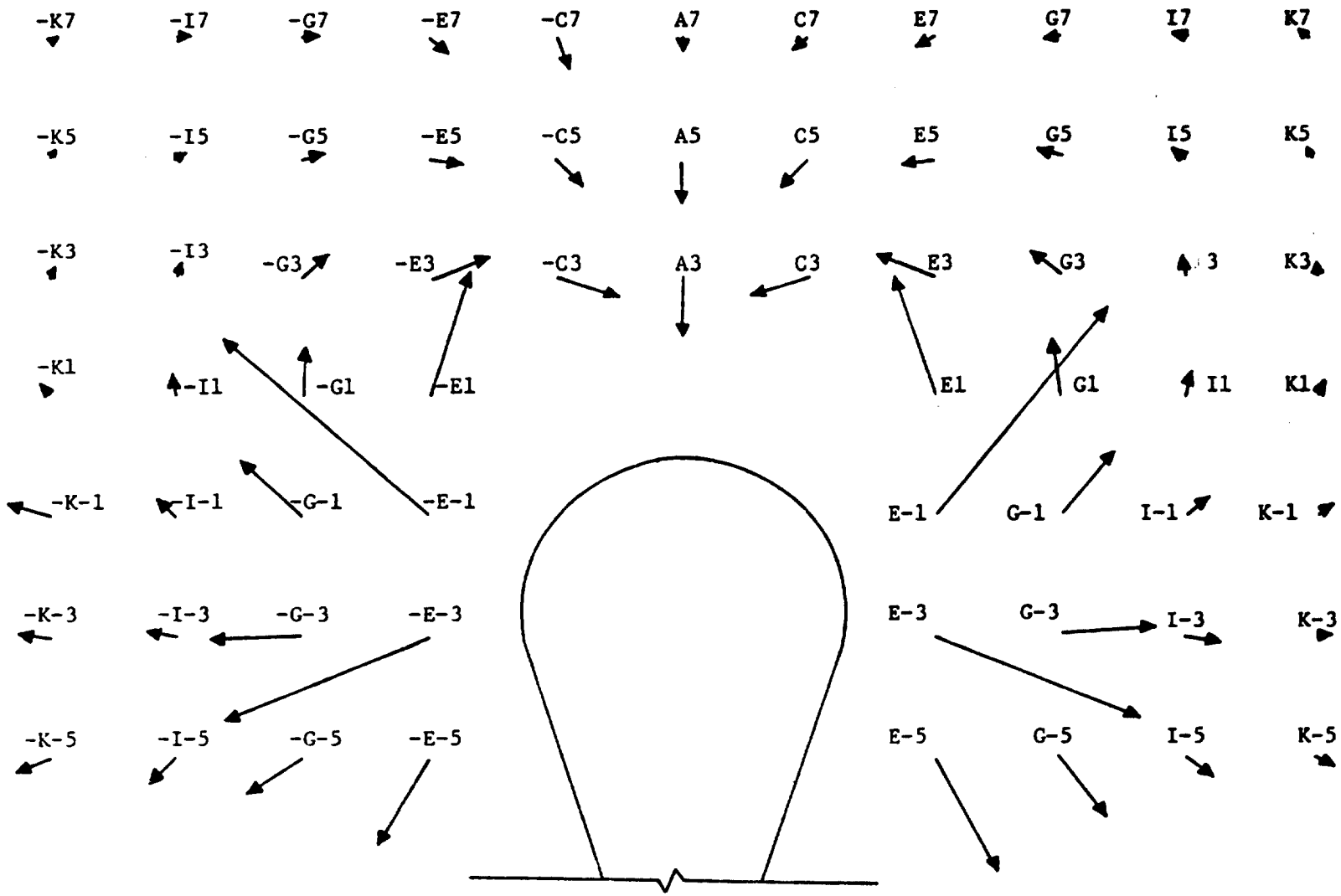

Fig. 5.13 Pressure Gradient Map for the Forward Half of the Teardrop Body

TABLE 5.1 OMNIDIRECTIONAL WALL SHEAR DATA FOR THE TEARDROP FLOW.

TEMPERATURE (DEGREES C)	BAROMETRIC PRESSURE (MM OF HG)	INLET DELTA H (CM OF H2O)	WALL SHEAR (PA)	WALL SHEAR UNCERTAINTY (PA)	ANGLE (DEGREES)	ANGLE UNCERTAINTY (DEGREES)	STATION	RE UNIT (1/M X 10**6)
26.1	712.7	2.794	0.76	0.020	-0.8	1.7	T A13	1.335
26.1	712.7	2.794	0.76	0.020	-0.2	1.7	T A13	1.335
26.1	712.7	2.794	0.71	0.020	-0.5	1.8	T A11	1.335
26.1	712.7	2.794	0.72	0.019	-1.2	1.7	T A11	1.335
26.1	712.7	2.794	0.69	0.017	-1.3	1.8	T A9	1.335
26.7	712.7	2.794	0.66	0.019	-0.9	1.8	T A9	1.332
26.7	712.5	2.794	0.56	0.016	-1.0	1.9	T A7	1.332
26.7	712.5	2.794	0.54	0.016	-0.7	1.9	T A7	1.332
26.7	712.5	2.794	0.49	0.015	-0.6	2.0	T A6	1.332
26.7	712.5	2.794	0.48	0.015	0.4	2.0	T A6	1.332
26.7	712.5	2.794	0.29	0.015	-2.2	3.0	T A4	1.332
26.7	712.5	2.794	0.28	0.015	-3.7	3.1	T A4	1.332
26.7	712.5	2.794	0.40	0.016	-1.7	2.4	T A5	1.332
26.7	712.5	2.791	0.40	0.013	-1.9	2.0	T A5	1.331
26.7	712.2	2.791	0.06	0.014	-6.4	13.3	T A3	1.331
26.7	712.2	2.791	0.06	0.010	-12.2	9.2	T A3	1.331
26.7	712.2	2.766	0.06	0.042	-127.8	26.5	T A2	1.330
26.7	712.0	2.784	0.04	0.059	-128.0	71.9	T A2	1.329
26.7	712.0	2.764	1.24	0.101	176.6	4.8	T A1	1.329
26.7	712.0	2.784	1.22	0.087	177.0	4.2	T A1	1.329
26.7	712.0	2.764	0.54	0.015	3.7	1.8	T B7	1.329
26.7	712.0	2.786	0.54	0.017	3.4	1.9	T B7	1.329
27.2	712.0	2.789	0.39	0.015	14.2	2.4	T B5	1.327
27.2	712.0	2.786	0.39	0.012	13.3	2.0	T B5	1.326
26.7	712.0	2.766	0.32	0.029	30.6	4.0	T B4	1.329
27.2	712.0	2.786	0.31	0.012	29.5	2.4	T B4	1.326
27.8	712.2	2.786	0.29	0.030	59.1	4.5	T B3	1.323
27.2	712.2	2.786	0.29	0.012	58.8	2.6	T B3	1.326
27.8	712.2	2.786	0.42	0.053	73.2	6.5	T B2	1.323
27.8	712.2	2.766	0.42	0.037	69.3	3.5	T B2	1.323
27.8	712.2	2.776	1.43	0.090	119.3	3.0	T B1	1.321
27.8	712.2	2.776	1.45	0.093	118.9	3.0	T B1	1.321
27.8	711.7	2.784	0.54	0.016	7.5	2.0	T C7	1.322
28.3	711.7	2.784	0.54	0.016	7.6	1.9	T C7	1.320
28.3	711.7	2.784	0.51	0.015	11.9	1.9	T C6	1.320
28.3	711.7	2.784	0.51	0.016	12.0	2.0	T C6	1.320
28.9	711.7	2.784	0.46	0.014	20.3	2.2	T C5	1.316

TABLE 5.2 OMNIDIRECTIONAL WALL SHEAR DATA FOR THE TEARDROP FLOW.

TEMPERATURE (DEGREES C)	BAROMETRIC PRESSURE (MM OF HG)	INLET DELTA H (CM OF H2O)	WALL SHEAR (PA)	WALL SHEAR UNCERTAINTY (PA)	ANGLE (DEGREES)	ANGLE UNCERTAINTY (DEGREES)	STATION	RE UNIT (1/M X 10**6)
28.9	711.7	2.784	0.45	0.015	20.4	1.8	T C5	1.316
28.3	711.5	2.784	0.44	0.014	34.1	2.2	T C4	1.319
28.3	711.5	2.771	0.46	0.015	33.4	2.1	T C4	1.316
28.9	707.4	2.769	0.50	0.018	53.1	2.1	T C3	1.309
28.9	707.4	2.769	0.51	0.016	51.6	2.0	T C3	1.309
28.9	707.4	2.769	0.72	0.035	58.6	2.9	T C2	1.309
29.4	707.4	2.769	0.74	0.028	57.8	2.4	T C2	1.305
25.7	710.2	2.771	1.59	0.071	73.6	2.6	T C1	1.324
27.2	710.2	2.771	1.59	0.059	74.8	2.8	T C1	1.321
26.7	710.4	2.776	0.62	0.018	9.4	1.8	T D7	1.326
27.2	710.4	2.776	0.60	0.017	9.3	1.9	T D7	1.322
27.2	710.9	2.784	0.55	0.016	21.6	1.7	T D5	1.325
27.2	710.9	2.784	0.55	0.017	18.7	1.9	T D5	1.325
27.2	710.9	2.784	0.56	0.021	30.8	2.0	T D4	1.325
27.2	710.9	2.784	0.56	0.021	30.6	1.7	T D4	1.325
26.7	711.5	2.774	0.65	0.019	43.4	1.6	T D3	1.326
26.7	711.5	2.774	0.66	0.019	42.6	1.7	T D3	1.326
26.7	711.5	2.774	0.92	0.024	48.2	1.6	T D2	1.326
26.7	711.5	2.774	0.90	0.023	47.8	1.6	T D2	1.326
26.7	711.5	2.774	1.49	0.038	39.5	2.0	T D1	1.326
26.7	711.5	2.771	1.50	0.047	39.3	2.0	T D1	1.325
26.7	711.5	2.771	1.85	0.061	42.0	2.6	T D0	1.325
26.7	711.5	2.766	1.86	0.049	42.3	2.1	T D0	1.324
26.7	710.7	2.781	0.63	0.018	10.5	1.8	T E7	1.327
26.7	710.7	2.779	0.65	0.017	9.7	1.8	T E7	1.326
26.7	709.9	2.779	0.60	0.017	14.4	1.9	T E6	1.326
26.7	709.9	2.774	0.63	0.018	14.0	1.7	T E6	1.324
26.7	709.9	2.774	0.61	0.017	19.2	1.8	T E5	1.324
26.7	709.9	2.774	0.59	0.017	18.5	1.9	T E5	1.324
26.7	708.9	2.776	0.66	0.018	25.8	1.9	T E4	1.324
26.7	708.9	2.774	0.67	0.020	25.4	1.6	T E4	1.324
26.7	708.9	2.774	0.76	0.018	32.0	1.7	T E3	1.324
26.7	709.2	2.766	0.77	0.021	31.4	1.6	T E3	1.322
26.7	709.2	2.769	0.94	0.024	35.2	1.6	T E2	1.323
26.7	709.2	2.769	0.95	0.024	35.3	1.6	T E2	1.323
26.7	709.2	2.769	1.27	0.030	31.3	1.5	T E1	1.323
26.7	709.2	2.769	1.24	0.028	31.0	1.5	T E1	1.323
25.6	709.4	2.771	1.66	0.056	18.1	2.0	T E0	1.330

TABLE 5.3 OMNIDIRECTIONAL WALL SHEAR DATA FOR THE TEARDROP FLOW.

TEMPERATURE (DEGREES C)	BAROMETRIC PRESSURE (MM OF HG)	INLET DELTA H (CM OF H20)	WALL SHEAR (PA)	WALL SHEAR UNCERTAINTY (PA)	ANGLE (DEGREES)	ANGLE UNCERTAINTY (DEGREES)	STATION	RE UNIT (1/M X 10**6)
25.6	709.7	2.771	1.68	0.048	18.4	1.9	T E0	1.330
25.6	709.7	2.771	1.76	0.079	14.7	3.0	T E-1	1.330
25.6	709.7	2.771	1.75	0.057	15.3	2.3	T E-1	1.330
25.6	709.9	2.771	1.82	0.066	11.4	2.6	T E-2	1.331
25.6	709.9	2.771	1.82	0.067	10.8	2.6	T E-2	1.331
25.6	709.9	2.771	1.86	0.077	6.2	2.6	T E-3	1.331
26.1	710.2	2.771	1.86	0.063	5.9	2.0	T E-3	1.327
25.6	710.2	2.781	1.85	0.051	6.3	1.7	T E-4	1.333
25.6	710.2	2.781	1.86	0.053	6.3	1.8	T E-4	1.333
25.6	710.2	2.779	1.69	0.048	5.9	1.8	T E-5	1.333
25.6	710.2	2.779	1.69	0.048	5.6	1.8	T E-5	1.333
26.1	710.2	2.784	0.67	0.020	10.3	1.8	T F7	1.331
26.1	710.2	2.784	0.67	0.020	10.2	1.8	T F7	1.331
26.1	710.2	2.784	0.66	0.019	17.5	1.9	T F5	1.331
26.1	710.2	2.784	0.68	0.020	16.7	1.8	T F5	1.331
26.7	709.9	2.779	0.74	0.020	19.8	1.8	T F4	1.326
26.7	709.9	2.771	0.76	0.022	19.6	1.8	T F4	1.324
26.7	709.9	2.771	0.83	0.021	23.1	1.6	T F3	1.324
26.7	709.9	2.766	0.82	0.022	22.5	1.7	T F3	1.323
27.2	705.4	2.756	0.89	0.022	25.7	1.6	T F2	1.313
27.2	705.4	2.751	0.89	0.023	25.9	1.6	T F2	1.311
27.2	705.1	2.751	1.05	0.027	23.0	1.6	T F1	1.311
27.2	705.1	2.751	1.04	0.026	23.0	1.6	T F1	1.311
27.2	705.1	2.751	1.22	0.029	15.4	1.5	T F0	1.311
27.2	705.1	2.751	1.20	0.028	15.2	1.5	T F0	1.311
27.2	705.1	2.751	1.42	0.032	6.0	1.5	T F-1	1.311
27.2	705.1	2.751	1.42	0.032	6.2	1.6	T F-1	1.311
25.6	708.7	2.809	1.66	0.037	-1.6	1.5	T F-2	1.339
25.6	708.9	2.779	1.68	0.038	-1.2	1.5	T F-2	1.332
25.6	710.2	2.779	1.60	0.037	-5.3	1.6	T F-3	1.333
26.1	710.2	2.779	1.59	0.036	-4.9	1.6	T F-3	1.329
26.1	710.2	2.779	1.42	0.041	-6.5	2.0	T F-4	1.329
26.1	710.2	2.779	1.42	0.032	-7.0	1.5	T F-4	1.329
26.1	710.2	2.779	1.25	0.030	-6.5	1.6	T F-5	1.329
26.1	710.2	2.779	1.25	0.038	-5.9	2.0	T F-5	1.329
26.1	710.2	2.779	0.71	0.018	9.8	1.6	T G7	1.329
26.1	710.2	2.779	0.73	0.019	9.1	1.7	T G7	1.329
26.1	710.2	2.779	0.73	0.019	12.1	1.6	T G6	1.329

TABLE 5.4 OMNIDIRECTIONAL WALL SHEAR DATA FOR THE TEARDROP FLOW.

TEMPERATURE (DEGREES C)	BAROMETRIC PRESSURE (MM OF HG)	INLET DELTA H (CM OF H2O)	WALL SHEAR (PA)	WALL SHEAR UNCERTAINTY (PA)	ANGLE (DEGREES)	ANGLE UNCERTAINTY (DEGREES)	STATION	RE UNIT (1/M X 10**6)
26.1	710.2	2.779	0.73	0.020	11.4	1.8	T G6	1.329
26.7	709.9	2.769	0.78	0.019	13.8	1.6	T G5	1.323
26.7	709.9	2.769	0.79	0.020	13.6	1.7	T G5	1.323
26.1	709.9	2.769	0.80	0.020	15.6	1.6	T G4	1.327
26.7	709.9	2.769	0.82	0.020	15.3	1.6	T G4	1.323
26.7	709.9	2.769	0.86	0.023	16.7	1.7	T G3	1.323
26.7	709.9	2.766	0.87	0.023	17.2	1.7	T G3	1.323
26.7	709.9	2.766	0.94	0.023	16.9	1.6	T G2	1.323
26.7	709.9	2.766	0.94	0.024	17.1	1.7	T G2	1.323
26.7	709.9	2.766	1.01	0.024	14.7	1.6	T G1	1.323
26.7	709.9	2.766	1.00	0.024	14.7	1.6	T G1	1.323
26.7	709.7	2.766	1.11	0.027	10.2	1.6	T G0	1.322
26.7	709.7	2.766	1.11	0.026	10.3	1.6	T G0	1.322
26.7	709.7	2.766	1.20	0.026	4.0	1.6	T G-1	1.322
26.7	709.7	2.766	1.20	0.028	3.9	1.6	T G-1	1.322
26.7	709.7	2.766	1.27	0.029	-2.0	1.6	T G-2	1.322
26.7	709.7	2.766	1.28	0.029	-2.1	1.6	T G-2	1.322
26.7	709.7	2.766	1.26	0.029	-7.0	1.6	T G-3	1.322
26.7	709.7	2.766	1.28	0.030	-6.8	1.6	T G-3	1.322
26.1	709.7	2.774	1.23	0.029	-10.1	1.6	T G-4	1.328
26.1	709.9	2.774	1.23	0.028	-10.1	1.5	T G-4	1.328
25.6	709.9	2.774	1.11	0.026	-11.9	1.6	T G-5	1.331
26.7	710.2	2.776	1.10	0.026	-11.9	1.5	T G-5	1.325
26.1	710.2	2.776	0.79	0.021	7.8	1.7	T H7	1.329
26.7	710.2	2.776	0.79	0.021	7.4	1.7	T H7	1.325
26.7	710.2	2.776	0.80	0.029	10.5	2.1	T H5	1.325
26.7	710.2	2.776	0.81	0.022	10.0	1.7	T H5	1.325
26.7	710.2	2.776	0.85	0.022	12.0	1.7	T H4	1.325
26.7	710.2	2.776	0.84	0.022	12.1	1.7	T H4	1.325
26.7	710.2	2.776	0.87	0.036	12.6	2.6	T H3	1.325
26.7	710.4	2.776	0.87	0.021	12.2	1.6	T H3	1.326
26.1	712.2	2.781	0.96	0.024	11.9	1.7	T H2	1.332
26.1	712.2	2.781	0.97	0.024	11.9	1.7	T H2	1.332
26.1	712.2	2.781	1.00	0.024	9.9	1.6	T H1	1.332
26.1	712.2	2.781	1.02	0.024	10.0	1.6	T H1	1.332
26.1	712.2	2.781	1.06	0.025	7.0	1.6	T H0	1.332
26.1	712.2	2.781	1.11	0.026	2.7	1.6	T H-1	1.332
26.7	712.2	2.781	1.11	0.026	2.8	1.6	T H-1	1.328

TABLE 5.5 OMNIDIRECTIONAL WALL SHEAR DATA FOR THE TEARDROP FLOW.

TEMPERATURE (DEGREES C)	BAROMETRIC PRESSURE (MM OF HG)	INLET DELTA H (CM OF H2O)	WALL SHEAR (PA)	WALL SHEAR UNCERTAINTY (PA)	ANGLE (DEGREES)	ANGLE UNCERTAINTY (DEGREES)	STATION	RE UNIT (1/M X 10**6)
26.1	712.2	2.781	1.04	0.025	7.1	1.6	T H0	1.332
26.1	712.2	2.781	1.12	0.026	-1.5	1.6	T H-2	1.332
26.7	712.2	2.781	1.14	0.026	-1.5	1.6	T H-2	1.328
26.1	712.2	2.781	1.14	0.027	-5.3	1.6	T H-3	1.332
26.1	712.5	2.781	1.13	0.026	-5.2	1.6	T H-3	1.332
26.7	714.6	2.799	1.12	0.026	-7.7	1.6	T H-4	1.335
26.7	715.0	2.799	1.11	0.027	-8.0	1.6	T H-4	1.335
26.1	715.0	2.799	1.03	0.024	-9.7	1.6	T H-5	1.339
26.7	715.0	2.799	1.03	0.024	-9.6	1.6	T H-5	1.335
26.7	715.0	2.799	0.78	0.020	6.5	1.7	T I7	1.335
26.7	715.0	2.799	0.78	0.020	6.4	1.7	T I7	1.335
26.7	715.0	2.799	0.81	0.021	8.2	1.7	T I5	1.335
26.7	715.0	2.794	0.81	0.022	8.2	1.7	T I5	1.334
26.7	714.8	2.794	0.88	0.022	9.3	1.7	T I3	1.334
26.7	714.8	2.791	0.88	0.022	9.3	1.7	T I3	1.333
26.7	714.8	2.791	0.95	0.024	7.1	1.7	T I1	1.333
26.7	714.8	2.791	0.95	0.023	6.7	1.6	T I1	1.333
26.7	714.5	2.791	1.04	0.025	1.5	1.6	T I-1	1.333
26.7	714.5	2.791	1.04	0.025	1.5	1.6	T I-1	1.333
26.7	714.5	2.791	1.05	0.025	-4.6	1.6	T I-3	1.333
26.7	714.5	2.791	1.06	0.026	-4.5	1.6	T I-3	1.333
26.7	714.5	2.791	0.99	0.024	-8.2	1.6	T I-5	1.333
26.7	714.5	2.791	0.98	0.024	-8.1	1.6	T I-5	1.333
26.7	714.5	2.791	0.74	0.020	4.4	1.8	T I9	1.333
26.7	714.5	2.791	0.74	0.020	3.9	1.8	T I9	1.333
26.7	714.5	2.791	0.72	0.020	4.6	1.8	T G9	1.333
26.7	714.5	2.791	0.72	0.019	4.7	1.7	T G9	1.333
26.7	714.5	2.791	0.48	0.016	-23.9	2.0	T -C5	1.333
26.7	714.5	2.791	0.48	0.017	-24.0	1.8	T -C5	1.333
26.7	714.5	2.791	0.80	0.022	-31.2	1.6	T -E3	1.333
26.7	714.5	2.791	0.81	0.022	-31.3	1.7	T -E3	1.333
26.1	718.8	2.814	0.65	0.018	3.5	1.8	T C9	1.346
26.7	718.8	2.814	0.67	0.019	2.7	1.8	T C9	1.342
26.1	718.8	2.814	0.47	0.015	22.1	1.9	T C5	1.346
26.7	719.1	2.814	0.48	0.017	20.7	2.0	T C5	1.343
26.7	719.1	2.814	0.70	0.019	4.8	1.8	T E9	1.343
26.7	719.1	2.814	0.70	0.018	4.6	1.7	T E9	1.343
26.7	719.3	2.814	0.80	0.021	31.9	1.6	T E3	1.343

was used. Additional wall shear values were obtained in a row 9 inches in front of the tear drop nose and at stations A11 and A13. The wall shear vectors at the flow stations shown in Fig. 5.1 have been drawn to scale in Fig. 5.14. The curvilinear rectangle at each vector tip indicates the uncertainty estimated for the magnitude and direction of each shear vector shown. The separation line shown in the figure was determined from a oil streak visualization study shown in Fig. 5.15 and obtained with titanium dioxide particles suspended in a diesel fuel-mineral oil mix.

Figure 5.16 shows a comparison of the preliminary data of Tennant (1977) with that reported here. These data are not directly comparable since they were obtained at different tunnel unit Reynolds numbers. The larger wall shear stress magnitudes of Tennant's data are a result of a 12% higher unit Reynolds number. For comparison purposes it is noted that extensive measurements in a nominally two-dimensional flow indicated a 20% higher wall shear for the higher Reynolds number tunnel conditions than for the lower speed conditions. It is noted that the pseudo two-dimensional nominally symmetric flow at station A7 shown in Fig. 5.16 reflects an equal difference. It is not possible to predict shear magnitude differences between the readings in the fully three-dimensional flow field. Agreement between the wall shear stress angles is generally within the uncertainty bands shown, although it should be noted that these angles would also be expected to change slightly for a change in tunnel unit Reynolds number. Note that the largest differences appear near the separation horseshoe vortex where measurements were very difficult because of larger fluctuations in the detected wall shear. Overall, each data set gives similar results for the two different unit Reynolds numbers showing the repeatability of the omnidirectional meter between the two studies. Repeatability of measured data within each study was generally well within the indicated uncertainty bands.

As the leading edge of the body was approached a reversal of the wall shear direction was noted near station A3. A complete flow reversal was recorded at station A1 with a very high local shear stress identified with the horseshoe vortex behind the upstream separation sheet. It appears that station C1 is also within the separation vortex. The shear vector direction indicates a significant downstream wall flow component develops

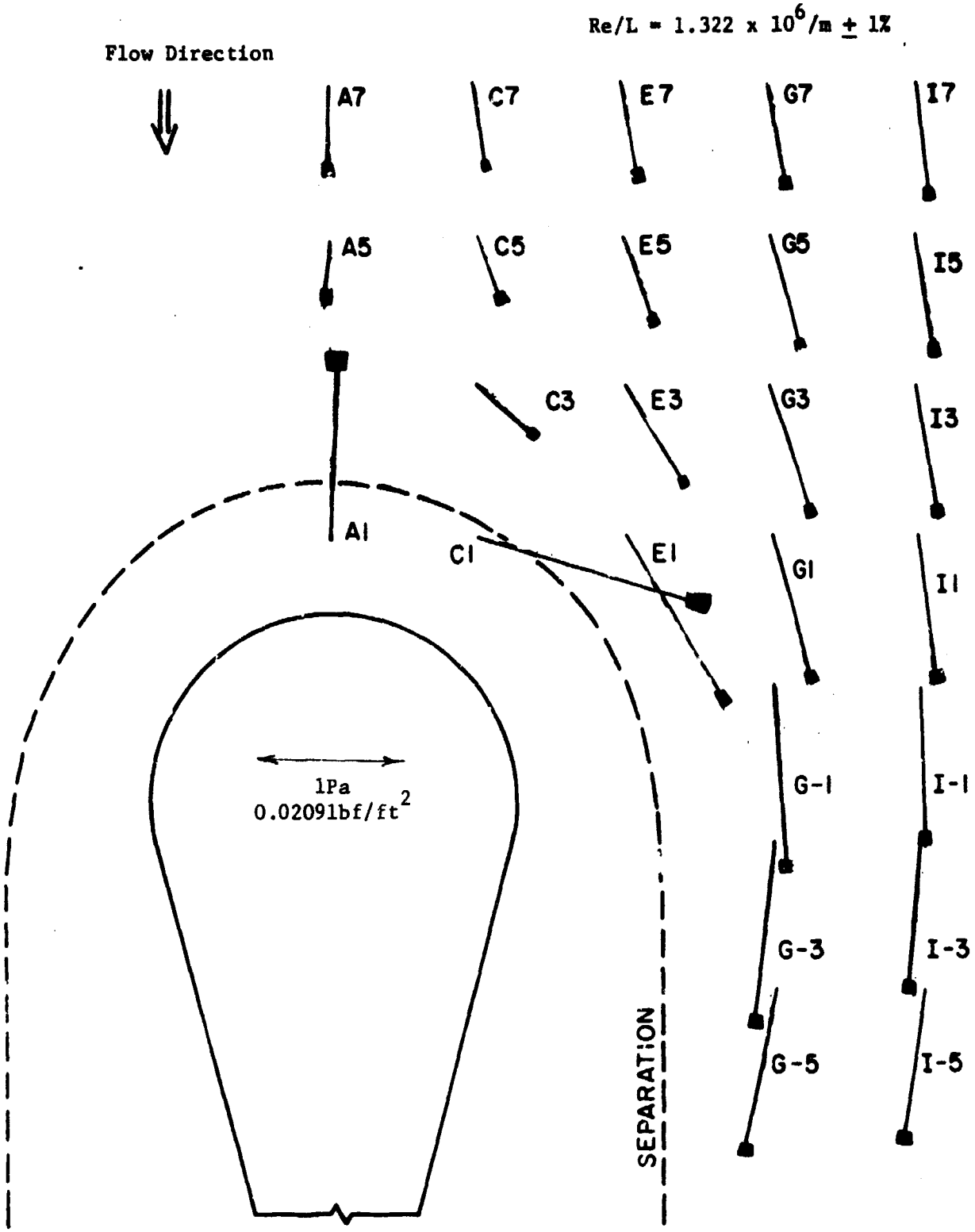

Fig. 5.14 Wall Shear Vector Map

Fig. 5.15 Oil Streak Pattern

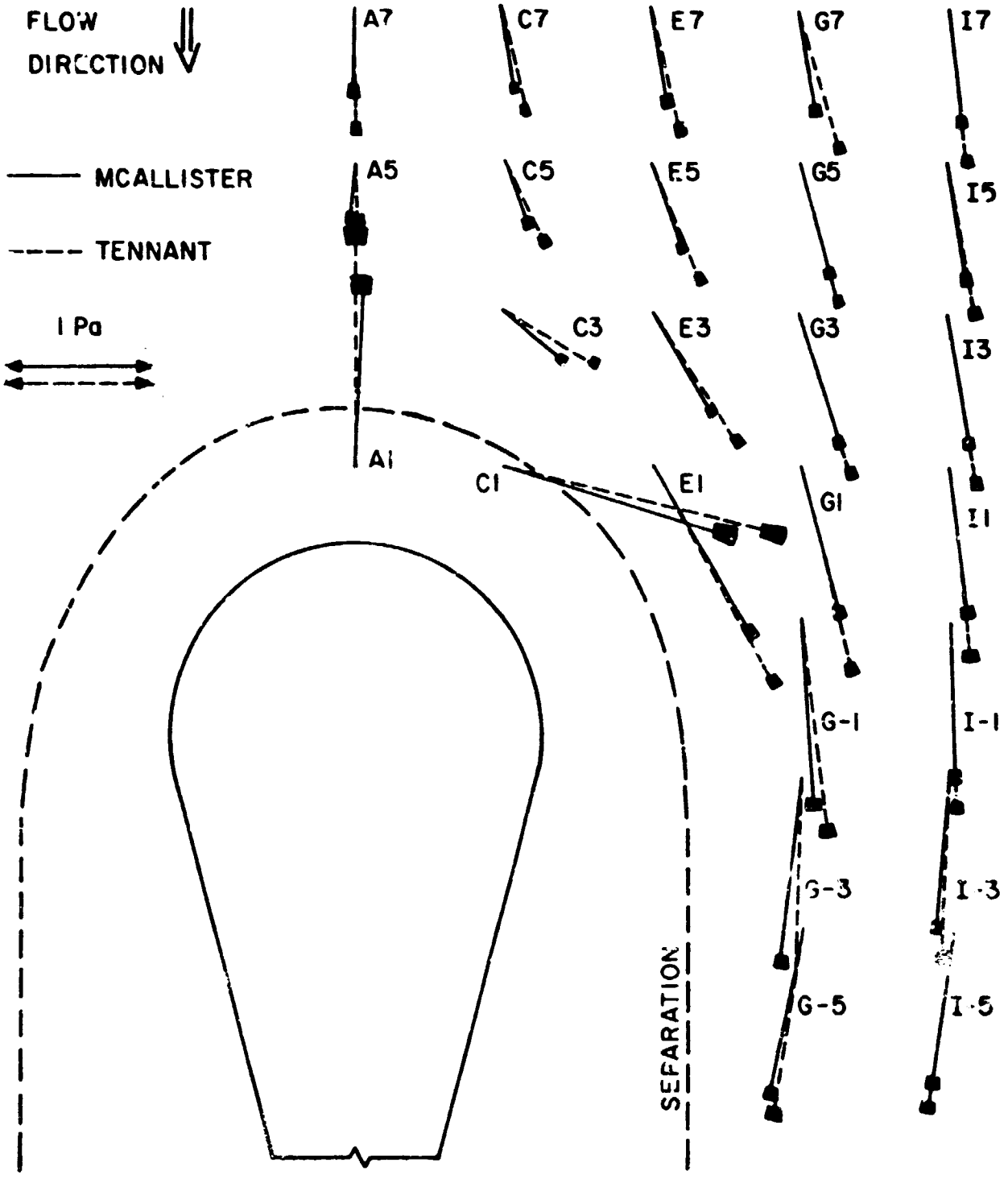

Fig. 5.16 Comparison of Wall Shear Maps of McAllister (1979) and Tennant (1977)

in a relatively short distance from the symmetry plane. This separated flow near the cylinder-floor corner appears to be complex and is being investigated by LDV techniques in a subsequent study. In the unseparated region the wall shear appears well behaved as its angle turns first away from the body as the flow approaches and moves around the cylinder, and then turns toward the body as the flow reverses direction to follow the trailing edge.

A superposition of the wall shear map and the pressure gradient map shown in Fig. 5.17 indicates the very wide range of pressure gradient-wall shear stress vector orientations varying from nearly collateral and in the same sense along the center line (the A) stations, to nearly collateral and in the opposite sense at E-1 and G-1, to nearly orthogonal at station G-1. These results confirm the anticipated further difficulties in the application of any pressure gradient corrections such as those in Fig. 3.15 to three-dimensional flow measurements.

Wall Streamline Directions

As discussed earlier, recent experiments (Rogers and Head (1969), Hebbar and Melnik (1978)) and analyses (Pierce and East (1972), Klinksiek and Pierce (1973)) do not support the assumption of a collateral near-wall layer in three-dimensional turbulent flow as suggested by polar representations of velocity profiles as in Fig. 2.4. Thus the assumption that the limiting wall streamline direction or the wall shear stress direction can be taken as the flow direction indicated by a small velocity probe very near to the wall is at best highly suspect. Figure 5.18 compares the velocity vector direction at 0.25 mm (0.010 in.) from the wall and the measured wall shear stress directions from the omnidirectional meter. The wall shear stress and velocity vector angles can differ significantly; for example, at station C3 the angles differ by over 13°, and are well outside any reasonable uncertainties for both measurements. These results are consistent with studies noted earlier which indicate that the velocity vector generally changes direction continuously to the wall. Since the measurements of local wall shear stress direction can be significantly different from the typical nearest wall velocity direction, the common practice of inferring the limiting wall stream line angle from the latter

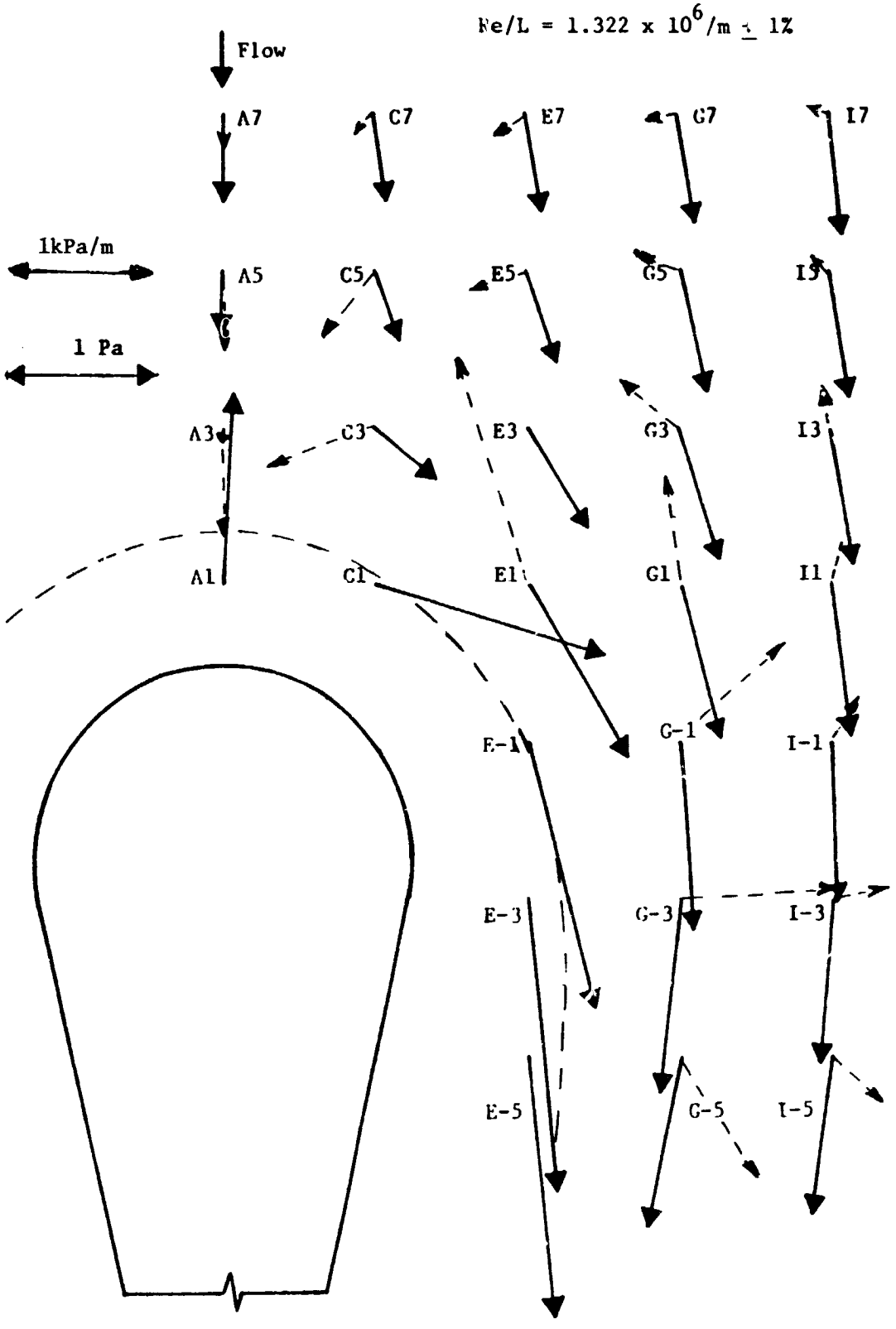

Fig. 5.1 Wall Shear-Pressure Gradient Orientations

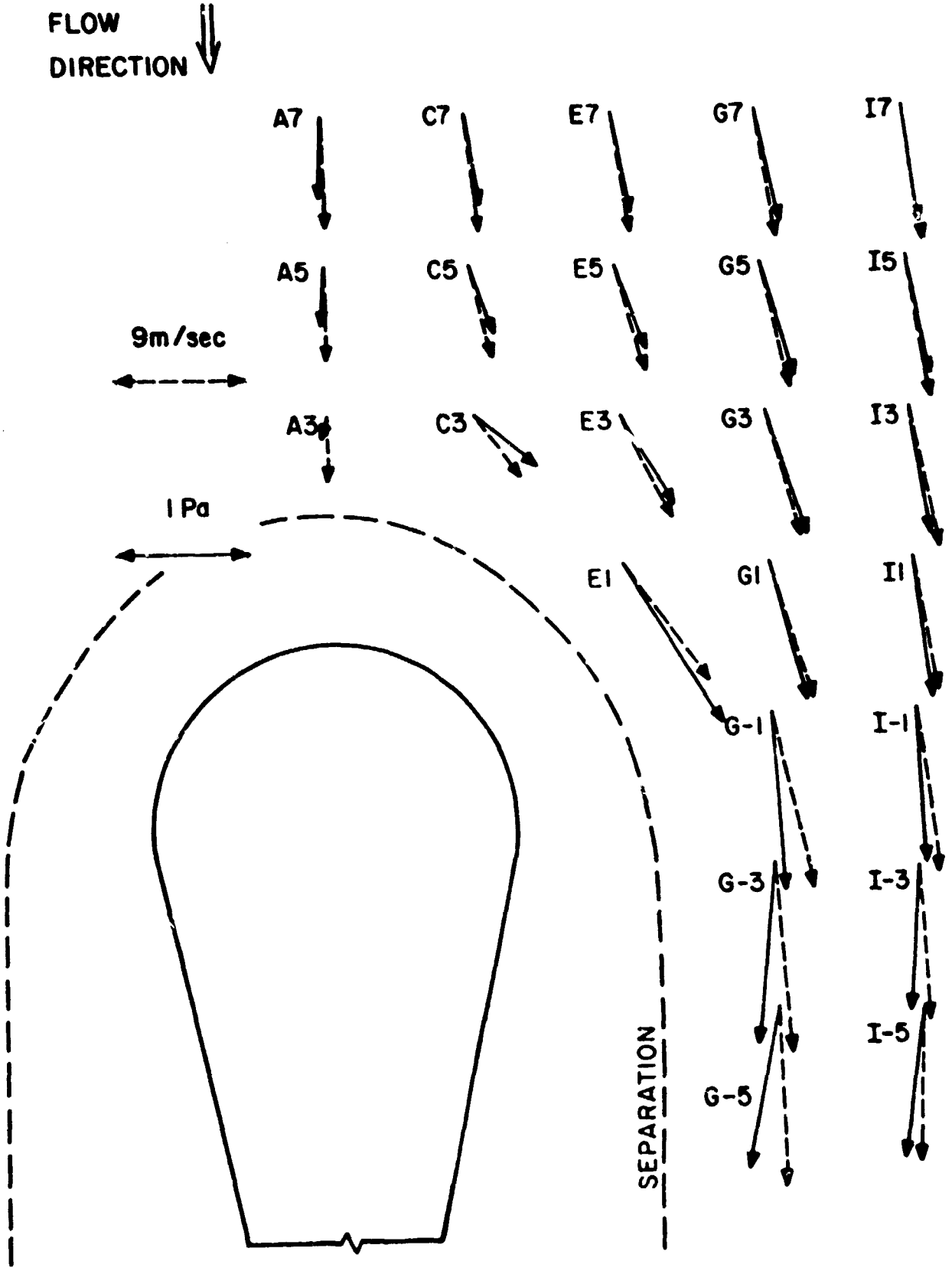

Fig. 5.18 Wall Shear and Nearest Wall Velocity Vector Map

can yield significant errors for at least some flow conditions. Limiting wall streamline directions were measured from the oil streak patterns shown in Fig. 5.15 and the results are presented in Table 5.6. With only a few exceptions, there is excellent agreement between the oil streak directions and the direct force wall shear directions, and as noted above, these directions are different from those of the nearest wall velocity vector indicating further turning of the velocity vector down to the wall.

The strong agreement between the oil streak limiting wall stream line directions and the direct force wall shear directions suggests that any pressure gradient effects on the direct force sensing shear meter affected the wall shear directions minimally, if at all. The results in Table 5.6 are interesting from another point of view. It has been suggested, at least informally, that the demonstrated use of miniature, dual sensor, buried wire flush mounted heat meters in a three-dimensional turbulent flow by Higuchi and Peake (1978) in effect validates the use of such devices for quantitative results in other such three-dimensional flows. It has been inferred that the smallness of such miniature heat meter sensors would result in a minimal thermal penetration into the skewed near-wall flow so that the limiting wall streamline direction would be accurately measured. The comparison of wall flow angles measured by oil streak patterns and the dual element heat sensor calibrated in a two-dimensional flow and reported in Heguchi and Peake show consistent and typical differences ranging from about 5° to as much as 15°. Based on the high degree of agreement found in this study between the wall flow angles measured from the oil streak patterns and the wall shear direction measured by the direct force sensing shear meter, at this point in time it would seem somewhat presumptuous to assume that such miniature heat sensors do in fact report limiting wall streamline directions accurately. Parenthetically, it is also noted that the wall shear magnitude values reported by Higuchi and Peake were based on a two-dimensional calibration using a Preston tube. No validation of this two-dimensional calibration was attempted in any three-dimensional flow.

Finally Fig. 5.19 shows the relative orientations of the freestream streamline directions and the local wall shear stress directions. As

Table 5.6

Comparison of Flow Angles[#]

Station	Shear Meter	Velocity Probe*	Oil Streaks
A7	- 0.9°	1.3°	+ 0.5°
A5	- 1.8	1.7	
C7	7.5	6.8	7.0
C5	20.3	14.2	20.5
C3	52.3	39.1	47.0
E7	10.1	8.4	10.0
E5	18.8	14.7	18.0
E3	31.7	26.6	31.5
E1	31.1	36.2	32.5
G7	9.4	9.1	10.5
G5	13.7	12.7	16.0
G3	16.9	16.5	16.5
G1	14.7	17.8	15.5
G-1	3.9	13.1	5.5
G-3	- 6.9	3.9	- 4.0
G-5	-11.9	2.0	-10.5
I7	6.4	7.6	7.0
I5	8.2	9.0	8.0
I3	9.3	11.0	9.0
I1	6.9	10.0	7.3
I-1	1.5	7.2	4.0
I-3	- 4.6	1.1	- 3.0
I-5	- 8.1	- 2.7	- 7.0

[#]Tunnel inlet unit Reynolds number of 1.30×10^6/m

*Probe OD = 0.25 mm (0.020 in.) with the probe on the wall

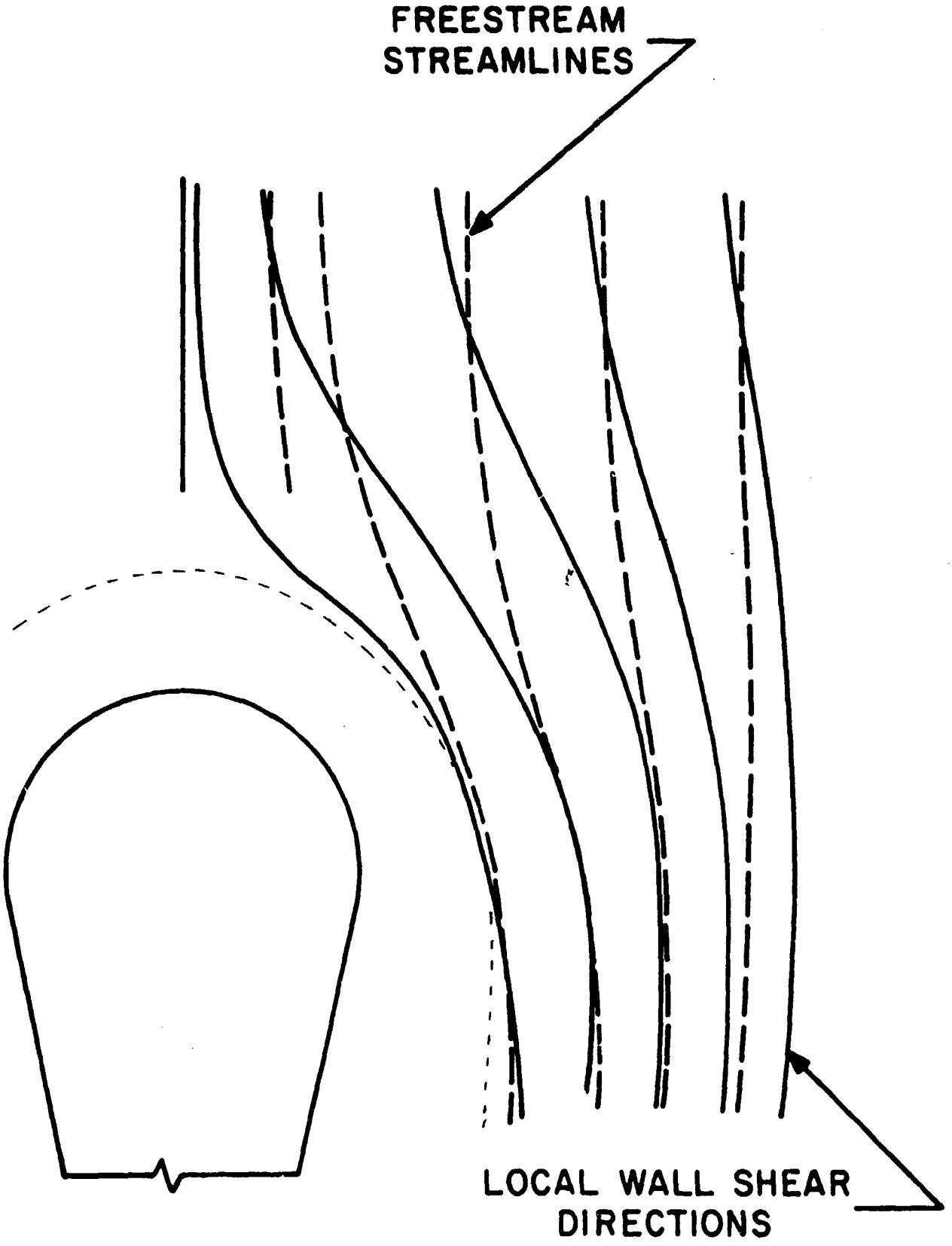

Fig. 5.19 Freestream Streamline and Local Wall Shear Directions

expected, the collinear upstream character of these two families is quickly lost when significant freestream streamline curvature begins with the corresponding pressure-driven secondary flow in the boundary layer. The figure also suggests that if one identifies wall streamlines with the local wall shear stress, then these wall streamlines appear to turn substantially less than the freestream streamlines. An ultimate return toward parallelism appears downstream when the freestream streamlines lose their curvature. The freestream streamlines in the lower quandrant of Fig. 5.19 tend to become parallel with the body centerline, rather than follow the body contour. This behavior appears to relate to the thickening of the separation horseshoe vortex as it wraps itself around the body as evidenced by the nearly constant width shown for the downstream portions of the separation line in Fig. 5.15. The influence of this separation vortex and the free-stream flow in close proximity to the body, particularly in the regions downstream of the midplane of the body, remains to be determined in further work in this three-dimensional, separated flow.

VI. THREE-DIMENSIONAL SIMILARITY MODEL RESULTS

Introduction

In making an assessment of the validity of any near-wall similarity model for a three-dimensional flow, the first question that arises is that of over what range of y^+ values might one expect to find similarity. As discussed earlier, in his extensive study of 2DTBL data, Coles (1956, 1968) suggests that the logarithmic behavior begins at about y^+ of 50 and for moderate pressure gradient flows extends to about 300. Questions on possible inaccuracies in velocity measurements arising from high-turbulence effects and wall interference or wall proximity effects for data in the lower range of this $50 \leq y^+ < 300$ interval for two-dimensional flows would also likely be valid for these dimensional flows as well. It is also noted that the upper limit of $y^+ \approx 300$ is reduced in adverse pressure gradient flows and tends to increase in favorable pressure gradient flows. For the two-dimensional case Perry (1966) and Brown and Joubert (1969) suggest a formal measure of the departure of the near-wall velocity profile from the logarithmic form in terms of a pressure gradient parameter and based on the half power model used to describe the flow in this region.

For the three-dimensional data in this study this two-dimensional experience will be used as a guide in the test for similarity. For the six simpler similarity models, for the Perry and Joubert model, and for the principal flow component of the three more complex models, the primary focus will be on data in the $50 \leq y^+ < 300$ range and clearly this upper limit of 300 must be considered flexible just as in the two-dimensional case. One might expect the six simple similarity models to behave as in the 2DTBL where pressure gradient strongly affects the range of similarity. Some of the more complex models incorporate pressure gradient information and in these cases the agreement with experimental velocity-wall shear data might be expected to be maintained at these higher y^+ values even in pressure gradient circumstances.

It is worth noting, however, that in the early study of three-dimensional flows with indirect wall shear measurements with Preston tubes (which presumes the existence of two-dimensional like near-wall

similarity in three-dimensional flows), Prahlad (1968) showed a high degree of velocity profile data consistency in the $y^+ < 50$ range though not with the logarithmic like law. Such consistency was also found in the velocity data of a few others including Ezekwe (1974), and in the measurements in this study as well.* It will prove to be useful to evaluate these similarity models in a secondary focus in this $y^+ < 50$ range as well.

In the case of the three models which propose a transverse component of the flow (in the coordinate system unique to each model), there is no firm basis for a choice as to the y^+ region to focus on in looking for near-wall similarity.

In the following discussion and related figures the ten similarity models tested are frequently indentified by letter rather than name designation and while the designations are obvious Table 6.1 summarizes the short-form usage.

The test of the suitability of the ten similarity models evaluated here is a graphical or visual test. In each case an "analytical" similarity line is shown as a solid line of q^+ (or u^+ and w^+) vs. y^+. In some models (PJ, B, and WLC) input from experimental data is required to construct this analytical line while in the others this line is independent of experimental data. Next, the experimentally measured velocity profile and local wall shear stress are combined as the various models specify to provide pairs of q^+ (or u^+ and w^+) and y^+ coordinates and these are shown as symbols. For the ten similarity models including all velocity components, each velocity profile-[illegible]ar station would require 13 figures. To reduce the number of figures re[illegible]ed, multiple plotting was used to show the ten similarity models in a sequence of six figures on a single page. The following describes the general scheme and specific exceptions will be noted in the text as they occur. The first two figures on the top of each page combine the six, simpler similarity models, three to a figure. This is convenient since for these six similarity models the analytical model is identical--it is the equivalent velocity used in constructing the q^+ and y^+ pairs from experimental data that differs among the models. In these first two figures the analytical model line is the two-dimensional near-wall similarity model and this has been drawn for the Spalding third order

*Similar consistent behavior is reported by K. C. Brown. See footnote on page 89.

Table 6.1. Three-Dimensional Similarity Model Designations

Model	Short Forms
Coles (1956)	C
Johnston (1960)	J
Prahlad (1968)	P
Hornung & Joubert (1963)	HJ
Freestream Profile Pierce and Krommenhoek (1968)	F
East & Hoxey (1969)	EH
Perry & Joubert (1965)	PJ
van den Berg (1973)	B
Chandrashekhar & Swamy (1976)	CS
White, Lessmann, & Christoph (1975)	WLC

equation. This choice allows a comparison of these models in the $50 \leq y^+ < 300$ range of principal focus as well as the very near-wall interval of $y^+ < 50$ of secondary focus. Analytical lines for both the NPL and Patel constants are shown for comparison purposes. The four more complex similarity models are shown in pairs in the next four figures. For these figures only the model lines for the Patel constants are shown except for the CS model, where the specific constants given by the model authors are used. Additionally, since these four models all return the two-dimensional like logarithmic law, the model lines are terminated at $y^+ = 50$ since one does not expect log-like behavior below this value. The first figure of the first pair shows the PJ model and the principal flow component, u^+, of the WLC model, with the PJ analytical model line labeled. In many instances these two analytical lines appear nearly identical. The second figure of the pair shows the transverse, w^+, component of the WLC model, with the analytical model line arbitrarily drawn only up to y^+ of 300. In several instances this figure is omitted because flow conditions were such as to prohibit the calculation of this component or because the component model is not appropriate to the flow conditions. The last pair of figures shows the principal and transverse components of the B and CS models, with the CS analytical model line labeled. The transverse analytical model line of the B model is shown up to y^+ of 300 while the CS line is limited to y^+ of 150. This latter arbitrary choice was made based on the region of similarity shown by Chandrashekhar and Swamy (1976) when the model was proposed. The reader is again cautioned that the two-component similarity models do not use the same coordinate systems and this should be recognized in any attempted generalizations. Thus the ten three-dimensional similarity models can be compared to the velocity-wall shear data in six figures. To facilitate the comparative evaluation of the ability of these ten similarity models to predict the measured data, the set of six graphs corresponding to each station has been grouped and reduced in size to fit on a single sheet and these are shown as Figs. 6.1 - 6.25.

Before studying these graphical results it is further worth noting that the ability to accurately assess the three-dimensional near-wall similarity models depends on the accuracy of the experimental data. The q^+ (or u^+ or w^+) and y^+ uncertainties in plotting the results from the <u>same</u>

experimental data generally vary for each similarity model because of the different ways the data are manipulated to calculate these quantities for each model. Additionally, the uncertainties for a given model vary as one moves throughout the boundary layer. This variation was demonstrated across the boundary layer in the two-dimensional similarity plots by showing the uncertainty for the data nearest and most remote from the wall in Figs. 4.20 and 4.21.

In the three-dimensional case a comparison of experimental data with an analytical model can involve two kinds of uncertainty. Such a comparison requires that for each of the models an experimentally determined pair of q^+ (or u^+ or w^+) and y^+ values be plotted and there is an experimental uncertainty in the various quantities needed to calculate a q^+ (or u^+ or w^+), y^+ pair. This uncertainty is here called an experimental uncertainty in q^+ (or u^+ or w^+) and y^+.

In the case of the six simpler models and one of four complex models, the analytical q^+ (or u^+ or w^+) and y^+ values (the solid lines) require no experimental data input and so no uncertainty is identified with the analytical model line. However, in the more complex models of WLC, PJ, and B, the analytical model line predicting the q^+ (or u^+ or w^+) and y^+ variations requires the input of specific experimentally measured data such as a measured pressure gradient vector, a wall shear vector, or gradients in the magnitude and direction of the wall shear vector. By inputing experimental data into an analytical model line there is introduced into that analytical model prediction an uncertainty here called a model uncertainty. Note that this model uncertainty is different from what has been called the experimental uncertainty in calculating a q^+ (or u^+ or w^+), y^+ pair from velocity profile-wall shear data, although both these kinds of uncertainties arise from various possible measurement errors. The CS model has no analytical model uncertainties as defined above because no experimental data input is needed to construct these lines. The total uncertainty for the WLC, B, and PJ comparisons in the similarity figures discussed here would combine the model uncertainty as defined above and the experimental uncertainty in calculating the q^+ (or u^+ or w^+), y^+ data point pair for the velocity profile and wall shear data. In comparing an experimentally measured q^+ (or u^+ or w^+), y^+ pair to a model, one would need to consider both the experimental

and analytical model uncertainties to establish a corresponding combined uncertainty. Two further points should be made in this regard. First, it should be noted that each of these models includes two empirical constants. Since these ten models all come directly from, or are developed from, variations of the traditional two-dimensional mixing length concept, these constants are designated κ and C and this insures the return of the two-dimensional model in the case of vanishing skew or transverse flow. The question of the uniqueness and accurate specifications of these two constants in the two-dimensional case has already been discussed and these ambiguities should also be recognized here. Secondly, the uncertainties reported for the local wall shear measurements include no pressure gradient effects. This is due to the lack of agreement among proposed corrections (and no corrections in pressure gradient flows should be included as one of these proposed corrections) for the limited studies reported in two-dimensional flows, coupled with the apparent strong dependence of proposed corrections on the geometric particulars of the mechanical meter used. An effort is currently being made to determine possible pressure gradient effects on the mechanical shear meter used in this study in two-dimensional flows.

In the following figures the direct force wall shear stress measured value is used to calculate the nondimensionalizing shear velocity particular to each model. Assuming the model is properly derived, perceived agreement between the nondimensionalized measured profile and the model line would support the relationship between the particular shear velocity and the local wall shear stress. The existence of uncertainties in the measured velocity and wall shear data in each q^+ (or u^+ or w^+) and y^+ pair as well as uncertainties in the analytical model line due to the constants κ, C and in some cases the input of experimental data as well, should be considered in these visual comparisons. It is worth reminding the reader that if one fits any portion of the near-wall or very near-wall data to any given similarity model with any given similarity constants by inferring a shear velocity from these data (Pierce and Zimmerman, (1973)) then one can expect a near perfect fit over the profile region used to infer the nondimensionalizing shear velocity. Such a superior fit does, however, not in general confirm any relationship between the shear velocity and the local wall shear stress.

Similarity Model Results

The three-dimensional similarity model comparisons for the ten models tested are shown in Figs. 6.1 through 6.25 for 25 stations as defined in Fig. 5.1. In an attempt to organize the comparisons the pressure driven velocity profiles are divided into four categories based on the total skewing of the local velocity vector relative to the freestream direction. The first category is for skew angles of from 0° to nominally 5° (actually less than 1.5°), the second two categories are for monotone increasing skew angles from 5° to 15°, and for more than 15°, and the last category is for profiles with first increasing and then decreasing skew angles. In all cases the changes in skew angle are with respect to a decreasing distance from the wall. It should be noted that the velocity profiles in this last group are incorrectly labeled by McAllister (1979) as s-shaped or bilaterally skewed when in fact only one of these profiles (station I-5) is of that type. Table 6.2 lists the profiles in each of these categories.

Only the pseudo two-dimensional plane of symmetry profiles along the A column, stations A7, A5, and A3, show the total velocity vector skewing less than 1.5° and these are shown in Figs. 6.1-6.3. As discussed in Chapter V, and similar to the two-dimensional profiles discussed in Chapter IV, the profiles at A7 and A5 show a monotone increasing and positive turning (per Fig. 4.1) of up to 1.4° as the wall is approached. The profile at A3 shows a turning of nearly one degree close to the wall, with return toward the freestream direction at the wall, hence this profile has a very slight bulge in its turning. While all these turning angles are less than 1.5° and a large measure of these angles can be accommodated in the angular uncertainty estimates, this behavior is consistent and taken to be real.

In an overall view, the six simpler models show a degree of agreement with the data for stations A7 and A5 not unlike that typical of early work in two-dimensional flows and shown in Fig. 2.2. There is closer agreement with the Patel line and as the adverse pressure gradient becomes more severe, a smaller region of apparent (or approximate) similarity is noted. In the limit of vanishing transverse flow these six simpler scalar similarity models all return the two-dimensional similarity law and from this view the results for A7 and A5 are not surprising. It is worth noting that there appears to be an inconsistent and slightly lesser slope to the data in the

Table 6.2. Velocity Profile Grouping by Skew Angle

Skewing Type	Monatone increasing			Increasing-Decreasing
	0 5°	5 15°	over 15°	
Velocity Profiles	A7	C7	C3	E-1
	A5	C5	E3	G-1
	A3	E7	E1	G-3
		E5		G-5
		G7		I-1
		G5		I-3
		G3		I-5
		G1		
		I7		
		I5		
		I3		
		I1		

region of primary y^+ focus. A similar result is reported for plane of symmetry flows by Brown* and is attributed to the lateral divergence of the streamlines with the transport of lower momentum wall flow upwards resulting in these slightly lower mean velocities. If this effect is to be included in any similarity model then the characteristics of the neighboring flow must be included and clearly the six simpler models are not adequate to include such an effect. In the y^+ range of secondary focus the data follows the general shape of the Spalding line very well though riding consistently higher. The possibility of a pressure gradient error in the wall shear must be noted since the slightly higher q^+ values shown could result from a low wall shear and hence low q^* and this would intuitively be the direction of such an error for these stations. Possible pressure gradient effects on the mechanical meter are currently being evaluated. The preliminary work of Tennant (1977) shows a better agreement with the theoretical model line for these six models at station A7 but similar behavior with the experimental data riding high for station A5. Finally, it is noted again that if one were to fit the lower y^+ data to the model lines then these several data would result in an excellent fit with the lesser slope of the following data more apparent.

The principal flow components of the four more complex models show good agreement and except for the CS model suggest no pressure gradient error in the wall shear measurements. For the A column these complex models are all in essentially the same direction and with the nearly zero skew measured none of the transverse model comparisons are meaningful. Since the complex models were developed around equilibrium and mixing length analyses following the 2DTBL case, it is not surprising to see this kind of agreement in the typical y^+ range of primary focus. At station A7 the PJ, WLC, and the B models all predict the effect of the modest rising pressure well but at A5, where the adverse pressure gradient becomes larger, the B model appears to account for this effect more effectively, with the PJ and WLC models overpredicting the pressure gradient effect. For these data the better agreement in the region of expected similarity for the PJ, WLC, and B models than for the six simpler two-dimensional-like models

---

*See footnote on page 90.

suggests that the ability to include pressure gradient effects is important in this y^+ region. The station A3 shows generally poor agreement with all models and this appears to be due to the close proximity to separation. These models can be traced to Townsend's (1956) equilibrium balance between turbulent energy production and dissipation in 2DTBL similarity, and in close proximity to a separation region boundary the existence of equilibrium can be questioned.

The second group of profiles considered all showed a monotone increasing skew angle relative to the local freestream direction and limited to 15°. These are shown in Figs. 6.4-6.15. Profiles C7, E7, G7, G5, I7, I5, I3, and I1 all show an increase in the local skew angle a maximum wall value of between 5° and 10° as measured with the claw probe resting on the wall. Profiles C5, E5, G3 and G1 show a maximum value between 10° and 15°. These two subgroups are considered together as listed in Table 6.2. In general, the six simpler models all show about the same kind of behavior relative to the experimental data with the data tending to ride above but closer to the Patel line than the NPL line. In the y^+ range of primary focus there is a tendency for the experimental data for the higher y^+ values to dip down somewhat and as with the plane of symmetry profiles one could argue that a better fit with the data would occur with a lesser slope in the logarithmic portion of the model lines. In the y^+ range of secondary focus it is worth noting that the data again tends to follow the general shape of the two-dimensional, Spalding single formula law of the wall rather consistently.

For this group of profiles the WLC model for these freestream flow components and the PJ model show generally good agreement with the data in the y^+ range of primary focus upward toward 150 or 200 depending on the profile with only profile G1 as an exception to this generalization. These profiles also show a very consistent behavior in that for $y^+ < 50$ the data drops down below the log like model lines and follows the form of the typical two-dimensional transition lines sketched between the $u^+ = y^+$ sublayer and the log-like behavior as for the six simpler models in the first two figures in each series. All of these profiles have modest transverse flow because of the limited skewing angle and five transverse profiles are shown for the WLC model with good agreement in the y^+ range of 10 to about 100 for skew angles up to 7°, and relatively poorer agreement with a maximum

skew angle approaching 12°. Only five of 12 transverse profiles are shown for th' model because of the difficulty in determining the nondimensional boundary layer thickness by evaluating the freestream model at the boundary layer edge as suggested by the model authors. In several cases this evaluation introduced a negative argument in a square root quantity. While other estimates could have been made for this required thickness, consistency suggested omitting such transverse profiles since some representative cases were available.

The CS and B models for the principal flow component (freestream component in the CS model and wall shear direction component in the B model) also show similar good agreement for these 12 profiles. Some care must be exercised in separating the CS and B lines in the figures. The CS model line is straight while the B model line generally shows some curvature. In general the B model line better approximates the data and tends to better represent the data at higher y^+ values shown in Fig. 6.5 for station C5. In some cases the CS model also shows reasonably close agreement with the experimental data as in stations G5 and G3 but the B model appears superior. For $y^+ < 50$ the data behaves as described above. For the transverse components of these 12 profiles the CS model generally shows very poor agreement. The choice of the principal flow direction in the B model results in an especially small transverse component near the wall with both the model line and the experimental data very close to zero for all profiles in the y^+ range less than 300. The data and model line both agree in the sense of showing small values but the small transverse flow does not seem to offer a reasonable test for the transverse model.

The third group of profiles is shown in Figs. 6.16-6.18 for stations C3, E3, and E1. These profiles are also characterized by a monotone increasing skew angle from the freestream toward the wall with a maximum skew angle ranging from 20° to 32°. For this group with the larger skew angles, the six simpler models begin to show significant differences as a result of the way the experimental data is manipulated to generate the equivalent q^+ values. The J, C, and EH models tend to show larger differences at the higher y^+ values. Any region of similarity seems to be in the y^+ range of secondary focus, but only up to a maximum skew of about 20°.

The PJ model and the freestream component of the WLC model show a small region of good agreement for a maximum skew of 20° with decreasing agreement with increase in maximum skew angle as in station E1 at 25° and C3 at 32°. The transverse component for the WLC model in Fig. 6.17 could not be computed for the reason noted earlier. For this figure the PJ and WLC models are repeated but this time using the NPL constants (rather than the Patel constants) in the model lines to show the effect of the choice of constants. Note that the NPL constants tend to lower slightly the model curves for both these models just as in the two-dimensional case as shown in the top two figures for the six simpler models.

The CS and B models show a small region of good agreement with the experimental data for the principal flow direction for the 20° maximum skew case of E3, with relatively poor agreement as the skew increases. The transverse component of the CS model generally shows poor agreement with the experimental data. Again, the choice of coordinate system aligning itself with the wall shear in the B model leads to small transverse velocities in the region where similarity would be expected even for these cases of large skew. For stations E3 and C3 the model lines and experimental data show poor agreement. Station E1 with 25° maximum skew shows some agreement over a modest y^+ range (at a near zero though slightly negative w^+ values) with the experimental data and model line going in opposite directions at y^+ of about 100. The transverse component of the B model is strongly dependent on the transverse pressure gradient of the flow field and the rate of change of the turning of the wall shear vector. These are the principal contributions to this component and the nature of the model line in these figures is largely determined by these gradients. Van den Berg (1973) does indicate that this similarity model be restricted to modest skewing, while this group has substantial skewing.

The fourth group of profiles includes stations E-1, G-1, G-3, G-5, I-1, I-3, and I-5 shown in Figs. 6.19-6.25. In the previous two groups of profiles, skewing of the velocity vector through the boundary layer was monotone increasing with the turning angle increasing continuously down to the wall relative to the local freestream direction. This kind of profile is typical of many, if not most, of the pressure-driven profiles for three-dimensional flows shown in the literature. The velocity profiles in this

last group are characterized by not having a monotone increasing skew angle. In all of these profiles as one moves through the boundary layer toward the wall there is first an increasing skew angle toward some maximum value away from the wall, with a subsequent decreasing of the skew angle to the wall. Two profiles in this group are singled out. Station E-1 in Fig. 6.19 has the widest range of skew angle, first increasing to about 29° and the decreasing to about 24°. Station I-5 in Fig. 6.25 is a bilaterally skewed profile such as shown in Figs. 2.5 and 2.6. In this case the skew angle range is only about $\pm$ 2° so that this is a modest case at best. Bilaterally skewed flows are typically identified with freestream streamline re-curvature where the change in direction of the curvature of the freestream streamlines changes the direction of the pressure gradient forces imposed on the boundary layer by the freestream flow. This change in direction of transverse pressure force acts to reverse the secondary flow direction of the boundary layer flow with the lower momentum fluid near the wall influenced more strongly and hence changing direction of the secondary flow more quickly. The first signs of this are the diminishing of the skew angle for the flow near the wall as shown in Klinksiek and Pierce (1970). The remaining five profiles of this group IV have their maximum skew angle between 0-10° and nominally all in the same direction. (Station G-5 shows a slight bilateral skew behavior but, while consistent, is within experimental angular uncertainty.)

For this group of profiles, with the exception of Station E-1, the six simpler models show varying degrees of agreement with the data, but generally in the lower y^+ range of secondary focus and with the velocity data typically somewhat high. Again, the high velocity data position could be explained by adverse pressure gradient force effects on the shear measurement but some of these stations showing this typically high velocity data are in near zero and even positive pressure gradients where such possible pressure effects should at least begin to show an opposite influence on the data. There is also a tendency for the velocity data to suggest a lower slope to the log line in the six simpler models. In the plane of symmetry case this has been attributed to lateral streamline divergence but such streamline divergence is somewhat more difficult to identify clearly in this group of profiles.

For this group of profiles, the six simpler models generally show reasonably good agreement with the experimental data although the profiles with large reversals in the skewing direction near the wall show a rapid drop off in the nondimensionalized velocity as the y^+ values increase as shown in Figs. 6.20 for station G-1 and especially in Fig. 6.19 for station E-1. The total turning angle in these figures is approximately 10° or less with the exception of station E-1. With such small turning angles the six simpler models all tend to show nearly identical results which, as in the earlier three groups of data, tend to lie somewhat above the theoretical line of the models in the lower y^+ regions. Figure 6.19 for station E-1 shows a singular behavior apart from the other profiles in this group. This is because of the relatively large turning angles which increase from 0° to about 29° and then decrease to about 24° at the wall. With such large turning angles the six simpler models show large differences in their equivalent velocities. None of the simpler models describe the flow at this station very well.

The WLC model for the freestream flow component and the PJ model show good agreement with the experimental data for the four profiles with skew of less than about 5° (Stations G-5, I-1, I-3, and I-5), with lesser agreement for the profiles showing skew in the 5° to 10° range (G-1 and G-3). Station E-1 in Fig. 6.19 shows poor agreement with the two models giving significantly different predictions. The transverse WLC model could only be computed for two of the seven profiles but the small transverse components again makes the comparison questionable. The CS and B models also show reasonably good agreement with the experimental data with the exception of station E-1. Again the good agreement is identified with the relatively modest skew and the poor agreement at station E-1 is identified with the large reversing skew. It is interesting to note that in Fig. 6.19 for station E-1 the B model tends to show very good qualitative agreement in predicting the general shape of the experimental data. The transverse component for the CS model again tends to show relatively poor agreement with the experimental data. The transverse component of the B model is again treating only very small velocity magnitudes. It is also noted that for this particular group of profiles there is a consistent disagreement between the direction of the transverse component predicted by the B model and measured for the profiles

in the region of expected similarity. Station E-1 provides a strong test of the transverse component CS model since large skewing is present. Figure 6.19 shows extremely poor agreement with this model.

Summary

Generalizing, it would appear that for profiles with monotone increasing skew and with skew angles up to about 15-20°, any of the six simpler models does a fair job of predicting near-wall similarity in a region of primary focus for $y^+ > 50$ with the qualification that in this study the experimental data tend to ride higher than the theoretical model lines. These (and many other) three-dimensional data show consistently better behavior in the lower y^+ range of secondary focus--the y^+ range where two-dimensional data are characterized by more scatter and disagreement among even carefully done experiments--and to some extent this better very near-near wall behavior compensates for the more rapid departure from similarity in the higher y^+ range of similarity more typical of two-dimensional flows. It would appear that shear velocity magnitudes inferred by Clauser chart type techniques using data in the y^+ range of 10 to about 100 would be within 5-10% of values calculated for the direct force measurements (uncorrected for any possible pressure gradient effects). It would of course be essential that the similarity law be of the type that reflects the very near-wall departure from the log law-like behavior in this range of smaller y^+ values. The third or fourth order Spalding formula such as used here or the two or three formula law of the wall described in Chapter II and adapted to the method Schraub and Kline (1965) by Pierce and Zimmerman (1973) should be adequate to accommodate this lower y^+ range data.

For profiles with an increasing and decreasing skew angle of 10° or less, as occurs with the change in direction of transverse pressure forces identified with freestream streamline curvature, and for plane of symmetry flow away from separation the agreement with the experimental data for the six simpler models is similar to that for the monotone increasing skew angle profiles with modest skewing described above as less than about 20°. For the profile with increasing and decreasing skew with large maximum skew angle (29°) none of the models, simple or complex, does an adequate job in representing the data.

For the above kinds of flows three of the four complex models generally are superior in describing the experimental data for the freestream or

principal flow component. The exception is the CS freestream model which behaves as the six simpler models. For modest transverse velocities the WLC and B models seem to be the most encouraging but the degree of agreement is generally not nearly as good as for the freestream or principal flow component. The PJ model and the freestream component of the WLC model and the principal flow component of the B model tend to show the best agreement with the data. A difficulty with these more complex models lies in the fact that each returns the two-dimensional logarithmic like law for small y^+ values. Thus, assuming these models could be used to infer local shear velocity magnitude (say to 5-10%) there is the problem of fixing a lower y^+ limit below which data would not be used since this and other studies suggest the typical data is better described by some kind of "transition" description in the very-near wall region of say $y^+ < 50$ as discussed earlier. Thus these models would not use well much of the data available to infer even an approximate shear velocity (or wall shear) magnitude.

Similarly, if one were to use these three more complex models in a computational scheme replacing the no slip wall boundary condition at the wall with a match to a similarity model near the wall then, for the flows described above, such a match should be made in this range of about $50 < y^+ < 100$. Practical difficulties will occur since these three more complex models (White, Lessmann and Christoph, Perry and Joubert, and van den Berg) all require an a priori knowledge of the pressure gradient magnitude and direction, and the latter two also require an a priori knowledge of at least the wall shear direction. Yet it is interesting to note that, in general, the corrections to the near wall similarity law for pressure gradient and inertial effects appear to contribute to the similarity model in a y^+ range that is often beyond any modest region of perceived similarity.

The question of pressure gradient effects or corrections to the direct force measurements is currently being pursued. It is noted, however, that while the high q^+ values of the plane of symmetry flows suggest a low wall shear value due to an adverse pressure gradient effect, a corrected, higher wall shear value would cause this same velocity data to appear low for the Perry and Joubert model and the principal flow direction components of the other two models which otherwise do a reasonable job of

predicting the near-wall flow, at least in modest y^+ regions. The various wall shear and pressure gradient orientations in Fig. 5.17 do not suggest a consistent behavior of possible pressure gradient effects on the measured wall shears. Additionally, preliminary work in a shear-driven flow in a near-zero pressure gradient field indicates results similar to those for this pressure-driven flow. This would also suggest small pressure gradient corrections at most.

In retrospect it is not surprising to find reasonably similar and fair agreement among these ten similarity models (the principal flow component in the three vector models) for the monotone increasing skew profiles of modest skew as well as the plane of symmetry profiles. All these models can trace their origin directly to the classic Townsend equilibrium concept for two-dimensional turbulent boundary layers and subsequent variations of the classic mixing length hypothesis. It can be argued that skewing in the three-dimensional case taxes the applicability of this basically two-dimensional approach with an approximate upper limit of 15°-20° of skew. Within this upper skew limit for these flows it appears that the local wall shear stress and nondimensionalizing shear velocity for the various similarity plots are related within a modest uncertainty. This implies that at least an approximate magnitude of local wall shear stress would be inferred from such similarity models in a "Clauser chart" type of approach as developed by Pierce and Zimmerman (1973) for at least the simpler similarity models reviewed and tested here. This would also imply that with indirect diagnostic devices which are not strongly sensitive to yaw angles (such as Preston tubes and surface heat meters) would also give a reasonable good approximation to the magnitude of the wall shear stress in such modestly skewed flow as well, using a two-dimensional calibration. Note that without the supporting results of this study with directly measured local wall shear stresses, such use of a two-dimensional calibration in a three-dimensional flow would be speculative at best. The same relative insensitivity to yaw that would allow the use of such indirect devices in a skewed flow would, however, render such devices as relatively poor in indicating the local wall shear stress or limiting wall streamline direction. It would appear that for such modestly skewed flows the combination of say a Preston tube or surface heat meter together with an established wall flow visualization technique

could do a reasonable satisfactory job in mapping a wall shear field. The combination of indirect magnitude sensing device and flow visualization for the direction would be significantly easier to use than a direct force sensing three-dimensional wall shear meter such as used in this study.

It appears that for monotone, strongly skewed flows (say 20° and greater) and for flows with increasing-decreasing skew of more than about 10°, none of the ten three-dimensional similarity models tested here seems adequate to describe the near-wall velocity field even approximately.

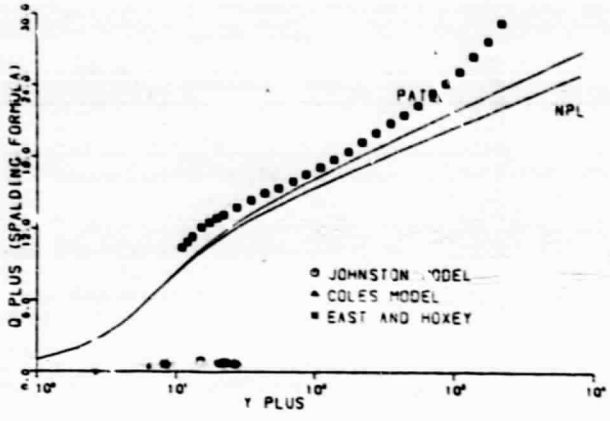

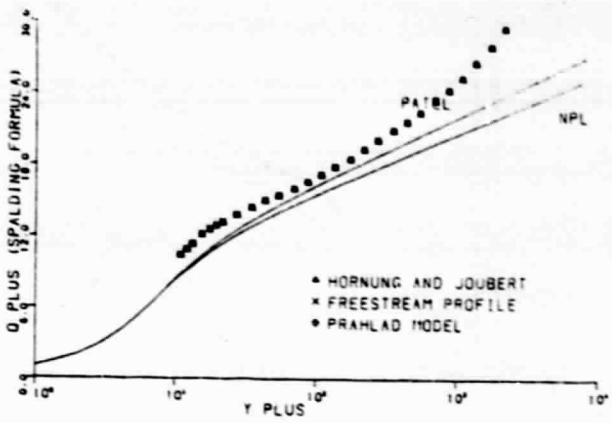

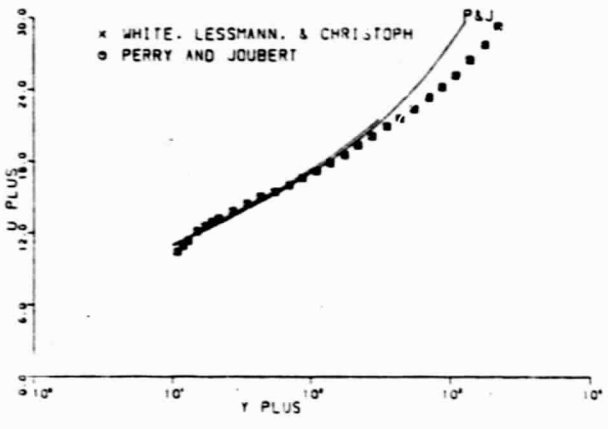

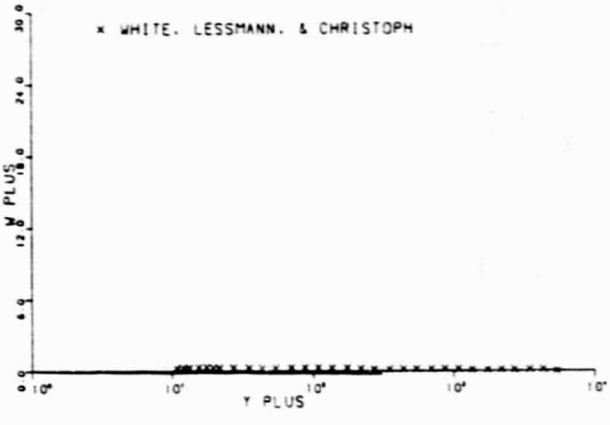

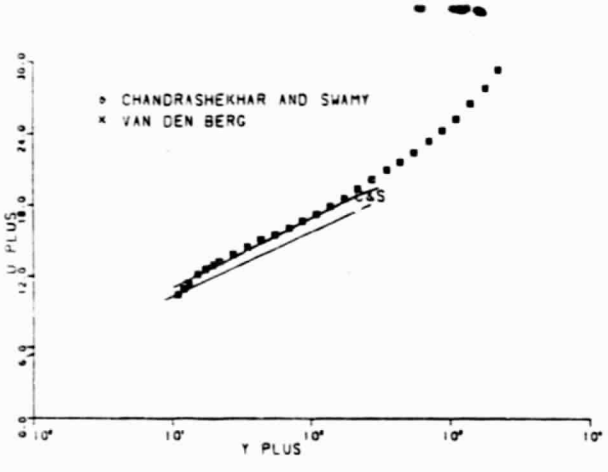

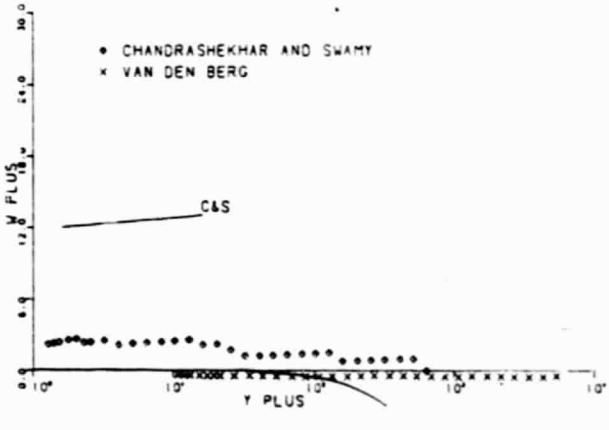

Fig. 6.1 Three-Dimensional Similarity Plots for A7

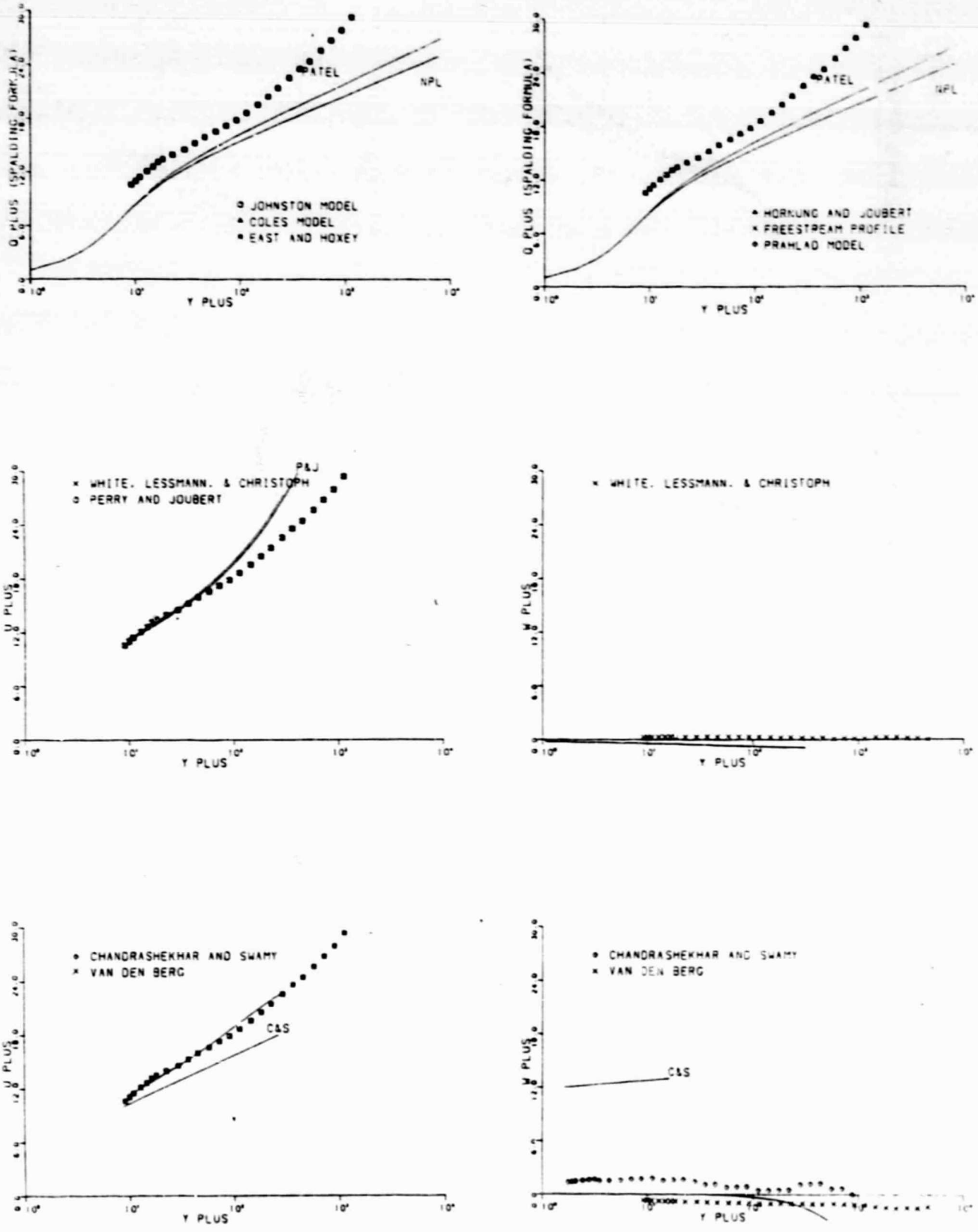

Fig. 6.2 Three-Dimensional Similarity Plots for A5

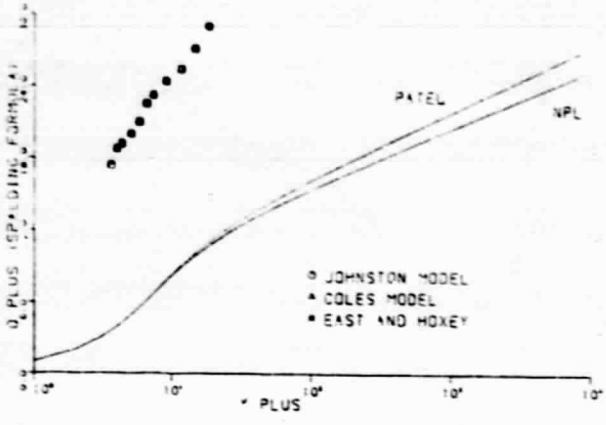

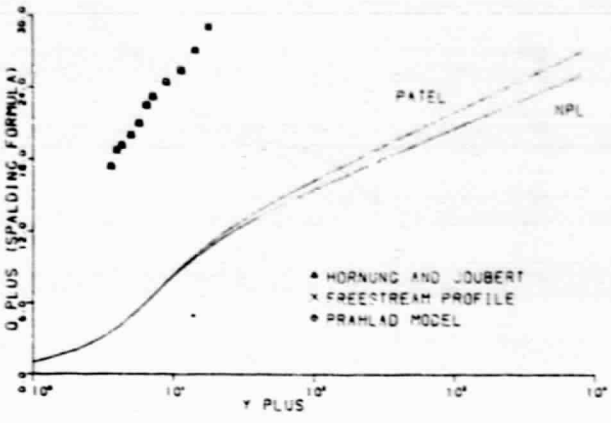

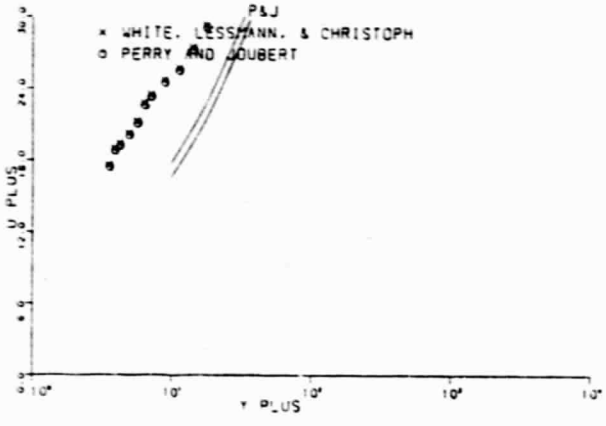

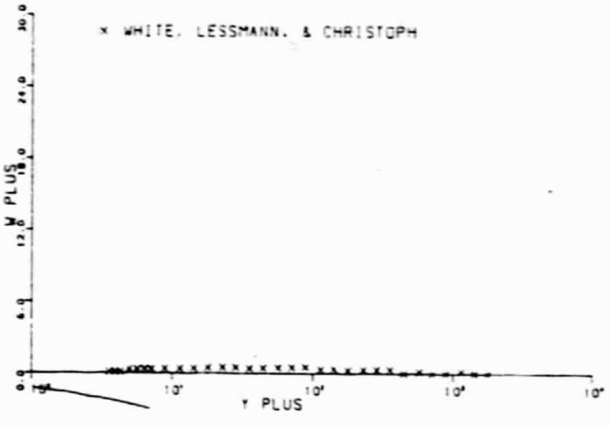

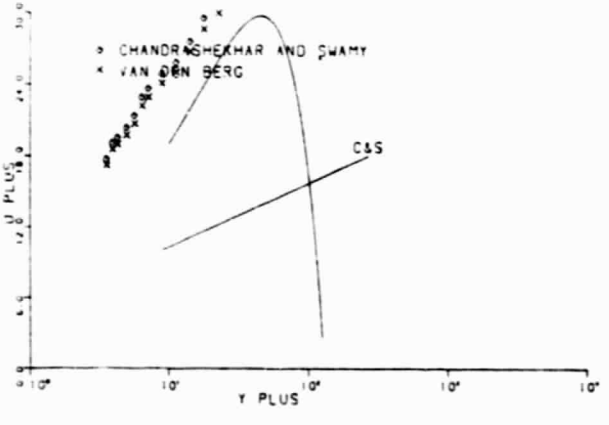

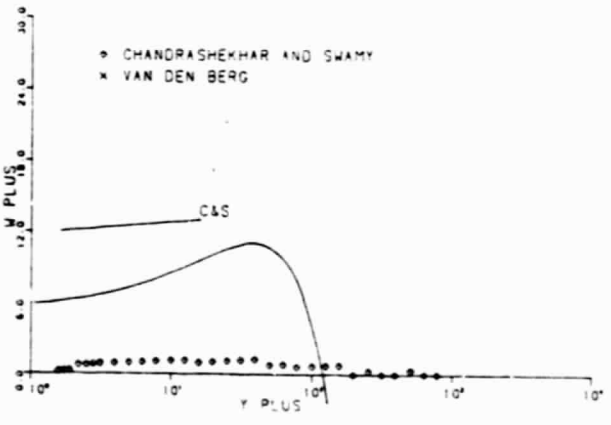

Fig. 6.3 Three-Dimensional Similarity Plots for A3

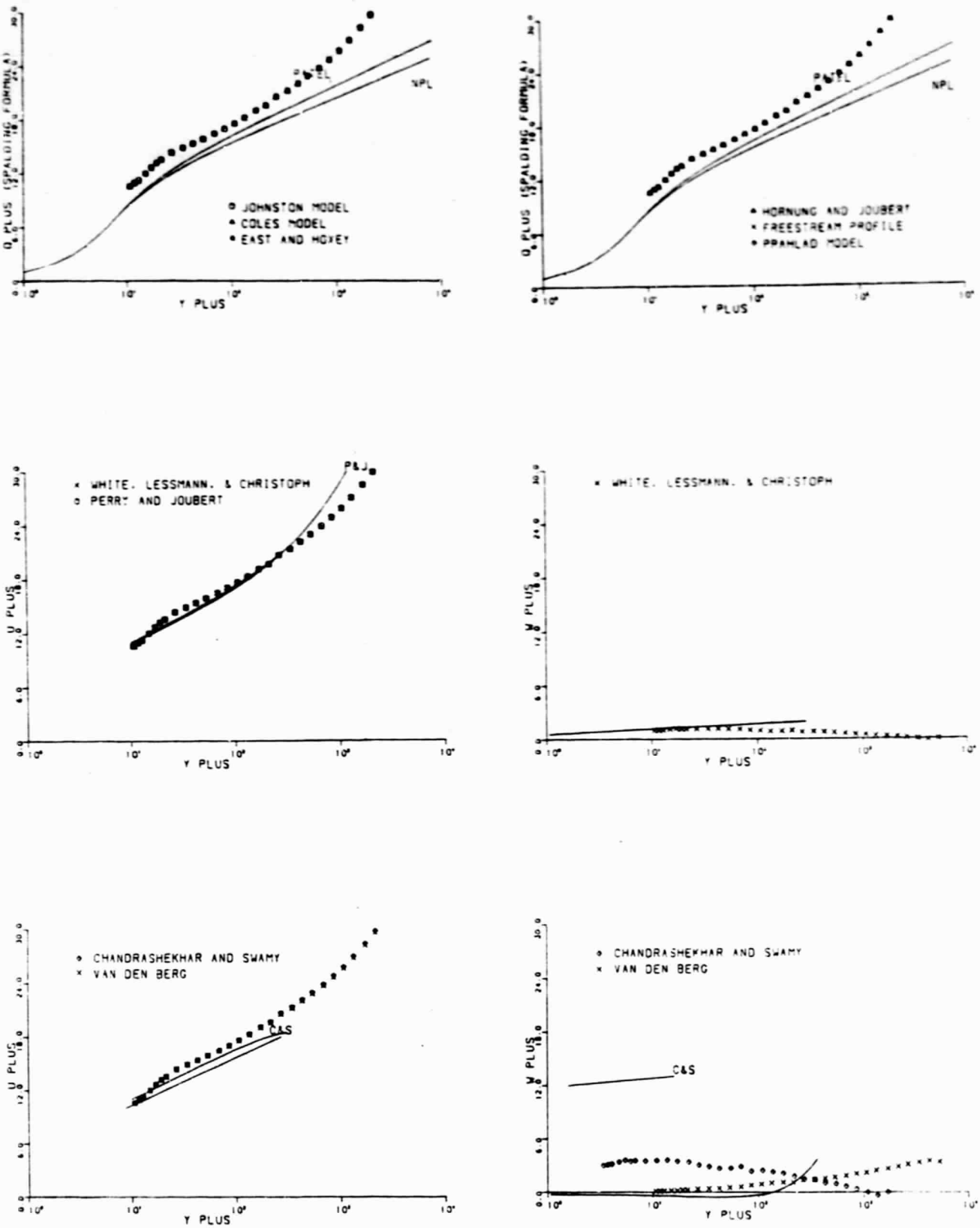

Fig. 6.4 Three-Dimensional Similarity Plots for C7

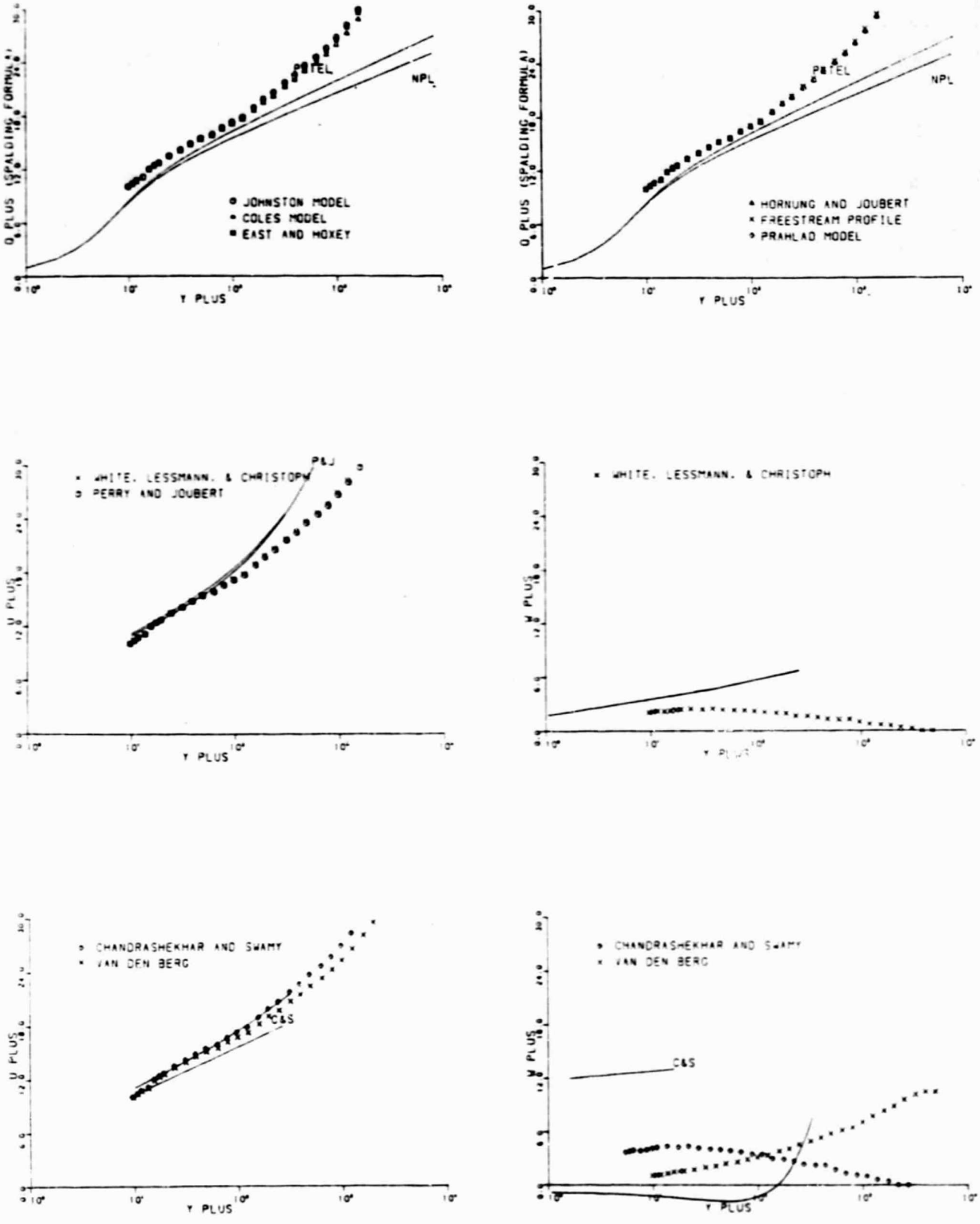

Fig. 6.5 Three-Dimensional Similarity Plots for C5

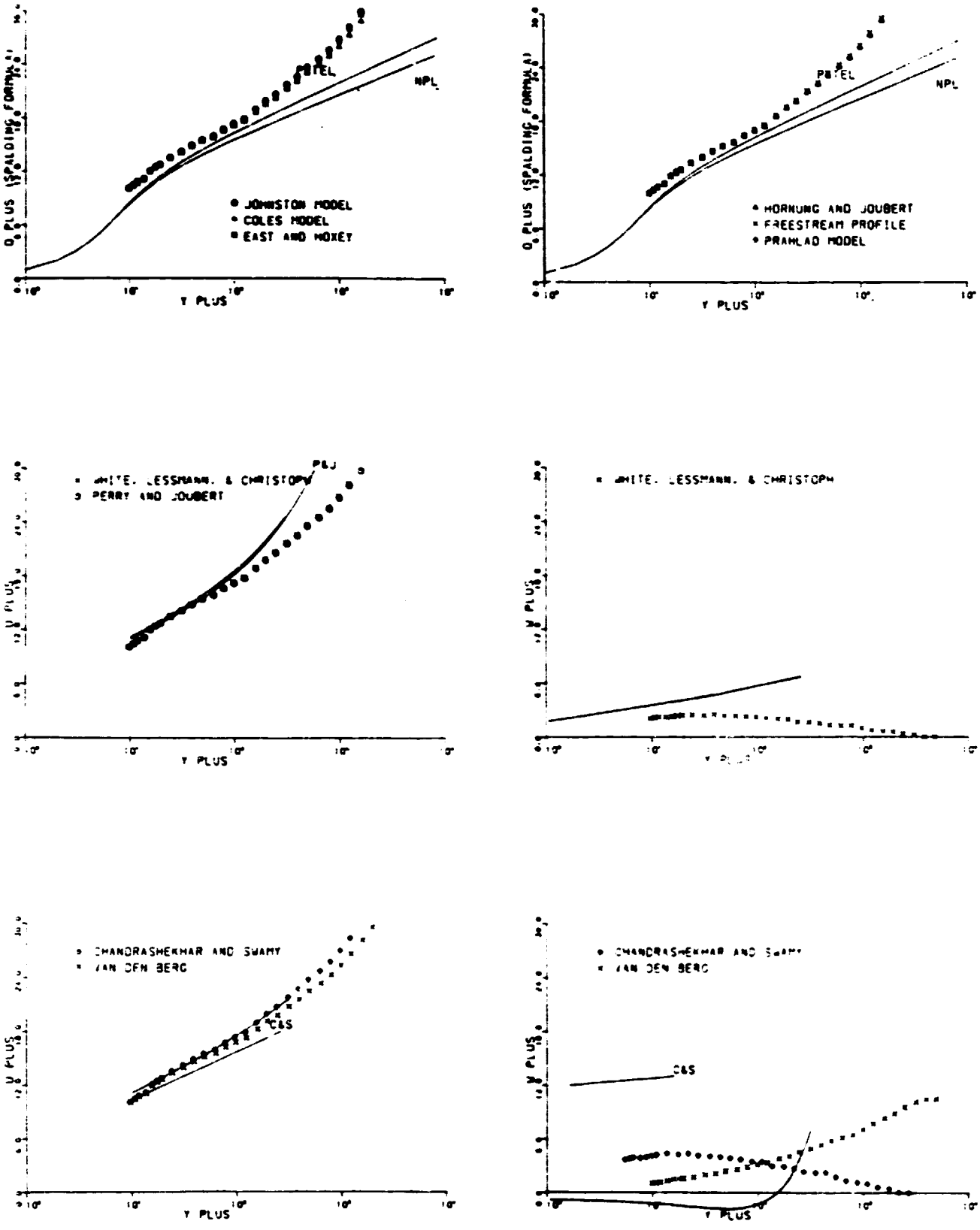

Fig. 6.5 Three-Dimensional Similarity Plots for C5

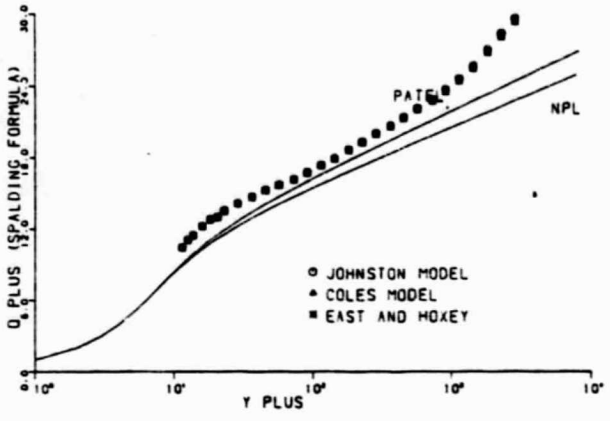

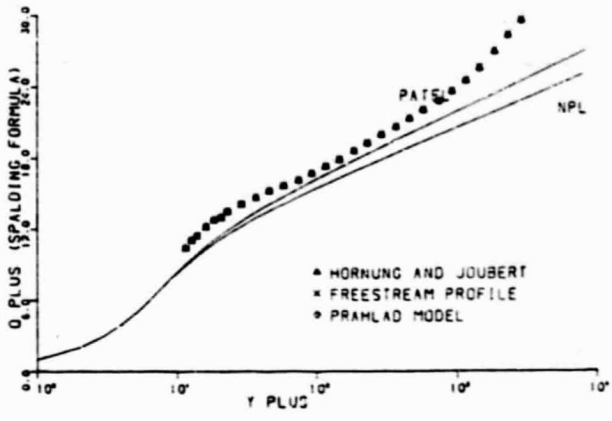

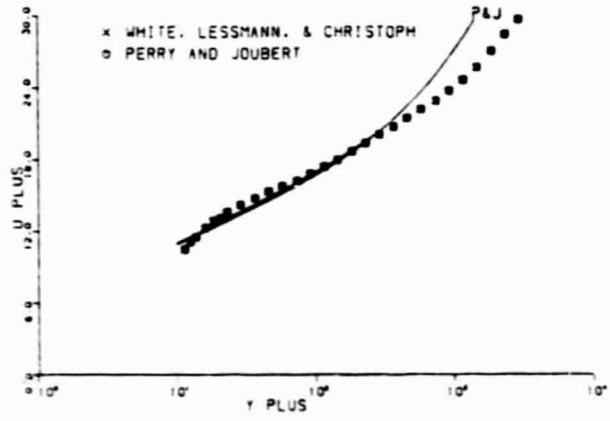

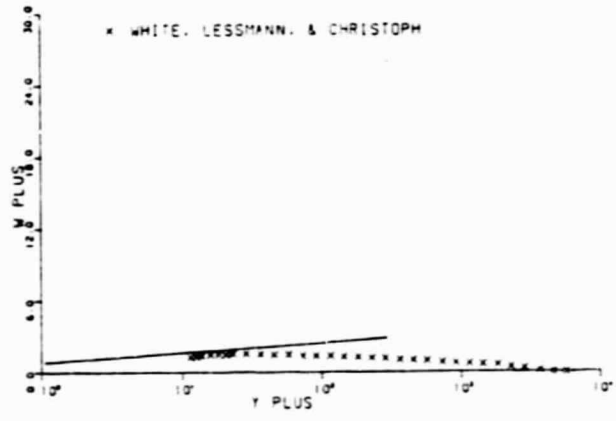

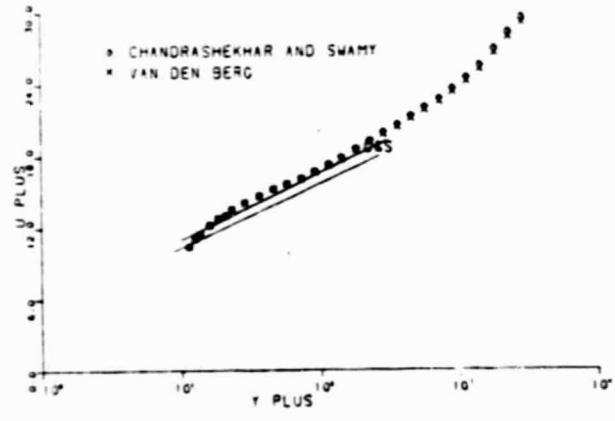

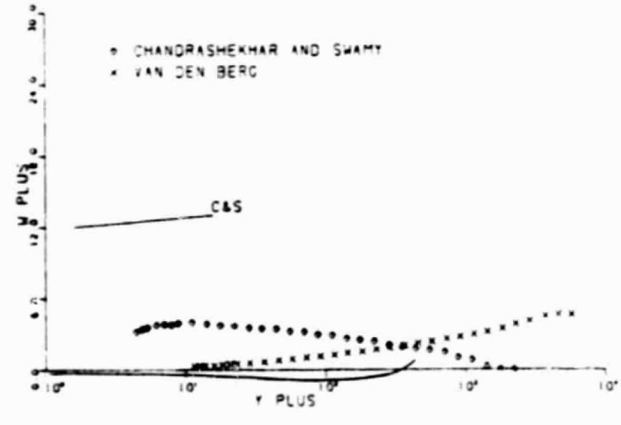

Fig. 6.6 Three-Dimensional Similarity Plots for E7

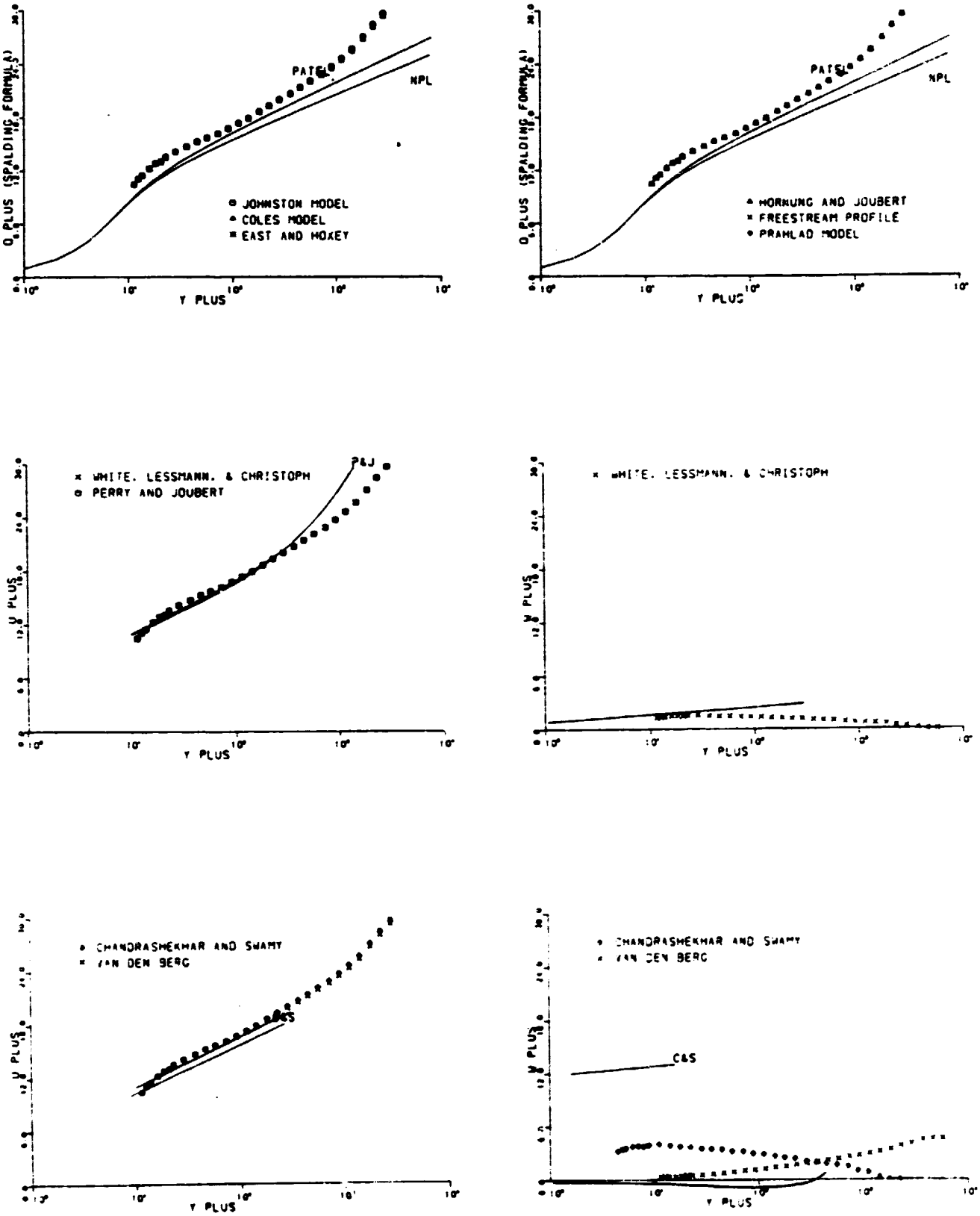

Fig. 6.6 Three-Dimensional Similarity Plots for E7

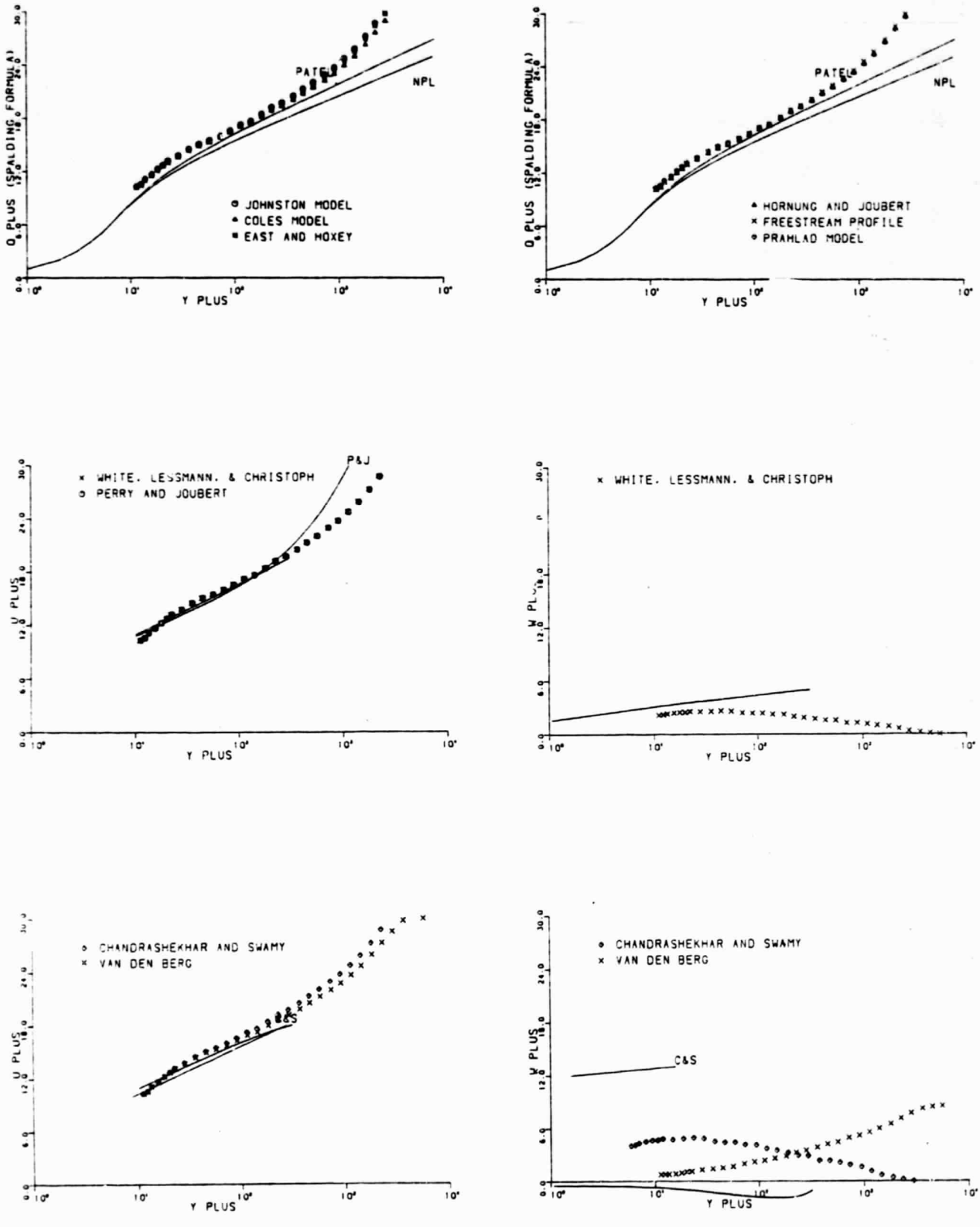

Fig. 6.7 Three-Dimensional Similarity Plots for E5

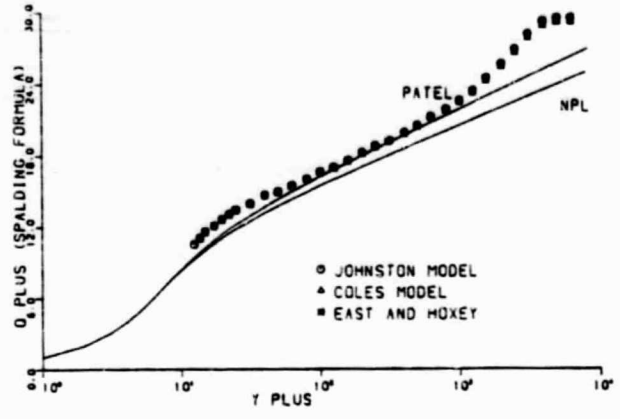

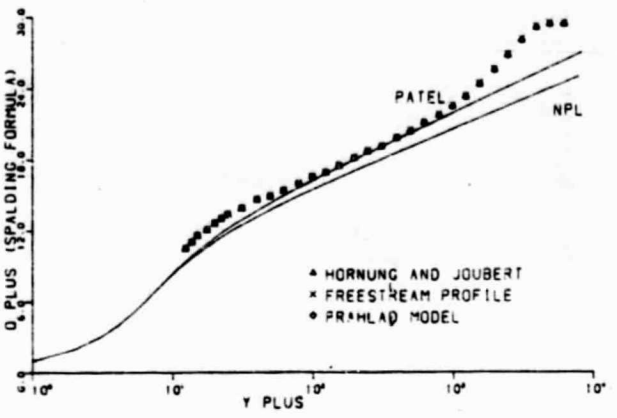

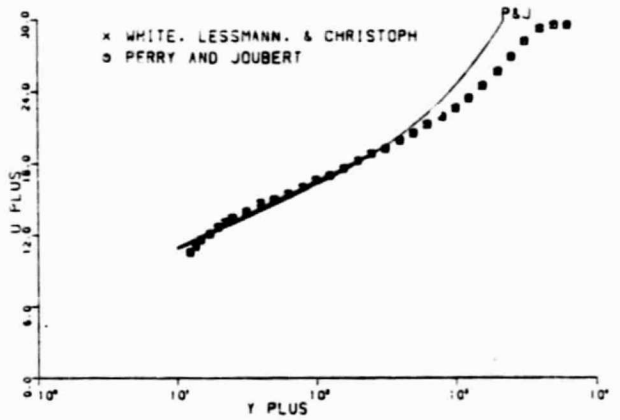

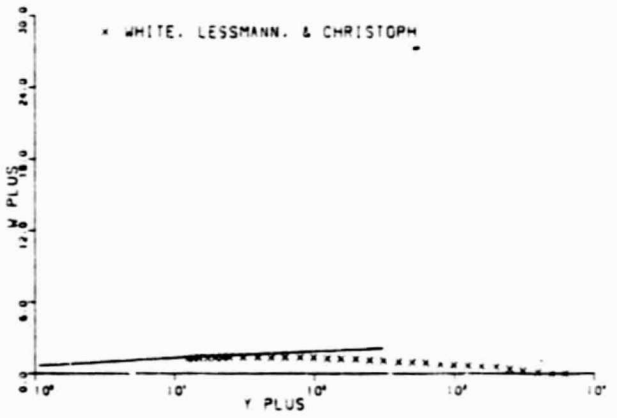

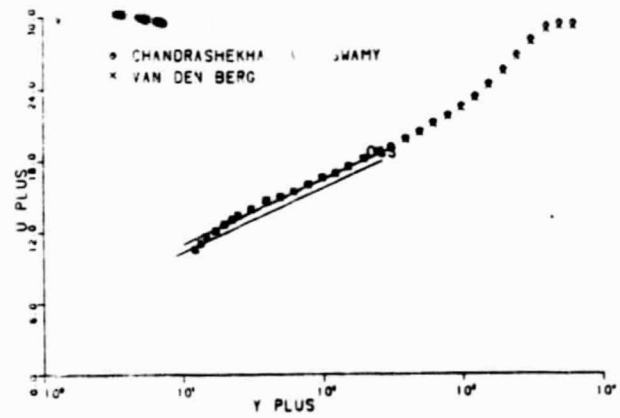

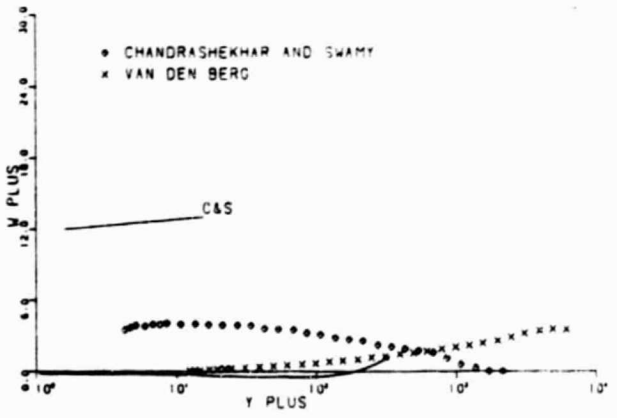

Fig. 6.8 Three-Dimensional Similarity Plots for G7

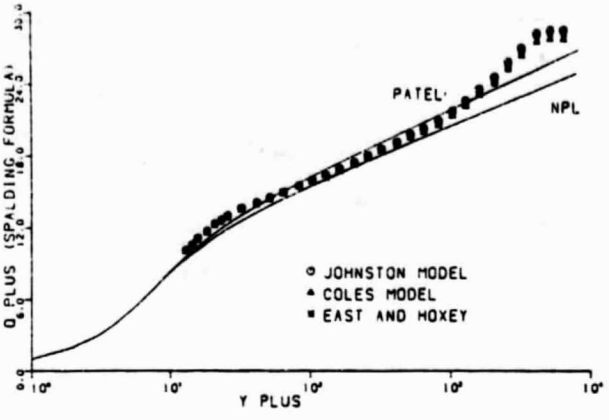

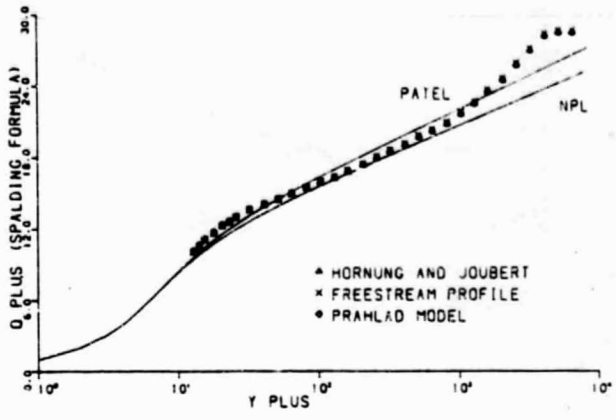

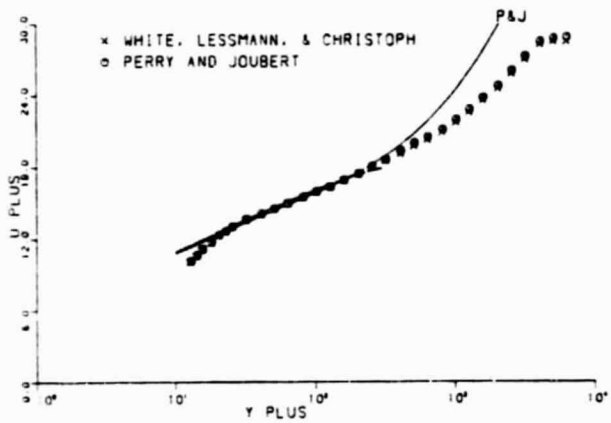

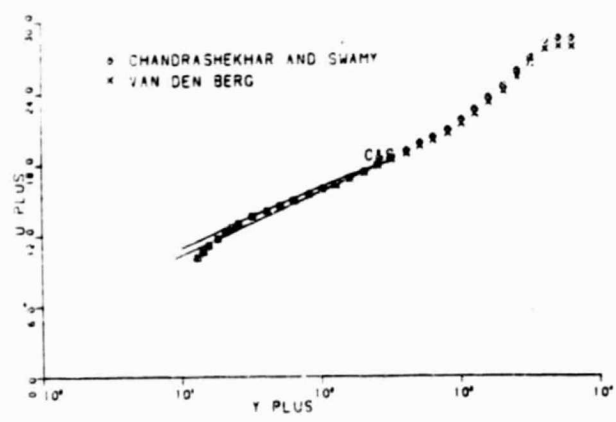

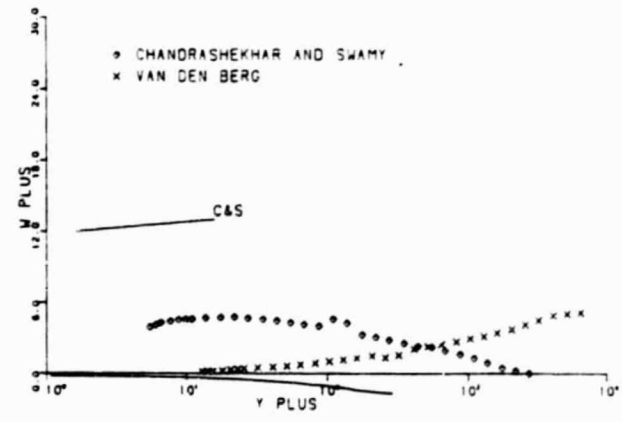

Fig. 6.9 Three-Dimensional Similarity Plots for G5

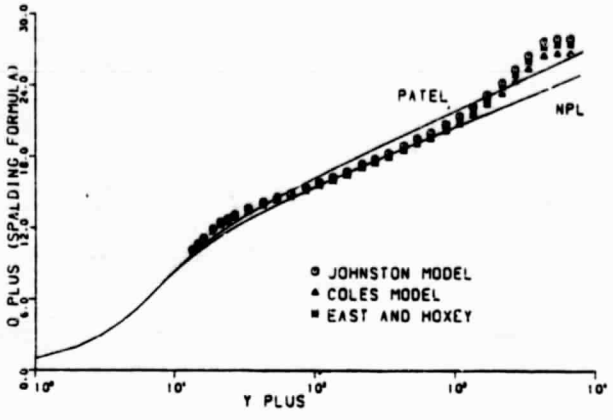

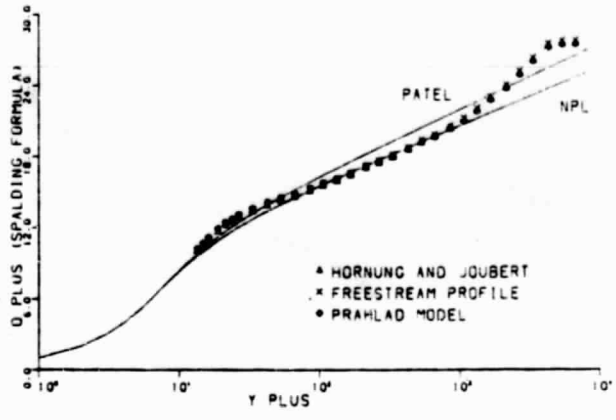

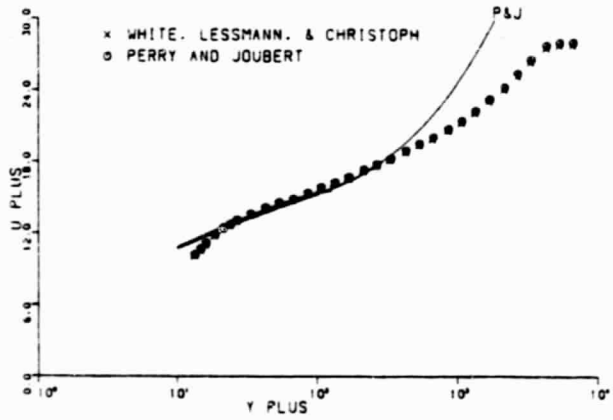

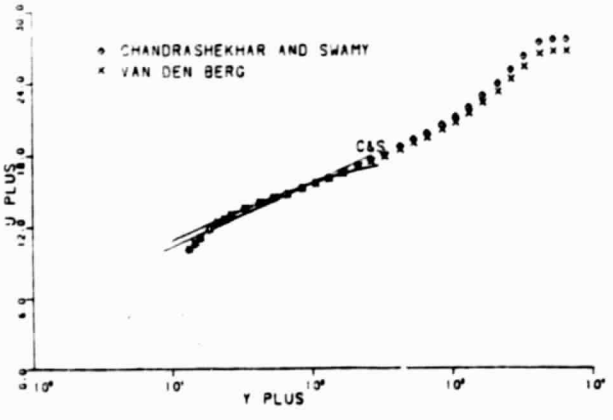

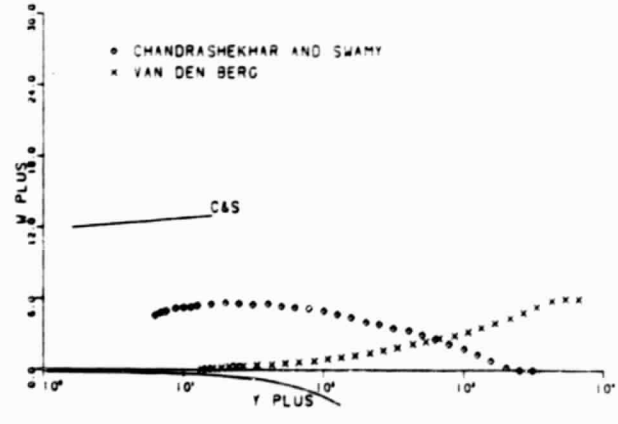

Fig. 6.10 Th-ee-Dimensional Similarity Plots for C3

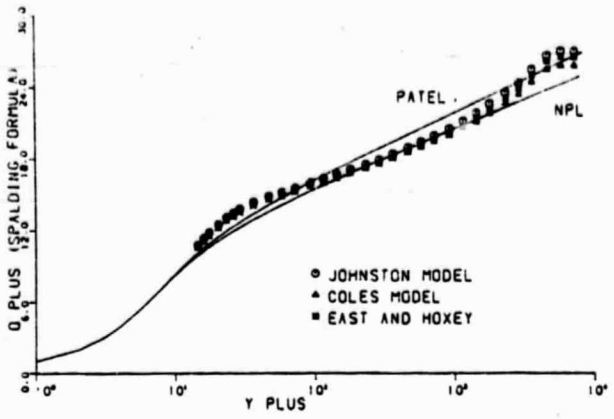

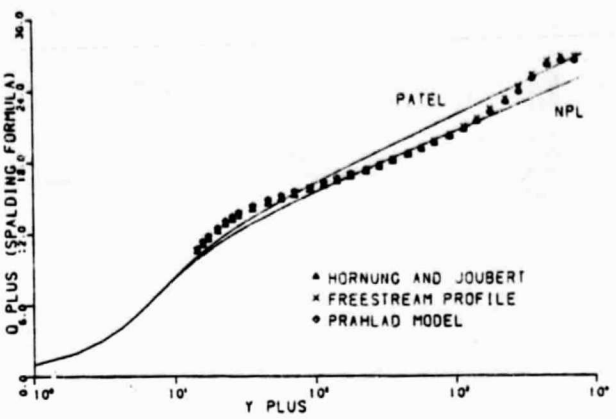

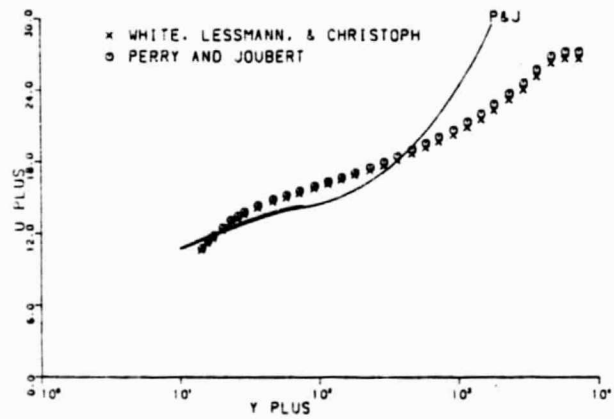

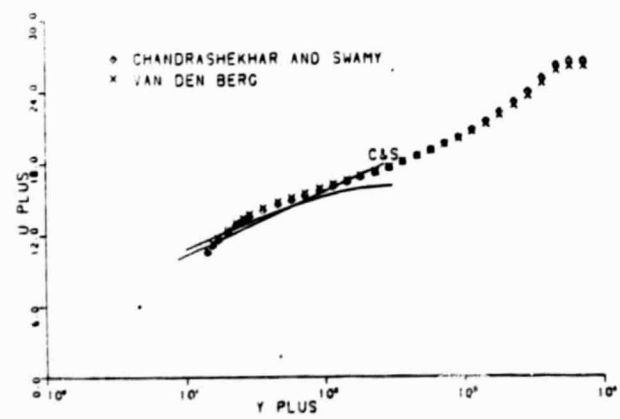

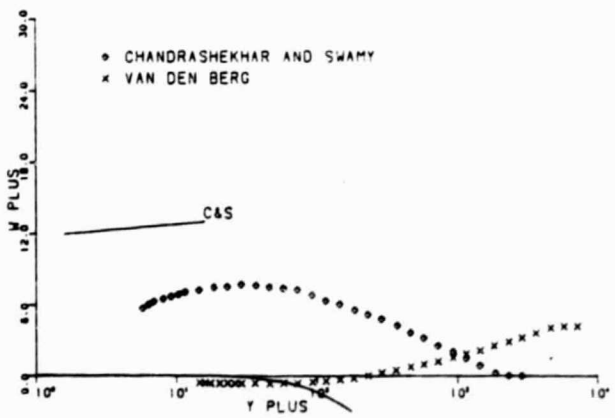

Fig. 6.11 Three-Dimensional Similarity Plots for G1

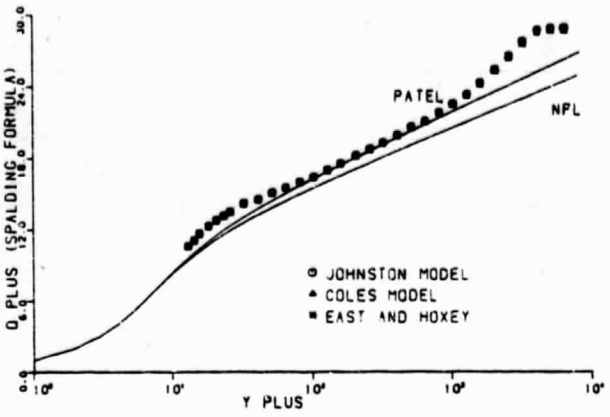

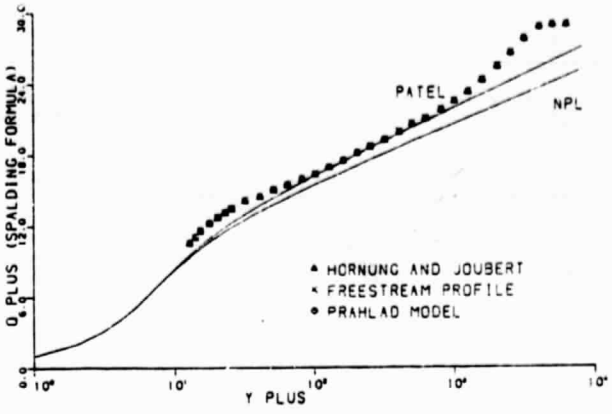

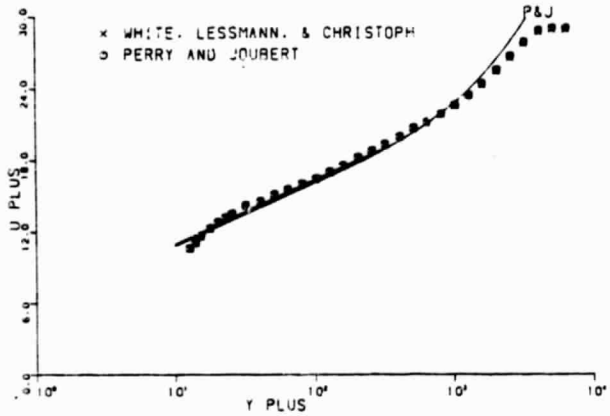

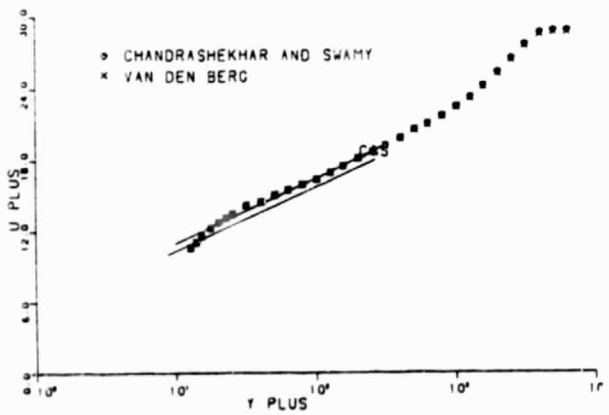

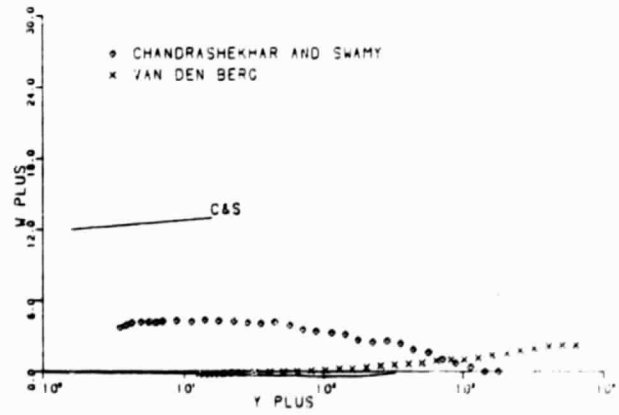

Fig. 6.12 Three-Dimensional Similarity Plots for I7

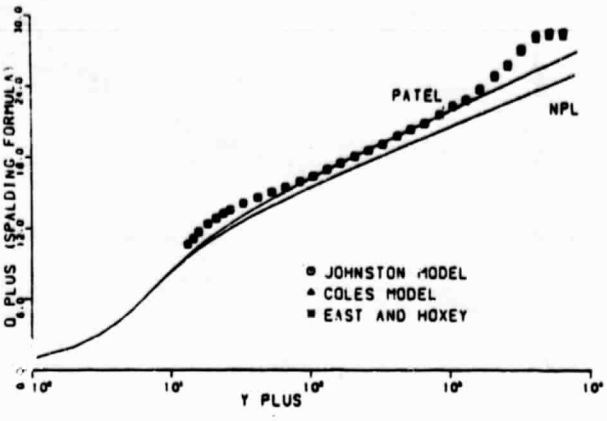

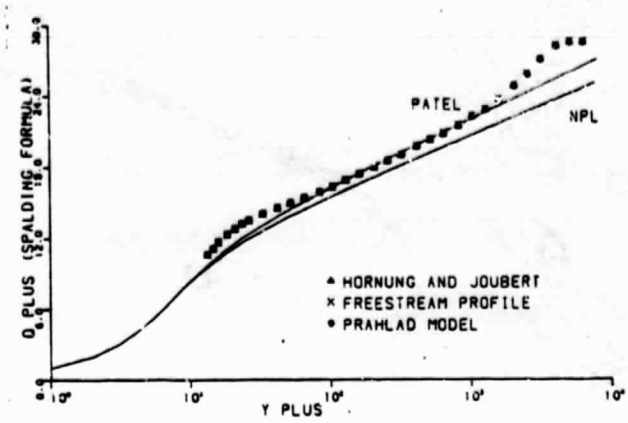

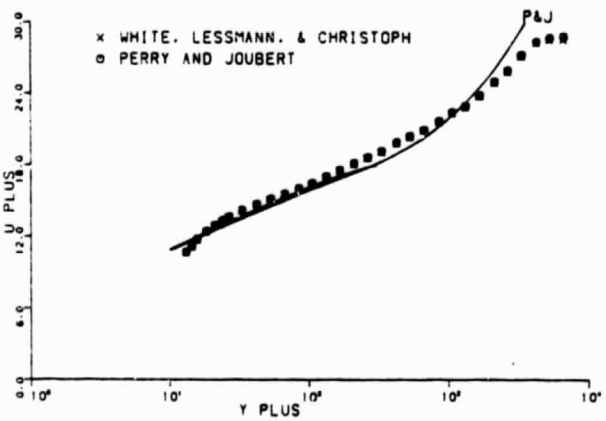

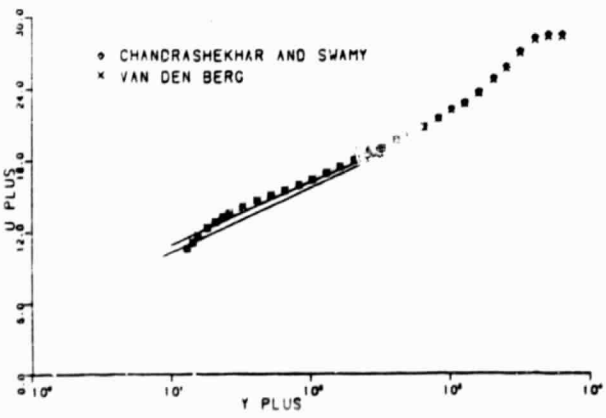

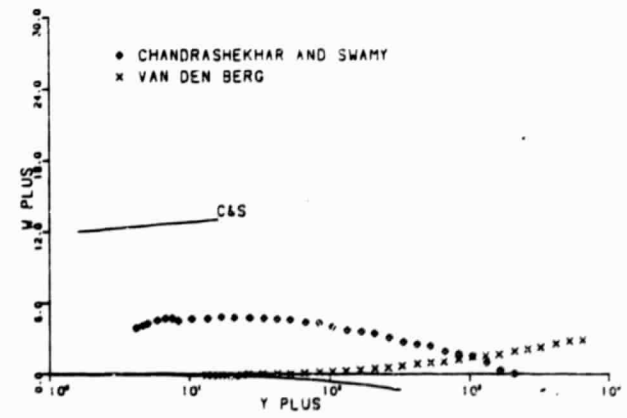

Fig. 6.13 Three-Dimensional Similarity Plots for I5

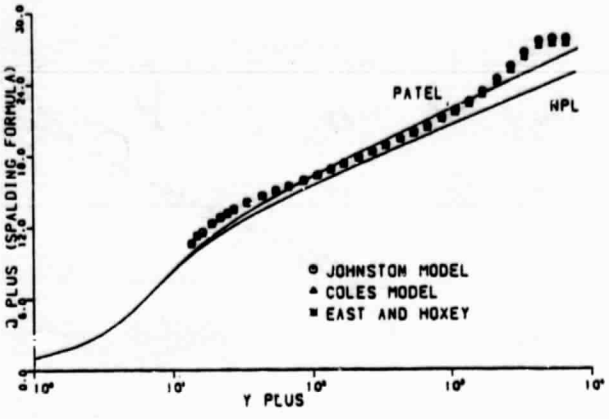

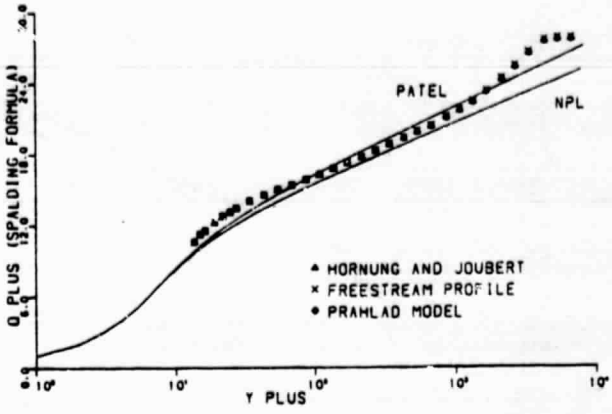

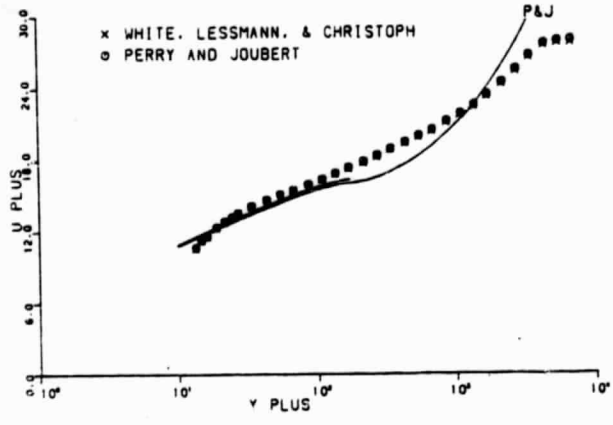

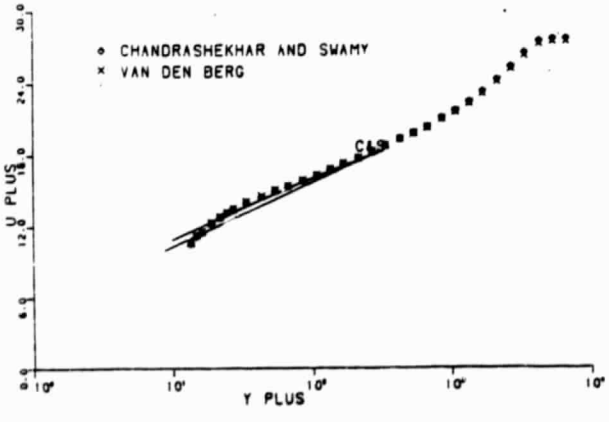

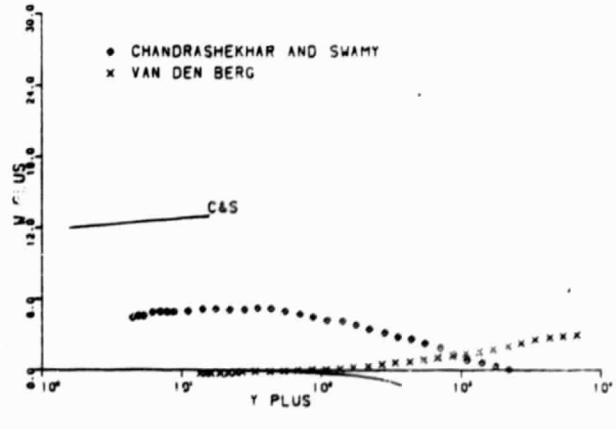

Fig. 6.14 Three-Dimensional Similarity Plots for I3

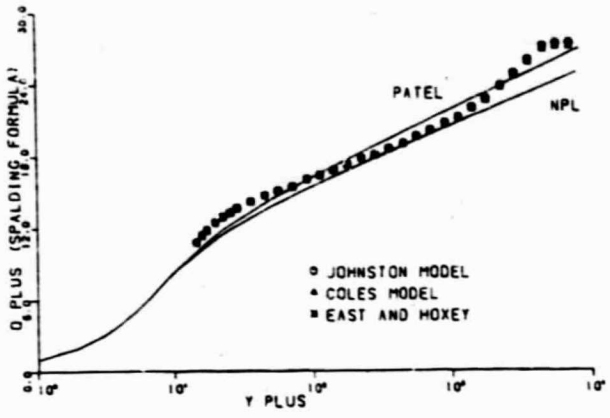

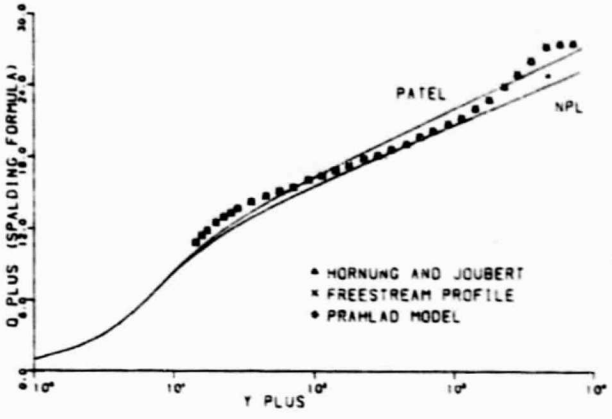

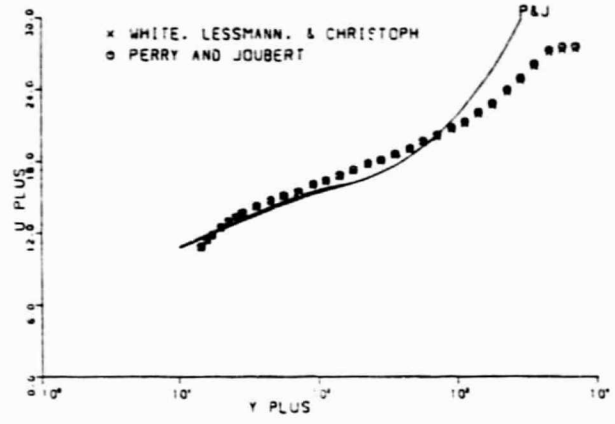

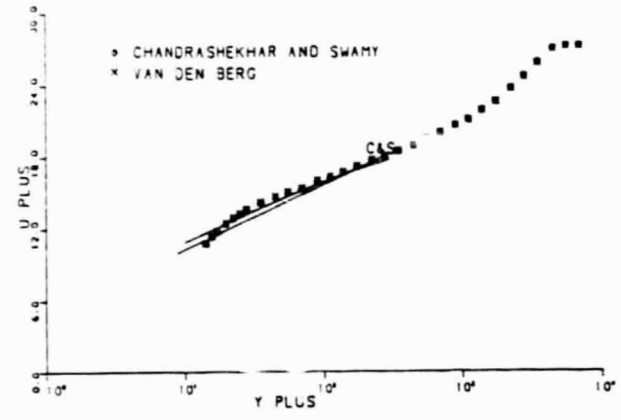

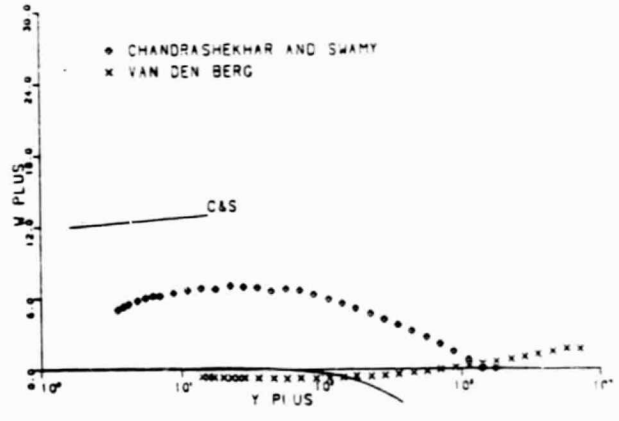

Fig. 6.15 Three-Dimensional Similarity Plots for I1

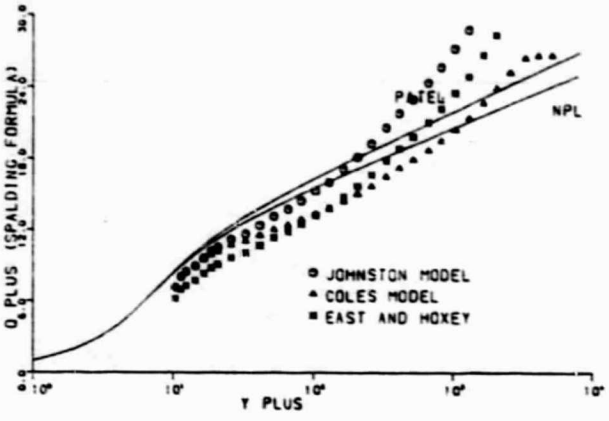

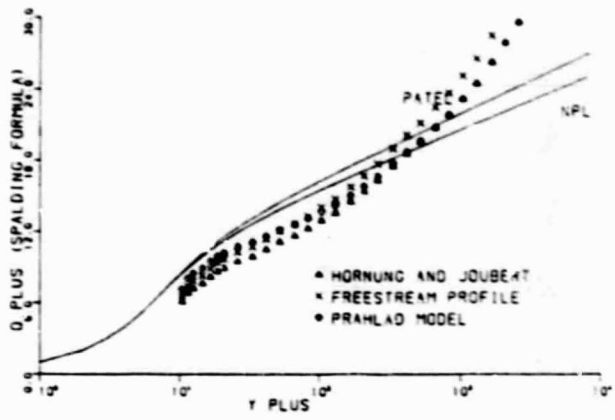

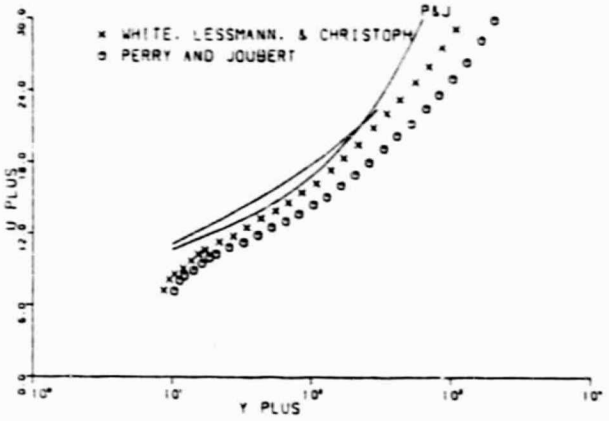

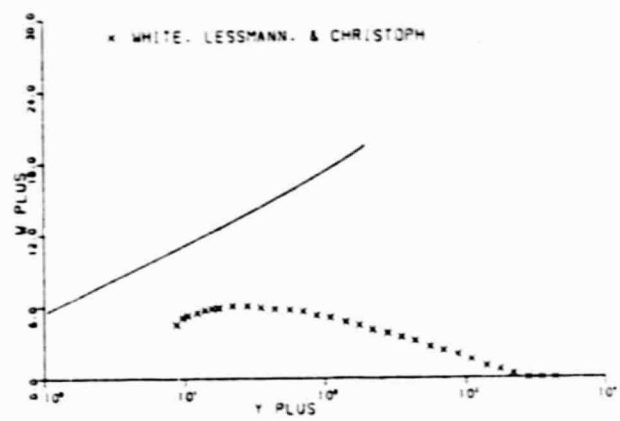

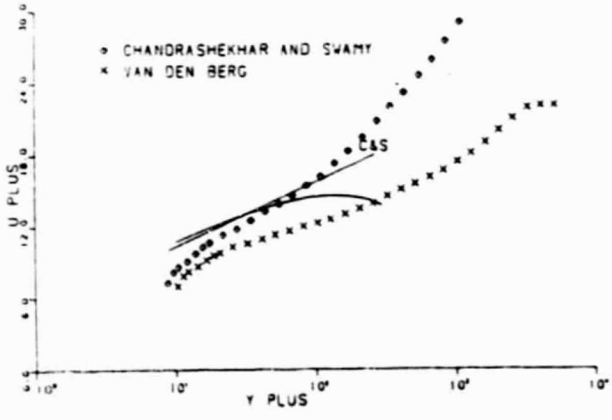

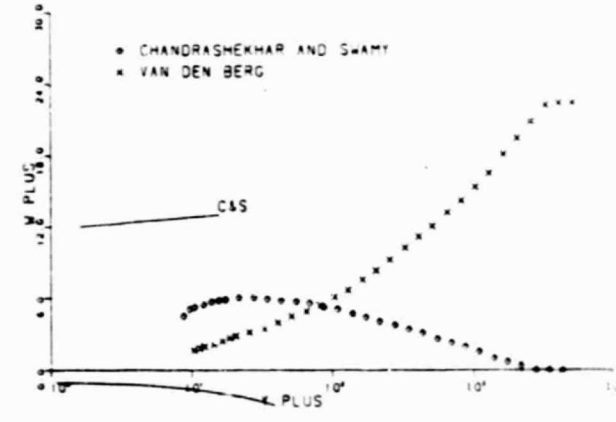

Fig. 6.16 Three-Dimensional Similarity Plots for C3

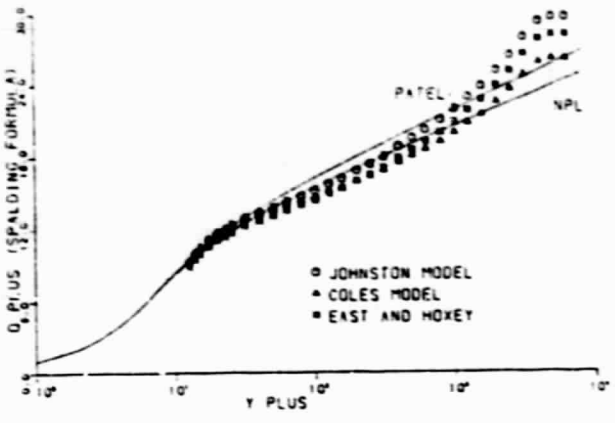

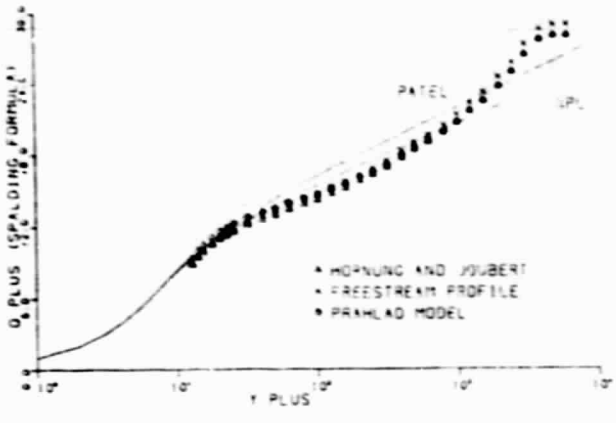

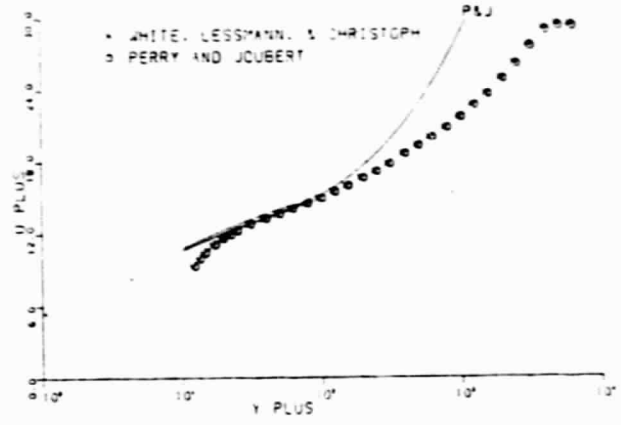

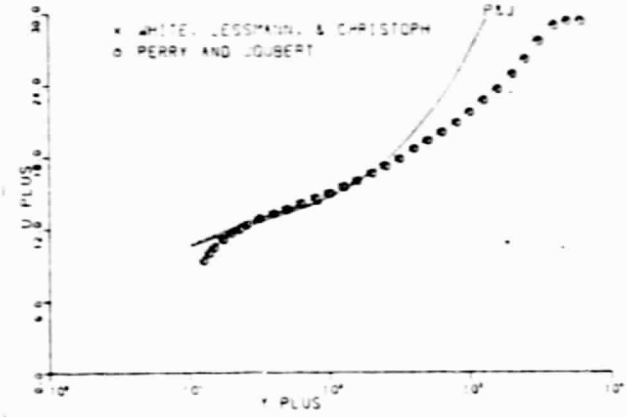

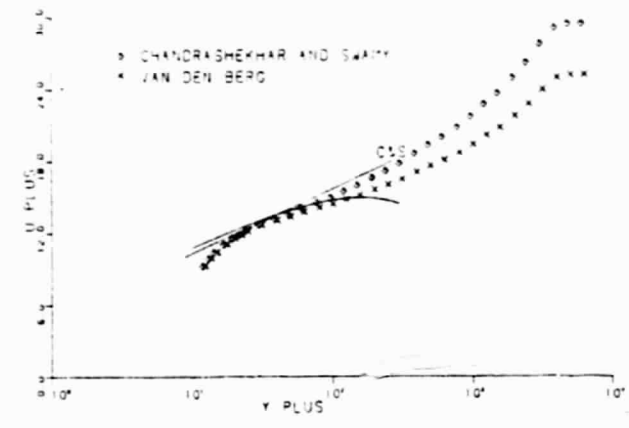

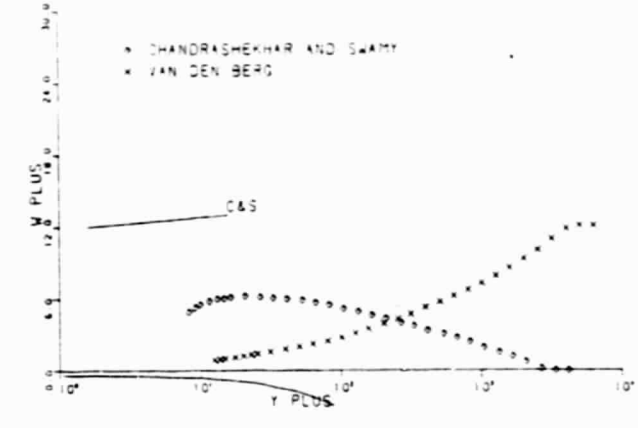

Fig. 6.17 Three-Dimensional Similarity Plots for E3

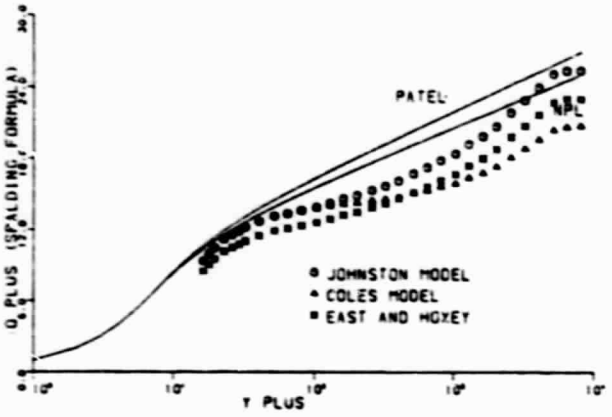

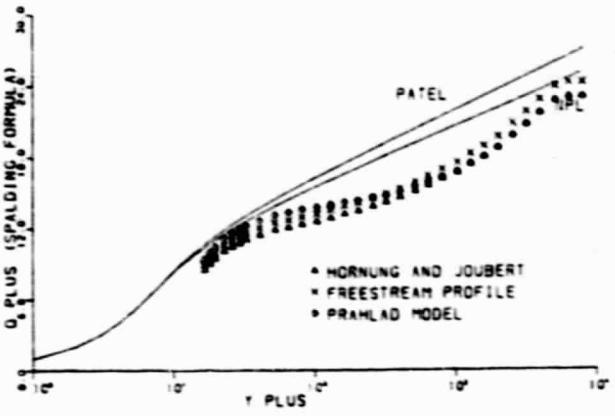

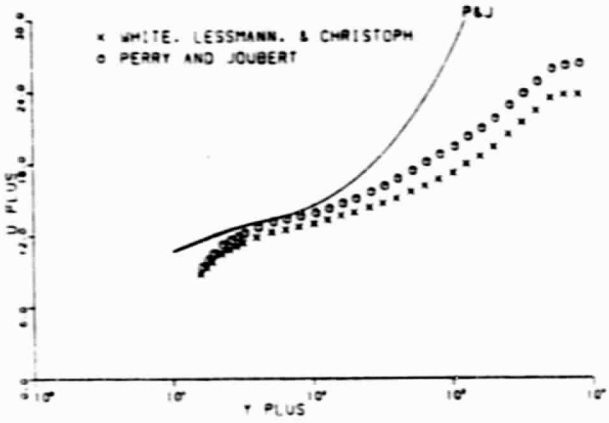

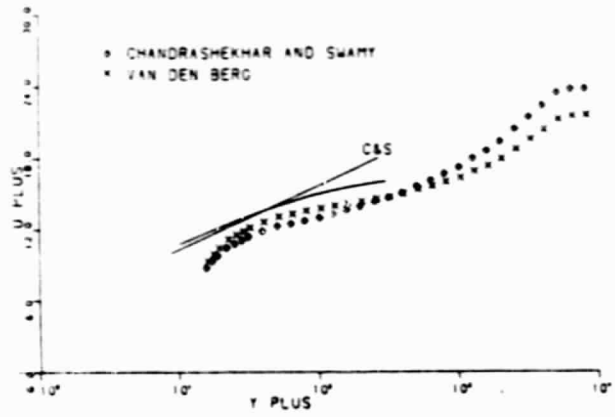

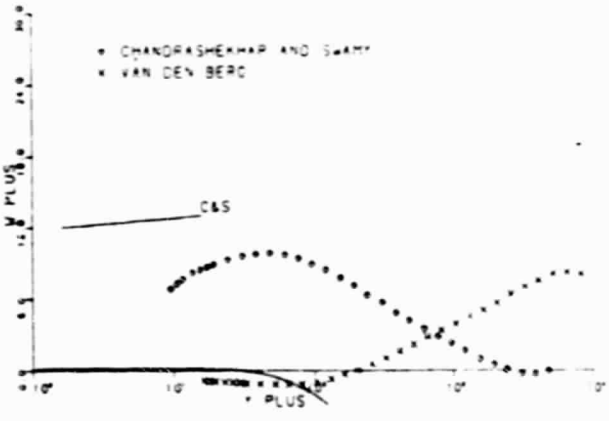

Fig. 6.18 Three-Dimensional Similarity Plots for E1

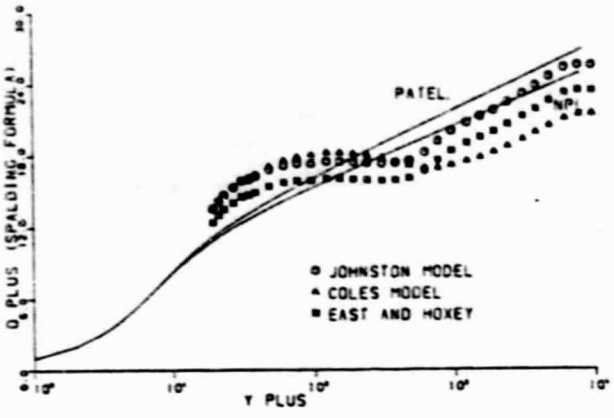

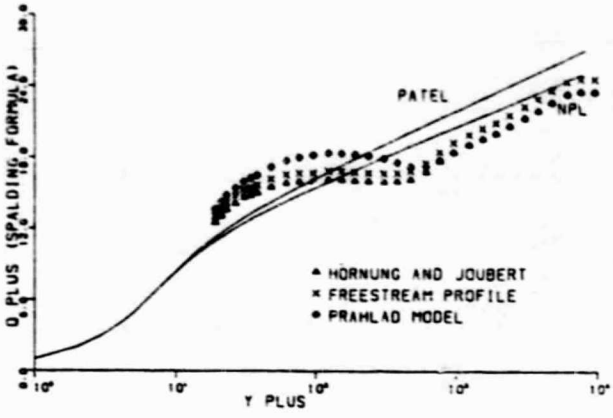

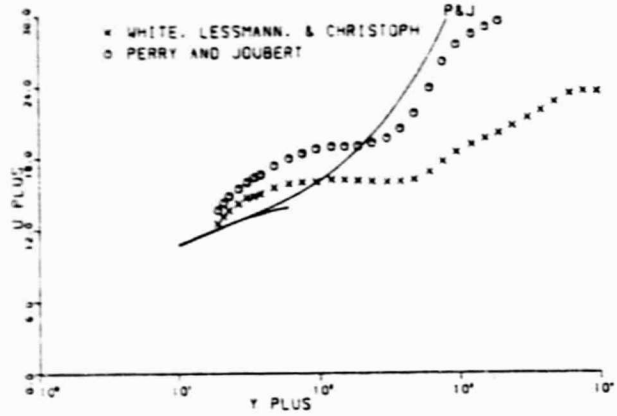

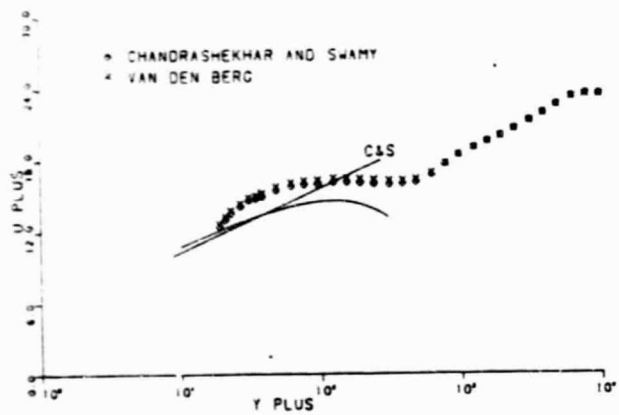

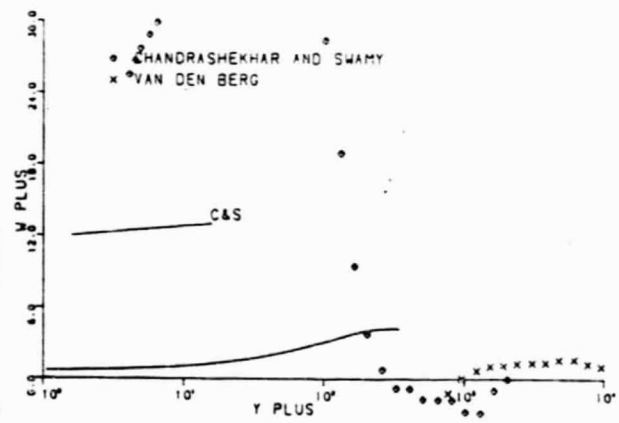

Fig. 6.19 Three-Dimensional Similarity Plots for E-1

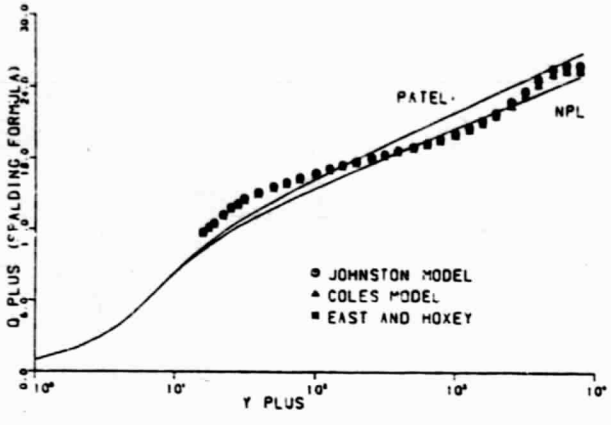

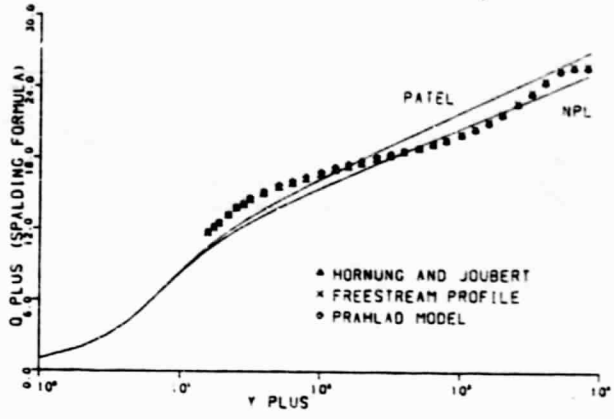

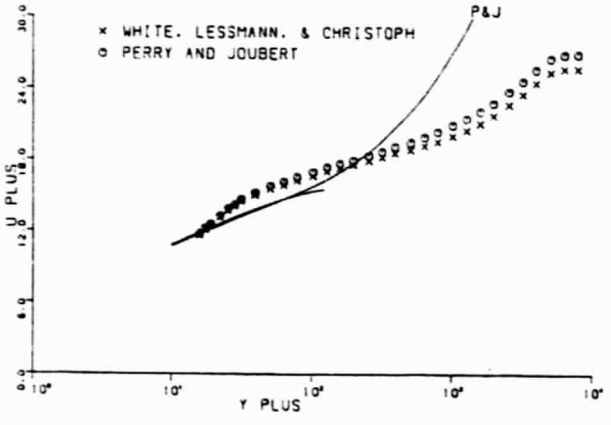

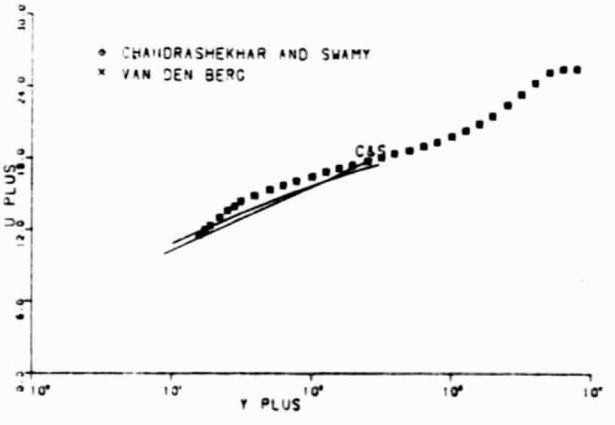

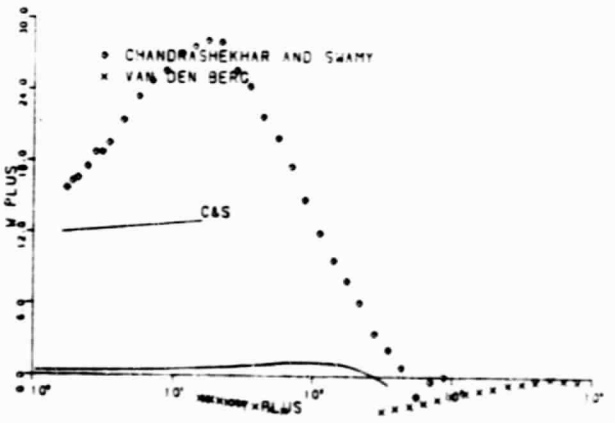

Fig. 6.20 Three-Dimensional Similarity Plots for G-1

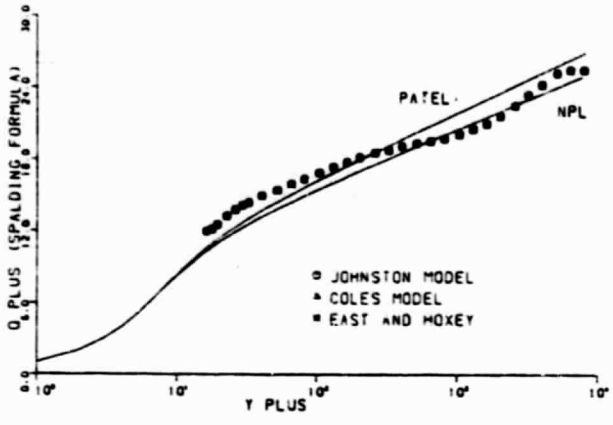

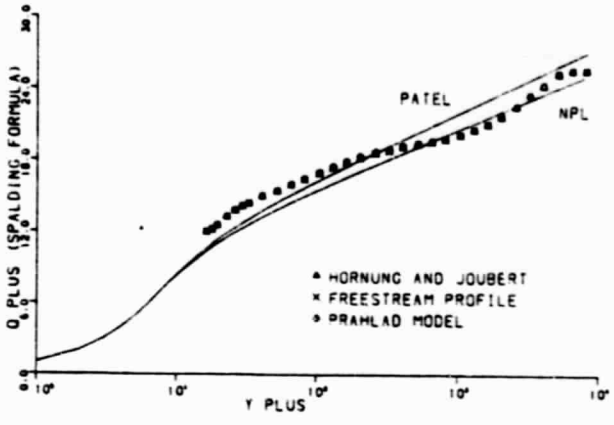

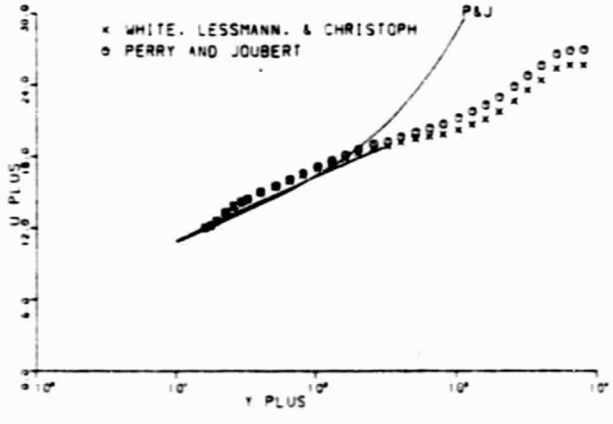

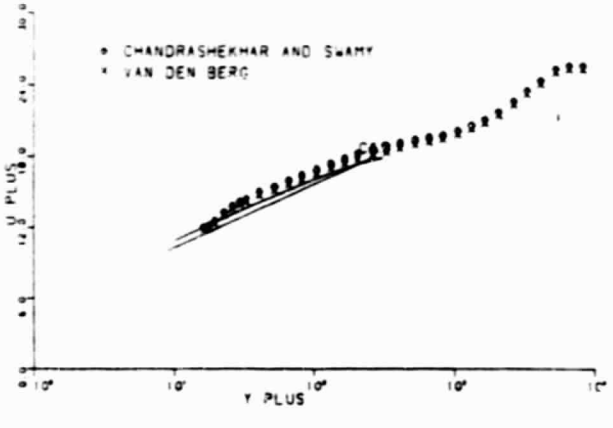

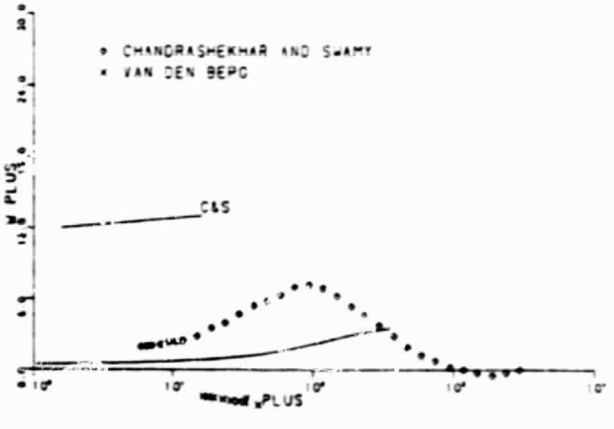

Fig. 6.21 Three-Dimensional Similarity Plots for G-3

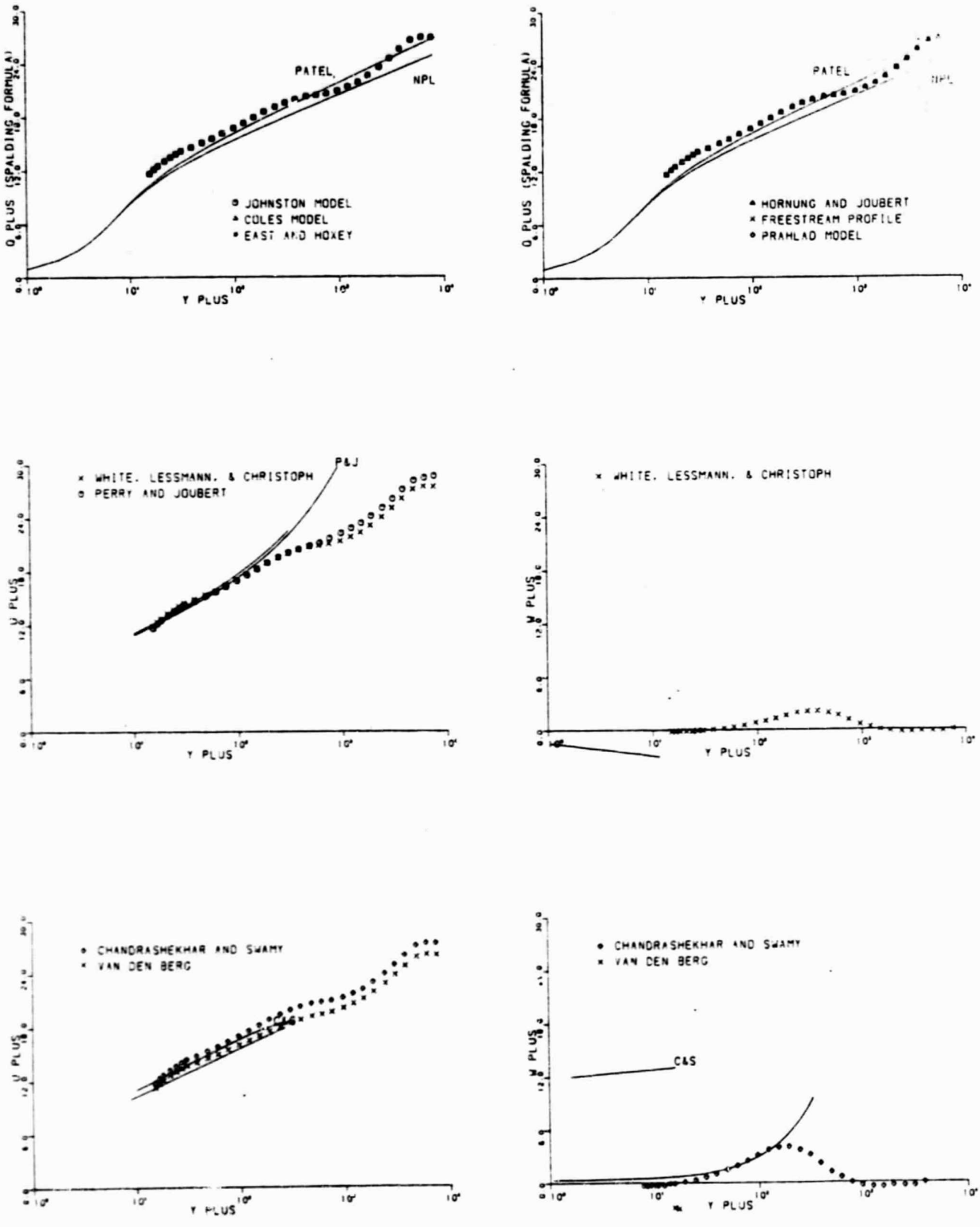

Fig. 6.22 Three-Dimensional Similarity Plots for G-5

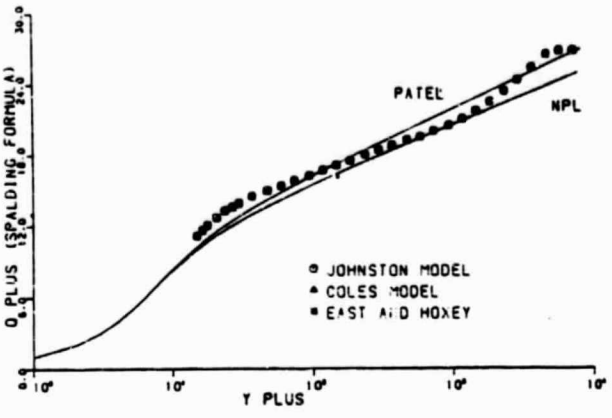

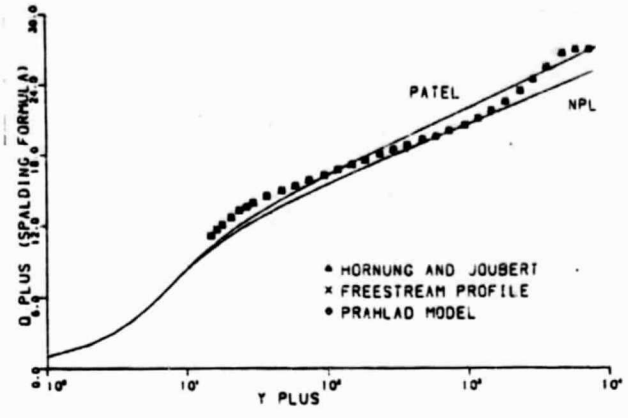

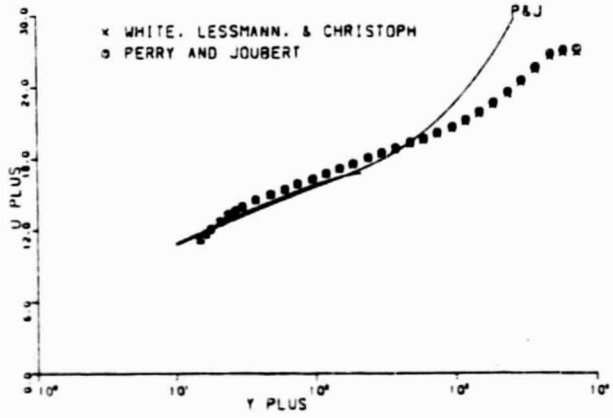

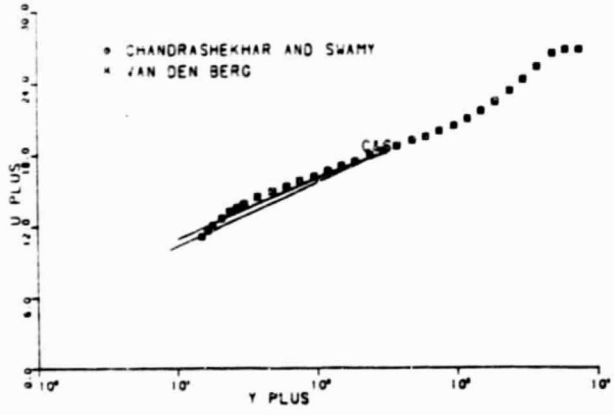

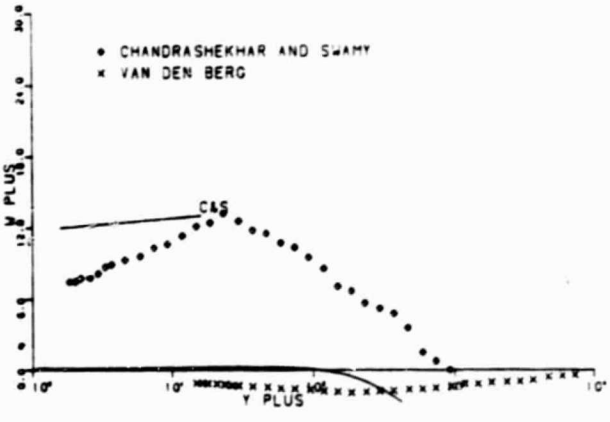

Fig. 6.23 Three-Dimensional Similarity Plots for I-1

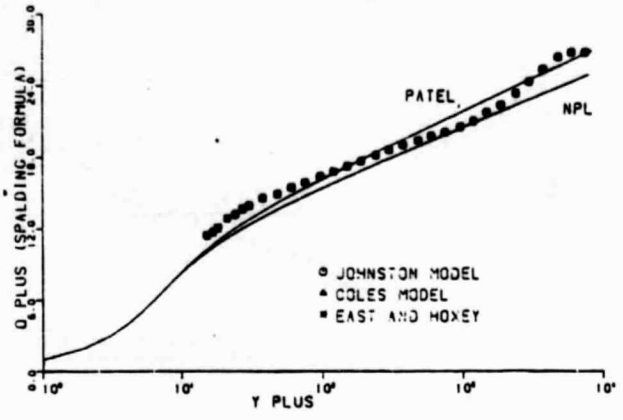

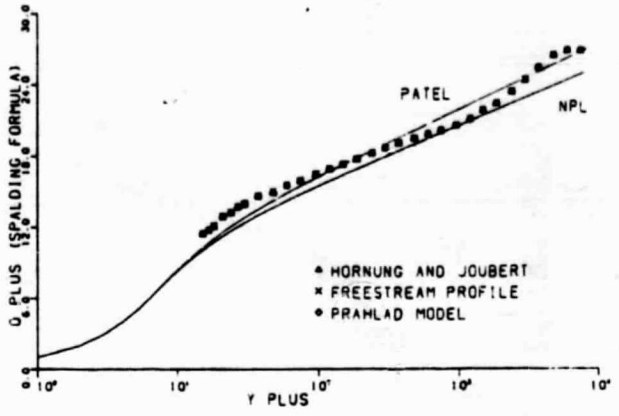

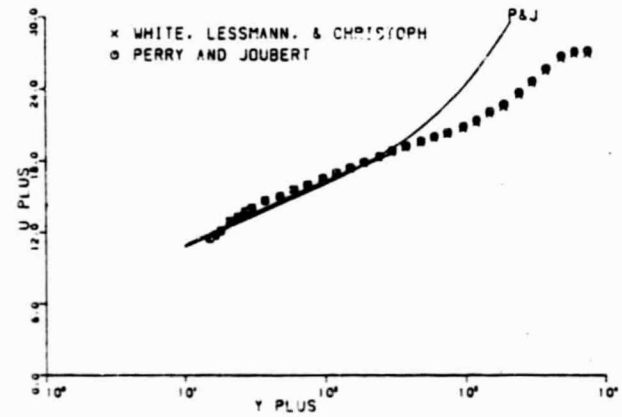

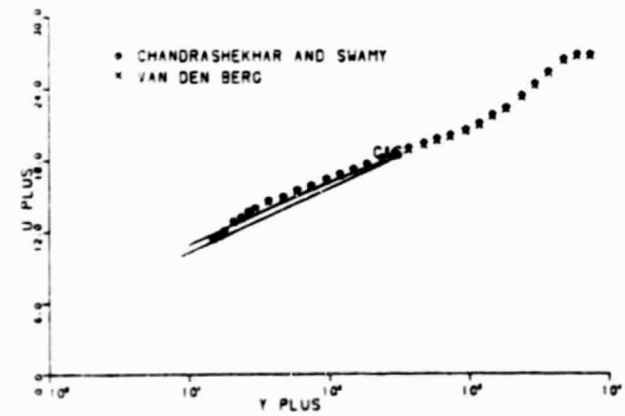

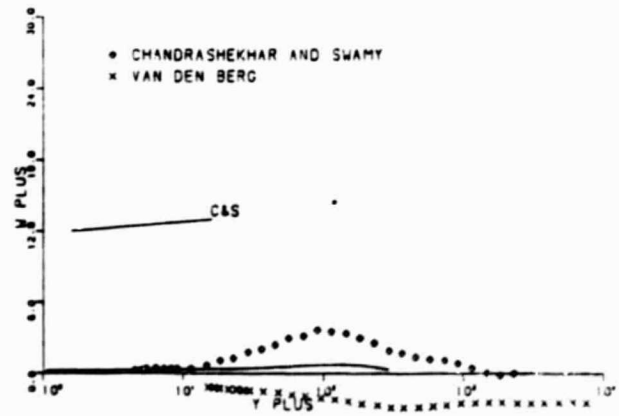

Fig. 6.24 Three-Dimensional Similarity Plots for 1-3

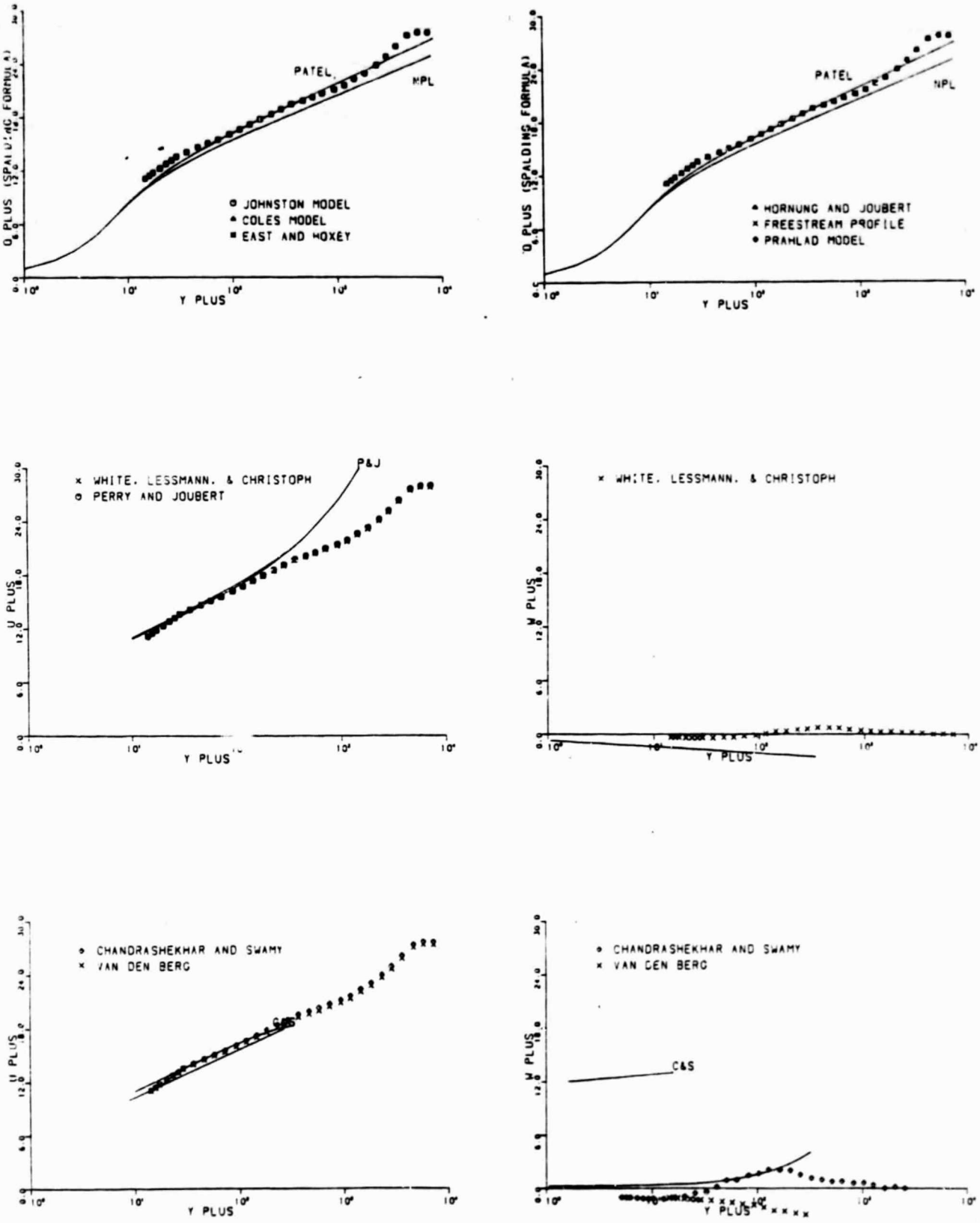

Fig. 6.25 Three-Dimensional Similarity Plots for I-5

REFERENCES

Abarbanel, S. S., R. J. Hakkinen, and L. Trilling, (1969) "Use of a Stanton Tube for Skin-Friction Measurements," NASA 2-17-59W.

Allen, J. M., (1973) "Evaluation of Prescon Tube Calibration Equations in Supersonic Flow," AIAA Journal, Vol. 11, No. 11, pp. 1461-1462.

Allen J. M., (1977) "Experimental Study of Error Sources in Skin Friction Balance Measurements," Trans. ASME, Journal of Fluid Engineering, Vol. 99, pp. 192-204.

Armistead, R. A. Jr., and J. J. Keyes Jr., (1968) "A Study of Wall-Turbulance Phenomena Using Hot-Film Sensors," Trans. ASME, Journal of Heat Transfer, Series C Vol. 90, pp. 13-21.

Bellhouse, B. J., and D. L. Schultz, (1966) "Determination of Mean and Dynamic Skin Friction, Separation, and Transition in Low-Speed Flow with a Thin-Film Heated Element," Journal of Fluid Mechanics, Vol. 24, Part 2, pp. 379-400.

Bellhouse, B. J., and D. L. Schultz, (1968) "The Measurement of Fluctuating Skin Friction in Air with Heated Thin-Film Gauges," Journal of Fluid Mechanics, Vol. 32, Part 4, pp. 675-680.

Bertelrud, A., (1972) "Skin Friction Measurement Techniques in Incompressible Turbulent Flow - A Literature Survey," Aeronautical Research Institute of Sweden, FFA Rept. AU-726, (available from NTIS as N73-17246).

Bertelrud, A., (1974) "Pipe Flow Calibration of Preston Tubes of Different Diameters and Relative Lengths Including Recommendations on Data Presentation for Best Accuracy," Aeronautical Research Institute of Sweden, FFA Rept. 125, (available from NTIS as N75-15000).

Bertelrud, A., (1976) "Surface Total/Static Tube for Skin Friction Measurement," Aeronautical Research Institute of Sweden, Technical Note AU-1133, (available as N76-26458).

Bertelrud, A., (1976A) "Preston Tube Calibration Accuracy," AIAA Journal, Vol. 14, No. 1, pp. 98-100.

Bertelrud, A., (1977) "Total Head/Static Measurements of Skin Friction and Surface Pressure," AIAA Journal, Vol. 15, No. 3, pp. 436-438.

Boyce, M. P. and E. F. Blick, (1969) "Fluid Flow Phenomena in Dusty Air," ASME Paper No. 69-WA/FE-24.

Boyce, M. P. and E. F. Blick, (1971) "Skin Friction Drag and Velocity Profile Measurement Techniques in Two-Phase Flow," ASME Paper No. 71-FE-32.

Bradshaw, P., (1959) "A Simple Method for Determining Turbulent Skin Friction From Velocity Profiles," Journal of Aerospace Sciences, Vol. 20, December, p. 841.

Bradshaw, P., (1965) "The Effect of Wind-Tunnel Screens on Nominally Two-Dimensional Boundary Layers," Journal of Fluid Mechanics, Vol. 22 Part 4, pp. 679-687.

Bradshaw, P., (1971) "Calculation of Three-Dimensional Turbulent Boundary Layers," Journal of Fluid Mechanics, Vol. 46, Part 3, pp. 417-445.

Bradshaw, P., (1975) "Complex Turbulent Flows," Trans. ASME, Journal of Fluids Engineering, Vol. 97, pp. 146-154.

Bradshaw, P., and N. Gregory, (1961) "The Determination of Local Turbulent Skin Friction from Observations in the Viscous Sub-Layer," ARC R & M 3203.

Bradshaw, P., D. H. Ferriss, and N. P. Atwell, (1967) "Calculation of Boundary-Layer Development Using the Turbulent Energy Equation," Journal of Fluid Mechanics, Vol. 28, pp. 593-616.

Brown, G. L., (1967) "Theory and Application of Heated Films for Skin Friction Measurement," Proceedings of the 1967 Heat Transfer and Fluid Mechanics Institute, Stanford University Press, Stanford, California, pp. 361-381.

Brown, K. C., and P. N. Joubert, (1969) "The Measurement of Skin Friction In Turbulent Boundary Layers with Adverse Pressure Gradients," Journal of Fluid Mechanics, Vol. 35, Part 4, pp. 732-757.

Burr, I. W., (1974) Applied Statistical Methods, Academic Press, New York.

Chandrashekhar, N., (1974) "Some Studies on Three-Dimensional Turbulent Boundary Layers," Ph.D. Dissertation, Department of Applied Mechanics, Indian Institute of Technology, Madras, India.

Chandrashekhar, N., and N. V. C. Swamy, (1976) "Wall Shear Stress Inference for Three-Dimensional Turbulent Boundary Layer Velocity Profiles," Journal of Applied Mechanics, Vol. 43, pp. 20-27.

Clauser, F., (1954) "Turbulent Boundary Layers in Adverse Pressure Gradients," Journal of Aeronautical Science, Vol. 21, No. 2, pp. 91-108.

Clauser, F. H., (1956) "The Turbulent Boundary Layer," Advances in Applied Mechanics, Vol. 4, pp. 1-51.

Coles, D., (1955) "The Law of the Wall in Turbulent Shear Flow," 50 Jahre Grenzschichtforschung, (ed.) H. Gortler and W. Tollmien, Friedr, Vieweg and Sohn, Braunschweig, pp. 153-163.

Coles, D., (1956) "The Law of the Wake in the Turbulent Boundary Layer," Journal of Fluid Mechanics, Vol. 1, pp. 191-227.

Coles, D., (1957) "Remarks on the Equilibrium Turbulent Boundary Layer," Journal of Aeronautical Science, Vol. 24, No. 7, pp. 495-506.

Coles, D., (1962) "The Turbulent Boundary Layer in a Compressible Fluid," USAF Project Rand R-403-PR, The Rand Corporation, Santa Monica.

Coles, D., (1968) "The Young Person's Guide to the Data," Proceedings Computation of Turbulent Boundary Layers - 1968, AFOSR-IFP-Stanford Conference Vol. II, pp. 1-45.

Cooke, J. C., and M. G. Hall, (1960) "Boundary Layers on Three-Dimensions," Royal Aircraft Establishment Report Aero. 2635.

Davies, P. O. A. L., (1958) "The Behavior of a Pitot Tube in Transverse Shear," Journal of Fluid Mechanics, Vol. 3, pp. 441-456.

Dean, R. B., (1976) "A Single Formula for the Complete Velocity Profile in a Turbulent Boundary Layer," Trans. ASME, Journal of Fluid Engineering, pp. 723-727.

Dean, R. C., Jr., (1958) Aerodynamics Measurements, Gas Turbine Laboratory, Massachusetts Institute of Technology, Eagle Enterprise.

de Bray, B. G., (1965) "Some Investigations into the Spanwise Non-Uniformity of Nominally Two-Dimensional Incompressible Boundary Layers Downstream of Gauze Screens," Aeronautical Research Council, A.R.C. 29 271.

Dechow, R., (1976) "Mittlera Geschwindigkeit und Reynoldsscher Spannungstensor in der dreidimensionalen turbulenten Wandgrenzschicht vor einen stehenden Zylinder," dissertation, Universitat (TH) Karlsruhe.

Dechow, R. and K. O. Felsch, (1977) "Measurements on the Mean Velocity and the Reynolds Stress Fenon in a Three-Dimensional Turbulent Boundary Layer Inclosed by a Cylinder Standing in a Flat Wall," Symposium on Turbulent Shear Flows, Pennsylvania State University, University Park, Pennsylvania, pp. 9.11-9.20.

Deissler, R. G., (1955) "Analysis of Turbulent Heat Transfer, Mass Transfer, and Friction in Smooth Tubes at High Prandtl and Schmidt Number's" NACA TR 1210.

Depooter, K., Brundrett, E. and A. B. Strong, (1977) "Direct Measurement of Wall Shear Stress With Mass Transfer in a Low Speed Boundary Layer," Journal of Fluids Engineering, Vol. 99, pp. 580-584.

Depooter, K., Brundrett, E., and A. B. Strong, (1978) "The Calibration of Preston Tubes in Transpired Turbulent Boundary Layers," Journal of Fluids Engineering, Vol. 100, pp. 10-16.

Dershin, H., Leonard, C. A., and W. H. Gallaher, (1967) "Direct Measurement of Skin Friction on a Porous Flat Plate with Mass Injection," AIAA Journal, Vol. 5, No. 11, pp. 1934-1939.

Dhawan, S., (1952) "Direct Measurements of Skin Friction," NACA TN 2567.

Dickinson, J., and V. Ozarapoglu, (1969) "The Determination of Turbulent Skin Friction," Progress Report DRB 9550-23 Universite Laval, Canada.

Doench, F., (1926) "Divergente und Konvergente turbulente Stroemungen mit kleinen Oeffnungswinkeln," Forch.-Arb. Geb. Ing.-Wes., Heft 282.

Drinkuth, R. H., and F. J. Pierce, (1966) "Directional Heat Meter for Wall Shear Stress Measurements in Turbulent Boundary Layers," Review of Scientific Instruments, Vol. 37, pp. 740-741.

East, L. F., (1968) "Measurement of Skin Friction at Low Subsonic Speeds by the Razor-Blade Technique," Aeronautical Research Council R & M 3525.

East, L. F., (1972) "A Prediction of the Law of the Wall in Compressible Three-Dimensional Turbulent Boundary Layers," Royal Aircraft Establishment Technical Report 72178.

East, L. F., and R. P. Hoxey, (1969) "Low-Speed Three-Dimensional Turbulent Boundary Layer Data," Parts 1 and 2, Aeronautical Research Council R & M 3653.

Elrod, H. G., Jr., (1957) "Note on the Turbulent Shear Stress Near a Wall," J. of the Aero. Sciences, Vol. 24, pp. 468-469.

Everett, H. U., (1958) "Calibration of Skin Friction Balance Discs for Pressure Gradient," Defense Research Laboratory, DRL-426, CF-2708.

Ezekwe, C. I., (1974) "Turbulent Stress Tenons in a Three-Dimensional Boundary Layer," Dissertation, Virginia Polytechnic Institute and State University, Blacksburg, Virgina.

Fage, A., and V. M. Falkner, (1931) "On the Relation Between Heat Transfer and Surface Friction for Laminar Flow," Aeronautical Research Council R & M No. 1408.

Ferriss, D. H., (1965) "Preston Tube Measurements in Turbulent Boundary Layers and Fully Developed Pipe Flow," ARC-CP-831.

Finley, P. J., Phoe, and Poh, (1966) "Velocity Measurements in a Thin Turbulent Water Layer," La Houille Blanche, Vol. 21, pp. 713-721.

Fowke, J. G., (1969) "Development of a Skin-Friction Balance to Investigate Sources of Error in Direct Skin-Friction Measurements," M.S. Thesis, University of Virginia.

Franklin, R. E., (1961) "A Force-Displacement Indicator for a Drag Balance," Ministry of Aviation, Aeronautical REsearch Council, C.P. No. 549, London.

Furuya, Y. and H. Osaka, (1975) "The Spanwise Non-Uniformity of Nominally Two-Dimensional Turbulent Boundary Layer I-- Characteristics of Spanwise Velocity Distribution," JSME Bulletin. Vol. 18, No. 121, pp. 664-672.

Furuya, Y., I. Nakamura, H. Osaka, and H. Honda, (1975) "The Spanwise Non-Uniformity of Nominally Two-Dimensional Turbulent Boundary Layer II--Wall Shear Stress and Flow Field," JSME Bulletin, Vol. 18, pp. 673-680.

Gold, D. S., (1974) "Near-Wall Velocity Measurements in Two-Dimensional Turbulent Boundary Layers," M.S. Thesis, Va. Polytechnic Inst. and State Univ., Blacksburg, Virginia.

Granville, P. S., (1975) "A Modified Law of the Wake for Turbulent Shear Layers," Naval Ship Research and Development Center - 4369, Bethesda, Maryland.

Gruschwitz, E., (1935) "Turbulente Reibungsschichten Mit Secundarstromung," Ingenieur-Archiv., Vol. 6.

Gupta, R. P., (1975) "New Device for Skin-Friction Measurement in Three-Dimensional Flows," AIAA Journal, Vol. 13, No. 2, pp. 236-238.

Hakkinen, R. J., (1955) "Measurements of Turbulent Skin Friction on a Flat Plate at Transonic Speeds," NACA TN 3486.

Head, M. R. and V. V. Ram, (1971) "Simplified Presentation of Preston Tube Calibration," Aeronautical Quarterly, Vol. 22, Part 3, pp. 295-300.

Head, M. R. and I. Rechenberg, (1962) "The Preston Tube as a Means of Measuring Skin Friction," Journal of Fluid Mechanics, Vol. 14, pp. 1-17.

Headley, J. W., (1966) "A Simple Calibration Technique for Skin Friction Balances," AIAA Journal, Vol. 4, p. 1862.

Hebbar, K. S., and W. L. Melnik, (1976) "Measurements in the Near-Wall Region of a Relaxing Three-Dimensional Low Speed Turbulent Air Boundary Layer," University of Maryland, T. R. No. AE-76-1.

Higuchi, H., and D. J. Peake, (1978) "Bi-Directional Buried-Wire Skin-Friction Gage," NASA TM 78531, Ames Research Center.

Hinze, J. O., (1975) Turbulence, 2 ed., McGraw Hill, New York.

Hornung, H. G., and P. N. Joubert, (1963) "The Mean Velocity in Three-Dimensional Turbulent Boundary Layers," Journal of Fluid Mechanics, Vol. 15, Part 3, pp. 368-384.

Huffman, G. D. and P. Bradshaw, (1972) "A Note on von Karman's Constant in Low Reynolds Number Turbulent Flows," Journal of Fluid Mechanics, Vol. 53, Part 1, pp. 45-60.

Johnston, J. P., (1960) "On Three-Dimensional Turbulent Boundary Layer Generated by Secondary Flow," Trans. ASME, Journal of Basic Engineering, Vol. 82, pp. 233-248.

Johnston, J. P., (1976) "Experimental Studies in Three-Dimensional Turbulent Boundary Layers," Report MD-34, Department of Mechanical Engineering, Stanford University, Stanford, California.

Kashinskiy, O. N., S. S. Kutateladze, and V. A. Mukhin, (1974) "Skin Friction in a Turbulent Boundary Layer with a Positive Pressure Gradient," NASA Translation from Z. H. Prikl. Mekh. Tekh. Fiz. (USSR), No. 6, pp. 92-96.

Kempf, G., (1929) "Neue Ergebnisse der Widerstands forschung," Werft Reederei Hafen, Vol. 10, pp. 234-239.

Klebanoff, P. S., and F. W. Diehl, (1951) "Some Features of Artifically Thickened Fully Developed Turbulent Boundary Layers with Zero Pressure Gradient," NACA TN 2475.

Kleinstein, G., (1967) "Generalized Law of the Wall and Eddy-Viscosity Model for Wall Boundary Layers," AIAA Journal, Vol. 5, No. 8, pp. 1402-1407.

Kline, S. J. and F. A. McClintock, (1953) "Describing Uncertainties in Single-Sample Experiments," Mechanical Engineering, p. 3.

Kline, S. J., and F. Schraub, (1965) "A Study of the Structure of the Turbulent Boundary Layer With and Without Longitudinal Pressure Gradients," Thermosciences Division, Stanford University Report MD-12.

Klinksiek, W. F., and F. J. Pierce, (1970) "Simultaneous Lateral Skewing in a Three-Dimensional Turbulent Boundary Layer," Trans. ASME, Journal of Basic Engineering, Vol. 92, pp. 834-[illegible].

Klinksiek, W. F. and F. J. Pierce, (1973) "A Finite Difference Solution of the Two- and Three-Dimensional Incompressible Turbulent Boundary Layer Equations," Journal of Fluids Engineering, Vol. 95, pp. 445-458.

Konstantinov, N. I., and G. L. Dragnysh, (1960) "The Measurement of Friction Stress on a Surface," English Translation, DSIR RTS 1499.

Kuethe, A., P. McKee, and W. Curry, (1949) "Measurements in the Boundary Layer with Zero Pressure Gradient," NACA TN 1946.

Landweber, L., (1960) "Reanalysis of Boundary-Layer Data on a Flat Plate," written discussion of Ninth International Toning Tank Conference, Paris, 1960. Iowa Institute of Hydraulic Research, State University of Iowa.

Landweber, L., and T. T. Siao, (1958) "Comparison of Two Analyses of Boundary Layer Data on a Flat Plate," Journal of Ship Research, Vol. 1.

Laufer, J., (1950) "Investigation of Turbulent Flow in a Two-Dimensional Channel," NACA TN 2123.

Laufer, J., (1953) "The Structure of Turbulence in Fully Developed Pipe Flow," NACA Tech. Note 2954.

Laufer, J., (1954) "The Structure of Turbulence in Fully Developed Pipe Flow, NACA TR 1174.

Liepmann, H. W., and G. T. Skinner, (1954) "Shearing-Stress Measurements by Use of a Heated Element," NACA Technical Note 3268.

Lindgren, E. R., and J. Chao, (1969) "Average Velocity Distribution of Turbulent Pipe Flow with Emphasis on the Viscous Sublayer," Physics of Fluids, Vol. 12, pp. 1364-1371.

Livesey, J. L., (1956) "The Behavior of Transverse Cylinderical and Forward Facing Total Pressure Probes in Transverse Total Pressure Gradients," Journal of Aeronautical Science, Vol. 23.

Ludwieg, H., (1950) "Instrument for Measuring the Wall Shearing Stress of Turbulent Boundary Layers," NACA Technical Memorandum 1284, (translated from Ingenier Arch., Vol. 17, 1949), pp. 207-218.

Ludwieg, H., and W. Tillmann, (1950) "Investigations of the Wall-Shearing Stress in Turbulent Boundary Layers," NACA TM 1285.

MacMillan, F. A., (1954) "Viscous Effects on Pitot Tubes at Low Speeds," Journal of the Royal Aeronautical Society, Vol. 58, pp. 570-572.

MacMillan, F., (1956) "Experiments on Pitot-Tubes in Shear Flow," ARC R & M No. 3028.

Mager, A., (1951) "Generalization of Boundary Layer Momentum Integral Equations to Three-Dimensional Flows, Including Those of a Rotating Disk," NACA TN 2310.

McAllister, J. E., (1979) "Near-Wall Similarity in Two- and Three-Dimensional Turbulent Boundary Layers," Dissertation, Virginia Polytechnic Institute and State University, Blacksburg, Virginia.

McCroskey, W. J., and E. J. Durbin, (1972) "Flow Angle and Shear Stress Measurements Using Heated Films and Wires," Trans. ASME, Journal of Basic Engineering, Vol. 94, pp. 46-52.

McDonald, H., (1969) "The Effect of Pressure Gradient on the Law of the Wall in Turbulent Flow," Journal of Fluid Mechanics, Vol. 35, Part 2, pp. 311-336.

Mellor, G. L., (1966) "The Effects of Pressure Gradients on Turbulent Flow Near a Smooth Wall," Journal of Fluid Mechanics, Vol. 24, Part 2, pp. 255-274.

Mellor, G. L., (1968) "Review of the Empirical Content of Some Turbulent Boundary Layer Prediction Methods," Proc. Symp. Fluidics and Internal Flows, Vol., Penn State Univ., pp. 151-175.

Miller, B. L. P., (1972) "The Measurement of Wall Shearing Stress in Turbulent Boundary Layers," Ph.D. Dissertation, University of Leicester, Great Britain.

Millikan, C. B., (1938) "A Critical Discussion of Turbulent Flows in Channels and Circular Tubes," Proc. 5th Int. Congr. Appl. Mech., Cambridge, Mass., pp. 386-392.

Mitchell, J. E., and T. J. Hanratty, (1966) "A Study of Turbulence at a Wall Using an Electrochemical Wall Shear Stressmeter," Journal of Fluid Mechanics, Vol. 26, Part 1, pp. 199-221.

Moffat, R. J., (1980) "Contributions to the Theory of Uncertainty Analysis for Single-Sample Experiments," in The 1980-81 AFOSR-HTTM-Stanford Conference on Complex Turbulent Flows: Comparison of Computation and Experiment, 1980 Meeting, Stanford University, Stanford, California. To be published.

Morsy, M. G., (1974) "An Instrument for the Direct Measurement of the Local Shear Stress on Circular Cylinders," Journal of Physics, Part E - Scientific Instruments, Vol. 7, pp. 83-86.

Musker, A. J., (1979) "Explicit Expression for the Smooth Wall Velocity Distribution in a Turbulent Boundary Layer," AIAA Journal, Vol. 17, No. 6, pp. 655-657.

Nash, J. F., and V. C. Patel, (1972) Three-Dimensional Turbulent Boundary Layers, SBC Technical Books.

Nash-Weber, J. L. and G. C. Oates, (1971) "An Instrument for Shin Friction Measurements in Thin Boundary Layers, ASME Paper 71-FE-27.

Nelson, D. J., (1979) "Pressure and Velocity Fields in a Relaxing Three-Dimensional Turbulent Boundary Layer," M.S. Thesis, Virginia Polytechnic Institute and State University, Blacksburg, Virginia.

NPL Staff, (1955) "On the Measurement of Local Surface Friction on a Flat Plate by Means of Preston Tubes," ARC R & M 3185.

O'Donnell, F. B., Jr., (1964) "A Study of the Effect of Floating-Element Misalignment on Skin-Friction-Balance Accuracy," Defense Research Laboratory, DRL-515, CR-10.

Owen, F. K., (1970) "Transition Experiments on a Flat Plate at Subsonic and Supersonic Speeds," AIAA Journal, Vol. 8, pp. 518-523.

Pai, B. R., and J. H. Whitelaw, (1969) "Simplification of the Razor-Blade Technique and its Application to the Measurement of Wall-Shear Stress in Wall-Jet Flows," Aero. Quarterly, Vol. 20, pp. 355-364.

Paros, J. M., (1970) "Application of the Force-Balance Principle to Pressure and Skin Friction Sensors," 16th Annual Technical Meeting Proceedings, Institute of Environmental Science, pp. 363-368.

Patel, V. C., (1965) "Calibration of the Preston Tube and Limitations on Its Use in Pressure Gradients," Journal Fluid Mechanics, Vol. 23, Part 1, pp. 185-208.

Patel, V. C., (1973) "A Unified View of the Law of the Wall Using Mixing-Length Theory," Aeronautical Quarterly, Vol. 24, pp. 55-70.

Patel, V. C. and M. R. Head, (1968) "Reversion of Turbulent to Laminar Flow," Journal of Fluid Mechanics, Vol. 34, Part 2, pp. 371-392.

Patel, V. C. and M. R. Head, (1969) "Some Observations on Skin Friction and Velocity Profiles in Fully Developed Pipe and Channel Flows," Journal of Fluid Mechanics, Vol. 38, Part 1, pp. 181-201.

Perry, A. E., (1966) "Turbulent Boundary Layers in Decreasing Adverse Pressure Gradients," Journal of Fluid Mechanics, Vol. 26, Part 3, pp. 481-506.

Perry, A. E., and P. N. Joubert, (1965) "A Three-Dimensional Turbulent Boundary Layers," Journal of Fluid Mechanics, Vol. 22, Part 2, pp. 285-304.

Pierce, F. J., and J. L. East, (1972) "Near-Wall Collateral Flow in Three-Dimensional Turbulent Boundary Layers," AIAA Journal, Vol. 10, No. 3, pp. 334-336.

Pierce, F. J. and D. S. Gold, (1977) "Near-Wall Velocity Measurements for Wall Shear Inference in Turbulent Flows," Flow Measurement in Open Channels and Closed Conduits, NBS Special Publication 484, Vol. 2, pp. 621-648.

Pierce, F. J., and D. H. Krommenhoek, (1968) "Wall Shear Stress Diagnostics in Three-Dimensional Turbulent Boundary Layers," Interim Technical Report No. 2, ARO-D Project 6858E, Virginia Polytechnic Institute and State University.

Pierce, F. J., M. H. Tennant, and J. A. Rule, (1976) "Near-Wall Similarity in Three-Dimensional Turbulent Flows-Experimental Systems," Int. Rpt. NSF Grant ENG 73-03737-A01, (VPI & SU Rpt. VPI-E-76-16, available NTIS).

Pierce, F. J., Tennant, M. H. and J. E. McAllister, (1980) "An Omnidirectional Wall Shear Meter," Trans. ASME, Journal of Fluids Engineering, Vol. 102, pp. 21-25.

Pierce, F. J. and B. B. Zimmerman, (1973) "Wall Shear Stress Inference from Two- and Three-Dimensional Turbulent Boundary Layer Velocity Profiles," Journal of Fluids Engineering, Vol. 95, pp. 61-67.

Pilkey, W. D., (1969) "Manual for the Response of Structural Members," IIT Research Institute, Vols. I and II.

Power, J. L., (1973) "Wall Shear Stress and Mean-Velocity Measurements in a Three-Dimensional Turbulent Boundary Layer," Naval Ship and Development Center Report 4056.

Prahlad, T. S., (1968) "Wall Similarity in Three-Dimensional Turbulent Boundary Layers," AIAA Journal, Vol. 6, No. 9, pp. 1772-1774.

Prahlad, T. S., (1972) "Yaw Characteristics of Preston Tubes," AIAA Journal, Vol. 10, No. 3, pp. 357-359.

Prahlad, T. S., (1973) "Mean Velocity Profiles in Three-Dimensional Incompressible Turbulent Boundary Layers," AIAA Journal, Vol. 11, No. 3, pp. 359-365.

Prandtl, L., (1933) "Neuere Ergebnisse der Turbulenzforschung," Z. Ver. Dtsch. Ing., Vol. 77, pp. 105-114, (translation NACA Tech. Mem. 720).

Preston, J. H., (1954) "The Determination of Turbulent Skin Friction by Means of Pitot Tubes," J. Roy. Aer. Soc., Vol. 38, pp. 109-121.

Quarmby, A. and H. K. Das, (1969) "Measurement of Skin Friction Using a Rectangular Mouthed Preston Tube," Journal of the Royal Aeronautical Society, Vol. 73, pp. 228-230.

Rasmussen, M. L., (1975) "On Compressible Turbulent Boundary Layer in the Presence of Favourable Pressure Gradients," ASME Paper 75-WA/HT-53.

Rechenberg, I., (1963) "The Measurement of Turbulent Wall Shear Stress," Zeitschrift fur Flugwissenschaften, Vol. 11, (A.R.A. Library Translation No. 11).

Reichardt, H., (1951) "Vollstandige Darstelling der turbulenten Geschwindigkeitsverteilung in glatten Leitungen," Z. Angew. Math Mech. Vol. 31, No. 7, pp. 208-219.

Rogers, B. K., and M. R. Head, (1969) "Measurement of Three-Dimensional Turbulent Boundary Layers," The Aero. Journal of the Royal Aero. Scoeity, Vol. 73, pp. 796-798.

Rotta, J., (1950) "Das in Wandnähe gültige Geschwindigkeitsgesetz turbulenter Strömungen," Ing. Arch., Vol. 18, pp. 277-279.

Rubesin, M. W., Okuno, A. F., Mateer, G. G., and A. Brosh, (1975) "A Hot-Wire Surface Gage for Skin Friction and Separation Detection Measurements, NASA TMX-62, 465, Ames Research Center.

Rule, J. A., Jr., (1976) "Near-Wall Similarity and Wall Shear Stress Measurements in a Two-Dimensional Wind Tunnel," M.S. Thesis, Va. Polytechnic Inst. and State Univ., Blacksburg, Virginia.

Samuel, A. E., and P. N. Joubert, (1974) "A Boundary Layer Developing in an Increasing Adverse Pressure Gradient," Journal of Fluid Mechanics, Vol. 66, pp. 481-505.

Schraub, F. A., and S. J. Kline, (1965) "A Study of the Structure of the Turbulent Boundary Layer With and Without Longitudinal Pressure Gradients," Rpt. MD-12, Thermosciences Division, Mechanical Engineering, Stanford University.

Schultz-Grunow, F. Von, (1940) "Neues Reibungswiderstands gesetz für glatte Platten," Luftfahrtforschung, Band 7, 5.239, (translation NACA TM 986).

Shutts, W. H., Hartwig, H. H., and J. E. Weiler, (1955) "Turbulent Boundary Layer and Skin-Friction Measurements on a Smooth, Thermally Insulated Flat Plate at Supersonic Speeds," Defense Research Laboratory, DRL-364, Cm-823.

Sigalla, A., (1958) "Measurements of Skin Friction in a Plane Turbulent Wall Jet," Journal of the Royal Aeronautical Scoeity, Vol. 62, pp. 873-877.

Simpson, R. L., and D. G. Whitten, (1968) "Preston Tubes in the Transpired Turbulent Boundary Layer," AIAA Journal, Vol. 6, No. 11, pp. 1776-1777.

Smith, D. W., and J. H. Walker, (1958) "Skin-Friction Measurements in Incompressible Flow," NACA TN 4231.

Smith, S. L., C. J. Lawn, and M. J. Hamlin, (1968) "The Direct Measurement of Wall Shear Stress in an Annulus," C.E. G.B. RD/B/N 1232.

Spalding, D. B., (1961) "A Single Formula for the Law of the Wall," Trans. ASME, Journal of Applied Mechanics, Vol. 83, pp. 455-458.

Stanton, T. E., D. Marshall, and C. N. Bryant, (1920) "On the Conditions at the Boundary of a Fluid in Turbulent Motion," Proceedings Royal Society London, Vol. 97.

Tennant, M. H., (1977) "Near-Wall Similarity in Three-Dimensional Turbulent Boundary Layers," Ph.D. Dissertation, Virginia Polytechnic Institute and State University, Blacksburg, Va.

Tennekes, H., and J. L. Lumley, (1972) A First Course in Turbulence, MIT Press, Cambridge, Mass.

Townsend, A. A., (1956) The Structure of Turbulent Shear Flows, Cambridge University Press.

Townsend, A. A., (1961) "Equilibrium Layers and Wall Turbulence," Journal of Fluid Mechanics, Vol. 11, pp. 97-120.

Townsend, A. A., (1976) The Structure of Turbulent Shear Flow, 2 ed., Cambridge University Press, Cambridge.

Vagt, J. D., and H. Fernholz, (1973) "Use of Surface Fences to Measure Wall Shear Stress in Three-Dimensional Boundary Layers," The Aeronautical Quarterly, Vol. 24, pp. 87-91.

van den Berg, B., (1973) "The Law of the Wall in Two- and Three-Dimensional Turbulent Boundary Layers," National Aerospace Laboratory, TR 72111 U, Netherlands.

van den Berg, B., (1975) "A Three-Dimensional Law of the Wall for Turbulent Shear Flows," Journal of Fluid Mechanics, Vol. 70, Part 1, pp. 149-160.

van den Berg, B., (1976) "Investigations of Three-Dimensional Incompressible Turbulent Boundary Layers," National Aerospace Laboratory, TR 76001 U, Netherlands.

van den Berg, B., and A. Elsenaar, (1972) "Measurements in a Three-Dimensional Incompressible Turbulent Boundary Layer in an Adverse Pressure Gradient under Infinite Swept Wing Conditions," National Aerospace Laboratory TR 72072 U, Netherlands.

van Driest, E. R., (1956) "On Turbulent Flow Near a Wall," J. of Aero. Sci., Vol. 23, pp. 1007-1011.

Vermeulen, A., (1971) "Measurements of Three-Dimensional Turbulent Boundary Layers," Ph.D. Thesis, Cambridge University.

Vinh, M. N. D., (1973) "Sur less erreurs concernant less measures de frottement pariétal à l'aide d'une balance à élément flottant dans un écoulement turbulent avec gradient de pression adverse modéré," C.R. Acad. Sc. Paris, t. 277, Série A. pp. 1115-1117.

Von Kármán, T., (1930) "Mechanische Ähnlichkeit und Turbulenz," Proceedings Third International Congress for Applied Mechanics, Stockholm.

Waltrup, P. J., (1971) "An Experimental Investigation of a Compressible Turbulent Boundary Layer Subjected to a Systematic Variation of Adverse Pressure Gradients," Ph.D. Thesis, Virginia Polytechnic Institute and State University.

Wanschkuhn, P., and V. I. Vasanta Ram, (1975) "Turbulent Boundary Layer Behind a Separation Zone," Zeitschrift für Flugwissenchaften, Vol. 23, pp. 1-9.

Nash-Weber, J. L., and G. C. Oates, (1971) "An Instrument for Skin-Friction Measurements in Thin Boundary Layers," ASME Paper No. 71-EF-27.

White, F. M., (1974) Viscous Fluid Flow, McGraw Hill, New York.

White, F. M. and G. H. Christoph, (1972) "A Simple Theory for the Two-Dimensional Compressible Turbulent Boundary Layer," ASME Paper No. 72-EF-15.

White, F. M., R. C. Lessmann, and G. H. Christoph, (1975) "A Three-Dimension Integral Method for Calculating Incompressible Skin Friction," Trans. ASME, Journal of Fluids Engineering, Vol. 97, pp. 550-557.

White, J. K., and R. E. Franklin, (1964) "Measurements of Skin-Friction in an Annulus by the Floating Element Technique," A.R.C. 25 661, F.M. 3419.

Wills, J. A. B., (1963) "Note on a Method of Measuring Skin Friction," A.R.C. 24, No. 655.

Winter, K. G., (1977) "An Outline of the Techniques Available for the Measurement of Skin Friction in Turbulent Boundary Layers, Progress in Aeronatuics Sciences, Vol. 18, pp. 1-57.

Wyatt, L. A., and L. F. East, (1968) "Low Speed Measurements of Skin Friction on a Slender Ring," A.R.C. R & M 3499.

Young, A. B., and J. N. Maas, (1936) "The Behavior of a Pitot-Tube in a Transverse Pressure Gradient," ARC R & M No. 1770.